IAEA-TECDOC-1034

Handbook for calculations of nuclear reaction data

Reference input parameter library

Final report of a co-ordinated research project

INTERNATIONAL ATOMIC ENERGY AGENCY IAEA

The originating Section of this publication in the IAEA was:

Nuclear Data Section
International Atomic Energy Agency
Wagramer Strasse 5
P.O. Box 100
A-1400 Vienna, Austria

HANDBOOK FOR CALCULATIONS OF NUCLEAR REACTION DATA
REFERENCE INPUT PARAMETER LIBRARY
IAEA, VIENNA, 1998
IAEA-TECDOC-1034
ISSN 1011-4289

Printed by the IAEA in Austria
August 1998

The IAEA does not normally maintain stocks of reports in this series. However, microfiche copies of these reports can be obtained from

INIS Clearinghouse
International Atomic Energy Agency
Wagramerstrasse 5
P.O. Box 100
A-1400 Vienna, Austria

Orders should be accompanied by prepayment of Austrian Schillings 100,— in the form of a cheque or in the form of IAEA microfiche service coupons which may be ordered separately from the INIS Clearinghouse.

FOREWORD

Nuclear data for applications constitute an integral part of the IAEA programme of activities. When considering low-energy nuclear reactions induced with light particles, such as neutrons, protons, deuterons, alphas and photons, one addresses a broad range of applications, from nuclear power reactors and shielding design through cyclotron production of medical radioisotopes and radiotherapy to transmutation of nuclear waste. In all these and many other applications one needs a detailed knowledge of cross sections, spectra of emitted particles and their angular distributions and of isotope production.

A long-standing problem — how to meet nuclear data needs of the future with limited experimental resources — puts a considerable demand upon nuclear model computation capabilities. Originally almost all nuclear data was provided by measurement programs. Over time, theoretical understanding of nuclear phenomena has reached a considerable degree of reliability, and nuclear modeling has become an important source of evaluated nuclear data (with measurements remaining critical for data testing and benchmarking).

The practical use of nuclear model codes requires a considerable numerical input that describes properties of the nuclei and interactions involved. Leading nuclear data laboratories and experts have used a variety of different input sets, often developed over years in their own laboratories. Many of these partial input databases were poorly documented, or not documented at all, and not always available for other users. With the trend of reduced funds for nuclear data evaluations, there is a real threat that the accumulated immense knowledge on input parameters and the related state-of-the-art may be reduced or even lost for the future applications.

Given this situation, a project was proposed, with the aim to develop an internationally recognized input parameter library, with contributions from all major players around the world. The idea was discussed in the nuclear data community in the beginning of 1990s and it was enthusiastically supported by the International Nuclear Data Committee as a top priority nuclear data project.

An ultimate objective of any international effort along these lines is to develop a library of evaluated and tested nuclear-model input parameters. Considering that such a task indeed is immense, the IAEA decided to proceed in two major steps. First, to summarize the present knowledge on input parameters, and whenever possible to critically analyze these parameters and to develop a single Starter File of input model parameters. This data base will be of immediate practical value for a number of users and should represent a firm basis for any future improvements and developments. The second step will focus on the testing, validation and related improvement of the Starter File.

With these objective in mind the IAEA initiated a Co-ordinated Research Project (CRP) under the title "*Development of Reference Input Parameter Library for Nuclear Model Calculations of Nuclear Data (Phase I: Starter File)*". The project, co-ordinated by the IAEA between 1994 and 1997, produced two major results. First, the complete electronic Starter File was developed and made available to users cost-free throughout the world. Second, the present Handbook was prepared, containing a detailed description of the library.

The Reference Input Parameter Library (Starter File) contains input parameters for theoretical calculations of nuclear reaction cross sections. The library is targeted at users of nuclear reaction codes interested in low-energy nuclear applications. Incident and outgoing particles include n, p, d, t, ^{3}He, ^{4}He and γ, with the energies up to about 100 MeV.

The Starter File contains numerical data arranged in seven segments/directories:

No	Directory	Contents
1	MASSES	Atomic Masses and Deformations
2	LEVELS	Discrete Level Schemes
3	RESONANCES	Average Neutron Resonance Parameters
4	OPTICAL	Optical Model Parameters
5	DENSITIES	Level Densities (Total, Fission, Partial)
6	GAMMA	Gamma-Ray Strength Functions
7	ANGULAR	Continuum Angular Distributions

Each segment/directory is split into two subdirectories:

- RECOMMENDED (for recommended input parameters), and
- OTHER_FILES (for alternative input parameters and other useful data).

The Starter File, physically located at the DEC Alpha server operated by the IAEA Nuclear Data Section, can be conveniently accessed using the Web interface or by using FTP. The address of the Web site reads http://www-nds.iaea.or.at/ripl/

while for FTP one should use ftp iaeand.iaea.or.at
username: ripl

with no password required. In addition, complete Starter File on a CD-ROM is available from the IAEA Nuclear Data Section cost-free upon request.

The IAEA wishes to thank all the participants of the CRP, and also other scientists associated with the project, for their diligent work that lead to the creation of the Reference Input Parameter Library. The assistance of M.B. Chadwick, T. Fukahori, A.V. Ignatyuk, S. Kailas, J. Kopecky, G. Molnár, G. Reffo, Z. Su, M. Uhl and P.G. Young, and also of O. Bersillon, E. Běták, R. Capote Noy and V.M. Maslov in the preparation of this publication is gratefully acknowledged. The responsible IAEA staff member for this report was P. Obložinský, Division of Physical and Chemical Sciences.

EDITORIAL NOTE

CONTENTS

INTRODUCTION

An important trend in the evaluation of neutron and charged-particle nuclear data at low energies (0-30 MeV) is the increased use of nuclear reaction theory codes to compute the cross sections, spectra, and angular distributions required by a large variety of applications. As a method of evaluation, such model codes offer, in comparison with simpler approaches, many advantages such as the preservation of the energy balance or the coherence of partial cross sections with the total or the reaction cross section, which are essential properties for nuclear data used in transport calculations. In addition, the theoretical approach is the only one that allows to predict data for unstable nuclei.

For any nuclear reaction calculation nuclear masses are very basic data for getting binding energies or Q-values. They are presented in **Chapter 1** together with other useful information such as ground state deformations.

Discrete level schemes, including spins, parities, γ-transitions and branching are important for establishing of low-energy nuclear level densities and for related cross section calculations. Most of the corresponding experimental information are contained in the ENSDF library and **Chapter 2** describes the procedures used to retrieve the needed data.

As is well known, the neutron cross sections at low incident energies present a resonant behaviour, and a careful statistical analysis of the experimental results leads to the average neutron resonance parameters, as described in **Chapter 3**. These average quantities are not directly used in the model calculations but are important data for constraining the parameters of different models:

- the average spacing of resonances is the only measure of the level density near the neutron binding energy,
- the neutron strength functions have to be reproduced by the optical model at low energy, and
- the average radiative width is used as a normalization for the gamma-ray strength functions.

Above the resonance energy region, the nuclear reaction models only reproduce the smooth behavior of the cross sections, and the evaluation of nuclear data is generally divided into two major steps.

By using the optical model in the first step, the elastic channel and the direct inelastic ones for deformed nuclei are explicitly calculated whereas all other channels are lumped together in the reaction cross section. **Chapter 4** gives an extensive compilation optical model parameter sets for different types of incident particles, from neutron to ^{4}He. In order to produce a consistent evaluation, it is recommended to use, for each interacting system, a unique parameterization which reproduces the relevant observables (total or reaction cross sections, elastic angular distributions, analysing powers) over an energy range as broad as possible, including, in the case of neutron interaction, the low energy region where the calculated neutron strength function and scattering radius should match the experimental values. Furthermore, the parameters should have a smooth energy dependence.

The second step consists in sharing the reaction cross section among all the possible individual channels, as illustrated by Figure 0.1. For incident energies lower than around 10 MeV, this is done by using the statistical decay of the compound nucleus, a formalism often referred to as the Hauser-Feshbach theory. Written in a compact form, the Hauser-Feshbach formula giving

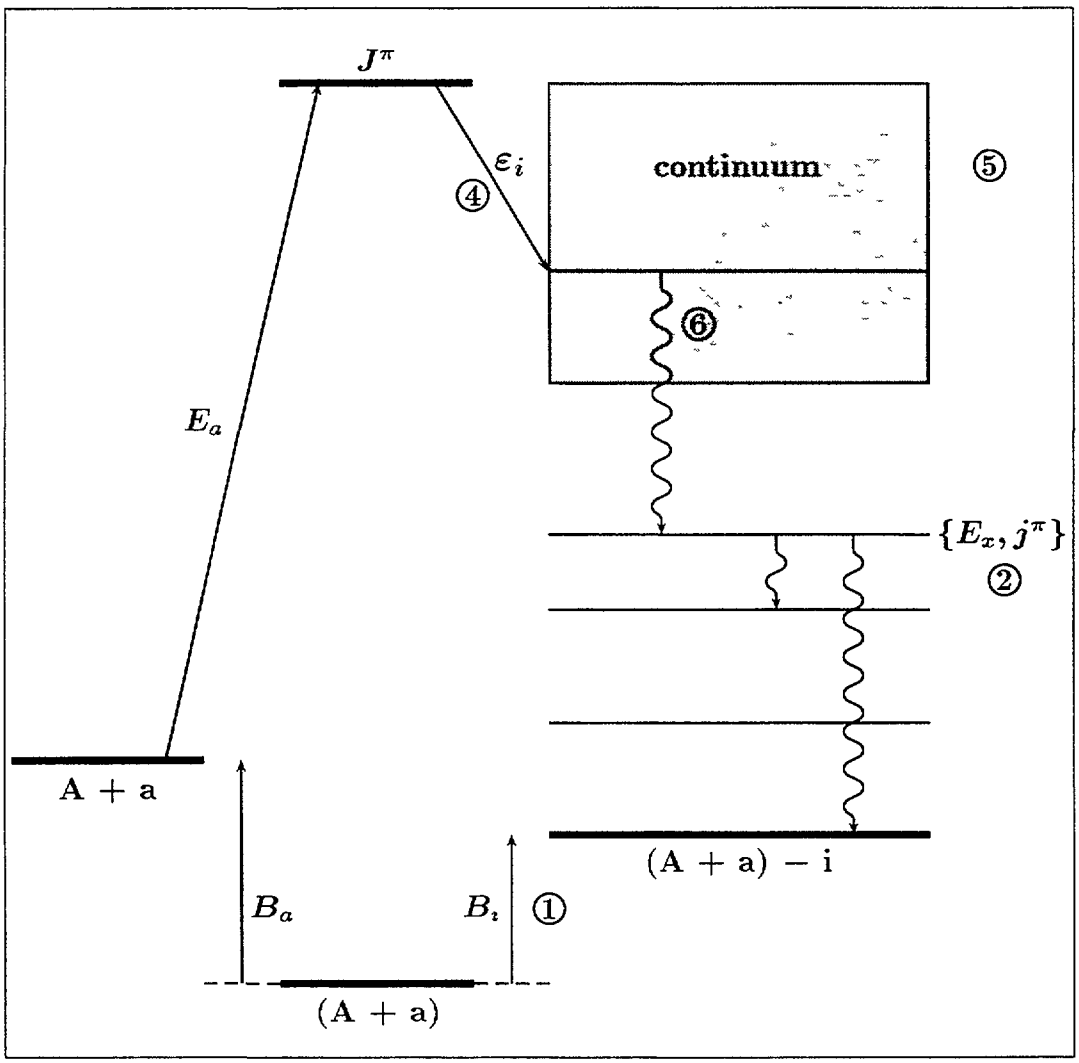

Figure 0.1: Schematic energy diagram of a nuclear reaction. Circled numbers refer to chapters where the parameters are described.

the cross section for the A(a,b)B reaction reads

$$\sigma_{a\to b} = \sum_{J^\pi} \frac{T_a\, T_b}{\sum_i \sum_c T_{ic}}$$

where the index i stands for the different types of outgoing particles[1] (or the fission channel, if any), and the T's are the transmission coefficients calculated by the optical model for this particle. The index c represents all the accessible final states which are either discrete excited levels of the residual nucleus or a continuum of levels described by a level density.

In the case of discrete levels one should only take into account the low-lying levels of known excitation energy, spin, parity, and decay branchings (if γ-production is needed).

Above the energy of the last level for which one of the previous quantities is missing or uncertain, one has to consider a continuum of levels described by a total level density which, at low excitation energy, must match the cumulative number of discrete levels, and, at the neutron binding energy, must reproduce the average spacing of resonances. **Chapter 5.1** presents different theoretical approaches of this longstanding problem.

[1] Generally, the considered outgoing particles are p, n, d, t, ^{3}He, α, and γ

The fission cross section calculation strongly depend on two key ingredients:

- the fission level density (the level density of the fissioning nucleus at the saddle point deformation), and
- the fission barrier.

These two strongly interdependent parameters are described in **Chapter 5.2.**

For incident energies higher than about 10 MeV, the pre-equilibrium reaction mechanism constitutes the bridge between fast, direct processes and slow compound processes and provides an explanation for the high-energy tails in spectra and the smoothly forward peaked angular distributions. Methods for calculating partial (or particle-hole) level densities for use in pre-equilibrium model calculations are given in **Chapter 5.3.**

Gamma-ray emission channel is an almost universal reaction channel since gamma rays, in general, accompany the emission of any other emitted particle. Here, the basic quantity is the gamma-ray strength function which is discussed in **Chapter 6.**

Besides sophisticated quantum-mechanical models of pre-equilibrium reactions such as the one by Feshbach, Kerman and Koonin, the Kalbach systematics formula to describe the continuum angular distributions of emitted particles represents for most applications an invaluable tool due to its wide-ranging applicability; it is described in **Chapter 7.**

Finally, it should be reminded that many of the parameters needed in the calculations are model dependent and should therefore be used within the strict frame of their definitions.

All the parameters reported in this Handbook can already be used but some of them still need improvements, in particular the optical model part in the light of new developments, and the total level densities which have to reproduce in a consistent way different pieces of information.

The main **Chapters** are followed by three **Appendices. Appendix I** brings the basic information on the **recommended files**, which are printed using **bold** font throughout this Handbook as well as on *other* RIPL files (their names are given in *italics*), the directory structure and the file access.

Appendices II and **III** summarize experiences with use of the optical model and its parameters at Los Alamos, where systematics study of this topic has been performed over years.

1 Atomic Masses and Deformations

Coordinator: M.B. Chadwick

Summary

This chapter discusses recommendations for nuclear masses, binding energies and ground-state deformations, for use in nuclear reaction model calculations. We recommend that the Möller *et al.* file **moller.dat** with data for nearly 9000 nuclides be used for these quantities. The whole region of masses is covered by **audi_95.dat**, which brings recommended masses for nearly 3000 nuclides based on experimental values. As a general rule, where experimental values exists, they should be used for calculations.

1.1 Calculated Masses and Deformations

1.1.1 Introduction

The file **moller.dat** contains tabulations of the atomic mass excesses and nuclear ground-state deformations of 8979 nuclei ranging from ^{16}O to $A = 339$. The calculations are based on the finite-range droplet macroscopic model and the folded-Yukawa single-particle microscopic model. Relative to the Möller *et. al.* 1981 mass table the current results are obtained with an improved macroscopic model, an improved pairing model with a new form for the effective-interaction pairing gap, and minimization of the ground-state energy with respect to additional shape degrees of freedom. The values of only nine constants are determined directly from a least-squares adjustment to the ground-state masses of 1654 nuclei ranging from ^{16}O to [$Z = 106$, $A = 263$] and to 28 fission-barrier heights. The error of the mass model is 0.669 MeV for the entire region of nuclei considered, but is only 0.448 MeV for the region N greater than or equal to 65.

Within the Möller *et al.* table, results are given for ground-state deformations within two different nuclear shape parameterizations: the "ϵ parameterization" (Nilsson perturbed-spheroid parameterization); and the "β parameterization" (a spherical harmonic expansion). Möller *et al.* discuss the relation between these two parameterizations in Ref. [1.1], and note that their ϵ tabulations completely specify the nuclear shape, but the β tabulations do not since β_5 is not tabulated. For this reason, use of the "ϵ parameterization" is preferred.

The Möller *et al.* table also shows calculated ground-state microscopic energies (shell-corrections [2]), and calculated ground-state atomic mass excesses, for two different models. the finite-range liquid drop model (FRLDM); and the finite-range droplet model (FRDM). As discussed in Ref. [1.1], the more recent FRDM is preferred.

Figures 1.1 and 1.2 show the microscopic energy (shell-correction energy) and the ground state quadrupole deformation, from Möller *et al.*'s work [1.1].

[2] As discussed in Ref [1 1], the microscopic energy includes the shell plus pairing correction, but it also includes the difference in macroscopic energy between the deformed and spherical nucleus It is therefore defined to represent all additional effects over and above the *spherical* macroscopic energy

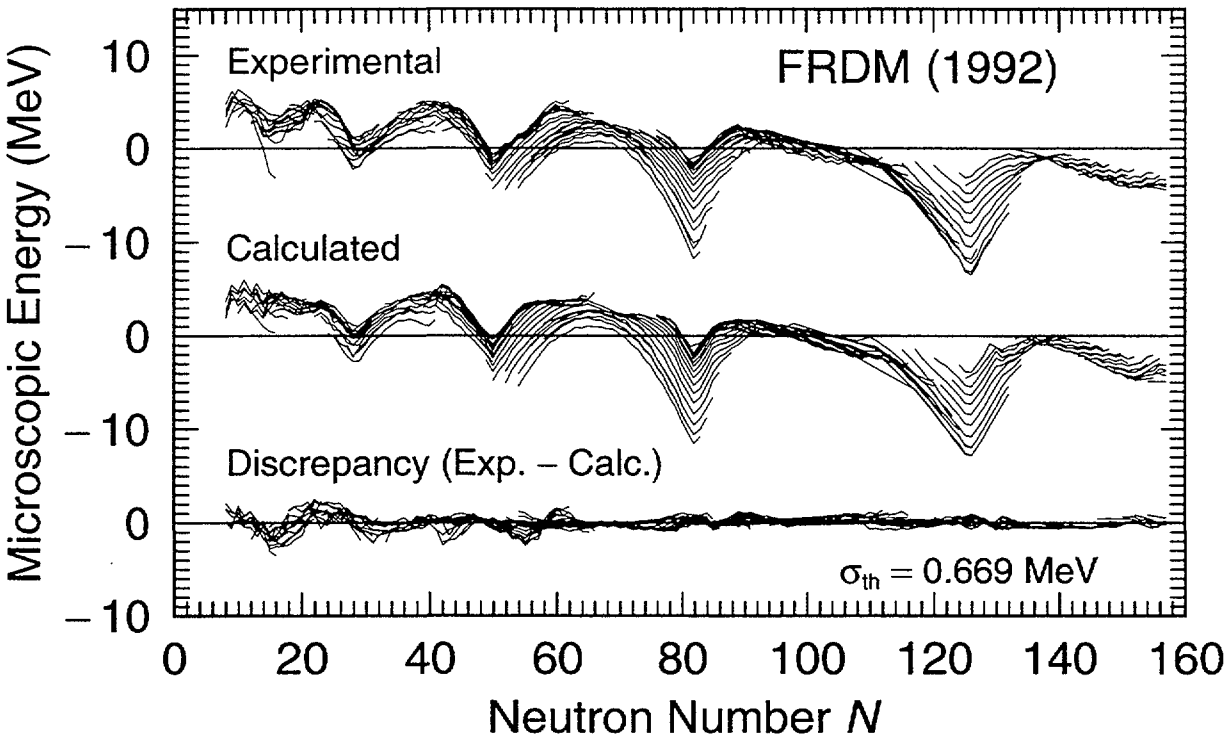

Figure 1.1: Comparison of experimental and calculated microscopic energies $E_{\rm mic}$ for 1654 nuclei, for Möller *et al.*'s FRDM model. The lines are drawn through isotopic chains. (Taken from Fig. 1 of Ref. [1.1]).

1.1.2 Format

EXPLANATION OF TABLE VARIABLES:

Z proton number. The mass table is ordered by increasing proton number. The corresponding chemical symbol of each named element is given in parentheses.

N neutron number.

A mass number.

ϵ_2 calculated ground-state quadrupole deformation in the Nilsson perturbed-spheroid parameterization.

ϵ_3 calculated ground-state octopole deformation in the Nilsson perturbed-spheroid parameterization.

ϵ_4 calculated ground-state hexadecapole deformation in the Nilsson perturbed-spheroid parameterization.

ϵ_6 calculated ground-state hexacontatetrapole deformation in the Nilsson perturbed-spheroid parameterization.

$\epsilon_6^{\rm sym}$ calculated ground-state hexacontatetrapole deformation in the Nilsson perturbed-spheroid parameterization for ϵ_3 =0.

β_2 calculated quadrupole deformation of the nuclear ground-state expressed in the spherical-harmonics expansion defined by Eq. (37) in Ref. [1.1].

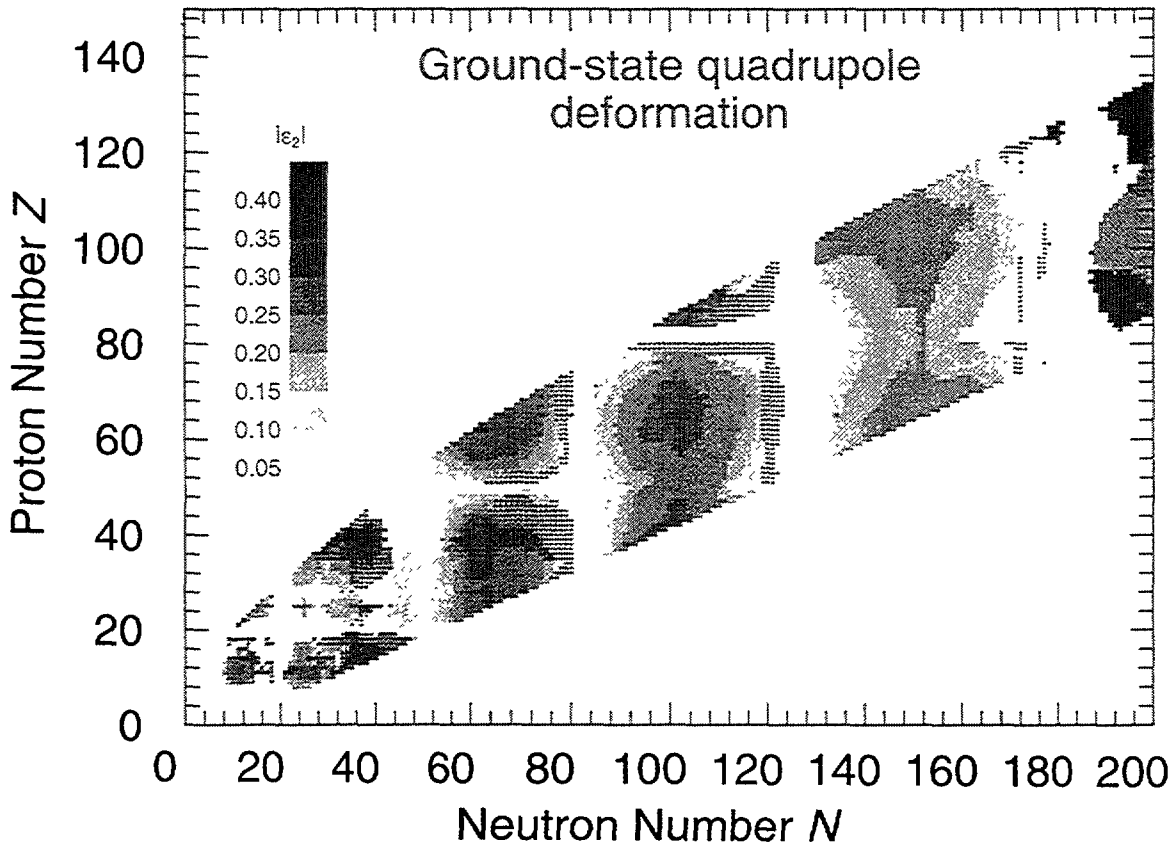

Figure 1.2: Calculated ground-state deformation values $|\epsilon_2|$ for 7969 nuclei using Möller *et al.*'s FRDM model. This figure is a grey-scale version of the color Fig. 9 in Ref. [1.1].

β_3 calculated octopole deformation of the nuclear ground-state expressed in the spherical-harmonics expansion defined by Eq. (37) in Ref. [1.1].

β_4 calculated hexadecapole deformation of the nuclear ground-state expressed in the spherical-harmonics expansion defined by Eq. (37) in Ref. [1.1].

β_6 calculated hexacontatetrapole deformation of the nuclear ground-state expressed in the spherical-harmonics expansion defined by Eq. (37) in Ref. [1.1].

E_{mic} calculated ground-state microscopic energy, given by the difference between the calculated ground-state atomic mass excess and the spherical macroscopic energy calculated from Eq. (40), in the preferred Möller *et al.* model, the FRDM (see Ref. [1.1]). Since this microscopic energy represents the difference compared to the spherical energy, and not the macroscopic energy at equilibrium nuclear deformation, it should not be used for the shell corrections needed in the level density formulation, described in Chapter 5.

M_{th} calculated ground-state atomic mass excess, in the preferred Möller *et al.* model, the FRDM.

M_{exp} experimental ground-state atomic mass excess in the 1989 midstream evaluation of Audi with 4 revisions [1.2].

σ_{exp} experimental error associated with the ground-state atomic mass excess in the 1989 midstream evaluation of Audi with 4 revisions [1.2].

$E_{\rm mic}^{\rm FL}$ calculated ground-state microscopic energy, given by the difference between the calculated ground-state atomic mass excess and the spherical macroscopic energy calculated from Eq. (62) of Ref. [1.1], in the FRLDM model [1.1]. Since this microscopic energy represents the difference compared to the spherical energy, and not the macroscopic energy at equilibrium nuclear deformation, it should not be used for the shell corrections needed in the level density formulation, described in Chapter 5.

$M_{\rm mic}^{\rm FL}$ calculated ground-state atomic mass excess, in the FRLDM model [1.1].

1.2 Experimental Masses

File **audi_95.dat** brings recent compilation of masses, binding energies, β-decay energies (not needed within RIPL) and atomic masses for 2931 nuclides ranging from the neutron and the proton up to $A = 273$ [1.3]. The values given there are not purely experimental data, but recommended values based on the experimental ones. These values are very close to the experimental values of Möller *et al.* [1.1]; the differences can be neglected for most nuclear reaction calculation applications.

The file contains just the energies mentioned above together of the error or uncertainity derived from the adjusted masses and the correlation matrix. Nuclei denoted by # in the file give values and error estimated from systematic trends. The file is organized using 124 character long lines, what may cause some inconvenience to a not sufficiently careful user at 80-columns wide display and/or narrow printout.

1.3 Other Files

For completeness, we also include two other electronic files: *beijing.dat* and *jaeri_deform.dat*, these are described below.

The *beijing.dat* file contains a compilation of experimental masses, calculated masses by Möller *et al.*, as well as ground state spins and parities, and abundances and half-lives.

The *jaeri_deform.dat* is a compilation of deformation parameters of excited states for calculating DWBA direct reactions involving the excitation of various multipolarities, from the Japan Atomic Energy Research Institute.

1.4 Conclusions and Recommendations

The files to be used for obtaining nuclear masses, binding energies, Q-values and ground-state deformations are **moller.dat**, which brings all quantities quoted above for nearly 9000 nuclei, and **audi_95.dat**, restricted to recommended masses based on experimental values. Where experimental values exists, they should be used.

When Q-values are calculated, it is necessary to make use of the masses of a number of different nuclei. We note the importance of using the same source of information for all masses in such calculations. This is particularly important for nuclei far from stability, where experimental masses may only exist for certain of the nuclides involved. In such cases, one should make use of calculated masses for all the nuclei involved in the reaction, for consistency purposes.

REFERENCES

[1.1] P. Möller, J.R. Nix, W.D. Myers and W.J. Swiatecki, Atomic Data Nucl. Data Tbl. **59**, 185 (1995). This publication can also be accessed at the WWW address: http://t2.lanl.gov/publications/publications.html.

[1.2] G. Audi, Midstream Atomic Mass Evaluation, private communication to P. Möller (1989), with 4 revisions.

[1.3] G. Audi and A.H. Wapstra, Nuclear Physics **A595**, 409 (1995). RIPL file **audi_95.dat** is the original file 'mass_rmd.mas95' of Audi and Wapstra. The other files of these authors do not enter RIPL.

2 Discrete Level Schemes

Coordinator: G.L. Molnár

Summary

An entirely new discrete levels segment has been created by the Budapest group according to the recommended principles, using the Evaluated Nuclear Structure Data File, ENSDF as a source. The resulting segment contains 96,834 levels and 105,423 gamma rays for 2,585 nuclei, with their characteristics such as energy, spin, parity, half-life as well as gamma-ray energy and branching percentage. Isomer flags for half-lives longer than 1 s have been introduced. For those 1,277 nuclei having at least ten known levels the cutoff level numbers N_m have been determined from fits to the cumulative number of levels. The level numbers N_c associated with the cutoff energies U_c, corresponding to the upper energy limit of levels with unique spin and parity, have been included for each nuclide. The segment has the form of an ASCII file which follows the extended ENEA Bologna convention.

For the RIPL Starter File the new Budapest file is recommended as a Discrete Level Schemes Segment because it is most complete, up-to-date, and also well documented. Moreover, the cutoff energies have been determined in a consistent way, giving also hints about basic level density parameters. The recommended files are **budapest_levels.dat** and **budapest_cumulative.dat**.

As alternative choices, the libraries from Beijing, Bologna, JAERI, Obninsk and Livermore may also be used for special applications.

2.1 Introduction

Nuclear reaction model calculations require the knowledge of complete discrete nuclear level schemes, in order to specify all possible outgoing reaction channels. This knowledge is also important for the test of total level density models, which necessarily replace the discrete schemes at higher excitation energies, approaching the continuum regime. The term "completeness" means here that for a given nucleus all discrete levels are observed in a specified energy and spin window, and they are all characterized by unique energy, spin and parity values. The knowledge of particle and gamma-ray decay branchings is also required in addition, especially when isomeric states are populated by gamma-ray cascades.

Complete level schemes can be obtained only from complete spectroscopy using nonselective reactions. Statistical reactions, e. g. the $(n, n'\gamma)$ reaction and averaged resonance capture, are especially suitable from the viewpoints of nonselectivity of the excitation mechanism and completeness of information obtained with the rich arsenal of gamma-ray spectroscopy [2.1]. For practical reasons the vast majority of nuclei cannot be studied by such means, hence the degree of knowledge of the experimentally determined discrete level schemes varies widely throughout the nuclear chart. While this knowledge is incorporated in the Evaluated Nuclear Structure Data File, ENSDF [2.2], it has to be extracted and put in a format appropriate for practical applications.

In the course of the Co-ordinated Research Project *RIPL* a Discrete Level Schemes Segment, DLSS, had to be prepared for the RIPL Starter File, according to the following principles [2.3, 2.4]:

- A single recommended DLSS file has to be created on the basis of the Evaluated Nuclear Structure Data File, ENSDF, as the primary source of input data.
- The starter file should keep the format of the ENEA Bologna discrete levels file, LIVELLI [2.5], with some extensions to incorporate additional information.
- Separate cutoff energies must be defined for each nucleus to indicate the limits of completeness of level scheme with regard to levels as well as level spins and parities, respectively.
- The starter file should be compared with other existing files not used for creating it.

2.2 Budapest Discrete Levels File

A new discrete levels file has been created by the Budapest group according to the recommended principles. The ENSDF data set "Adopted levels and gammas", as of 23 February 1996 [2.2], has been used as data source. The major steps are outlined below.

- The adopted discrete nuclear levels and gamma-ray transitions have been retrieved on line, using the program NUDAT [2.6].
- The retrieved ENSDF data have been filtered for errors and converted into a file in the extended Bologna format, as described in detail below.
- The cutoff energy, U_{max}, and the cumulative number, N_{max}, of levels up to this energy have been determined from exponential fits to the staircase plots for those nuclei for which at least 10 levels were known [2.7] and have been included in the file as a cutoff value up to which the discrete level scheme is complete.
- A second energy cutoff, U_c, corresponding to the upper energy limit of levels characterized by an unique spin and parity has been determined for all nuclei on the basis of ENSDF data alone.

2.2.1 Retrieval of ENSDF Data

Filtering of adopted level and gamma data sets

The data on discrete levels and gamma-ray transitions were retrieved from the Online Nuclear Data Service at IAEA, with the help of NUDAT [2.6]. Adopted levels and gamma rays had to be retrieved separately, since attempts to retrieve adopted levels and gammas together had failed. Inspection of the retrieved files "Adopted Levels" and "Adopted Gammas" revealed a number of syntax errors.

After performing the syntactical tests the data have been loaded into a Borland PARADOX database, running on IBM-PC. The resulting *relational database of discrete levels and gammas*, consisting of the files 'ensdflev.db' and 'ensdfgam.db' [2.8], contains the mass and charge of each nuclide, the initial level energies with uncertainties, the gamma transition energies and relative intensities with their uncertainties, level half-lives, spins and parities, as well as the date of evaluation. ENSDF notations for ambiguous spins and parities had to be tokenized and level half-lives be converted to seconds, in order to facilitate further database operations.

The original ENSDF file (update as of 23 February 1996) contains 106,234 adopted levels for 2,807 nuclei within the range $A = 1 - 266$, $Z = 0 - 109$. There are 148,129 adopted gamma transitions in 1,592 nuclei with $A = 5 - 266$ and $Z = 3 - 103$. More details can be found in the database files 'l_zstat.db' and 'l_astat.db' for levels and in 'g_zstat.db' and 'g_astat.db' for gamma rays. The ASCII table versions of these database files are available on request [2.8].

Each discrete level has to be unique and has to be unambiguously placed in the level scheme. Hence only nuclides with a firmly established ground state can be kept. Duplicated ground states (isomers or band heads with unknown energy, e.g. 0 + X) as well as duplicated excited states - altogether 9,400 levels - had to be eliminated, leaving us with 96,834 levels in 2,585 nuclides.

The number of gamma rays has also been reduced by 13,650 due to the deletion of 9,214 level duplicates, decaying by gamma rays. Furthermore, 57 duplicated gamma rays were found which had to be deleted as well. Finally, another 11,425 gammas had to be deleted because they fell in at least one of the following classes:

- the energy of the initial level is zero or unknown - 744 cases
- the gamma-ray energy is zero - 13 cases
- the gamma-ray intensity is missing or zero - 11,242 cases

Eventually, 122,997 gamma rays have been kept in 1,354 nuclides.

Placement of gammas and calculation of branchings

The gamma-ray branching percentages can be calculated from the intensities of gamma rays de-exciting the given level. Unfortunately, for each gamma ray only the initial levels are usually specified in the ENSDF file, the final levels have not been encoded. Hence each gamma ray had to be placed anew in the level scheme.

For this purpose the energies of final levels were computed for all gamma transitions assigned to a given initial level, and the resulting energy values were identified with adopted level energies. This procedure was preceded by a correction for recoil shift of the transition energy, calculated as $\Delta E_\gamma = E_\gamma^2/(2 \cdot A \cdot 931.494 \text{ MeV})$. The correction exceeds 0.1 keV for 12,842 gamma rays, mainly belonging to light nuclides. The criterion for a proper assignment was that the difference between computed and adopted level energies had to be less than three standard deviations, where the latter were computed from the given uncertainties added in square.

Unfortunately, no energy uncertainties have been specified in ENSDF for 10,688 levels and 19,734 gammas, respectively. In these cases average uncertainty values, calculated for each individual nuclide, have been used. Whenever this average value exceeded the interval of 0.15 keV to 5 keV, the closest limiting value has been adopted instead. The distribution of generated uncertainties is given in Table 2.1 both for the levels and gamma rays, respectively.

Only for those gamma transitions which could be placed firmly could the branching percentages be computed, while gamma rays without placement or intensity value had to be omitted. Within the 3σ combined uncertainty 1,466 gammas could not be placed. On the other hand, 13,164 gammas matched more than one final level, and 11 gammas were duplicate placements (i.e. connect the same levels). Another 11 gammas were just marked as weak. After eliminating

Table 2.1: Distribution of levels according to energy uncertainty bins.

ΔE_{level} (keV)	Number of cases
5.00	540
≥ 4.00	156
≥ 3.00	248
≥ 2.00	346
≥ 1.00	1,236
> 0.15	4,460
0.15	3,702
Total	10,688

Distribution of γ-rays according to energy uncertainty bins.

ΔE_{γ} (keV)	Number of cases
5.00	79
≥ 4.00	0
≥ 3.00	0
≥ 2.00	2
≥ 1.00	69
> 0.15	551
0.15	19,033
Total	19,734

those falling in at least one of the enlisted categories there remained 108,345 uniquely placed gamma rays, for which the branching percentages have been determined.

2.2.2 Determination of Cutoff Energies

Determination of the cutoff energy up to which the discrete level scheme can be considered complete is a difficult task for which no universal recipes have been available. Therefore, a reliable automatic procedure had to be found.

Histograms of the cumulative number of levels against excitation energy (staircase plots) have been created first, using the database described above. At least 10 known levels have been required, including the ground state. This constraint has left us with 1422 nuclei. For 145 nuclei out of this selection ENSDF contains more than one zero-energy level, rendering the level scheme ambiguous. Hence those 145 nuclei also had to be excluded from the procedure which has been carried out for the remaining 1277 nuclei, from ^{6}Li to ^{251}Es.

The cutoff energies U_{max} and the corresponding *cumulative numbers of levels* N_m have been determined by fitting the histograms with the constant-temperature exponential formula:

$$N(E) = \exp((E - U_0)/T) \ , \tag{2.1}$$

where T is the nuclear temperature, and U_0 is the backshift energy. The excitation energy, E, has been used as a weighting factor in order to minimize the influence of $N(E)$ values at the high-energy end where our knowledge becomes incomplete.

Based on the fits T, U_0 and U_{max} have been determined for all 1277 nuclei considered. The whole procedure is described in detail elsewhere [2.7]. Here we only note that the level number

associated with the minimal value of χ^2 determines in turn the cutoff energy, U_{max}, above which the level density starts deviating from the expected exponential law. The results have been presented in the form of tables and plots which may also be found in a separate publication [2.7]. Only a short description of those is given here, with some illustrative examples.

Fig. 2.1 is an example of the histograms of the cumulative number of levels, $N(E)$, created for the 1277 nuclei considered. In the plots the continuous line always represents the accepted level density fit as explained above. The diamond symbol marks the cutoff energy, U_{max}, and the associated cumulative level number, N_{max}, corresponding to that local minimum of χ^2 which is characterized by the maximal slope of $\ln(N(E))$. The other cutoff energy, U_c, is determined by the energy of the highest level up to (and including) which both the spin and parity are unambiguously established, while N_c is the corresponding level number. The numerical values of U_{max} and U_c are also indicated in the plots. The whole set of plots is included in Ref. [2.7].

Table 2.2: Excerpt from the file **budapest_cumulative.dat**. Notations: * means $U_{max} > S_n$ or S_p, # marks cases where the accepted local minimum is different from the absolute minimum.

						Accepted local minimum				Absolute minimum			
A	Z	n	Nc	Nmax	Uc (MeV)	Umax (MeV)	U0 (MeV)	T (MeV)	Chi^2	Umax (MeV)	U0 (MeV)	T (MeV)	Chi^2
6	3	13	12	13	26.600	31.000*	-25.167	21.027	0.026	31.000	-25.167	21.027	0.026
8	3	11	4	10	3.210	9.000*	-4.007	5.527	0.005	9.000	-4.007	5.527	0.005
8	4	26	15	22	20.900	24.000*	7.010	5.350	0.028	24.000	7.010	5.350	0.028
9	4	31	5	29	3.049	22.400*	-10.644	9.623	0.010	22.400	-10.644	9.623	0.010
9	5	18	1	15	0.000	17.076*	-10.841	10.621	0.014	15.290	-11.590	11.155	0.014#
10	4	16	8	11	7.542	10.570*	-0.328	4.252	0.046	10.570	-0.328	4.252	0.046
10	5	38	12	25	6.127	8.894*	-2.041	3.370	0.009	8.894	-2.041	3.370	0.009
11	4	15	2	12	0.320	7.030*	-2.706	3.842	0.009	7.030	-2.706	3.842	0.009
11	5	41	8	23	7.978	12.000*	0.182	3.740	0.003	12.000	0.182	3.740	0.003
11	6	36	13	17	9.200	10.083*	0.313	3.481	0.003	10.083	0.313	3.481	0.003
12	5	50	16	11	7.060	5.000*	-1.091	2.514	0.004	5.000	-1.091	2.514	0.004
12	6	56	4	10	9.641	13.352	2.987	4.413	0.006	13.352	2.987	4.413	0.006
12	7	19	5	10	2.439	5.600*	-3.009	3.558	0.012	5.600	-3.009	3.558	0.012
13	5	23	1	11	0.000	5.557*	1.075	1.861	0.017	5.557	1.075	1.861	0.017
13	6	73	5	33	6.864	14.582*	-1.484	4.509	0.008	14.582	-1.484	4.509	0.008
13	7	54	12	24	9.476	12.937*	-2.132	4.715	0.007	12.937	-2.132	4.715	0.007
14	6	46	11	23	10.425	12.963*	1.180	3.686	0.019	12.963	1.180	3.686	0.019
14	7	120	23	10	9.703	7.029	1.399	2.358	0.005	7.029	1.399	2.358	0.005
14	8	18	5	15	6.590	13.010*	-1.141	5.016	0.022	13.010	-1.141	5.016	0.022
15	6	31	6	21	4.780	8.110*	0.663	2.410	0.010	6.417	0.017	2.852	0.006#
15	7	113	22	36	10.804	12.551*	2.197	2.867	0.003	12.551	2.197	2.867	0.003
15	8	85	12	39	8.922	12.471*	2.024	2.811	0.003	12.471	2.024	2.811	0.003
...													

The parameters obtained from the fits to the cumulative level numbers for 1277 nuclei have been tabulated in the form shown in Table 2.2. For increasing mass and charge numbers we have printed the results of the least-square fits for the accepted and absolute minima and other relevant quantities in one line. A and Z are mass and charge numbers, respectively, n is the total number of levels, N_c is the cumulative level number at cutoff energy U_c for completeness with respect to spin/parity and the rest comes from the fits. In 111 out of the 1277 fits the U_{max} value has been found to be larger than the lowest of the two single-nucleon separation energies S_n, S_p [2.9]. In other words, these fits include unbound states as well. In Table 2.2 the corresponding U_{max} values have been marked with an asterisk. The whole table is available in the form of an ASCII text file called **budapest_cumulative.dat** as part of the DLS Segment. A printed version is included in a separate report [2.7].

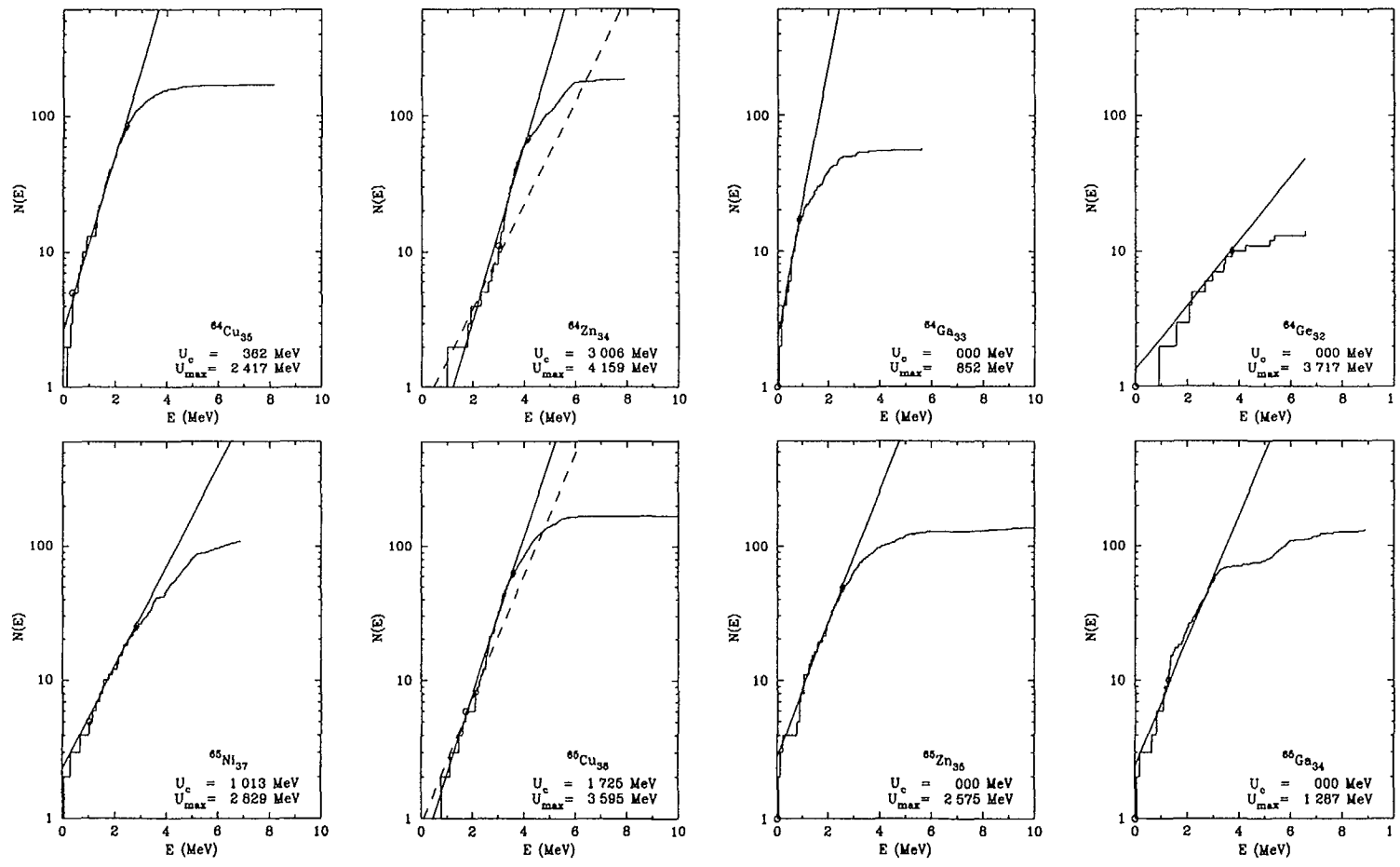

Figure 2.1: Sample histogram plots of cumulative number of levels versus excitation energy.

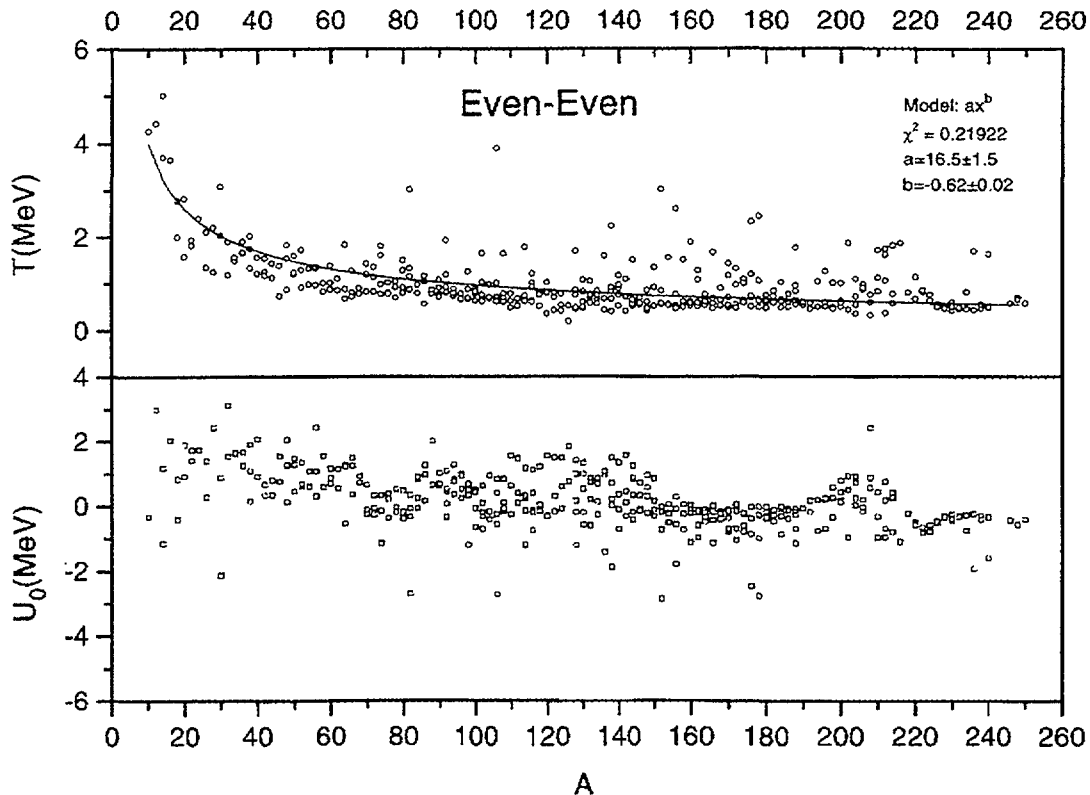

Figure 2.2: Nuclear temperature T and shift energy U_0 versus mass number for even-even nuclei.

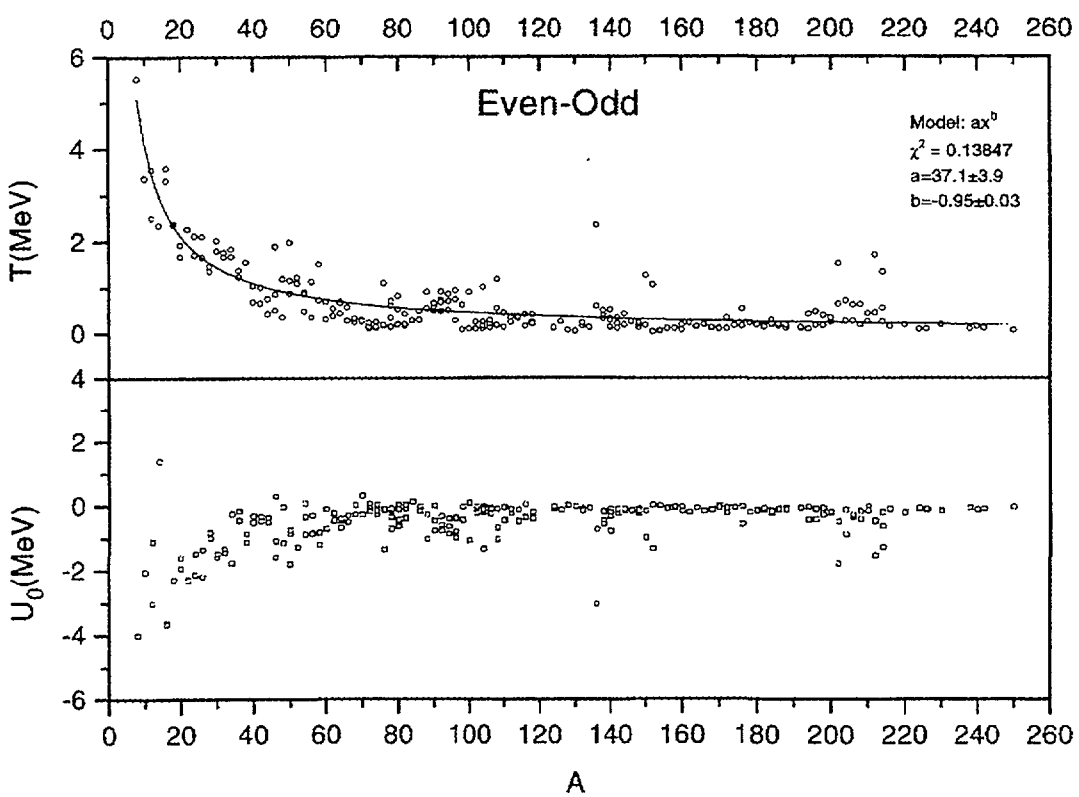

Figure 2.3: Nuclear temperature T and shift energy U_0 versus mass number for even-odd nuclei.

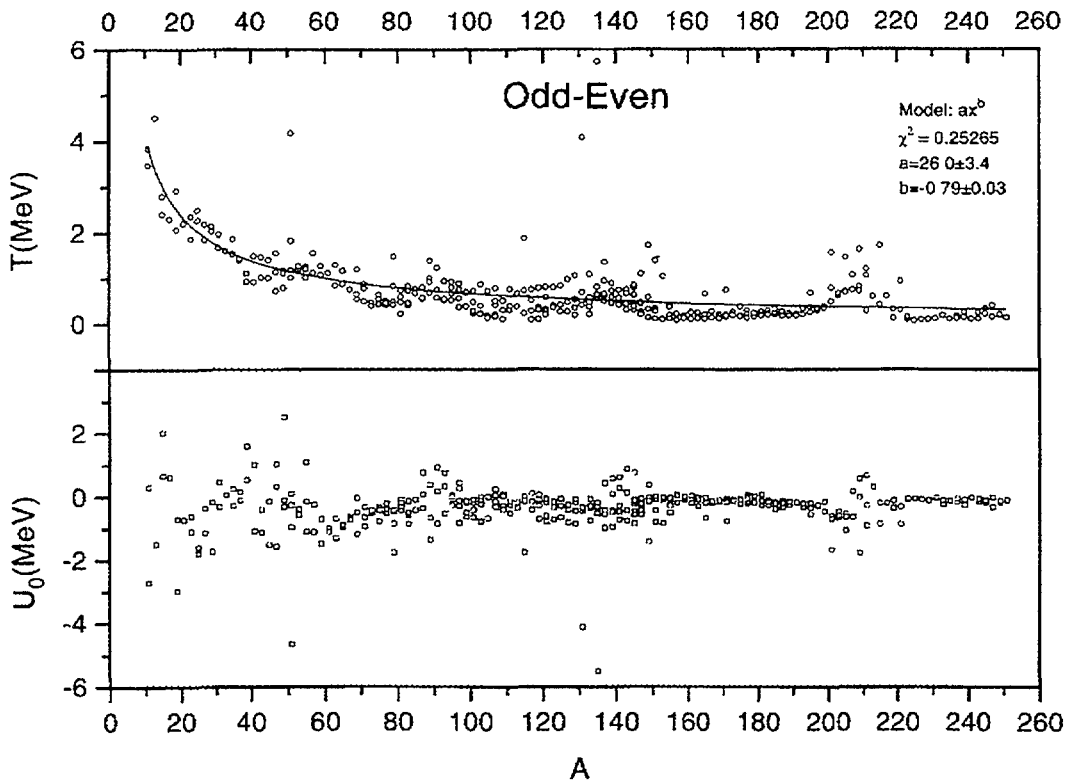

Figure 2.4: Nuclear temperature T and shift energy U_0 versus mass number for odd-even nuclei.

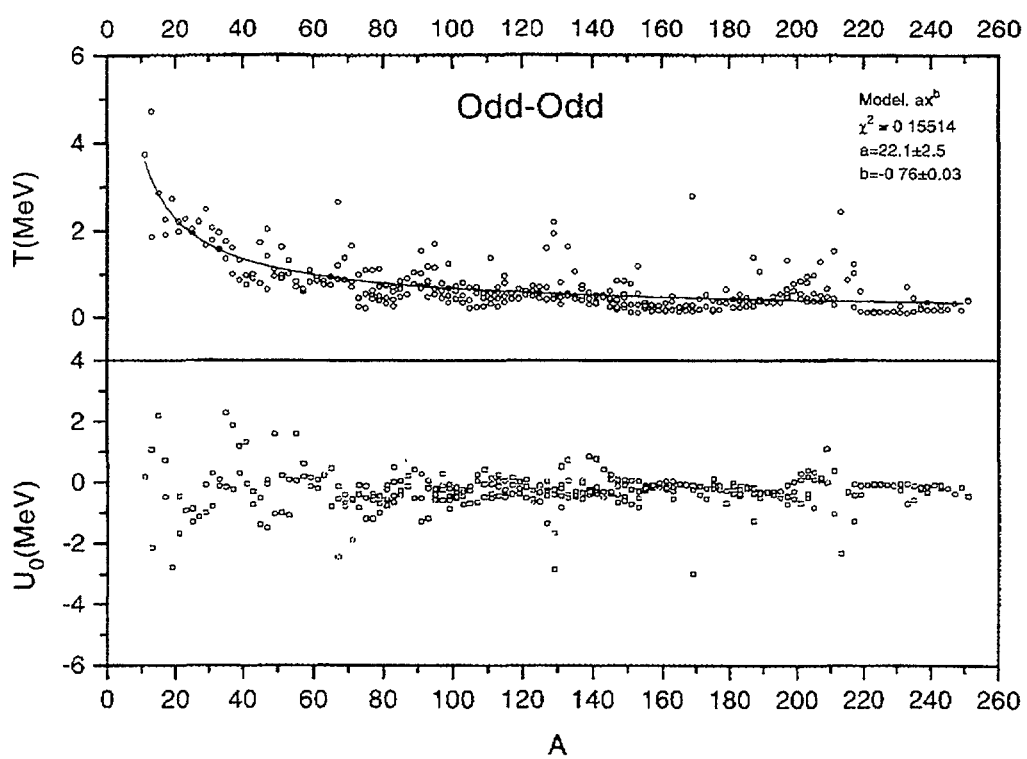

Figure 2.5: Nuclear temperature T and shift energy U_0 versus mass number for odd-odd nuclei.

Plots of nuclear temperature T and backshift energy U_0 against mass number have been created separately for even-even, odd-even, even-odd and odd-odd nuclei using the results from Table 2.2. The data points have been fitted (unweighted) with power trend lines. The corresponding plots are shown in Figs. 2.2 to 2.5 where the fitted power functions are also indicated.

Needless to say that the applied model is very crude and it has been meant only for finding an approximate cutoff energy for each nucleus in a uniform manner. **It should not be considered as a uniformly valid model for level density, nor should the parameters T and U_0, determined with eq. (2.1), be taken for "real" nuclear temperatures and backshift energies.** Nevertheless, they are indicative in that they show some regularity with mass, resembling the behavior of analogous parameters from more physical models (see Figs. 2.2 to 2.5).

2.2.3 Format

The discrete levels database, created at Budapest, contains *96,834 levels* and 108,345 placed gamma rays, in *2,585 nuclides*. In a final step, it has been converted into an ASCII file having the extended Bologna format, specified elsewhere [2.4]. The format and contents of the resulting Discrete Level Schemes Segment are described below.

In order to perform the conversion to Bologna format, the levels for each nuclide had to be numbered first. As in the Bologna format the final levels are identified by their two-digit integer serial number, the sets of gammas had to be truncated to keep the serial number of *final levels below 100* for each individual nuclide. (There is no limit to the number of initial levels, however.) Similarly, for branching percentages also only two digit integer numbers (100% is given as 00) are allowed by the Bologna format. Therefore all branching values had to be rounded to integers, and gammas with branchings below 0.5% had to be deleted. The truncation has affected 2,922 gammas, reducing their total number to *105,423 gamma rays*.

Level spins and parities have been included in the file. In cases of multiple spin choices tentative values have been inferred according to the following rule: out of two alternative spins the higher value, out of three the middle value has been adopted. For the rest of cases no spin values were given at all, and no attempts were made to infer parities either. Separate flags mark uncertain or undefined spin and parity, respectively. The extended Bologna format also allows the inclusion of half-lives. Those excited levels with half-lives greater than one second have been flagged as isomers. Detailed statistics are given in Table 2.3.

Finally, the *cumulative level numbers* N_{max}, corresponding to the cutoff energies U_{max} have also been included in the file for those 1,277 nuclides which have at least ten known levels. On the other hand, the cumulative level numbers N_c, associated with the upper energy limit U_c for levels characterized by unique spin and parity values, have been included for every nuclide.

The Budapest Discrete Level Schemes Segment consists of three files:

1. **budapest_levels.dat** - the actual segment, ASCII text file with 132-character lines, about 5 Mbyte size;
   first version: 16 November 1996, last modified: 15 September 1997
2. **budapest_cumulative.dat** - ASCII table of the fitted cumulative numbers, cutoff energies and level density parameters;
   first version: 16 November 1996, last modified: 15 September 1997
3. **budapest.readme** - describes the Segment's format, contains illustrative example;
   first version: 16 November 1996, last modified: 15 September 1997

The latter file describing the format is reproduced in Table 2.4 for convenience.

Table 2.3: Data statistics for the Discrete Level Schemes Segment file **budapest_levels.dat**.

Mass region	Nuclei #	Stable nuclei #	Level #	Gamma #	Spin No. unamb.	Parity # unamb.	J^{π} unamb.
1-10	36	8	245	31	131	145	129
11-20	62	10	2,206	1,211	1,123	1,157	1,089
21-30	86	10	3,047	3,929	1,468	1,687	1,368
31-40	97	13	3,238	3,573	1,321	1,722	1,236
41-50	111	14	5,192	4,332	1,473	1,870	1,357
51-60	107	12	6,767	4,863	1,783	2,079	1,656
61-70	100	12	4,251	3,563	933	1,141	858
71-80	109	14	4,699	5,577	919	1,266	869
81-90	113	14	4,703	4,788	877	1,241	862
91-100	119	17	5,491	6,076	979	1,420	907
101-110	126	13	4,547	5,870	1,114	1,391	1,030
111-120	119	16	4,279	4,858	1,023	1,287	994
121-130	119	18	4,564	4,591	606	945	564
131-140	119	15	4,653	6,635	963	1,192	888
141-150	139	15	5,571	6,546	1,475	1,688	1,312
151-160	124	14	5,777	8,434	2,155	2,296	2,058
161-170	118	13	5,436	6,617	1,662	2,013	1,594
171-180	109	14	4,784	5,132	833	1,084	783
181-190	94	14	4,258	5,593	916	1,498	875
191-200	75	13	3,034	3,872	623	920	615
201-210	97	11	4,323	4,013	1,155	1,618	1,088
211-220	85	0	1,315	1,049	254	327	246
221-230	77	0	1,063	1,502	225	309	217
231-240	76	4	2,165	2,040	606	658	575
241-250	58	1	965	600	170	197	164
251-260	71	0	221	128	39	42	39
261-270	39	0	40	0	9	9	9
All	2,585	285	96,834	105,423	24,835	31,202	23,382

2.3 Other Files

In the course of the present project several other discrete level schemes files have been provided by the participants of the RIPL project. These are characterized briefly below. The list goes according to laboratory. Description of the actual file formats may be found in the accompanying README files.

- File: *beijing.dat*
  Provided by Su Zongdi, as of 1 February 1996
  Chinese Nuclear Data Center, CIAE Beijing, China

  The Chinese Segment of Discrete Level Schemes and Gamma-Ray Branching Ratios, CENPL-DLS.1, contains a data file and a management-retrieval code system [2.10]. It is part of the Chinese Evaluated Nuclear Parameter Library, CENPL, version 1, as of 12 October 1995. Contains data for 79,461 levels and 93,177 gamma rays in 1,908 nuclides, originating from the 1991 version of ENSDF [2.2].

Table 2.4: Format description for the Discrete Level Schemes Segment file **budapest_levels.dat**, including an example.

```
IAEA Project RIPL - Phase I (1994/97)
DISCRETE LEVEL SCHEMES SUBLIBRARY - Version 1996
Prepared by: J. Ostor, T. Belgya and G. Molnar,
Institute of Isotopes, Budapest, Hungary
Format: ASCII, 132 characters per line
Data format: extended version of original Bologna format
by G. Reffo et al. (ENEA Bologna, Italy)

1. First line

Number of levels (format I5); 18 blanks; mass, charge, 0 (format 3I3);
40 characters for bibliographic information

2. Second line - new!

Level number for cutoff Umax,
level number for spin/parity cutoff Uc (blank if not available, format 2I3); 23 blanks;
                                                                          0 (format I3)

3. All other lines

Col 1: * flag = uncertain parity (blank otherwise)
Col 2-4: parity (+1 or -1 or blank, format I3)
Col 5-13: level energy in MeV (format F8.5)
Col 14-20: spin (format F8.5)
Col 21: X flag = isomeric level
Col 22: * flag = uncertain energy - not used!
Col 23: * flag = uncertain spin
Col 24-32: mass, charge, level number (format 3I3)
Col 33-112: data for 18 gamma decay events (format 18I4;
first 2 digits = number of final level, second 2 digits = branching percentage
                                                          /100 percent given as 00)
Col 113-119 : level half-life in seconds (scientific format)
-------------------------------------------------------------------------------

Example: Co-60

  286                  60 27  0*** FROM NUDAT 1996 FEB 23
 10 10                        0
   1 0       5          60 27  1                      ...           4.017E7
   1 .05859  2       X  60 27  2 100                  ...           6.28E2
   1 .2772   4          60 27  3
   1 .2884   3          60 27  4 200
   1 .43571  5          60 27  5 139 361
   1 .5062   3          60 27  6 299 4 1
   1 .54282  2          60 27  7 200
   1 .61455  3          60 27  8 296 3 4
   1 .7388   1          60 27  9 259 741
   1 .78571  4          60 27 10 153 444 5 2 8 1     ...           3.2E-12
*    .94               * 60 27 11
*    1.00391           * 60 27 12 249 323 4 2 726
*    1.0058   4          60 27 13 1 6 440 85110 2
*    1.13198           * 60 27 14 900
*  1 1.1507            * 60 27 15 400
   1 1.20783 5          60 27 16 129 371
   1 1.21645 6          60 27 17 100                  ...           2.8E-13
...
```

- File: *bologna.dat*
  Provided by G. Reffo, as of 15 November 1995
  Nuclear Data Centre, ENEA Bologna, Italy

  The Bologna Nuclear Level File, BNLF, contains 81916 levels for 2258 nuclei and has a size of 3.26 Mbytes. It replaces the older Bologna file LIVELLI [2.5], version 1993-1994. Data were extracted from ENSDF [2.2] using the conversion code JANUS and stored in the old Bologna format. Uncertain or redundant data have been marked by warning asterisks.

  In the new file the maximal number of levels per nucleus is still limited to 99. Data affected by this truncation, as well as data for nuclei where the translation has failed, have been preserved in separate files.

- Files: *obninsk_levels.dat* and *obninsk_branchings.dat*
  Provided by A. V. Ignatyuk, as of 28 October 1994
  Nuclear Data Center, FEI Obninsk, Russia

  The evaluated data segment of discrete levels and branching ratio data from Obninsk consists of two files.

  The first version of the segment Schemes of Experimental Discrete Levels (SEDL) was prepared in 1989 [2.12]. Usage of SEDL in applied and fundamental fields shows that some improvements of the file are desirable. For example, more than 50 levels and lists of possible level spins must be added into the file. A modern version of the segment [2.13] contains experimental schemes (extracted from ENSDF [2.2]) for nuclei with $21 < A < 250$ (1170 nuclides): energy, spin and parity of levels (up to 400 levels in a nuclide).

  To provide input data for isomer yield calculations the SEDL-RADA file has been prepared [2.13]. In the current version of the file the following data are included for each nuclide: energy, spin and parity of γ-decaying levels, number of γ-transitions, number of final levels and the branching ratio for each transition.

- File: *jaeri.dat*
  Provided by T. Fukahori, as of 15 September 1997.
  Nuclear Data Center, JAERI Tokai-mura, Japan

  Discrete level scheme data for 644 nuclei from $^{4}_{2}$He to $^{255}_{100}$Fm were taken from ENSDF and were slightly modified for use in the Japanese Evaluated Nuclear Data Library (JENDL-3) evaluation. Level energies, spins and parities for 12109 levels are included. For some levels gamma-ray branching ratios are also given. A comparison with the LIVELLI file [2.5] of Bologna has shown no significant differences for overlapping nuclei.

  Basically, the level scheme data form part of the Evaluation Data File, EVLDF, which is mainly used in the Integrated Nuclear Data Evaluation System (INDES) to provide basic input parameters for various theoretical model codes. Description of the format is available in Ref. [2.11].

- File: *livermore.dat*
  Provided by M. B. Chadwick, as of 1 November 1994.
  LLNL Livermore, USA

  The Livermore Biological File of Discrete Levels contains information on discrete levels for $A < 18$ nuclei, from ^{4}He to ^{17}F. The number of the maximum level below which information on energy, spin and parity of levels was judged "complete" and the corresponding cutoff energy have been obtained from a level density analysis at Livermore in 1993, using evaluations by F. Ajzenberg-Selove [2.14] and other compilations. Note that not every nuclide with $A < 18$ is included.

2.4 Conclusions and Recommendations

To meet the needs of nuclear reaction model calculations, as well as level density analysis, a most complete and up-to-date Discrete Level Schemes Segment has been created by the Budapest group, using the 1996 version of the Evaluated Nuclear Structure Data File ENSDF [2.2] as input data. The segment contains data for 2,585 nuclei: 96,834 levels and 105,423 gamma rays with their characteristics such as energy, spin, parity, half-life, as well as gamma-ray placements and branching percentages, respectively.

The original data were retrieved from ENSDF using the NUDAT on-line database [2.6], exported into a relational database management system, carefully checked for consistency and converted into an ASCII file. The new segment is substantially larger than any earlier file and is virtually free of ambiguous data. Moreover, it contains cutoff values indicating the limit of completeness of the level scheme for those 1,277 nuclei having at least ten known levels, as well as other cutoffs with regard to complete knowledge of spin and parity for all 2,585 nuclei included. The Segment file has the recommended extended Bologna format [2.4], which is computer readable.

For the above reasons we *recommend* that the Budapest Discrete Levels File **budapest_levels.dat**, together with the data file **budapest_cumulative.dat** containing the fitted cutoff energies and level density parameters, be selected as the Discrete Level Schemes Segment of the RIPL Starter File. The U_0 and T parameters, obtained in a simplified model, should not be taken as realistic level density parameters, however. A brief description of the contents and formats of the above Budapest files is included in the accompanying file **budapest.readme**.

As alternative choices, the libraries from Beijing, Bologna, JAERI, Obninsk and Livermore, described in section 2.3, may also be used for special applications, but with the understanding of their limitations. The relevant files are: *beijing.dat*, *bologna.dat*, *obninsk_levels.dat*, *obninsk_branchings.dat*, *jaeri.dat* and *livermore.dat*.

REFERENCES

[2.1] G. Molnár, T. Belgya and B. Fazekas, *in* First Research Co-ordination Meeting on Development of Reference Input Parameter Library for Nuclear Model Calculations of Nuclear Data, Cervia (Ravenna), Italy, 19-23 September 1994, Report INDC(NDS)-335 (IAEA Vienna 1995), p. 97.

[2.2] *Evaluated Nuclear Structure Data File (ENSDF)*, produced by members of the International Nuclear Structure and Decay Data Network, and maintained by the National Nuclear Data Center, BNL, USA. Also available online from IAEA Nuclear Data Section, Vienna.

[2.3] Summary Report of the First Research Co-ordination Meeting on Development of Reference Input Parameter Library for Nuclear Model Calculations of Nuclear Data, Cervia (Ravenna), Italy, 19-23 September 1994, Report INDC(NDS)-312 (IAEA Vienna 1994).

[2.4] Summary Report of the Second Research Co-ordination Meeting on Development of Reference Input Parameter Library for Nuclear Model Calculations of Nuclear Data, IAEA Vienna, 30 October - 4 November 1995, Report INDC(NDS)-350 (IAEA Vienna 1996).

[2.5] Bologna Discrete Nuclear Levels File LIVELLI (ENEA Bologna, Italy, 1993-94).

[2.6] *NUDAT database, version 23 February 1996*, maintained by the National Nuclear Data Center, BNL, USA. Also available online from IAEA Nuclear Data Section, Vienna.

[2.7] T. Belgya, G.L. Molnár, B. Fazekas and J. Östör, Report INDC(NDS)-367 (IAEA Vienna 1997).

[2.8] J. Östör, T. Belgya and G. Molnár, Institute of Isotopes, Budapest, H-1525 Hungary, unpublished.

[2.9] G. Audi and A.H. Wapstra, Nucl. Phys. **A595**, 409 (1995).

[2.10] Su Zongdi, Zhang Limin, Zhou Chunmei and Sun Zhengjun, *in* First Research Co-ordination Meeting on Development of Reference Input Parameter Library for Nuclear Model Calculations of Nuclear Data, Cervia (Ravenna), Italy, 19-23 September 1994, Report INDC(NDS)-335 (IAEA Vienna 1995), p. 67.

[2.11] T. Fukahori and T. Nakagawa *in* First Research Co-ordination Meeting on Development of Reference Input Parameter Library for Nuclear Model Calculations of Nuclear Data, Cervia (Ravenna), Italy, 19-23 September 1994, Report INDC(NDS)-335 (IAEA Vienna 1995), p. 7; T. Nakagawa, *ibid.*, p. 21.

[2.12] O.T. Grudzevich, A.V. Zelenetsky and A.B. Pashchenko, Preprint FEI-2209 (Obninsk 1989).

[2.13] O.T. Grudzevich, A.V. Zelenetsky and A.B. Pashchenko, Reference Nuclear Parameter Library, Preprint FEI-2306 (Obninsk 1993).

[2.14] F. Ajzenberg-Selove, Nucl. Phys. **A523**, 1 (1991).

3 Average Neutron Resonance Parameters

Coordinator: G. Reffo

Summary

Required parameters for statistical model calculations are neutron strength functions, average radiative widths and average spacing of resonances. These parameters are generally obtained from the analysis of parameter sets for the resolved resonances. The fact that the experimental resolution and sensitivity are limited in quality results in an incomplete (missing resonances) or distorted (errors on width determination) information on the resonance parameters. That is why the average widths and resonance spacings cannot be directly deduced from available resonance sequences, and they should always be estimated with account of missing resonances. Various methods for statistical analysis of missing resonances were developed, and most of them were applied for evaluation of average resonance parameters during RIPL project. Advantages and shortcomings of such methods are briefly discussed below for the purpose to obtain some objective estimation for an accuracy of recommended parameters.

For the RIPL Starter File the resonance parameters evaluated by Obninsk group are chosen as recommended ones mainly due a more reliable estimation of parameter uncertainities. These parameters are included into the **obninsk.dat** file. Alternative parameters evaluated by Beijing group are given in *beijing.dat* file, and average resonance parameters evaluated by Minsk group for the actinides are given in *minsk.dat* file.

3.1 Introduction

Before describing statistical methods for resonance analysis we would like to point out that statistical methods of resonance analysis are effective only when applied to pure resonance samples. Therefore, results of analysis become less and less accurate with the sample deficiencies.

Cases of pure resonance sample are pretty rare. In order to overcome this difficulty, one adopts different statistical analysis methods as well as sampling criteria in order to identify for each set of resonances a reduced sample where missing resonances and/or distortion are reduced. Getting average resonance parameters consists therefore of an iterative procedure where one tries to reach convergence of results from different methods of analysis. The spread of values obtained using different statistics is meaningful as uncertainty affecting results. Anyway, even such iterative procedure of statistical resonance analysis is not sufficient to guarantee the absolute value of parameters in many cases, and is to be validated by use of supplementary information like e.g. capture cross sections and radiative widths wherever possible. The formats of data are explained in the corresponding **readme** files.

3.2 Evaluation Methods

The neutron strength functions for a given orbital angular momentum l are defined by the relation

$$S_l = \frac{< g\Gamma_n^l >}{(2l+1)D_l} = \frac{1}{(2l+1)\Delta E} \sum_r g_r \Gamma_{nr}^l, \tag{3.1}$$

where the summation is performed over N resonances in the energy interval ΔE, $g_r = (2J_r+1)/2(2I_0+1)$ is the statistical weight factor that depends on the angular momentum J_r of a resonance and the spin I_0 of the target nucleus; Γ^l_{nr} are the reduced neutron widths of resonances, and D_l is the average resonance spacing, defined as

$$D_l = \Delta E/(N-1). \tag{3.2}$$

The reliable identification of s- and p-wave resonances is the most important for an accurate evaluation of average parameters. If such identification is available the neutron strength functions can be evaluated rather simply from the linear approximation of the cumulative sum of the products $g_r\Gamma^l_{nr}$. A departure from linearity may indicate the missing of resonances. The relative error of the evaluation can be defined from the relation

$$\frac{\delta S_l}{S_l} = \sqrt{2/N}, \tag{3.3}$$

which is based on an asymptotic estimation for the variance of the sum of neutron widths distributed in accordance with the Porter-Thomas law [3.1].

As dominant contributions to the sum in Eq. (3.1) give resonances with a large neutron width the missing of some weak resonances or admixture of p-wave resonances has a rather small effect on evaluation of strength functions for s-neutrons. The situation is not so favorable for p-neutrons, strength function of which can be strongly distorted by any admixture of incorrectly identified s-wave resonances. It is the main reason that for many nuclei the relative accuracy of p-wave strength functions is much lower than for s-wave ones.

For a rather full set of resonances the relative statistical error of the resonance spacing evaluation can be determined by the relation

$$\frac{\delta D_l}{D_l} = \frac{0.45\sqrt{\ln N + 2.18}}{N} \approx \frac{1}{N}, \tag{3.4}$$

which was obtained by Dyson and Mehta for the Gaussian orthogonal ensemble [3.2]. It is obvious that a missing of some resonances in a analyzed set results in a mistake that essentially exceeds the statistical one. So the estimation of missing resonances is a crucial problem for an accurate evaluation of the average resonance spacings. Another problem in resonance analysis arises in the separation of p-waves by s-waves. This is also crucial in order to be able to treat pure samples.

Three categories of methods were developed for the statistical account of missing or erroneously identified resonances: *i)* the methods exploiting the statistics of level spacings, *ii)* the methods based on the fit of the reduced neutron width distribution by a Porter-Thomas law, *iii)* the methods using combined simulation of the level and width statistics. Advantages and weaknesses of various methods have been broadly discussed in Refs. [3.3–3.8]. Some new developments connected the third class of methods were proposed recently too [3.9–3.12].

The simplest method of resonance analysis, often used even nowadays, is the staircase plot of the cumulative number $N(E)$ of resonances as a function of energy. It is usually assumed that at low energy range there are no missing resonances, and a linear approximation of this part of the plot gives a direct estimation of D_l. Some variety of this method is the approach based on the Δ_3 statistics given by Dyson and Mehta [3.2]. The best fit of $N(E)$ is searched by the least squares procedure of the parameter

$$\Delta = \min\left[\frac{1}{\Delta E}\int_0^{\Delta E}[N(E) - AE - B]^2 \mathrm{d}E\right]. \tag{3.5}$$

For a compete set of levels the value and variance of this parameter are defined by the relations:

$$\Delta_3 =< \Delta >= \frac{1}{\pi^2}(\ln N - 0.0687), \qquad \sigma = \frac{1}{\pi^2}\sqrt{\frac{4\pi^2}{45} + \frac{7}{24}} = 0.11. \tag{3.6}$$

Absence of levels or presence of spurious levels from another sequences obviously increases Δ_3. Therefore, if the fitted value of Δ satisfies the condition $\Delta_3 - \sigma < \Delta < \Delta_3 + \sigma$, the analyzed set of resonances may be considered as a pure and complete set. Unfortunately the Δ_3 statistics does not give any recipe to correct a bad set of resonance parameters. Besides in practice one finds that the Δ_3 test criteria are often satisfied for samples that are known to be neither pure nor complete [3.6, 3.8].

In contrast to the spacing distribution the neutron width distribution is only slightly affected by missing or spurious weak resonances. The upper part of the Porter-Thomas distribution, corresponding to the strong resonances, can be regarded as virtually unperturbed. A number of resonances that have reduced neutron width above a given value should be described by the function

$$N(\Gamma) = N_0 \int_{\Gamma/\overline{\Gamma}}^{\infty} \frac{\exp(-x/2)\mathrm{d}x}{\sqrt{2\pi x}} = N_0 \left[1 - \mathrm{erf}\sqrt{\Gamma/2\overline{\Gamma}}\right]. \tag{3.7}$$

So by fitting the corresponding distribution of neutron widths with a maximum likelihood approach we can find both the average reduced neutron width and total number of resonances N_0 at considered energy interval. The versions of the method were developed too that take into account of energy variations of neutron width measurement threshold and some other experimental conditions [3.8, 3.9].

The methods of the third class try to account simultaneously of limitations imposed on estimation of a mean width and resonance spacing by the Wigner and Porter-Thomas laws. Simulations of the neutron cross section by the Monte-Carlo methods with an account of experimental resolution and other conditions are applied in most cases. Some analytical treatments that could replace Monte-Carlo simulation in some cases were discussed in Refs. [3.9].

On the basis of the resonance parameter analyses performed by different groups one conclusion should be stressed that none of the methods developed permits an unambiguous identification of missed or spurious resonances in a general case. A critical analysis of experimental conditions and of the approaches used to obtain individual resonance parameters is very important for many cases. The priority in average parameter evaluations should be given to the quality of the selected resonance set rather than to the total number of resonances included into consideration [3.9, 3.13]. Only for a rather small number of nuclei the accuracy of evaluated resonance spacings is better than 10%. The best examples of such nuclei are the isotopes U-235 and U-238 for which the relative errors of the recommended D_0 are better than 2%, and for the isotopes Pu-239, Pu-240 and Pu-242 such errors are about 5% [3.9, 3.11].

3.3 Files of Average Neutron Resonance Parameters

The complete tables of average resonance parameters have been provided to the NDS by Beijing, Bologna and Obninsk groups in the beginning of the RIPL project. They were obtained by each group on the basis of methods used for neutron data evaluations in the corresponding Centers.

Combined tables of average parameters for the resonance spacings D_0, the neutron strength function S_0 and the average radiative widths were prepared by the Bologna group. Obninsk group has compiled the tables to computer readable format errors. This results provided the

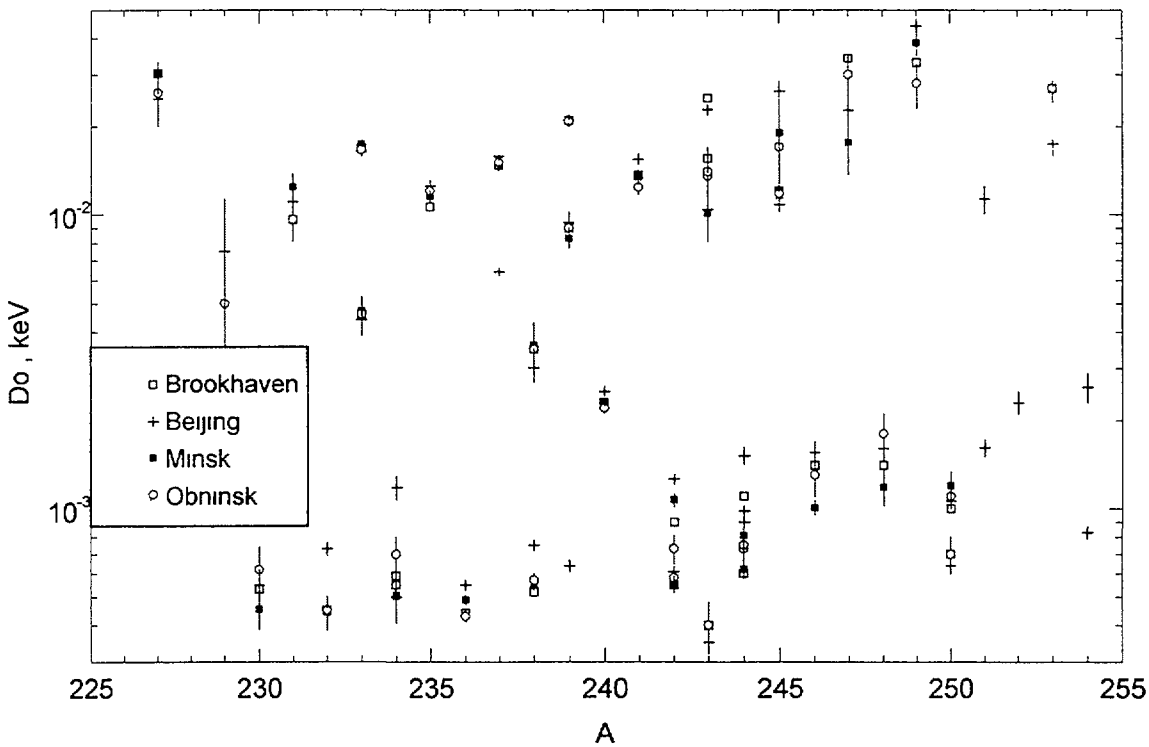

Figure 3.1: Average resonance spacings for actinides evaluated by Brookhaven (empty squares), Beijing (+) Obninsk (circles), and Minsk (full squares) groups.

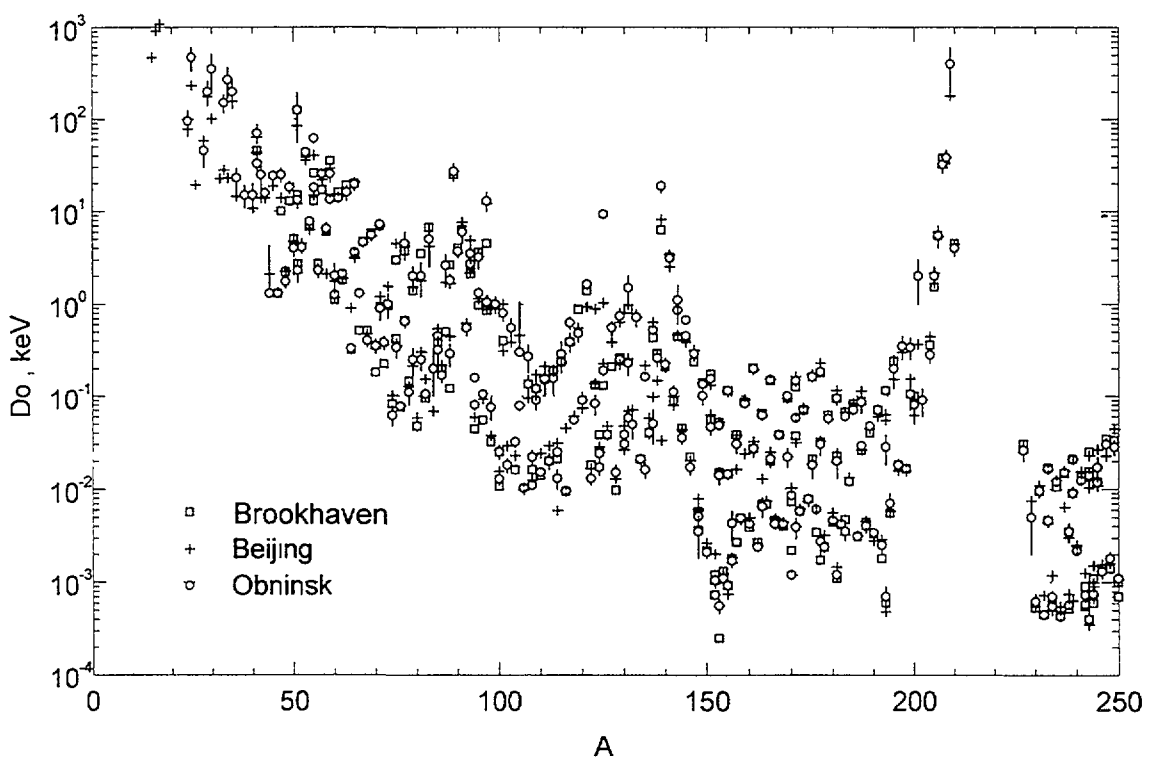

Figure 3.2: Average resonance spacings for full mass region evaluated by Brookhaven (squares), Beijing (+) and Obninsk (circles) groups. Uncertainties are shown for Obninsk evaluations only.

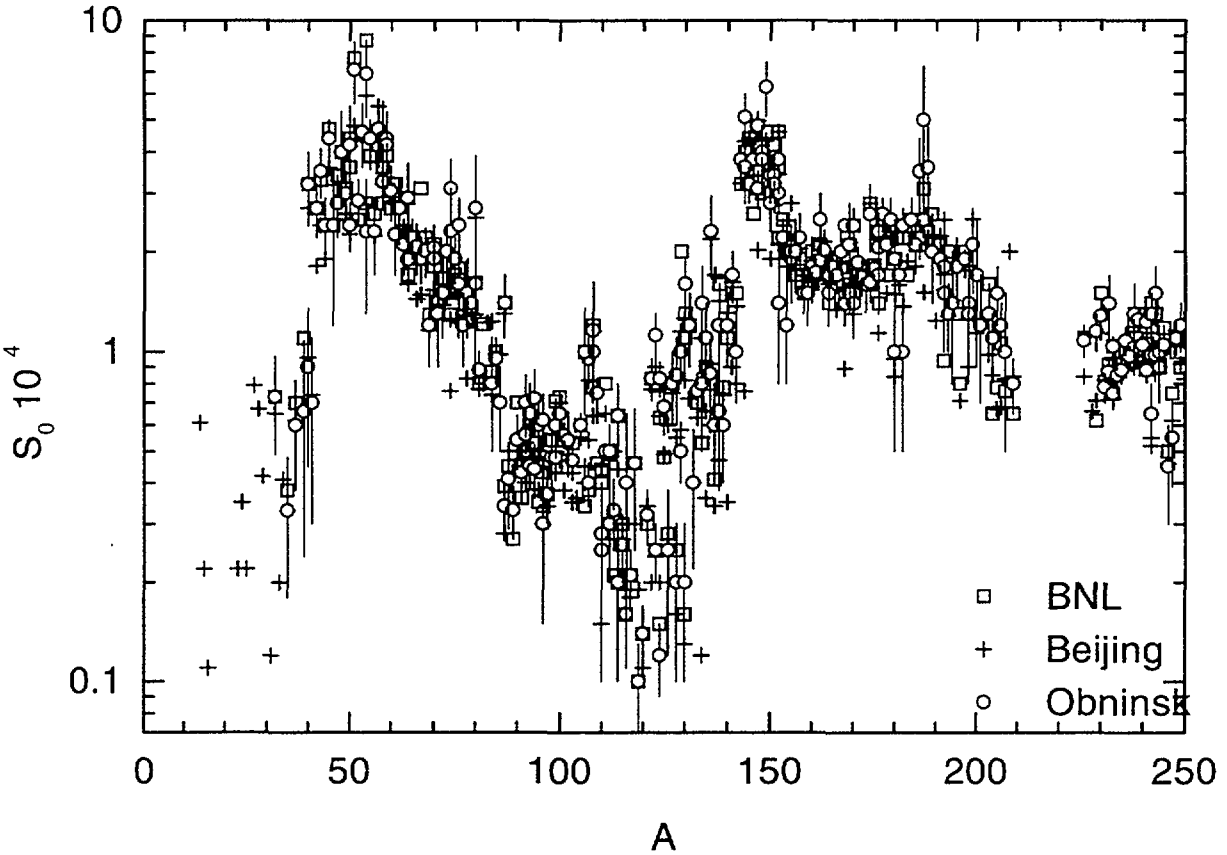

Figure 3.3: The s-wave neutron strength functions evaluated by BNL (squares), Beijing (+) and Obninsk (circles) groups. Uncertainties are shown for Obninsk evaluations only.

basis for detailed comparison and discussion of evaluated average parameters carried out by means of frequent consultations between Obninsk and Bologna.

Many discrepancies were found and the reasons for such discrepancies were traced. After the analysis of the available files, namely from Bologna, Obninsk and Beijing, meetings were held between Bologna and Obninsk groups where statistical methods of resonance analysis were carefully discussed in order to clarify the meaning of errors as well as the meaning of the different quantities. To better understand the nature of discrepancies, a restricted number of nuclei have been analyzed more carefully on the basis of methods used in Bologna and Obninsk. This has clarified the different philosophies adopted as well as the significance of the quoted quantities. In particular Obninsk group spends more attention to the limitation of energy interval on which the resonance parameters are analyzed and complements the statistical estimation of errors with some experience guesses about associated methodical errors. Bologna group approach is more formal and conservative in the sense that all information available about resonances is involved in the statistical analysis. The quoted uncertainties in this case represent the intrinsic limit and deficiency of the statistical sample, and they are in general larger than those obtained for the other confidence limit estimates.

After consideration of existing discrepancies Obninsk took care of the re-analysis of 80% of nuclei and new tables of the evaluated neutron strength functions and resonance spacings were prepared. For heavy actinides a new analysis of average resonance parameters was performed also by Minsk group.

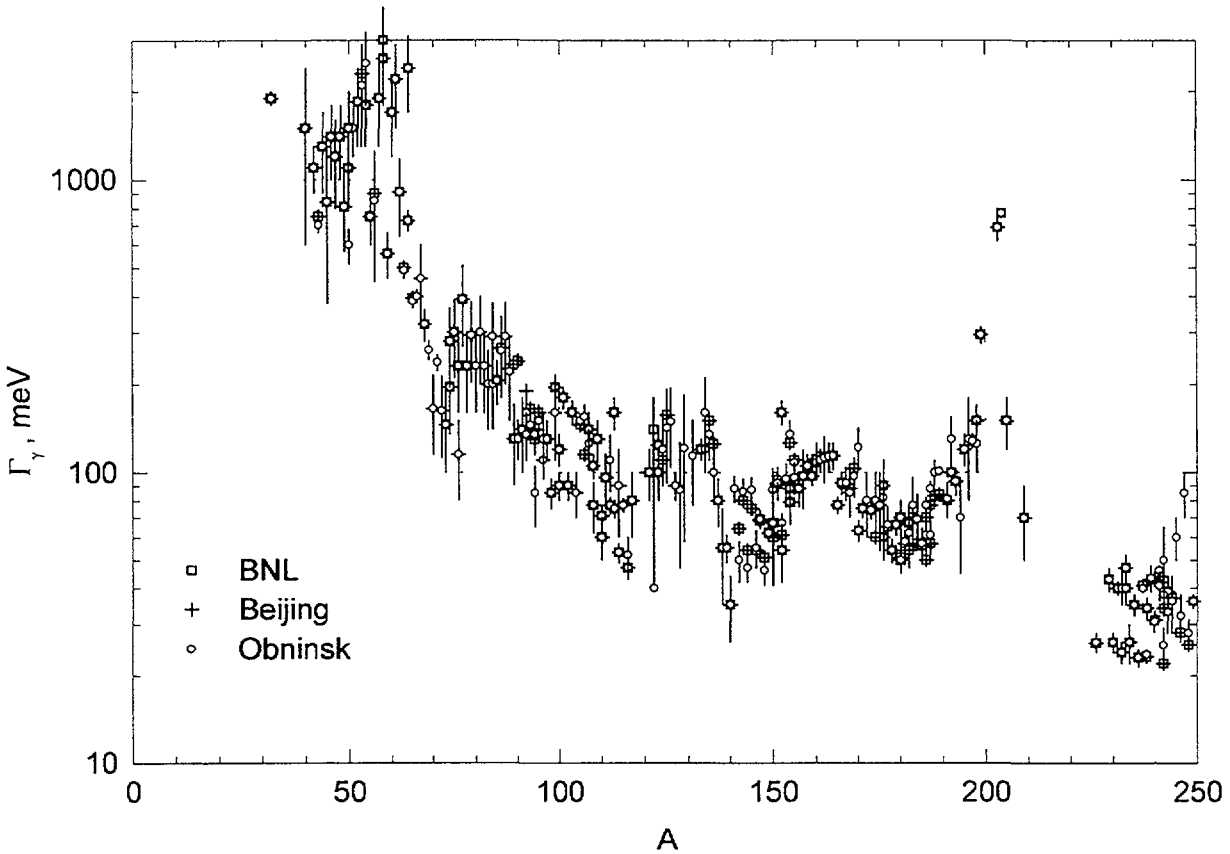

Figure 3.4: Average radiative widths evaluated by Beijing (+) and Obninsk (circles) groups.

The resonance spacings evaluated by Beijing, Minsk and Obninsk groups for actinides are shown in Fig. 3.1. The results of all groups demonstrate a rather good agreement for most cases where data are available for more than 30 resonances. The quoted uncertainties of Obninsk, as a rule, are higher than the uncertainties given by Beijing and Minsk groups. This difference of uncertainties mainly connected with the reduction of energy interval that used Obninsk group to improve quality of analyzed statistical samples. Taking into account the big difference between uncertainties obtained for various methods of resonance spacing estimation, the uncertainties of Obninsk group seem more reliable than Beijing or Minsk ones.

Evaluations of the resonance spacings for full mass range are shown in Fig. 3.2. The last Obninsk evaluations for some nuclei are based on more recent experimental data than included in Mughabghab compilations [3.14, 3.15] analyzed by Beijing group. As an alternative set is included into the RIPL Starter File the average resonance spacings evaluated by Beijing group [3.17]. The recent compilation of the resonance spacings published in Ref. [3.16] and based on evaluations of different authors is also included into the *iljinov_gc.dat* file which is placed in Segment 5 of the Starter File as more related to the nuclear level density parameters.

The results of new evaluations of Beijing and Obninsk groups for the s-wave neutron strength functions are shown in Fig. 3.3 in comparison with old BNL evaluations. There are no essential differences between the two evaluations for most nuclei. Uncertainties of Obninsk group are a little higher again because to some extent they take account of sample quality effects in addition to pure statistical errors.

Table 3.1: Table of recommended average parameters of the s-wave neutron resonances (file **obninsk.dat**).

Z and A are the element and mass numbers of the compound nucleus, I_0 is the spin of the target nucleus, Bn is the neutron binding energy, Nr is the number of resonances included in the analysis, D_0 and δD_0 are the evaluated resonance spacing and its uncertainty, S_0 and δS_0 are the neutron strength function and its uncertainty, Γ_γ and $\delta\Gamma_\gamma$ are the average radiative width and its uncertainity. The references relate to the works in which the resonance spacings and neutron strength functions were evaluated, the average radiative widths are mainly taken from Ref. [3.13].

Z	Sy	A	I_0	Bn MeV	Nr	D_0 keV	δD_0 keV	S_0 10^{-4}	δS_0 10^{-4}	Ref	Γ_γ meV	$\delta\Gamma_\gamma$ meV
11	Na	24	1.5	6.959	3	9.50E+01	3.00E+01			[3.18]		
12	Mg	25	0	7.330	4	4.70E+02	1.40E+02			[3.18]		
13	Al	28	2.5	7.725	7	4.50E+01	1.50E+01			[3.18]		
14	Si	29	0	8.474	5	2.00E+02	6.00E+01			[3.18]		
14	Si	30	0.5	10.610	5	3.50E+02	1.60E+02			[3.19]		
16	S	33	0	8.641	41	1.50E+02	3.50E+01	0.73	0.24	[3.18]	1900	
16	S	34	1.5	11.416	7	2.70E+02	1.00E+02			[3.18]		
16	S	35	0	6.985	3	2.00E+02	7.00E+01			[3.18]		
17	Cl	36	1.5	8.580	10	2.30E+01	6.00E+00	0.33	0.15	[3.20]		
17	Cl	38	1.5	6.108	14	1.50E+01	4.00E+00	0.60	0.22	[3.20]		
18	Ar	41	0	6.098	7	7.02E+01	1.70E+01	0.90	0.45	[3.21]		
19	K	40	1.5	7.799	7	1.50E+01	5.00E+00	0.66	0.42	[3.18]		
19	K	42	1.5	7.533	5	2.50E+01	1.00E+01	0.70	0.40	[3.20]		
20	Ca	41	0	8.362	31	3.26E+01	4.30E+00	3.20	0.80	[3.21]	1500	1000
20	Ca	43	0	7.932	27	1.58E+01	2.10E+00	2.70	0.50	[3.21]	1100	200
20	Ca	44	3.5	11.132	23	1.30E+00	3.00E+00	3.50	0.60	[3.20]	750	40
20	Ca	45	0	7.414	21	2.41E+01	3.20E+00	2.40	0.50	[3.21]	1300	400
21	Sc	46	3.5	8.760	74	1.30E+00	1.00E-01	4.40	0.60	[3.20]	840	460
22	Ti	47	0	8.877	12	2.50E+01	4.40E+00	2.40	1.20	[3.21]	1400	400
22	Ti	48	2.5	11.627	40	1.75E+00	2.50E-01	2.80	0.60	[3.20]	1200	400
22	Ti	49	0	8.142	16	1.83E+01	2.90E+00	4.00	1.30	[3.21]	1400	400
22	Ti	50	3.5	10.939	35	4.00E+00	8.00E-01	3.00	0.50	[3.20]	810	240
22	Ti	51	0	6.371	3	1.25E+02	7.00E+01			[3.14]	1100	300
23	V	51	6	11.051	16	2.30E+00	6.00E-01	4.20	1.30	[3.20]	600	80
23	V	52	3.5	7.310	48	4.10E+00	6.00E-01	7.10	1.50	[3.20]	1500	300
24	Cr	51	0	9.261	41	1.33E+01	1.30E+00	2.40	0.40	[3.21]	1500	500
24	Cr	53	0	7.939	23	4.34E+01	4.37E+00	2.85	0.45	[3.22]	1850	550
24	Cr	54	1.5	9.719	34	7.80E+00	8.00E-01	4.60	1.00	[3.22]	2100	800
24	Cr	55	0	6.246	15	6.20E+01	8.00E+00	2.30	1.00	[3.22]	2500	700
25	Mn	56	2.5	7.270	52	2.30E+00	4.00E-01	4.40	0.60	[3.20]	750	150
26	Fe	55	0	9.297	52	1.80E+01	2.40E+00	6.90	1.80	[3.21]	1800	500
26	Fe	57	0	7.646	41	2.54E+01	2.20E+00	2.30	0.60	[3.23]	920	410
26	Fe	58	0.5	10.044	22	6.50E+00	1.00E+00	4.70	1.10	[3.20]	1900	600
26	Fe	59	0	6.581	12	2.54E+01	4.90E+00	4.40	1.30	[3.21]	3000	900
27	Co	60	3.5	7.491	96	1.25E+00	1.50E-01	4.40	0.80	[3.20]	560	100

Table 3.1. (Cont.)

28	Ni	59	0	8.999	61	1.34E+01	9.00E-01	3.26	0.59	[3.24]	2600	800
28	Ni	60	1.5	11.388	7	2.00E+00	7.00E-01	4.20	1.10	[3.20]	2200	700
28	Ni	61	0	7.820	58	1.38E+01	9.00E-01	3.05	0.57	[3.24]	1700	500
28	Ni	62	1.5	10.597	31	2.10E+00	1.50E-01	2.25	0.55	[3.20]	2200	700
28	Ni	63	0	6.838	29	1.60E+01	3.00E+00	2.70	0.60	[3.20]	910	270
28	Ni	65	0	6.097	28	1.96E+01	3.00E+00	2.90	0.80	[3.20]	2400	700
29	Cu	64	1.5	7.916	153	3.30E-01	4.00E-02	2.10	0.40	[3.20]	490	30
29	Cu	66	1.5	7.065	129	1.30E+00	1.10E-01	2.20	0.30	[3.20]	385	20
30	Zn	65	0	7.979	22	3.59E+00	1.60E-01	1.89	0.26	[3.25]	726	60
30	Zn	67	0	7.052	64	4.62E+00	5.50E-01	2.06	0.36	[3.25]	390	60
30	Zn	68	2.5	10.198	345	4.00E-01	6.00E-02	1.90	0.30	[3.20]	460	140
30	Zn	69	0	6.482	45	5.56E+00	4.30E-01	2.01	0.34	[3.25]	320	40
30	Zn	71	0	5.833	48	7.20E+00	8.00E-01	2.05	0.35	[3.25]		
31	Ga	70	1.5	7.654	19	3.50E-01	6.00E-02	1.20	0.30	[3.20]	262	25
31	Ga	72	1.5	6.521	14	3.80E-01	6.00E-02	1.30	0.40	[3.20]	237	20
32	Ge	71	0	7.416	21	8.90E-01	2.40E-01	1.90	0.30	[3.20]	165	50
32	Ge	73	0	6.783	14	1.00E+00	3.00E-01	1.50	0.40	[3.20]	162	50
32	Ge	74	4.5	10.199	35	6.20E-02	1.50E-02	2.00	0.40	[3.20]	195	45
32	Ge	75	0	6.506	8	3.00E+00	1.00E+00	2.30	0.80	[3.20]	195	60
32	Ge	77	0	6.073	8	4.50E+00	1.50E-00	1.60	0.50	[3.20]	115	35
33	As	76	1.5	7.326	243	7.70E-02	8.00E-03	1.90	0.30	[3.20]	300	90
34	Se	75	0	8.027	7	3.40E-01	8.00E-02	3.10	0.70	[3.20]	280	80
34	Se	77	0	7.418	15	6.50E-01	1.00E-01	2.40	0.50	[3.20]	230	60
34	Se	78	0.5	10.498	27	1.10E-01	3.00E-02	1.20	0.30	[3.20]	390	90
34	Se	79	0	6.963	16	2.00E+00	5.00E-01	1.50	0.40	[3.20]	230	60
34	Se	81	0	6.701	10	2.00E+00	8.00E-01	2.70	1.20	[3.20]	230	70
34	Se	83	0	5.818	4	5.00E+00	2.50E+00			[3.20]		
35	Br	80	1.5	7.892	111	4.70E-02	5.00E-03	1.40	0.15	[3.20]	293	90
35	Br	82	1.5	7.592	99	1.05E-01	1.50E-02	0.88	0.12	[3.20]	300	100
36	Kr	79	0	8.369	3	2.50E-01	8.00E-02			[3.20]		
36	Kr	81	0	7.874	4	2.50E-01	6.00E-02	1.60	0.80	[3.20]	230	60
36	Kr	84	4.5	10.519	4	2.00E-01	1.00E-01			[3.20]	210	60
36	Kr	85	0	7.118	3	4.50E-01	1.70E-01			[3.20]		
37	Rb	86	2.5	8.651	63	1.70E-01	3.00E-02	0.95	0.15	[3.20]	205	35
37	Rb	88	1.5	6.079	14	1.80E+00	3.00E-01	1.40	0.30	[3.20]		
38	Sr	85	0	8.529	9	3.20E-01	1.20E-01	0.80	0.30	[3.20]	290	90
38	Sr	87	0	8.428	24	2.60E+00	8.00E-01	0.70	0.20	[3.20]	260	80
38	Sr	88	4.5	11.112	50	2.90E-01	8.00E-02	0.34	0.06	[3.20]	290	90
38	Sr	89	0	6.366	8	2.70E+01	6.00E+00	0.41	0.12	[3.20]	220	70
39	Y	90	0.5	6.856	66	3.70E+00	4.00E-01	0.33	0.06	[3.20]	130	40
40	Zr	91	0	7.194	28	6.00E+00	1.40E+00	0.54	0.10	[3.20]	130	20
40	Zr	92	2.5	8.635	30	5.50E-01	1.00E-01	0.43	0.08	[3.20]	140	40
40	Zr	93	0	6.734	31	3.50E+00	8.00E-01	0.70	0.15	[3.20]	135	25
40	Zr	94	2.5	8.219	114	1.60E-01	1.50E-02	0.65	0.15	[3.20]		
40	Zr	95	0	6.462	17	3.20E+00	8.00E-01	0.72	0.16	[3.20]	85	20
40	Zr	97	0	5.579	8	1.30E+01	3.00E+00	0.30	0.15	[3.20]	130	
41	Nb	94	4.5	7.229	79	8.00E-02	1.00E-02	0.45	0.07	[3.20]	145	10
42	Mo	93	0	8.067	14	2.70E+00	5.00E-01	0.56	0.07	[3.20]	160	20
42	Mo	95	0	7.367	12	1.32E+00	1.80E-01	0.44	0.08	[3.20]	135	20

Table 3.1. (Cont.)

42	Mo	96	2.5	9.154	22	1.05E-01	1.00E-02	0.60	0.10	[3.20]	150	20
42	Mo	97	0	6.821	12	1.05E+00	2.00E-01	0.62	0.12	[3.20]	110	15
42	Mo	98	2.5	8.642	22	7.50E-02	2.00E-02	0.37	0.07	[3.20]	130	20
42	Mo	99	0	5.925	28	1.00E+00	2.00E-01	0.48	0.09	[3.20]	85	10
42	Mo	101	0	5.398	32	8.00E-01	1.50E-01	0.65	0.10	[3.20]	90	10
43	Tc	100	4.5	6.764	106	1.28E-02	1.80E-03	0.48	0.07	[3.20]	160	50
44	Ru	100	2.5	9.673	35	2.50E-02	4.00E-03	0.60	0.12	[3.20]	195	20
44	Ru	102	2.5	9.220	41	1.80E-02	3.00E-03	0.56	0.05	[3.20]	180	15
44	Ru	103	0	6.232	21	5.50E-01	1.50E-01	0.54	0.12	[3.8]	90	10
44	Ru	105	0	5.910	17	3.00E-01	7.50E-01			[3.8]	85	15
45	Rh	104	0.5	6.999	30	3.20E-02	4.00E-03	0.47	0.06	[3.20]	160	15
46	Pd	105	0	7.094	29	7.80E-02	9.00E-03			[3.31]		
46	Pd	106	2.5	9.562	193	1.03E-02	5.00E-04	0.60	0.05	[3.20]	150	8
46	Pd	107	0	6.538	29	2.70E-01	9.00E-02			[3.20]		
46	Pd	108	2.5	9.220	51	1.10E-02	9.00E-04	0.95	0.15	[3.20]	125	15
46	Pd	109	0	6.153	20	9.00E-02	2.00E-02	1.00	0.30	[3.20]	77	5
46	Pd	111	0	5.756	40	1.50E-01	5.00E-02	0.25	0.15	[3.20]	60	10
47	Ag	108	0.5	7.269	39	2.20E-02	4.00E-03	0.40	0.06	[3.20]	140	20
47	Ag	110	0.5	6.809	61	1.51E-02	1.40E-03	0.75	0.08	[3.20]	130	20
48	Cd	107	0	7.926	56	1.35E-01	3.50E-02	1.00	0.35	[3.26]	155	15
48	Cd	109	0	7.325	52	1.20E-01	3.00E-02	1.16	0.46	[3.26]	105	10
48	Cd	111	0	6.974	43	1.55E-01	2.00E-02	0.28	0.07	[3.26]	71	6
48	Cd	112	0.5	9.398	78	2.00E-02	4.00E-03	0.50		[3.26]	96	20
48	Cd	113	0	6.540	34	1.90E-01	2.50E-02	0.50	0.10	[3.26]	77	5
48	Cd	114	0.5	9.042	122	2.48E-02	2.60E-03	0.32	0.06	[3.27]	160	20
48	Cd	115	0	6.141	34	2.35E-01	3.50E-02	0.64	0.16	[3.26]	53	4
48	Cd	117	0	5.767	26	3.90E-01	9.00E-02	0.16	0.05	[3.26]	47	4
49	In	114	4.5	7.274	38	1.30E-02	3.00E-03	0.33	0.08	[3.20]	75	5
49	In	116	4.5	6.784	205	9.50E-03	5.00E-04	0.26	0.06	[3.20]	77	4
50	Sn	113	0	7.743	7	1.57E-01	5.20E-02	0.30	0.10	[3.28]	110	25
50	Sn	115	0	7.545	4	2.86E-01	1.06E-01	0.20	0.10	[3.28]	90	30
50	Sn	117	0	6.944	4	6.29E-01	9.80E-02	0.40	0.25	[3.28]	52	10
50	Sn	118	0.5	9.326	56	5.50E-02	5.00E-03	0.21	0.04	[3.28]	80	20
50	Sn	119	0	6.485	10	4.80E-01	9.00E-02	0.46	0.21	[3.28]		
50	Sn	120	0.5	9.106	16	9.00E-02	2.00E-02	0.10	0.03	[3.28]		
50	Sn	121	0	6.171	31	1.64E+00	2.00E-01	0.14	0.03	[3.29]		
50	Sn	125	0	5.732	32	9.30E+00	9.00E-01	0.12	0.03	[3.30]		
51	Sb	122	2.5	6.807	60	1.30E-02	2.00E-03	0.32	0.06	[3.20]	100	20
51	Sb	124	3.5	6.467	48	2.40E-02	3.00E-03	0.25	0.05	[3.20]	100	20
52	Te	123	0	6.935	22	8.20E-02	2.00E-02	0.83	0.12	[3.20]	140	40
52	Te	124	0.5	9.425	27	1.70E-02	3.00E-03	1.12	0.18	[3.20]	124	20
52	Te	125	0	6.570	36	1.90E-01	2.00E-02	0.83	0.10	[3.20]	120	30
52	Te	126	0.5	9.114	65	3.80E-02	5.00E-03	0.68	0.12	[3.20]	157	30
52	Te	127	0	6.290	15	5.50E-01	1.00E-01	0.25	0.13	[3.20]	149	45
52	Te	129	0	6.085	11	7.40E-01	1.50E-01	0.20	0.10	[3.20]	87	40
52	Te	131	0	5.929	22	1.50E+00	5.00E-01	0.20	0.10	[3.20]		
53	I	128	2.5	6.825	328	1.50E-02	3.00E-03	0.80	0.20	[3.20]	90	10
53	I	130	3.5	6.461	62	3.00E-02	3.00E-03	0.50	0.10	[3.20]		
54	Xe	129	0	6.909	10	2.50E-01	1.00E-03	0.85	0.25	[3.20]		

Table 3.1. (Cont.)

54	Xe	130	0.5	9.254	69	3.80E-02	5.00E-03	1.00	0.20	[3.20]	120	60
54	Xe	131	0	6.618	11	2.30E-01	6.00E-02	1.10	0.30	[3.20]		
54	Xe	132	1.5	8.935	20	4.90E-02	1.50E-02	1.20	0.30	[3.20]	114	37
54	Xe	133	0	6.438	5	7.17E-01	1.55E-01	0.40	0.18	[3.31]		
55	Cs	134	3.5	6.891	107	2.10E-02	2.00E-03	0.76	0.10	[3.20]	120	10
55	Cs	135	4	8.827	7	1.60E-02	3.00E-03	0.80	0.30	[3.20]	160	40
56	Ba	131	0	7.494	39	5.80E-02	1.00E-02	1.60	0.30	[3.32]	100	30
56	Ba	135	0	6.973	35	1.63E-01	1.10E-02	1.40	0.40	[3.33]	78	27
56	Ba	136	3.5	9.107	28	4.00E-02	6.00E-03	1.10	0.30	[3.32]	135	25
56	Ba	137	0	6.900	18	5.22E-01	3.40E-02	0.86	0.23	[3.33]	86	28
56	Ba	138	1.5	8.611	44	2.60E-01	5.00E-02	0.60	0.20	[3.32]	80	15
56	Ba	139	0	4.723	11	1.87E+01	2.90E+00	0.66	0.28	[3.24]	55	20
57	La	139	5	8.778	10	3.20E-02	6.00E-03	1.20	0.40	[3.20]	95	25
57	La	140	3.5	5.160	88	2.20E-01	4.00E-02	0.60	0.20	[3.20]	55	6
58	Ce	137	0	7.481	9	5.00E-02	2.00E-02	2.30	0.64	[3.20]		
58	Ce	141	0	5.428	40	3.10E+00	5.00E-01	1.20	0.30	[3.20]	35	9
58	Ce	143	0	5.145	4	1.10E+00	5.00E-01			[3.20]		
59	Pr	142	2.5	5.843	107	1.10E-01	2.00E-02	1.70	0.30	[3.20]	88	9
60	Nd	143	0	6.123	26	8.60E-01	8.00E-02	1.00	0.30	[3.20]	50	8
60	Nd	144	3.5	7.817	57	3.50E-02	5.00E-03	3.80	0.40	[3.20]	86	9
60	Nd	145	0	5.755	20	4.50E-01	5.00E-02	5.10	0.90	[3.20]	47	5
60	Nd	146	3.5	7.564	114	1.70E-02	3.00E-03	3.20	0.40	[3.20]	87	9
60	Nd	147	0	5.292	31	2.90E-01	5.00E-02	3.80	0.60	[3.20]	55	8
60	Nd	148	2.5	7.333	7	3.50E-03	1.70E-03			[3.20]		
60	Nd	149	0	5.038	39	1.35E-01	2.00E-02	4.00	0.80	[3.20]	46	5
60	Nd	151	0	5.334	77	1.55E-01	2.00E-02	2.80	0.50	[3.20]	67	25
61	Pm	148	3.5	5.893	43	5.20E-03	1.20E-03	3.10	0.40	[3.20]	69	5
62	Sm	145	0	6.762	50	6.70E-01	6.00E-02	3.60	0.80	[3.34]	75	5
62	Sm	148	3.5	8.141	89	5.10E-03	5.00E-04	4.80	0.50	[3.32]	69	2
62	Sm	149	0	5.871	26	1.00E-01	2.00E-02	3.80	0.80	[3.32]		
62	Sm	150	3.5	7.985	86	2.10E-03	3.00E-04	6.30	1.20	[3.32]	62	2
62	Sm	151	0	5.598	11	4.60E-02	8.00E-03	3.40	0.60	[3.32]	87	16
62	Sm	152	2.5	8.257	62	1.04E-03	1.50E-04	3.40	0.50	[3.32]	95	4
62	Sm	153	0	5.867	41	4.80E-02	5.00E-03	3.00	0.40	[3.32]	67	5
62	Sm	155	0	5.807	22	1.14E-01	1.50E-02	2.00	0.50	[3.32]	79	13
63	Eu	152	2.5	6.307	90	7.30E-04	7.00E-05	3.20	0.40	[3.32]	92	12
63	Eu	153	3	8.550	17	5.60E-04	1.00E-04	1.40	0.60	[3.32]	160	25
63	Eu	154	2.5	6.441	70	1.10E-03	2.00E-04	2.20	0.30	[3.32]	95	12
63	Eu	155	3	8.152	19	9.20E-04	1.20E-04	1.20	0.40	[3.32]	135	25
63	Eu	156	2.5	6.338	7	4.30E-03	1.50E-03	1.90	0.50	[3.32]	96	18
64	Gd	153	0	6.246	17	1.40E-02	3.00E-03	3.80	0.80	[3.32]	54	12
64	Gd	155	0	6.435	47	1.45E-02	1.50E-03	2.00	0.40	[3.32]	88	10
64	Gd	156	1.5	8.536	92	1.70E-03	2.00E-04	2.00	0.30	[3.32]	108	10
64	Gd	157	0	6.359	33	3.00E-02	6.00E-03	2.00	0.50	[3.32]	88	12
64	Gd	158	1.5	7.938	56	4.90E-03	5.00E-04	2.20	0.40	[3.32]	97	22
64	Gd	159	0	5.942	60	8.20E-02	6.00E-03	1.50	0.20	[3.32]	105	10
64	Gd	161	0	5.635	38	2.00E-01	2.00E-02	1.80	0.40	[3.32]	111	15
65	Tb	160	1.5	6.375	201	4.20E-03	3.00E-04	1.50	0.30	[3.32]	97	7
66	Dy	161	0	6.453	34	2.70E-02	5.00E-03	2.00	0.36	[3.20]	108	10

Table 3.1. (Cont.)

66	Dy	162	2.5	8.196	53	2.40E-03	2.00E-04	1.73	0.17	[3.20]	112	10
66	Dy	163	0	6.271	72	6.20E-02	5.00E-03	1.88	0.25	[3.20]	112	20
66	Dy	164	2.5	7.658	60	6.80E-03	6.00E-04	2.02	0.30	[3.20]	113	13
66	Dy	165	0	5.716	48	1.50E-01	1.00E-02	1.70	0.25	[3.20]	114	14
67	Ho	166	3.5	6.243	150	4.20E-03	5.00E-04	1.80	0.20	[3.35]	77	5
68	Er	163	0	6.902	17	6.50E-03	1.50E-03	2.50	0.50	[3.32]		
68	Er	165	0	6.649	18	2.10E-02	4.00E-03	1.50	0.30	[3.32]		
68	Er	167	0	6.436	115	3.80E-02	3.00E-03	1.70	0.20	[3.32]	92	8
68	Er	168	3.5	7.771	124	4.20E-03	3.00E-04	2.00	0.30	[3.32]	92	12
68	Er	169	0	6.003	82	1.00E-01	1.00E-02	1.40	0.20	[3.32]	85	15
68	Er	171	0	5.681	41	1.47E-01	2.00E-02	1.50	0.20	[3.32]		
69	Tm	170	0.5	6.593	192	8.50E-03	7.00E-04	1.50	0.20	[3.32]	97	15
69	Tm	171	1	7.486	13	3.90E-03	1.00E-03	1.40	0.30	[3.32]	122	20
70	Yb	169	0	6.867	5	2.20E-02	5.00E-03	2.40	0.80	[3.20]	64	20
70	Yb	170	3.5	8.470	21	1.19E-03	1.00E-04	2.10	0.70	[3.20]	80	25
70	Yb	171	0	6.615	23	5.80E-02	2.60E-03	2.40	0.30	[3.20]	63	5
70	Yb	172	0.5	8.019	168	5.79E-03	4.80E-04	1.86	0.20	[3.20]	75	5
70	Yb	173	0	6.367	100	7.03E-02	2.60E-03	1.68	0.20	[3.20]	79	20
70	Yb	174	2.5	7.464	166	7.81E-03	9.30E-04	1.60	0.28	[3.20]	74	5
70	Yb	175	0	5.822	78	1.62E-01	1.80E-02	1.62	0.21	[3.20]	80	20
70	Yb	177	0	5.566	68	1.85E-01	1.90E-02	2.30	0.32	[3.20]	82	25
71	Lu	176	3.5	6.294	227	6.05E-03	1.50E-04	1.78	0.12	[3.32]	77	23
71	Lu	177	7	7.071	59	2.75E-03	8.50E-04	2.06	0.44	[3.32]	90	20
72	Hf	175	0	6.708	10	1.80E-02	5.00E-03	2.60	0.60	[3.32]		
72	Hf	177	0	6.381	39	3.00E-02	7.00E-03	1.70	0.40	[3.32]	60	10
72	Hf	178	3.5	7.625	94	2.40E-03	3.00E-04	2.60	0.30	[3.32]	66	10
72	Hf	179	0	6.100	48	5.70E-02	6.00E-03	2.10	0.30	[3.32]	54	5
72	Hf	180	4.5	7.387	70	4.60E-03	3.00E-04	2.50	0.40	[3.32]	66	5
72	Hf	181	0	5.696	14	9.40E-02	1.50E-02	1.90	0.60	[3.32]	50	5
73	Ta	181	1	7.576	60	1.20E-03	2.00E-04	1.90	0.30	[3.32]	51	3
73	Ta	182	3.5	6.063	418	4.20E-03	3.00E-04	1.70	0.20	[3.32]	57	3
73	Ta	183	5	6.934	9	3.50E-03	7.00E-04	1.00	0.50	[3.32]	67	3
74	W	181	0	6.680	5	2.00E-02	7.00E-03	1.00	0.50	[3.20]	70	15
74	W	183	0	6.190	47	6.00E-02	6.00E-03	2.30	0.30	[3.20]	62	15
74	W	184	0.5	7.411	59	1.20E-02	1.00E-03	1.90	0.30	[3.20]	77	12
74	W	185	0	5.755	31	7.00E-02	7.00E-03	2.80	0.40	[3.20]	69	17
74	W	187	0	5.466	32	8.50E-02	8.00E-03	2.10	0.40	[3.20]	61	8
75	Re	186	2.5	6.178	237	3.10E-03	3.00E-04	2.70	0.30	[3.20]	57	7
75	Re	188	2.5	5.871	174	4.10E-03	3.00E-04	2.50	0.30	[3.20]	61	9
76	Os	187	0	6.292	32	2.90E-02	3.00E-03	3.50	0.90	[3.36]	77	10
76	Os	188	0.5	7.989	25	4.00E-03	6.00E-04	5.00	2.30	[3.36]	88	5
76	Os	189	0	5.922	20	4.70E-02	6.00E-03	3.60	1.20	[3.36]	100	10
76	Os	190	1.5	7.792	21	3.40E-03	4.00E-04	2.00	0.60	[3.20]	100	10
76	Os	191	0	5.758	23	7.00E-02	1.00E-02			[3.20]		
76	Os	193	0	5.584	19	1.15E-01	1.00E-02			[3.20]		
77	Ir	192	1.5	6.199	41	2.50E-03	5.00E-04	1.90	0.30	[3.32]	81	11
77	Ir	193	4	7.772	11	7.00E-04	2.00E-04	1.50	0.50	[3.32]	100	20
77	Ir	194	1.5	6.066	34	7.00E-03	2.00E-03	1.30	0.30	[3.32]	93	10
78	Pt	193	0	6.255	9	2.80E-02	1.00E-02	1.80	0.60	[3.32]	80	30

Table 3.1. (Cont.)

78	Pt	195	0	6.105	6	2.00E-01	8.00E-02	1.40	0.60	[3.32]	70	25
78	Pt	196	0.5	7.921	44	1.80E-02	3.00E-03	1.80	0.40	[3.32]	120	15
78	Pt	197	0	5.846	4	3.50E-01	1.00E-01			[3.32]		
78	Pt	199	0	5.571	4	3.40E-01	9.00E-02	1.40	0.60	[3.32]		
79	Au	198	1.5	6.512	151	1.65E-02	9.00E-04	1.90	0.12	[3.32]	128	6
80	Hg	199	0	6.664	5	1.05E-01	3.50E-02	1.30	0.50	[3.32]	150	20
80	Hg	200	0.5	8.028	9	8.00E-02	3.00E-02	2.10	0.60	[3.32]	295	20
80	Hg	201	0	6.230	4	2.00E+00	1.00E+00	1.70	0.80	[3.32]		
80	Hg	202	1.5	7.753	7	9.00E-02	3.00E-02	1.20	0.50	[3.32]		
81	Tl	204	0.5	6.656	48	2.80E-01	5.00E-02	1.30	0.30	[3.32]	690	70
81	Tl	206	0.5	6.503	10	5.50E+00	1.50E+00	1.50	0.30	[3.32]	1500	300
82	Pb	205	0	6.732	29	2.00E+00	5.00E-01	1.10	0.20	[3.32]	770	
82	Pb	207	0	6.738	22	3.20E+01	6.00E+00	1.20	0.20	[3.32]		
82	Pb	208	0.5	7.367	12	3.80E+01	8.00E+00	1.00	0.50	[3.32]		
82	Pb	209	0	3.937	2	1.00E+03				[3.32]		
83	Bi	210	4.5	4.604	42	4.00E+00	7.00E-01	0.80	0.15	[3.32]	70	20
88	Ra	227	0	4.561	33	2.60E-02	6.00E-03	1.08	0.12	[3.32]	26	3
90	Th	229	0	5.239	2	5.00E-03	3.00E-03			[3.32]		
90	Th	230	2.5	6.794	11	6.20E-04	1.20E-04	1.15	0.15	[3.32]	43	4
90	Th	231	0	5.117	20	9.60E-03	1.50E-03	1.28	0.15	[3.32]	26	2
90	Th	233	0	4.786	180	1.66E-02	6.00E-04	0.87	0.07	[3.32]	24	2
91	Pa	232	1.5	5.569	44	4.50E-04	5.00E-05	0.78	0.08	[3.32]	40	2
91	Pa	234	1.5	5.222	24	7.00E-04	1.00E-04	0.75	0.08	[3.32]	47	5
92	U	233	0	5.743	12	4.60E-03	7.00E-04	1.40	0.30	[3.32]		
92	U	234	2.5	6.845	160	5.50E-04	5.00E-05	1.04	0.07	[3.32]	40	5
92	U	235	0	5.297	115	1.20E-02	8.00E-04	0.85	0.10	[3.32]	26	4
92	U	236	3.5	6.545	200	4.30E-04	2.00E-05	0.88	0.08	[3.32]	35	3
92	U	237	0	5.125	161	1.50E-02	1.00E-03	1.08	0.10	[3.32]	23	2
92	U	238	0.5	6.153	27	3.50E-03	8.00E-04			[3.32]		
92	U	239	0	4.806	473	2.08E-02	3.00E-04	1.03	0.08	[3.32]	23.6	.8
93	Np	238	2.5	5.488	270	5.70E-04	3.00E-05	0.97	0.07	[3.32]	40.8	1.2
94	Pu	239	0	5.647	26	9.00E-03	1.00E-03	1.30	0.30	[3.32]	34.	3.0
94	Pu	240	0.5	6.533	258	2.20E-03	5.00E-05	1.25	0.10	[3.32]	43.3	4.5
94	Pu	241	0	5.241	173	1.24E-02	7.00E-04	1.05	0.10	[3.32]	30.7	2.5
94	Pu	242	0.5	6.310	123	7.30E-04	8.00E-05	1.23	0.13	[3.32]	40.8	4.6
94	Pu	243	0	5.033	77	1.35E-02	1.50E-03	0.98	0.08	[3.32]	25.4	3.7
94	Pu	245	0	4.698	14	1.70E-02	5.00E-03	0.90	0.20	[3.32]		
95	Am	242	2.5	5.539	190	5.80E-04	4.00E-05	0.88	0.06	[3.32]	46.0	2.0
95	Am	243	1	6.365	24	4.00E-04	8.00E-05	1.30	0.20	[3.32]		
95	Am	244	2.5	5.363	219	7.30E-04	6.00E-05	0.98	0.06	[3.32]	39.0	5.0
96	Cm	243	0	5.694	12	1.40E-02	3.00E-03	0.65	0.15	[3.32]	38.0	6.0
96	Cm	244	2.5	6.799	40	7.50E-04	1.50E-04	1.50	0.30	[3.32]	33.0	5.0
96	Cm	245	0	5.522	38	1.18E-02	1.20E-03	1.00	0.20	[3.32]	36.	8
96	Cm	246	0.5	6.455	38	1.30E-03	2.00E-04	1.05	0.15	[3.32]	60.	10
96	Cm	247	0	5.157	9	3.00E-02	5.00E-03	0.45	0.15	[3.32]	32.	6
96	Cm	248	4.5	6.211	34	1.80E-03	3.00E-04	0.55	0.16	[3.32]	85.	15
96	Cm	249	0	4.713	33	2.80E-02	5.00E-03	1.10	0.12	[3.32]	28.	3
97	Bk	250	3.5	4.962	33	1.10E-03	1.00E-04	1.20	0.20	[3.32]	36.	2
98	Cf	250	4.5	6.621	48	7.00E-04	1.00E-04	1.20	0.20	[3.32]		
98	Cf	253	0	4.805	30	2.70E-02	4.00E-03			[3.32]		

The results of the radiative width evaluations obtained by Beijing and Obninsk groups are very close (Fig. 3.4). The uncertainties estimated by Obninsk group seem reasonable for Beijing group too. So Obninsk evaluations should be taken as recommended for the RIPL Starter File.

3.4 Conclusions and Recommendations

All recent evaluations of average neutron resonance parameters are available in the computer readable format in the RIPL Starter File. The **obninsk.dat** is recommended file, and *beijing.dat* and *minsk.dat* contain useful alternative values of the parameters. In addition, *iljinov_gc.dat* (see Chapter 5.1, p. 74, Fig. 5.3) contains recent compilation of D_0 from Troitsk, Russia. Difference of parameters obtained by different groups reflects the systematic uncertainity of parameter estimation caused by the evaluation methods used.

Obninsk evaluations of average resonance parameters seem preferable as recommended ones for most nuclei due more reliable estimation of parameter uncertainties.

REFERENCES

[3.1] C.E. Porter and R.G. Thomas, Phys. Rev. **104**, 483 (1956).

[3.2] C.E. Porter (Editor), *Statistical Theories of Spectra* (Academic Press, New York 1965).

[3.3] M.L. Mehta, *Random Matrices* (Academic Press, New York 1967).

[3.4] J. Lynn, *Theory of Neutron Resonance Reactions* (Clarendon Press, Oxford 1968).

[3.5] H.S. Camarda *et al.*, *in Statistical Properties of Nuclei*, Ed. J.B. Card. (Plenum Press, New York 1972), p. 285.

[3.6] H.L. Liou *et al.*, Phys. Rev. **C5**, 973 (1972).

[3.7] G. Delfini and H. Gruppellaar, *in* Proc. Meeting on Neutron Cross Sections of Fission Product Nuclei. (Bologna, 1979) Ed. C. Coceva, G.C. Panini. Report NEANDC(E)-209, p. 169.

[3.8] E. Fort, H. Derrien and O. Lafond, *in* Proc. Meeting on Neutron Cross Sections of Fission Product Nuclei. (Bologna, 1979) Ed. C. Coceva, G.C. Panini. Report NEANDC(E) 209, p. 121.

[3.9] F.H. Fröhner, *in* IAEA Advisory Group Meeting on Basic and Applied Problems of Nuclear Level Densities. Ed. M.R. Bhat R. Report BNL-NCS-51694 (Brookhaven 1983), p. 219.

[3.10] P. Ribon, *ibid.* p. 245.

[3.11] Zongdi Su *et al.*, *in* Proc. Meet. on Nuclear Data Evaluation Methods. Ed. C. Dunford, (New York, 1992).

[3.12] Yu.V. Porodzinski and E.Sh. Sukhovitski, *in* Proc. ISTC Workshop on Nuclear Data for Minor Actinides (May 1996), Tokai, JAERI-97-001, p.34.

[3.13] T.S. Belanova, A.V. Ignatyuk, A.B. Pashchenko and V.I. Plyaskin, *Radiative Neutron Capture - Handbook* (in Russian). (Energoatomizdat, Moscow 1986).

[3.14] S.F. Mughabghab, M. Divadeenam and N.E. Holden, *Neutron Cross Sections, vol. 1, part A* (Academic Press, New York and London, 1981).

[3.15] S.F. Mughabghab, *Neutron Cross Sections, vol. 1, part B* (Academic Press, New York and London, 1985).

[3.16] A.S. Iljinov *et al.*, Nucl. Phys. **A543**, 517 (1992).

[3.17] Zongdi Su *et al.*, Contribution to the Third CRP Meeting on RIPL (Trieste, May 1997).

[3.18] G. Rohr *et al.*, *in* Proc. Meeting on Neutron Cross Sections of Fission Product Nuclei (Bologna, 1979). Ed. C. Coceva and G.C. Panini. NEANDC(E)-209, p. 197.

[3.19] J.A. Harvay *et al.*, Phys. Rev. **C28**, 24 (1983).

[3.20] A.V. Ignatyuk, Contribution to the Second CRP Meeting on RIPL (Vienna, November 1996).

[3.21] H. Vonach *et al.*, Phys. Rev. **C38**, 2541 (1988).

[3.22] G. Rohr *et al.*, Phys. Rev. **C39**, 426 (1989).

[3.23] C.M. Perey *et al.*, Report ORNL/TM-11742 (Oak Ridge 1990).

[3.24] A. Brusegan *et al.*, *in* Nuclear Data for Science and Technology (Gatlinburg 1994). Ed. J.K. Dickens, ORNL, 1994, pp. 224 and 227.

[3.25] J.B. Garg, V.K. Tikku and J.A. Harvay, Phys. Rev. **C23**, 671; **C24**, 1922 (1981).

[3.26] A.R. Masgrov *et al.*, *in* Proc. Conf. on Neutron Physics. Harwell, 1979, p. 449.

[3.27] C.M. Frankle *et al.*, Phys. Rev. **C50**, 2774 (1994).

[3.28] V. Benzi *et al.*, *in* Proc. Meeting on Neutron Cross Sections of Fission Product Nuclei (Bologna, 1979). Ed. C. Coceva and G.C. Panini. NEANDC(E)-209, p. 169.

[3.29] D.E. Cullen and C.R. Weisbin, Nucl. Sci. Eng. **60**, 199 (1976).

[3.30] R.F. Carlton, J.A. Harvey and N.W. Hill, Phys. Rev. **C54**, 2445 (1996).

[3.31] Zongdi Su *et al.*, Contribution to the Second CRP Meeting on RIPL (Vienna, November 1996).

[3.32] A.V. Ignatyuk, Contribution to the Third CRP Meeting on RIPL (Trieste, May 1997).

[3.33] P.E. Koehler *et al.*, Phys. Rev. **C54**, 1463 (1996).

[3.34] R.L. Maklin *et al.*, Phys. Rev. **C48**, 1120 (1993).

[3.35] C.M. Frankle *et al.*, Phys. Rev. **C54**, 2051 (1996).

[3.36] R.R. Winter *et al.*, Phys. Rev. **C34**, 840 (1986).

4 Optical Model Parameters

Coordinator: P.G. Young

Summary

This chapter contains a description of the optical model Segment of the Reference Input Parameter Library. The Segment consists of some 293 optical model potentials for incident neutrons (76), protons (125), deuterons (6), tritons (26), ^{3}He (53), and ^{4}He (7). Global as well as nuclide-specific potentials are included that utilize spherical, vibrational, or rotational models. The optical model parameterizations in the Starter File are given in a very general format, which is described here in detail together with the conventions used for numbering the potentials. In general, it is recommended that nuclide-specific potentials be used for materials where careful analyses have been made. For cases where global parameterizations must be used, recommendations are included. The recommended file, which is the main RIPL optical potential file, is named **losalamos_omlib.dat**. Additionally, there are supplemental files that define the parameters and specify the format (**losalamos.readme**) and that include subroutines and short codes for accessing and summarizing the file (*losalamos_omcode.for*).

4.1 Introduction

The optical model provides the basis for many theoretical analyses and/or evaluations of nuclear cross sections that are used in providing nuclear data for applied purposes. In addition to offering a convenient means for calculation of reaction, shape elastic, and (neutron) total cross sections, optical model potentials are widely used in quantum-mechanical preequilibrium and direct-reaction theory calculations and, most importantly, in supplying particle transmission coefficients for Hauser-Feshbach statistical-theory analyses used in nuclear data evaluations. The importance of optical model parameterizations is made even more apparent by the worldwide diminution of experimental facilities for low-energy nuclear physics measurements and the consequent increased reliance on theoretical methods for providing nuclear data for applications. Therefore, the preservation of past work aimed at describing experimental results with optical model potentials is vital for future development of nuclear data bases.

The optical model Segment of the RIPL CRP is aimed at compiling and developing a Segment of optical model parameterizations that are useful in evaluations of nuclear data. The planned product of this activity is a Reference Input Parameter Library that will contain reliable, state-of-the-art parameterizations for conventional optical model codes used in calculations of nuclear data for applications. In addition to preserving optical model parameterizations for future activities, the Segment will offer a convenient means for present day evaluators to access a wide body of optical model information. Subroutines have been developed for reading and writing the data library, and eventually processing codes will be written that will permit direct interfacing of the Segment with selected optical model codes.

4.2 Optical Model Parameterization

One of the primary goals of the optical model Segment is to provide a format for optical model parameterizations that is general enough to cover all commonly used potential representations and that is easily expanded for additional types of optical potentials. For the present Starter

File we have focused on standard, Schrödinger-type forms of optical model potentials, and have included spherical, coupled-channel rotational, and simple vibrational models. Eventually, the Segment will be expanded to include more complex rotational/vibrational configurations, dispersive potentials, and perhaps even folding model potentials.

As presently formulated, potentials of the form

$$\begin{aligned} V(r) &= -V_R f_R(r) - iW_V f_V(r) + 4ia_D W_D \frac{\mathrm{d}}{\mathrm{d}r} f_D(r) \\ &+ \frac{\lambda\!\!\!^{-2}_{\pi}}{r}\left[V_{SO}\frac{\mathrm{d}}{\mathrm{d}r} f_{VSO}(r) + iW_{SO}\frac{\mathrm{d}}{\mathrm{d}r} f_{WSO}(r)\right]\sigma\cdot l \end{aligned} \tag{4.1}$$

are allowed. In Eq. (4.1) V_R and W_V are the real and imaginary volume potential well depths, W_D is the well depth for the surface derivative term, V_{SO} and W_{SO} are the real and imaginary well depths for the spin-orbit potential, and $\lambda\!\!\!^{-2}_{\pi}$ is the pion Compton wavelength squared ($\simeq 2$). The quantity $\sigma\cdot l$ is the scalar product of the intrinsic and orbital angular momentum operators and is given by

$$\begin{aligned} \sigma\cdot l &= l \qquad\qquad \text{for } j = l + \frac{1}{2} \\ &= -(l+1) \qquad \text{for } j = l - \frac{1}{2}. \end{aligned} \tag{4.2}$$

The $f_i(r)$ are radial-dependent form factors and are defined below.

Any incident particle is permitted by the format, but we have limited our initial file to incident neutrons, protons, deuterons, tritons, ^{3}He, and ^{4}He particles. Our approach is to supply a general form for optical model potentials that is an extension of the representation implemented in the SCAT2 optical model code [4.1] and that describes most of the parameterizations commonly used in the past. Additionally, three more specialized formats are formulated that describe particular, less common, forms of potentials but which offer promise of being important for applied purposes.

The general form of the optical model potential used here is the following:

$$\begin{aligned} V_i(E) &= \alpha_1 + \alpha_7\eta + \alpha_8\Delta_c + \alpha_9 A + \alpha_{10}A^{1/3} + \alpha_{11}A^{-2/3} + \alpha_{12}\Delta_{c'} \\ &+(\alpha_2 + \alpha_{13}\eta + \alpha_{14}A)E + \alpha_3 E^2 + \alpha_4 E^3 + \alpha_6\sqrt{E} \\ &+(\alpha_5 + \alpha_{15}\eta + \alpha_{16}E)\ln(E) + \alpha_{17}\Delta_c E^{-2}, \end{aligned} \tag{4.3}$$

where $V_i(E)$ designates the i^{th} term of the potential (for example, V_R, W_D, V_{SO}, etc.) at incident laboratory energy E, $\eta = (N-Z)/A$, N and Z are the neutron and proton numbers of the target nucleus, and A is the atomic mass of the target. Two different forms of correction terms for Coulomb repulsion with incident protons are provided:

$$\Delta_c = \frac{0.4Z}{A^{1/3}} \quad \text{and} \quad \Delta_{c'} = \frac{1.73Z}{R_c}, \tag{4.4}$$

where R_c is the Coulomb radius. Δ_c and $\Delta_{c'}$ are zero for incident neutrons. Each of the potential terms in Eq. (4.1) can be represented over any number of defined energy ranges using as many of the terms given in Eq. (4.3) as required, with the coefficients of the unused terms set to zero.

The first special form of the potential is used to represent the potential of Smith *et al.* [4.2] and to accommodate exponential forms included in the Engelbrecht and Fiedeldey potential [4.3]:

$$V_i(E) = \alpha_1 + \alpha_2\eta + \alpha_3\cos[2\pi(A-\alpha_4)/\alpha_5] + \alpha_6\exp(\alpha_7 E + \alpha_8 E^2) + \alpha_9 E\exp(\alpha_{10}E^{\alpha_{11}}). \tag{4.5}$$

This formulation is activated by setting $\alpha_{18} > 0$.

The second special form is necessary to represent the potential determined in an extensive analysis of proton scattering cross sections and polarizations by Varner *et al.* [4.4], as well as an exponential form permitted in the SCAT2 code [4.1]:

$$V_i(E) = \frac{\alpha_1 + \alpha_2\eta}{1 + \exp\left(\frac{\alpha_3 - E + \alpha_4\Delta_{c'}}{\alpha_5}\right)} + \alpha_6 \exp\left(\frac{\alpha_7 E - \alpha_8}{\alpha_6}\right). \tag{4.6}$$

The formulation in Eq. (4.6) is activated by setting $\alpha_{19} > 0$.

Finally, the third special form, which was developed by Delaroche, is activated by setting $\alpha_{20} > 0$ and is used by Koning, van Wijk, and Delaroche [4.5] in a recent analysis of neutron reactions with isotopes of Zr

$$\begin{aligned} V_i(E) = \alpha_1 + \alpha_2 E + \alpha_3 \exp\left[-\alpha_4(E - \alpha_5 E_f)\right] + \frac{\alpha_6(E - E_f)^{\alpha_8}}{(E - E_f)^{\alpha_8} + (\alpha_7)^{\alpha_8}} \\ + \alpha_9 \exp[-\alpha_{10}(E - E_f)] \frac{(E - E_f)^{\alpha_{12}}}{(E - E_f)^{\alpha_{12}} + (\alpha_{11})^{\alpha_{12}}} \end{aligned} \tag{4.7}$$

where E_f is the Fermi energy in MeV and is given by

$$\begin{aligned} E_f &= -0.5\,[S_n(Z,A) + S_n(Z,A+1)] \qquad \text{(for incident neutrons)} \\ &= -0.5\,[S_p(Z,A) + S_p(Z+1,A+1)] \qquad \text{(for incident protons)}, \end{aligned} \tag{4.8}$$

where $S_n(Z,A)$ and $S_p(Z,A)$ are the neutron and proton separation energies for nucleus (Z,A).

Either Woods-Saxon or Gaussian form factors are permitted for the $f_i(r)$ terms in Eq. (4.1), that is,

$$f_i(r) = \frac{1}{1 + \exp\left(\frac{r - R_i}{a_i}\right)} \qquad \text{(Woods} - \text{Saxon form)} \tag{4.9}$$

or

$$f_i(r) = \exp\left(\frac{-(r - R_i)^2}{a_i^2}\right) \qquad \text{(Gaussian form)}. \tag{4.10}$$

The nuclear radius is given by $R_i = r_i A^{1/3}$ where r_i is given by

$$\begin{aligned} r_i(E) &= \beta_1 + \beta_2 E + \beta_3\eta + \beta_4 A^{-1} + \beta_5 A^{-1/2} + \beta_6 A^{2/3} + \beta_7 A \\ &\quad + \beta_8 A^2 + \beta_9 A^3 + \beta_{10} A^{1/3} + \beta_{11} A^{-1/3} \end{aligned} \tag{4.11}$$

and a similar form is used for the diffuseness, a_i,

$$\begin{aligned} a_i(E) &= \delta_1 + \delta_2 E + \delta_3\eta + \delta_4 A^{-1} + \delta_5 A^{-1/2} + \delta_6 A^{2/3} + \delta_7 A \\ &\quad + \delta_8 A^2 + \delta_9 A^3 + \delta_{10} A^{1/3} + \delta_{11} A^{-1/3}. \end{aligned} \tag{4.12}$$

Note that the $\beta_{11} A^{-1/3}$ term in Eq. (4.11) permits the inclusion of a constant (A-independent) quantity to the radius, that is, $R_i = r_o + r_i' A^{1/3} = \beta_{11} + r_i' A^{1/3}$, where r_i' includes terms in Eq. (4.11) through β_{10}.

The format also permits inputting of the relevant parameters for coupled-channel rotational, vibrational, and non-axial deformed models, including energies, spins and parities of vibrational and rotational states, deformation parameters, softness parameters, etc., that are required for the various models. At present the format is considered reasonably complete for spherical and rotational models, which permits calculations with codes like SCAT2 [4.1] for spherical models

and ECIS94 [4.6] for rotational and vibrational models. Extensions to the format are needed for certain forms of vibrational and non-axial deformed models.

Details of the format for the optical model parameterizations are given in Annex A. The description in Annex A is included in the **losalamos.readme** file in the RIPL data base at the IAEA/NDS.

4.3 Contents of the Optical Model Segment

To date, some 293 optical model parameterizations are included in the Segment. These potentials have been selected mainly from analyses made at Los Alamos for various applied calculations [4.7, 4.8]; from a set of parameters supplied by workers from the Japan Atomic Energy Research Institute, from the Bhabha Atomic Research Institute; and others specifically for the RIPL Starter File; and from several well known global optical model parameterizations. There are several optical model potential compilations and/or general references available that are useful in compiling data on potentials. For example, Perey and Perey [4.9] and Young [4.10] for neutrons; Mehta and Kailas [4.11] for low-energy protons; Daehnick *et al.* [4.12] and Bojowald *et al.* [4.13] for deuterons; and Avrigeanu *et al.* [4.14] for alpha particles.

Each potential included in the RIPL is given a unique reference number, according to a numbering system that is described in Annex B. This system was adopted in order to separate the potentials for different incident particles into different reference number regions, and to provide approximate information on the sources of the various potentials by geographical region. The latter information might be used, for example, if one wished to use only potentials from a particular source for a given set of calculations (for example, JAERI). To be very useful, of course, many more potentials must be added to the Starter File, for example, from China, Japan, Russia, Bologna, and the JEFF and ENDF communities in general. In addition to the numbering rules given in Annex B, we are following an informal numbering convention for neutron and proton potentials that are related through isospin by means of the Lane model [4.15]; that is, we assign a 3-digit reference number to the potential and then add 3000 for incident neutrons and 5000 for incident protons.

An example of a complete entry for one reference in the Starter File is given in Annex C. The example follows the format given in Annex A and the numbering convention in Annex B. The reference number (600) indicates that the incident particle is a neutron and that the source of the potential is a former Soviet Union country.

Summary information on all the potentials compiled thus far is given in Annex D, together with references for each potential. To date, the Segment includes 76 optical model parameterizations for incident neutrons, 125 parameterizations for incident protons, 6 for incident deuterons, 26 for incident tritons, 53 for incident ^{3}He particles, and 7 parameterizations for incident alpha particles.

4.4 Files in the Optical Model Segment

As described above, the recommended optical model parameter file in the RIPL Starter File is the **losalamos_omlib.dat** file. The format, numbering convention, and file summary is included in the **losalamos.readme** file. In addition, a second file, *losalamos_omcode.for*, is included in the RIPL supplemental file area and is comprised of the following:

1. OMSUMRY — a Fortran code that reads the **losalamos_omlib.dat** file and produces a summary of the authors, reference, and descriptive information for the entire file;

2. OMTABLE — a Fortran code that makes an abbreviated summary of the **losalamos_omlib.dat** file together with a list of the references (see Annex D);

3. OMIN — a Fortran subroutine that reads a single reference from the **losalamos_omlib.dat** file;

4. OMOUT — a Fortran subroutine that writes a single reference in the format used by the **losalamos_omlib.dat** file.

In addition to the main optical potential file described here, two supplemental optical model potential files, one from China (*beijing.dat*) and one from Japan (*jaeri.dat*), are also included as supplemental files in the RIPL Starter File. These potentials, which are in different formats from the main file, will eventually be merged into the main RIPL file but are made available now for the convenience of interested users. Please note that there is some duplication of potentials between these two supplemental files and the main RIPL file.

4.5 Validation of the Optical Model Segment

Validation of the potentials in the Segment must be carried out at two levels: (1) ensuring that the potentials in the Segment are both complete and accurate, and (2) testing how well the potentials agree with the available experimental data base. Some effort has been directed at checking the accuracy of entries into the file by careful proofreading. Additional efforts are needed in this area and, in particular, a processing code should be developed that will retrieve information from the file and print it out in standard, easily readable form.

We have also began efforts to compare a few of the potentials with experimental data, as reported by Kumar *et al.* [4.16]. In this study neutron total, reaction, and elastic scattering cross sections are compared with experimental data for 6 global potentials and 5 regional or nuclide-specific potentials. Examples of the results of comparisons obtained by Kumar *et al.* are included in Fig. 4.1, which compares calculated and measured total neutron cross sections for ^{12}C, and Fig. 4.2, which compares measured and calculated neutron reaction cross sections for ^{27}Al. It should be noted that the Kumar calculations for global optical potentiuals in Figs. 4.1 and 4.2 exceed the energy ranges of validity for all the potentials considered, so caution should be exercised in interpreting these comparions.

Additionally, the volume integrals from global potentials can be compared with the ones obtained from "best-fit" potentials for specific target nuclei. This exercise enables identification of the global potential that is closest to the best-fit potential and, in combination with cross section comparisons as described above, can serve as a basis for parameter recommendations. An example is given in Fig. 4.3 where the volume integrals computed for the ^{208}Pb+n system are shown for well known global potentials and some best-fit potentials.

4.6 Conclusions and Recommendations

Because of the limited number of potentials included in the Segment thus far and, especially, because of the very limited testing done, it is not possible to make general recommendations for optical model potentials at present. However, some specific comments can be made. In every

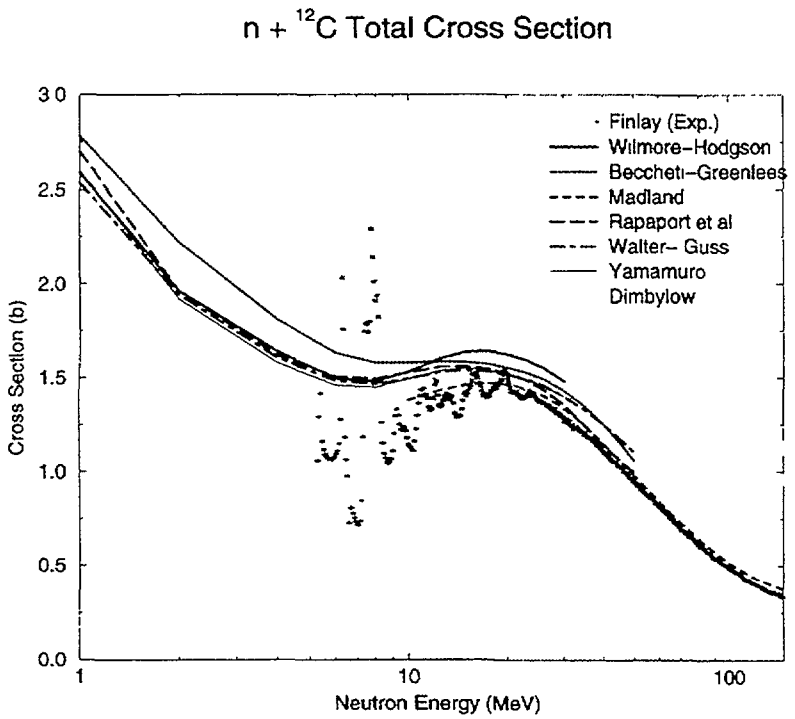

Figure 4.1: Calculated and measured neutron total cross sections for ^{12}C.

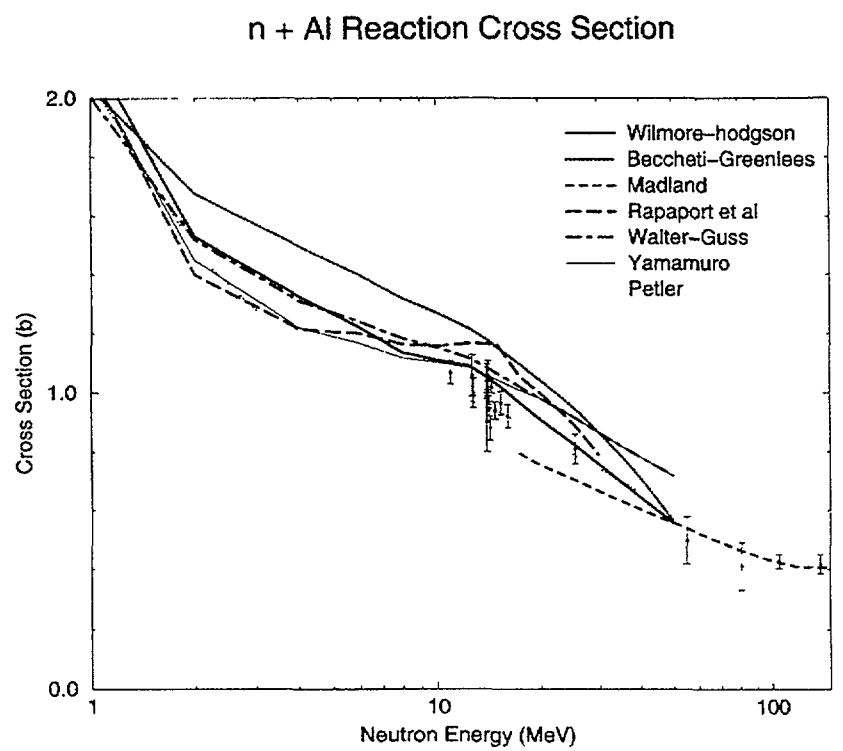

Figure 4.2: Calculated and measured neutron reaction cross sections for ^{27}Al.

case where local potentials were compared by Kumar *et al.* [4.16] to global potentials, the local parameterizations produced better agreement with the experimental data than did the global potentials. So one firm conclusion is that additional, carefully-chosen nuclide-specific potentials should be included in the RIPL Starter File. Also it was observed that, if a global optical

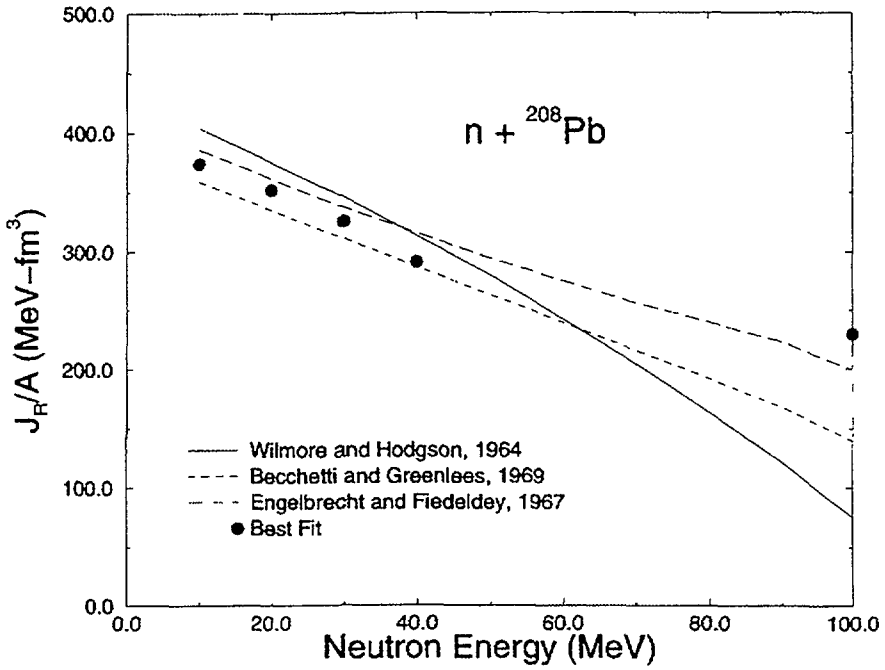

Figure 4.3: Comparison of volume integrals computed from global and "best-fit" optical model parameterizations for the ^{208}Pb+n system.

potential must be used for incident neutrons, then the Wilmore and Hodgson [4.17] potential often gave reasonable results below 30 MeV in the limited tests performed, and the Madland Semmering potential [4.18] usually gave reasonable results for both neutrons and protons from 30 to 200 MeV. These latter conclusions are particularly applicable for Hauser-Feshbach calculations where the reaction cross section is quite important. However, it should be again emphasized that the parameterizations included and the comparisons with experiment that have been made are very limited in scope and should be expanded.

The largest differences in the reaction cross sections calculated with the various potentials by Kumar *et al.* occurred at fairly low energies, which were not tested in the comparisons. To test the low energy reaction and elastic cross section predictions requires carrying out Hauser-Feshbach calculations. Such tests should clearly be performed.

In conclusion, it can be said that we have succeeded in developing an initial or Starter File of optical model parameterizations in a format that is easily expanded, together with initial codes and subroutines for handling the data. While the existing Starter File already promises to be useful, it is essential that follow-on activities occur to enhance its usefulness. A summary of improvements or areas where additional work is needed includes:

1. Additional potentials must be incorporated into the Segment. For example, potentials from programs in China, Japan, Russia, Bologna, and the JEFF and ENDF communities must be added.

2. Additional processing codes should be developed for checking, displaying, linking of the Segment to optical model codes, and comparing predictions from the parameter file with experimental data.

3. Extensive checking and validation of the Segment, especially when more processing codes become available.

As a final note, we should point out that most of the presently available optical model potentials have been derived over very limited energy and mass regions. For example, the Wilmore-Hodgson potential, which we recommend for use in certain circumstances, was derived at incident neutron energies between 1 and 15 MeV. Similarly, the recommended Madland Semering potential was derived over the energy range 50 MeV to 400 MeV. This obviously leaves a gap between 15 and 50 MeV where no potential is recommended. If, nonetheless, these two potentials are used over this energy range and are joined at, say, 30 MeV, then not only are they being used outside their range of validity but also a discontinuity results at 30 MeV. It is important that there be no such discontinuities in calculations of cross sections for applications.

The only potential having a truly broad energy range of validity in the present Segment is that of Koning, Wijk and Delaroche [4.5] for neutron reactions on ^{90}Zr (potential segment number 2404), which covers the neutron energy range from 0 to 220 MeV. Special mention should be made of the greatly advanced methodology used to derive this potential and the tremendous promise it offers for improved potentials in the future [4.19]. We are hopeful that in the coming years this methodology will be broadly applied over wide mass and energy ranges to produce greatly improved potentials for nuclear data calculations.

REFERENCES

[4.1] O. Bersillon, Report CEA-N-2227 (1978), and *in* Proc. ICTP Workshop on Computation and Analysis of Nuclear Data Relevant to Nuclear Energy and Safety, 10 February - 13 March, 1992, Trieste, Italy.

[4.2] A.B. Smith, P.T. Guenther and J.F. Whalen, Nucl. Phys. **A415**, 1 (1984).

[4.3] C.A. Engelbrecht and H. Fiedeldey, Ann. Phys. **42**, 262 (1967).

[4.4] R.L. Varner, W.J. Thompson, T.L. McAbee, E.J. Ludwig and T.B. Clegg, Phys. Rep. **201**, 57 (1991).

[4.5] A.J. Koning, J.J. van Wijk and J.P. Delaroche, personal communication (March, 1997).

[4.6] J. Raynal, personal communication through A. Koning (1996).

[4.7] P.G. Young, Report LA-UR-94-3104 (Los Alamos National Lab. 1994).

[4.8] P.G. Young, Report LA-UR-95-3654 (Los Alamos National Lab. 1995).

[4.9] C.M. Perey and F.G. Perey, Atomic Data Nucl. Data Tbl. **17**, 1 (1976).

[4.10] P.G. Young, *in* Proc. Specialists' Meeting on Use of the Optical Model for the Calculation of Neutron Cross Sections below 20 MeV, sponsored by the NEA NDC, Nov. 13-15, 1985, Chateau de la Muette, Paris, France, OECD/NEA Report NEANDC-222'U' (1986) p. 127 .

[4.11] M.K. Mehta and S. Kailas, Pramana. J. Phys. **27**, 139 (1986).

[4.12] W.W. Daehnick, J.D. Childs and Z. Vrcelj, Phys. Rev. **C21**, 2253 (1980).

[4.13] J. Bojowald, H. Machner, H. Nann, W. Oelert, M. Rogge and P. Turek, Phys. Rev. **C38**, 1153 (1988).

[4.14] V. Avrigeanu, P.E. Hodgson, and M. Avrigeanu, Phys. Rev. **C49**, 2136 (1994); see also M. Avrigeanu and V. Avrigeanu, Report NP-83-1994 (Inst. Atomic Phys. Bucharest 1994).

[4.15] A.M. Lane, Nucl. Phys. **35**, 676 (1962).

[4.16] A. Kumar, P.G. Young and M.B. Chadwick, Report LA-UR-97-1454 (Los Alamos National Laboratory 1997).

[4.17] D. Wilmore and P.E. Hodgson, Nucl. Phys. **55**, 673 (1964).

[4.18] D.G. Madland, *in* Proc. Specialists' Meeting Preequilibrium Nuclear Reactions, Semmering, Austria, 10-12 February 1988. Ed. B. Strohmaier, Report NEANDC-245 'U' (1988), p. 103.

[4.19] O. Bersillon *et al.*, to be published.

Annex A

OPTICAL MODEL PARAMETER FORMAT

```
iref
author
reference
summary
emin,emax
izmin,izmax
iamin,iamax
imodel,izproj,iaproj

       *****LOOP: i=1,5
jrange(i)
       *****LOOP j=1,jrange
epot(i,j)
(rco(i,j,k), k=1,11)
(aco(i,j,k), k=1,11)
(pot(i,j,k), k=1,20)
       *****END i AND j LOOPS

jcoul
       *****LOOP j=1,jcoul
ecoul(j),rcoul(j),rcoul0(j),beta(j)
       *****END j LOOP

    (1)*****SKIP TO (2)***** IF IMODEL NOT EQUAL TO 1

nisotopes
       *****LOOP n=1,nisotopes
iz(n),ia(n),ncoll(n),lmax(n),idef(n),bandk(n),[def(j,n),j=2,idef(n),2]
       *****LOOP k=1,ncoll(n)
ex(k,n),spin(k,n),ipar(k,n)
       *****END k AND n LOOPS

    (2)*****SKIP
TO (3)***** IF IMODEL NOT EQUAL TO 2

nisotopes
       *****LOOP n=1,nisotopes
iz(n),ia(n),nvib(n)
       *****LOOP k=1,nvib(n)
exv(k,n),spinv(k,n),iparv(k,n),nph(k,n),defv(k,n),thetm(k,n)
       *****END k LOOP
       *****END n LOOP

    (3)*****SKIP REMAINING LINES IF IMODEL NOT EQUAL TO 3

nisotopes
       *****LOOP n=1,nisotopes
iz(n),ia(n),beta0(n),gamma0(n),xmubeta(n)
       *****END n LOOP
```

```
      iref  = unique fixed point reference number for this potential
    author  = authors for this potential (up to 80 characters, 1 line)
 reference  = reference for this potential (up to 80 characters, 1 line)
   summary = short description of the potential (320 characters, 4 lines)
 emin,emax  = minimum and maximum energies for validity of this potential
izmin,izmax = minimum and maximum Z values for this potential
iamin,iamax = minimum and maximum A values for this potential
    imodel  = 0 for spherical potential
            = 1 for coupled-channel, rotational model
            = 2 for vibrational model
            = 3 for non-axial deformed model
    izproj  = Z for incident projectile
    iaproj  = A for incident projectile
    index i = 1 real potential (Woods-Saxon)
            = 2 surface imaginary potential
            = 3 volume imaginary potential (Woods-Saxon)
            = 4 real spin-orbit potential
            = 5 imaginary spin-orbit potential
    jrange  = number of energy ranges over which the potential is specified
            = positive for potential strengths
            = negative for volume integrals
            = 0 if potential of type i not used
  epot(i,j) = upper energy limit for jth energy range for potential i
  rco(i,j,k)= coefficients for multiplying A**(1/3) for
              specification of radius R in fm where:

     R(i,j) = {abs[rco(i,j,1)] + rco(i,j,2)*E + rco(i,j,3)*eta
              + rco(i,j,4)/A + rco(i,j,5)/sqrt(A)
              + rco(i,j,6)*A**(2/3) + rco(i,j,7)*A
              + rco(i,j,8)*A**2  + rco(i,j,9)*A**3
              + rco(i,j,10)*A**(1/3)
              + rco(i,j,11)*A**(-1/3)} * [A**(1/3)]

and

if rco(2,j,1) >0.0: Woods-Saxon derivative surface potential
if rco(2,j,1) <0.0: Gaussian surface potential.

[Note that the A dependence of rco(i,j,11) cancels out so that
rco(i,j,11) is equivalent to adding a constant of that magnitude to
the radius R(i,j)].


 aco(i,j,k) = coefficients for specification of diffuseness a in

          fm where:

     a(i,j) = abs(aco(i,j,1)) + aco(i,j,2)*E + aco(i,j,3)*eta
                + aco(i,j,4)/A + aco(i,j,5)/sqrt(A)
                + aco(i,j,6)*A**(2/3) + aco(i,j,7)*A
                + aco(i,j,8)*A**2 + aco(i,j,9)*A**3
                + aco(i,j,10)*A**(1/3) + aco(i,j,11)*A**(-1/3)

 pot(i,j,k) = strength parameters, as follows:
```

```
if pot(i,j,k>17) .eq. 0, then

V(i,j) = pot(i,j,1) + pot(i,j,7)*eta + pot(i,j,8)*Ecoul
       + pot(i,j,9)*A + pot(i,j,10)*A**(1/3)
       + pot(i,j,11)*A**(-2/3) + pot(i,j,12)*Ecoul2
       + [pot(i,j,2) + pot(i,j,13)*eta + pot(i,j,14)*A]*E
       + pot(i,j,3)*E*E + pot(i,j,4)*E*E*E + pot(i,j,6)*sqrt(E)
       + [pot(i,j,5) + pot(i,j,15)*eta + pot(i,j,16)*E]*ln(E)
       + pot(i,j,17)*Ecoul/E**2

if pot(i,j,18) .ne. 0, then

V(i,j) = pot(i,j,1) + pot(i,j,2)*eta
       + pot(i,j,3)*cos[2*pi*(A - pot(i,j,4))/pot(i,j,5)]
       + pot(i,j,6)*exp[pot(i,j,7)*E + pot(i,j,8)*E*E]
       + pot(i,j,9)*E*exp[pot(i,j,10)*E**pot(i,j,11)]

if pot(i,j,19) .ne. 0, then

V(i,j) = [pot(i,j,1) + pot(i,j,2)*eta]/
       {1 + exp[(pot(i,j,3) - E + pot(i,j,4)*Ecoul2)/pot(i,j,5)]}
       + pot(i,j,6)*exp[(pot(i,j,7)*E - pot(i,j,8))/pot(i,j,6)]

if pot(i,j,20) .ne. 0, then

V(i,j) = pot(i,j,1) + pot(i,j,2)*E
       + pot(i,j,3)*exp[-pot(i,j,4)*(E - pot(i,j,5)*EF)]
       + pot(i,j,6)*[(E-EF)**pot(i,j,8)]/[(E-EF)**pot(i,j,8)
       + pot(i,j,7)**pot(i,j,8)]
       + pot(i,j,9)*exp[-pot(i,j,10)*(E-EF)]*[(E-EF)**pot(i,j,12)]
       /[(E-EF)**pot(i,j,12) + pot(i,j,11)**pot(i,j,12)]


where
     E      = projectile laboratory energy in MeV
     eta    = (N-Z)/A
     Ecoul  = 0.4Z/A**(1/3)
     Ecoul2 = 1.73*Z/RC
     EF     = Fermi energy in MeV
            = -0.5*[SN(Z,A) + SN(Z,A+1)]   (for incident neutrons)
            = -0.5*[SP(Z,A) + SP(Z+1,A+1)] (for incident protons)
    SN(Z,A) = the neutron separation energy for nucleus (Z,A)
    SP(Z,A) = the proton separation energy for nucleus (Z,A).

And, continuing the definitions:

    jcoul    = number of energy ranges for specifying coulomb
               radius and nonlocality range
   ecoul(j)  = maximum energy of coulomb energy range j
   rcoul(j), = coefficients to determine the coulomb radius,
   rcoul0(j)   RC, from the expression
                          RC = rcoul*A**(1/3) + rcoul0
    beta(j)  = nonlocality range.  Note that when beta(j).ne.0.,
               then the imaginary potential is pure derivative
               Woods-Saxon for energy range j.
  nisotopes  = number of isotopes for which deformation parameters
               and discrete levels are given
     iz,ia   = Z and A for the deformation parameters and discrete
               levels that follow
```

```
 ncoll   = number of collective states in the coupled-channel
           rotational model for this iz, ia
  lmax   = maximum l value for multipole expansion
  idef   = largest order of deformation
 bandk   = k for the rotational band
   def   = deformation parameters, l=2,4,6,...through lmax
    ex   = rotational level excitation energy (MeV)
  spin   = rotational level spin
  ipar   = rotational level parity
  nvib   = number of vibrational states in the model for this iz, ia
   exv   = vibrational level excitation energy (MeV)
 spinv   = vibrational level spin
 iparv   = vibrational level parity
   nph   = 1 for pure 1-photon state
         = 2 for pure 2-photon state
         = 3 for mixture of 1- and 2-photon states
  defv   = vibrational model deformation parameter
 thetm   = mixing parameter (degrees) for nph=3
 beta0   = beta deformability parameter
gamma0   = gamma deformability parameter
xmubeta  = non-axiality parameter
```

Annex B

REFERENCE NUMBERING SYSTEM

DEFINITION ===> IREF = 1000*I + JREF

Incident Particles (leading digit, I)

IREF	I	Particle
1 - 3999	0 - 3	Neutrons
4000 - 5999	4 - 5	Protons
6000 - 6999	6	Deuterons
7000 - 7999	7	Tritons
8000 - 8999	8	He-3
9000 - 9999	9	He-4

Geographic Indicators (trailing 3 digits, JREF)

JREF	Region
1- 99	Los Alamos National Laboratory (LANL)
100 - 199	Other U.S. laboratories, universities
200 - 299	Japan, JAERI
300 - 399	Russia
400 - 499	Western Europe, JEF community
500 - 599	China
600 - 649	Former Soviet Union
650 - 699	India, Pakistan
700 - 799	Others
800 - 999	Reserved

Annex C

EXAMPLE OF A POTENTIAL

```
  600
G. Vladuca, A. Tudora, M. Sin
Rom. J. Phys.,tome 41, no. 7-8 (1996) 515-526
Regional phenomenological deformed optical potential for neutron interactions
with actinides. Coupled-channels calculations performed with ECIS-95 code


    0.001    20.000
   90  103
  227  260
    1    0    1
    1
    20.000
     1.25600  0.00000+0  0.00000+0  0.00000+0  0.00000+0  0.00000+0  0.00000+0
              0.00000+0  0.00000+0  0.00000+0  0.00000+0
     0.62000  0.00000+0  0.00000+0  0.00000+0  0.00000+0  0.00000+0  0.00000+0
              0.00000+0  0.00000+0  0.00000+0  0.00000+0
    51.32134 -5.70000-1  2.00000-2  0.00000+0  0.00000+0  0.00000+0 -2.40000+1
              0.00000+0  0.00000+0  0.00000+0  0.00000+0  0.00000+0  0.00000+0
              0.00000+0  0.00000+0  0.00000+0  0.00000+0  0.00000+0  0.00000+0
              0.00000+0
    1
    20.000
     1.26000  0.00000+0  0.00000+0  0.00000+0  0.00000+0  0.00000+0  0.00000+0
              0.00000+0  0.00000+0  0.00000+0  0.00000+0
     0.58000  0.00000+0  0.00000+0  0.00000+0  0.00000+0  0.00000+0  0.00000+0
              0.00000+0  0.00000+0  0.00000+0  0.00000+0
     5.04567  4.00000-1  1.00000-3  0.00000+0  0.00000+0  0.00000+0  0.00000+0
              0.00000+0  0.00000+0  0.00000+0  0.00000+0  0.00000+0  0.00000+0
              0.00000+0  0.00000+0  0.00000+0  0.00000+0  0.00000+0  0.00000+0
              0.00000+0
    0
    1
    20.000
     1.12000  0.00000+0  0.00000+0  0.00000+0  0.00000+0  0.00000+0  0.00000+0
              0.00000+0  0.00000+0  0.00000+0  0.00000+0
     0.50000  0.00000+0  0.00000+0  0.00000+0  0.00000+0  0.00000+0  0.00000+0
              0.00000+0  0.00000+0  0.00000+0  0.00000+0
     6.00000  0.00000+0  0.00000+0  0.00000+0  0.00000+0  0.00000+0  0.00000+0
              0.00000+0  0.00000+0  0.00000+0  0.00000+0  0.00000+0  0.00000+0
              0.00000+0  0.00000+0  0.00000+0  0.00000+0  0.00000+0  0.00000+0
              0.00000+0
    0
    0
    7
   90  232    5    4    4  0.0  1.950E-01  8.200E-02
  0.00000000    0.0   1
  0.04936900    2.0   1
  0.16212000    4.0   1
  0.33320000    6.0   1
  0.55690000    8.0   1
   92  233    5    4    4  2.5  2.200E-01  7.000E-02
  0.00000000    2.5   1
  0.04035000    3.5   1
  0.09219000    4.5   1
```

```
0.15527000    5.5   1
0.22940000    6.5   1
 92  238    5    4    4  0.0  1.980E-01  5.700E-02
0.00000000    0.0   1
0.04491000    2.0   1
0.14841000    4.0   1
0.30721000    6.0   1
0.51830000    8.0   1
 94  239    5    4    4  0.5  2.200E-01  7.000E-02
0.00000000    0.5   1
0.00786100    1.5   1
0.05727600    2.5   1
0.07570600    3.5   1
0.16376000    4.5   1
 94  240    5    4    4  0.0  2.000E-01  7.000E-02
0.00000000    0.0   1
0.04282400    2.0   1
0.14169000    4.0   1
0.29431900    6.0   1
0.49752000    8.0   1
 94  242    5    4    4  0.0  2.180E-01  4.600E-02
0.00000000    0.0   1
0.04454000    2.0   1
0.14730000    4.0   1
0.30640000    6.0   1
0.51810000    8.0   1
 95  241    5    4    4  2.5  2.200E-01  3.600E-02
0.00000000    2.5  -1
0.04117600    3.5  -1
0.09365000    4.5  -1
0.15800000    5.5  -1
0.23400000    6.5  -1
```

Annex D

SUMMARY OF ENTRIES AND REFERENCES

This annex contains a short summary of the optical model parameterizations that are included in the initial version of the RIPL optical potential data file. The results are given in tabular form (Table D-1), with each entry summarized in a single line and with a complete list of the references included in the Segment. The table and reference list were obtained using the OMTABLE computer code, which is included in the IAEA/NDS RIPL Starter File.

TABLE D-1. SUMMARY OF OPTICAL MODEL PARAMETERIZATIONS INCLUDED IN THE RIPL STARTER FILE

Lib. No.	Inc. Part.	Model Type	Z-Range	A-Range	E-Range (MeV)	Ref. No.	First Author
1	n	CC rot.	93-93	237-237	0.0- 30.0	1	P.G.Young
2	n	vibra.	82-82	208-208	0.0-200.0	2	H.Vonach
3	n	CC rot.	92-92	235-235	0.0- 30.0	1	P.G.Young
4	n	CC rot.	92-92	237-237	0.0- 30.0	3	P.G.Young
5	n	CC rot.	92-92	238-238	0.0- 30.0	3	P.G.Young
6	n	CC rot.	94-94	242-242	0.0- 20.0	4	D.G.Madland
7	n	CC rot.	94-94	239-239	0.0- 30.0	3	P.G.Young
8	n	CC rot.	95-95	241-243	0.0- 30.0	5	P.G.Young
9	n	spher.	90-95	230-250	0.0- 10.0	6	D.G.Madland
10	n	spher.	26-26	54- 56	0.0- 52.0	7	E.D.Arthur
11	n	spher.	27-27	59- 59	0.0- 27.5	8	E.D.Arthur
12	n	spher.	30-30	57- 81	0.0- 20.0	9	P.G.Young
13	n	spher.	39-39	89- 89	0.0- 21.0	10	E.D.Arthur
14	n	spher.	40-40	90- 90	0.0- 20.0	10	E.D.Arthur
15	n	spher.	6- 6	12- 12	0.0- 65.0	11	M.B.Chadwick
16	n	spher.	7- 7	14- 14	0.0- 60.0	11	M.B.Chadwick
17	n	spher.	8- 8	16- 16	0.0- 50.0	11	M.B.Chadwick
100	n	spher.	20-92	40-238	10.0- 50.0	12	F.D.Becchetti
101	n	spher.	12-83	24-209	11.0- 11.0	13	J.C.Ferrer
102	n	spher.	82-82	206-208	5.0- 50.0	14	R.W.Finlay
103	n	spher.	26-26	56- 56	0.0-100.0	15	A.Prince
104	n	spher.	26-26	54- 54	0.0-100.0	15	A.Prince
105	n	spher.	26-26	57- 57	0.0-100.0	15	A.Prince
106	n	spher.	26-26	58- 58	0.0-100.0	15	A.Prince
107	n	spher.	28-28	58- 58	0.0-100.0	15	A.Prince
108	n	spher.	28-28	60- 60	0.0-100.0	15	A.Prince
109	n	spher.	28-28	61- 61	0.0-100.0	15	A.Prince
110	n	spher.	28-28	62- 62	0.0-100.0	15	A.Prince
111	n	spher.	28-28	64- 64	0.0-100.0	15	A.Prince
112	n	spher.	24-24	50- 50	0.0-100.0	15	A.Prince
113	n	spher.	24-24	53- 53	0.0-100.0	15	A.Prince
114	n	spher.	24-24	52- 52	0.0-100.0	15	A.Prince
115	n	spher.	24-24	54- 54	0.0-100.0	15	A.Prince
116	n	spher.	20-83	40-209	0.0- 5.0	16	P.A.Moldauer
117	n	spher.	13-13	27- 27	0.0- 60.0	17	J.Petler
118	n	spher.	39-51	85-125	0.0- 5.0	18	A.B.Smith
200	n	spher.	0-69	0-146	0.0- 20.0	19	S.Igarasi
201	n	spher.	69-95	147-999	0.0- 20.0	19	S.Igarasi
202	n	spher.	33-37	61-107	0.0- 20.0	20	JAERI NDC
203	n	spher.	38-42	69-116	0.0- 20.0	20	JAERI NDC
204	n	spher.	43-45	80-125	0.0- 20.0	20	JAERI NDC
205	n	spher.	46-48	89-134	0.0- 20.0	20	JAERI NDC
206	n	spher.	49-51	97-141	0.0- 20.0	20	JAERI NDC

TABLE D-1. (CONT.)

207	n	spher.	52-54	103-150	0.0- 20.0	20	JAERI NDC
208	n	spher.	55-55	111-153	0.0- 20.0	20	JAERI NDC
209	n	spher.	56-56	112-154	0.0- 20.0	20	JAERI NDC
210	n	spher.	57-58	117-156	0.0- 20.0	20	JAERI NDC
211	n	spher.	59-59	119-160	0.0- 20.0	20	JAERI NDC
212	n	spher.	60-60	141-143	0.0- 20.0	20	JAERI NDC
213	n	spher.	60-60	144-148	0.0- 20.0	20	JAERI NDC
214	n	spher.	60-60	150-999	0.0- 20.0	20	JAERI NDC
215	n	spher.	61-61	147-999	0.0- 20.0	20	JAERI NDC
216	n	spher.	62-62	144-144	0.0- 20.0	20	JAERI NDC
217	n	spher.	62-62	147-147	0.0- 20.0	20	JAERI NDC
218	n	spher.	62-62	148-148	0.0- 20.0	20	JAERI NDC
219	n	spher.	62-62	149-149	0.0- 20.0	20	JAERI NDC
220	n	spher.	62-62	150-150	0.0- 20.0	20	JAERI NDC
221	n	spher.	63-63	151-999	0.0- 20.0	20	JAERI NDC
222	n	spher.	64-64	133-171	0.0- 20.0	20	JAERI NDC
223	n	spher.	65-65	138-175	0.0- 20.0	20	JAERI NDC
400	n	CC rot.	79-79	197-197	0.0- 57.0	21	J.P.Delaroche
401	n	spher.	20-92	40-238	0.0- 25.0	22	D.Wilmore
402	n	spher.	83-83	209-209	0.0- 30.0	23	O.Bersillon
403	n	spher.	74-74	182-186	0.0- 30.0	24	J.P.Delaroche
404	n	spher.	23-41	50- 95	0.0- 30.0	25	B.Strohmaier
600	n	CC rot.	90-**	227-260	0.0- 20.0	26	G.Vladuca
800	n	spher.	20-83	40-210	0.0-155.0	27	C.A.Engelbrecht
2001	n	spher.	13-82	12-208	50.0-400.0	28	D.G.Madland
2002	n	CC rot.	74-74	182-186	0.0-100.0	29	P.G.Young
2003	n	CC rot.	67-69	165-169	0.0-100.0	30	E.D.Arthur
2004	n	CC rot.	63-63	151-153	0.0- 20.0	31	R.Macklin
2005	n	CC rot.	75-75	185-187	0.0- 20.0	32	R.Macklin
2006	n	CC rot.	92-92	238-238	0.0-200.0	33	P.G.Young
2100	n	spher.	20-83	40-209	10.0- 26.0	34	R.L.Varner
2101	n	spher.	26-82	54-208	10.0- 80.0	35	R.L.Walter
2404	n	spher.	40-40	90- 90	0.0-200.0	36	A.J.Koning
4000	p	spher.	25-26	54- 56	0.0- 28.0	37	E.D.Arthur
4001	p	spher.	26-27	59- 59	0.0- 23.0	38	E.D.Arthur
4002	p	spher.	38-38	88- 89	0.0- 21.0	39	E.D.Arthur
4003	p	spher.	39-39	89- 89	0.0- 21.0	39	E.D.Arthur
4004	p	CC rot.	79-79	197-197	0.0- 57.0	40	P.G.Young
4015	p	spher.	6- 6	12- 12	0.0- 65.0	41	M.B.Chadwick
4016	p	spher.	7- 7	14- 14	0.0- 70.0	41	M.B.Chadwick
4017	p	spher.	8- 8	16- 16	0.0- 50.0	41	M.B.Chadwick
4100	p	spher.	16-49	30-100	0.0- 22.0	42	F.G.Perey
4101	p	spher.	20-83	40-209	10.0- 50.0	43	F.D.Becchetti
4102	p	spher.	6-82	12-208	30.0- 60.0	44	J.J.H.Menet
4103	p	spher.	26-26	56- 56	50.0- 50.0	45	G.S.Mani
4104	p	spher.	28-28	58- 58	100.0-100.0	46	K.Kwiatkowski
4105	p	spher.	40-40	90- 90	100.0-100.0	46	K.Kwiatkowski
4106	p	spher.	50-50	120-120	100.0-100.0	46	K.Kwiatkowski
4107	p	spher.	82-82	208-208	100.0-100.0	46	K.Kwiatkowski
4108	p	spher.	20-82	48-208	25.0- 45.0	47	D.M.Patterson
4109	p	spher.	39-39	89- 89	1.0- 7.0	48	C.H.Johnson
4110	p	spher.	41-41	93- 93	1.0- 7.0	48	C.H.Johnson
4111	p	spher.	45-45	103-103	1.0- 7.0	48	C.H.Johnson
4112	p	spher.	46-46	105-105	1.0- 7.0	48	C.H.Johnson
4113	p	spher.	47-47	107-107	1.0- 7.0	48	C.H.Johnson
4114	p	spher.	47-47	109-109	1.0- 7.0	48	C.H.Johnson
4115	p	spher.	48-48	110-110	1.0- 7.0	48	C.H.Johnson
4116	p	spher.	48-48	111-111	1.0- 7.0	48	C.H.Johnson
4117	p	spher.	48-48	113-113	1.0- 7.0	48	C.H.Johnson

TABLE D-1. (CONT.)

4118	p	spher.	48-48	114-114	1.0- 7.0	48	C.H.Johnson
4119	p	spher.	49-49	115-115	1.0- 7.0	48	C.H.Johnson
4120	p	spher.	50-50	116-116	1.0- 7.0	48	C.H.Johnson
4121	p	spher.	50-50	122-122	1.0- 7.0	48	C.H.Johnson
4122	p	spher.	50-50	124-124	1.0- 7.0	48	C.H.Johnson
4123	p	spher.	52-52	128-128	1.0- 7.0	48	C.H.Johnson
4124	p	spher.	52-52	130-130	1.0- 7.0	48	C.H.Johnson
4125	p	spher.	40-40	92- 92	2.0- 7.0	49	D.S.Flynn
4126	p	spher.	40-40	94- 94	2.0- 7.0	49	D.S.Flynn
4127	p	spher.	40-40	96- 96	2.0- 7.0	49	D.S.Flynn
4128	p	spher.	42-42	95- 95	2.0- 7.0	49	D.S.Flynn
4129	p	spher.	42-42	98- 98	2.0- 7.0	49	D.S.Flynn
4130	p	spher.	42-42	100-100	2.0- 7.0	49	D.S.Flynn
4200	p	spher.	8- 8	16- 16	65.0- 65.0	50	H.Sagaguchi
4201	p	spher.	10-10	20- 20	65.0- 65.0	50	H.Sagaguchi
4202	p	spher.	12-12	24- 24	65.0- 65.0	50	H.Sagaguchi
4203	p	spher.	14-14	28- 28	65.0- 65.0	50	H.Sagaguchi
4204	p	spher.	18-18	40- 40	65.0- 65.0	50	H.Sagaguchi
4205	p	spher.	20-20	40- 40	65.0- 65.0	50	H.Sagaguchi
4206	p	spher.	20-20	44- 44	65.0- 65.0	50	H.Sagaguchi
4207	p	spher.	20-20	48- 48	65.0- 65.0	50	H.Sagaguchi
4208	p	spher.	22-22	46- 46	65.0- 65.0	50	H.Sagaguchi
4209	p	spher.	22-22	48- 48	65.0- 65.0	50	H.Sagaguchi
4210	p	spher.	22-22	50- 50	65.0- 65.0	50	H.Sagaguchi
4211	p	spher.	26-26	54- 54	65.0- 65.0	50	H.Sagaguchi
4212	p	spher.	26-26	56- 56	65.0- 65.0	50	H.Sagaguchi
4213	p	spher.	27-27	59- 59	65.0- 65.0	50	H.Sagaguchi
4214	p	spher.	28-28	58- 58	65.0- 65.0	50	H.Sagaguchi
4215	p	spher.	28-28	60- 60	65.0- 65.0	50	H.Sagaguchi
4216	p	spher.	28-28	62- 62	65.0- 65.0	50	H.Sagaguchi
4217	p	spher.	28-28	64- 64	65.0- 65.0	50	H.Sagaguchi
4218	p	spher.	39-39	89- 89	65.0- 65.0	50	H.Sagaguchi
4219	p	spher.	40-40	90- 90	65.0- 65.0	50	H.Sagaguchi
4220	p	spher.	42-42	98- 98	65.0- 65.0	50	H.Sagaguchi
4221	p	spher.	42-42	100-100	65.0- 65.0	50	H.Sagaguchi
4222	p	spher.	62-62	144-144	65.0- 65.0	50	H.Sagaguchi
4223	p	spher.	82-82	208-208	65.0- 65.0	50	H.Sagaguchi
4224	p	spher.	83-83	209-209	65.0- 65.0	50	H.Sagaguchi
4401	p	spher.	42-42	92- 92	22.3- 22.3	51	E.Cereda
4402	p	spher.	42-42	94- 94	22.3- 22.3	51	E.Cereda
4403	p	spher.	42-42	96- 96	22.3- 22.3	51	E.Cereda
4404	p	spher.	42-42	98- 98	22.3- 22.3	51	E.Cereda
4405	p	spher.	42-42	100-100	22.3- 22.3	51	E.Cereda
4406	p	spher.	44-44	102-102	22.3- 22.3	51	E.Cereda
4407	p	spher.	46-46	104-104	22.3- 22.3	51	E.Cereda
4408	p	spher.	46-46	106-106	22.3- 22.3	51	E.Cereda
4409	p	spher.	46-46	108-108	22.3- 22.3	51	E.Cereda
4410	p	spher.	46-46	110-110	22.3- 22.3	51	E.Cereda
4411	p	spher.	48-48	106-106	22.3- 22.3	51	E.Cereda
4412	p	spher.	48-48	110-110	22.3- 22.3	51	E.Cereda
4413	p	spher.	48-48	112-112	22.3- 22.3	51	E.Cereda
4414	p	spher.	48-48	116-116	22.3- 22.3	51	E.Cereda
4415	p	spher.	47-47	109-109	6.1- 6.1	52	A.Feigel
4650	p	spher.	21-21	45- 45	3.0- 5.0	53	S.Kailas
4651	p	spher.	20-20	48- 48	3.0- 5.0	53	S.Kailas
4652	p	spher.	23-23	51- 51	3.0- 5.0	53	S.Kailas
4653	p	spher.	24-24	54- 54	3.0- 5.0	53	S.Kailas
4654	p	spher.	27-27	59- 59	3.0- 5.0	53	S.Kailas
4655	p	spher.	28-28	61- 61	3.0- 5.0	53	S.Kailas

TABLE D-1. (CONT.)

4656	p	spher.	29-29	65- 65	3.0- 5.0	53	S.Kailas
4657	p	spher.	31-31	71- 71	3.0- 5.0	53	S.Kailas
4658	p	spher.	33-33	75- 75	3.0- 5.0	53	S.Kailas
4659	p	spher.	34-34	80- 80	3.0- 5.0	53	S.Kailas
4660	p	spher.	19-19	41- 41	1.0- 7.0	54	Y.P.Viyogi
4661	p	spher.	21-21	45- 45	1.0- 7.0	54	Y.P.Viyogi
4662	p	spher.	20-20	48- 48	1.0- 7.0	54	Y.P.Viyogi
4663	p	spher.	22-22	49- 49	1.0- 7.0	54	Y.P.Viyogi
4664	p	spher.	23-23	51- 51	1.0- 7.0	54	Y.P.Viyogi
4665	p	spher.	25-25	55- 55	1.0- 7.0	54	Y.P.Viyogi
4666	p	spher.	27-27	59- 59	1.0- 7.0	54	Y.P.Viyogi
4667	p	spher.	28-28	61- 61	1.0- 7.0	54	Y.P.Viyogi
4668	p	spher.	29-29	65- 65	1.0- 7.0	54	Y.P.Viyogi
4669	p	spher.	30-30	68- 68	1.0- 7.0	54	Y.P.Viyogi
4670	p	spher.	31-31	71- 71	1.0- 7.0	54	Y.P.Viyogi
4671	p	spher.	33-33	75- 75	1.0- 7.0	54	Y.P.Viyogi
4672	p	spher.	34-34	80- 80	1.0- 7.0	54	Y.P.Viyogi
4673	p	spher.	39-39	89- 89	1.0- 7.0	54	Y.P.Viyogi
4674	p	spher.	41-41	93- 93	1.0- 7.0	54	Y.P.Viyogi
4675	p	spher.	42-42	96- 96	1.0- 7.0	54	Y.P.Viyogi
4676	p	spher.	42-42	98- 98	1.0- 7.0	54	Y.P.Viyogi
4677	p	spher.	45-45	103-103	1.0- 7.0	54	Y.P.Viyogi
4678	p	spher.	46-46	105-105	1.0- 7.0	54	Y.P.Viyogi
4679	p	spher.	47-47	107-107	1.0- 7.0	54	Y.P.Viyogi
4680	p	spher.	47-47	109-109	1.0- 7.0	54	Y.P.Viyogi
4681	p	spher.	48-48	110-110	1.0- 7.0	54	Y.P.Viyogi
4682	p	spher.	49-49	115-115	1.0- 7.0	54	Y.P.Viyogi
4683	p	spher.	50-50	120-120	1.0- 7.0	54	Y.P.Viyogi
4684	p	spher.	50-50	124-124	1.0- 7.0	54	Y.P.Viyogi
4685	p	spher.	52-52	128-128	1.0- 7.0	54	Y.P.Viyogi
4686	p	spher.	52-52	130-130	1.0- 7.0	54	Y.P.Viyogi
5001	p	spher.	13-82	12-208	50.0-400.0	28	D.G.Madland
5002	p	CC rot.	74-74	182-186	0.0-100.0	29	P.G.Young
5003	p	CC rot.	67-69	165-169	0.0-100.0	30	E.D.Arthur
5004	p	CC rot.	63-63	151-153	0.0- 20.0	31	R.Macklin
5005	p	CC rot.	75-75	185-187	0.0- 20.0	32	R.Macklin
5006	p	CC rot.	92-92	238-238	0.0-200.0	33	P.G.Young
5100	p	spher.	20-83	40-209	16.0- 65.0	34	R.L.Varner
5101	p	spher.	26-82	54-208	10.0- 80.0	55	R.L.Walter
5404	p	spher.	40-40	90- 90	0.0-200.0	36	A.J.Koning
6001	d	spher.	20-82	40-208	11.0- 27.0	56	C.M.Perey
6100	d	spher.	20-83	40-209	8.0- 13.0	57	J.M.Lohr
6300	d	spher.	22-22	48- 48	13.6- 13.6	58	O.P.Bilanyuk
6301	d	spher.	24-24	52- 52	13.6- 13.6	58	O.P.Bilanyuk
6302	d	spher.	24-24	54- 54	13.6- 13.6	58	O.P.Bilanyuk
6400	d	spher.	6-82	12-208	20.0-100.0	59	J.Bojowald
7001	t	spher.	20-20	40- 40	17.0- 17.0	60	R.Hardekopf
7002	t	spher.	22-22	46- 46	17.0- 17.0	60	R.Hardekopf
7003	t	spher.	22-22	48- 48	17.0- 17.0	60	R.Hardekopf
7004	t	spher.	26-26	54- 54	17.0- 17.0	60	R.Hardekopf
7005	t	spher.	26-26	56- 56	17.0- 17.0	60	R.Hardekopf
7006	t	spher.	28-28	58- 58	17.0- 17.0	60	R.Hardekopf
7007	t	spher.	28-28	60- 60	17.0- 17.0	60	R.Hardekopf
7008	t	spher.	30-30	68- 68	17.0- 17.0	60	R.Hardekopf
7009	t	spher.	40-40	90- 90	17.0- 17.0	60	R.Hardekopf
7010	t	spher.	40-40	94- 94	17.0- 17.0	60	R.Hardekopf
7011	t	spher.	50-50	116-116	17.0- 17.0	60	R.Hardekopf
7012	t	spher.	58-58	140-140	17.0- 17.0	60	R.Hardekopf
7013	t	spher.	82-82	208-208	17.0- 17.0	60	R.Hardekopf

TABLE D-1. (CONT.)

7100	t	spher.	20-82	40-208	1.0- 40.0	61	F.D.Becchetti
7101	t	spher.	20-20	40- 40	20.0- 20.0	62	P.P.Urone
7102	t	spher.	24-24	52- 52	20.0- 20.0	62	P.P.Urone
7103	t	spher.	26-26	54- 54	20.0- 20.0	62	P.P.Urone
7104	t	spher.	28-28	62- 62	20.0- 20.0	62	P.P.Urone
7105	t	spher.	28-28	64- 64	20.0- 20.0	62	P.P.Urone
7106	t	spher.	40-40	90- 90	20.0- 20.0	62	P.P.Urone
7107	t	spher.	40-40	92- 92	20.0- 20.0	62	P.P.Urone
7108	t	spher.	40-40	94- 94	20.0- 20.0	62	P.P.Urone
7109	t	spher.	50-50	118-118	20.0- 20.0	62	P.P.Urone
7110	t	spher.	12-12	26- 26	17.0- 17.0	63	P.Schwandt
7111	t	spher.	13-13	27- 27	17.0- 17.0	63	P.Schwandt
7112	t	spher.	14-14	28- 28	17.0- 17.0	63	P.Schwandt
8100	3He	spher.	20-82	40-208	1.0- 40.0	61	F.D.Becchetti
8101	3He	spher.	20-20	40- 40	21.0- 84.0	64	H.H.Chang
8102	3He	spher.	28-28	58- 58	22.0- 84.0	64	H.H.Chang
8103	3He	spher.	28-28	60- 60	29.6- 29.6	65	C.B.Fulmer
8104	3He	spher.	28-28	60- 60	35.1- 35.1	65	C.B.Fulmer
8105	3He	spher.	28-28	60- 60	49.7- 49.7	65	C.B.Fulmer
8106	3He	spher.	28-28	60- 60	59.8- 59.8	65	C.B.Fulmer
8107	3He	spher.	28-28	60- 60	71.1- 71.1	65	C.B.Fulmer
8108	3He	spher.	20-20	40- 40	21.0- 21.0	66	P.P.Urone
8109	3He	spher.	24-24	52- 52	21.0- 21.0	66	P.P.Urone
8110	3He	spher.	26-26	54- 54	21.0- 21.0	66	P.P.Urone
8111	3He	spher.	28-28	62- 62	21.0- 21.0	66	P.P.Urone
8112	3He	spher.	28-28	64- 64	21.0- 21.0	66	P.P.Urone
8113	3He	spher.	40-40	90- 90	21.0- 21.0	66	P.P.Urone
8114	3He	spher.	40-40	92- 92	21.0- 21.0	66	P.P.Urone
8115	3He	spher.	40-40	94- 94	21.0- 21.0	66	P.P.Urone
8116	3He	spher.	50-50	118-118	21.0- 21.0	66	P.P.Urone
8200	3He	spher.	20-20	40- 40	109.2-109.2	67	M.Hyakutake
8201	3He	spher.	28-28	58- 58	109.2-109.2	67	M.Hyakutake
8202	3He	spher.	40-40	90- 90	109.2-109.2	67	M.Hyakutake
8203	3He	spher.	50-50	116-116	109.2-109.2	67	M.Hyakutake
8204	3He	spher.	28-28	58- 58	89.3- 89.3	67	M.Hyakutake
8205	3He	spher.	28-28	58- 58	118.5-118.5	67	M.Hyakutake
8400	3He	spher.	12-12	24- 24	130.0-130.0	68	A.Djaloeis
8401	3He	spher.	40-40	90- 90	130.0-130.0	68	A.Djaloeis
8402	3He	spher.	50-50	120-120	130.0-130.0	68	A.Djaloeis
8403	3He	spher.	82-82	208-208	130.0-130.0	68	A.Djaloeis
8404	3He	spher.	3- 3	6- 6	217.0-217.0	69	N.Willis
8405	3He	spher.	4- 4	9- 9	217.0-217.0	69	N.Willis
8406	3He	spher.	6- 6	12- 12	217.0-217.0	69	N.Willis
8407	3He	spher.	14-14	28- 28	217.0-217.0	69	N.Willis
8408	3He	spher.	20-20	40- 40	217.0-217.0	69	N.Willis
8409	3He	spher.	28-28	58- 58	217.0-217.0	69	N.Willis
8410	3He	spher.	39-39	89- 89	217.0-217.0	69	N.Willis
8411	3He	spher.	40-40	90- 90	217.0-217.0	69	N.Willis
8412	3He	spher.	50-50	120-120	217.0-217.0	69	N.Willis
8413	3He	spher.	82-82	208-208	217.0-217.0	69	N.Willis
8414	3He	spher.	5- 5	10- 10	41.0- 41.0	70	H.J.Trost
8415	3He	spher.	6- 6	12- 12	41.0- 41.0	70	H.J.Trost
8416	3He	spher.	6- 6	13- 13	41.0- 41.0	70	H.J.Trost
8417	3He	spher.	8- 8	16- 16	41.0- 41.0	70	H.J.Trost
8418	3He	spher.	8- 8	18- 18	41.0- 41.0	70	H.J.Trost
8419	3He	spher.	11-11	23- 23	41.0- 41.0	70	H.J.Trost
8420	3He	spher.	12-12	24- 24	41.0- 41.0	70	H.J.Trost
8421	3He	spher.	12-12	25- 25	41.0- 41.0	70	H.J.Trost
8422	3He	spher.	12-12	26- 26	41.0- 41.0	70	H.J.Trost

TABLE D-1. (CONT.)

8423	3He	spher.	13-13	27- 27	41.0- 41.0	70	H.J.Trost
8424	3He	spher.	20-20	40- 40	41.0- 41.0	70	H.J.Trost
8425	3He	spher.	28-28	58- 58	41.0- 41.0	70	H.J.Trost
8650	3He	spher.	28-28	58- 58	270.0-270.0	71	P.P.Singh
8651	3He	spher.	40-40	90- 90	270.0-270.0	71	P.P.Singh
8652	3He	spher.	50-50	116-116	270.0-270.0	71	P.P.Singh
8653	3He	spher.	82-82	208-208	270.0-270.0	71	P.P.Singh
9000	4He	spher.	13-26	27- 56	1.0-100.0	72	E.D.Arthur
9001	4He	spher.	27-27	59- 59	1.0-100.0	73	E.D.Arthur
9100	4He	spher.	8-82	16-208	1.0- 25.0	74	L.McFadden
9101	4He	spher.	10-92	20-235	1.0- 46.0	75	J.R.Huizenga
9400	4He	spher.	20-45	40-100	1.0- 30.0	76	B.Strohmaier
9401	4He	spher.	22-30	37- 86	20.0- 30.0	77	O.F.Lemos
9600	4He	spher.	8-96	16-250	1.0- 73.0	78	V.Avrigeanu

REFERENCES (Annex D)

1. P.G.Young and E.D.Arthur, Proc.Int.Conf.Nucl.Data Sci.and Tech., Julich (1992) p894
2. H.Vonach,A.Pavlik,M.B.Chadwick,R.C.Haight,R.O.Nelson,S.A.Wender, P.G.Young, Phys. Rev. C 50, 1952 (1994)
3. P.G.Young and E.D.Arthur, LANL Report LA-UR-91-1424,894(1992)
4. D.G.Madland and P.G.Young, Report LA-7533-MS (1978)
5. P.G.Young and E.D.Arthur, LANL Report LA-UR-95-3654, paper at RIPL CRP Meeting, Vienna, Oct.30-Nov.3,1995.
6. D.G.Madland and P.G.Young, Int. Conf., Harwell, UK, Sept. 25-29, 1978
7. E.D.Arthur and P.G.Young, LA-UR-95-3654 (1995),BNL-NCS-51245 (1980) p.731, LA-8626-MS (1980)
8. E.D.Arthur, P.G.Young, and W.Matthes, BNL-51245 ,751 (1980); Nucl. Sci.Eng.124,271(1996)
9. P.G.Young and D.Rutherford, Report IAEA-TECDOC-483,167 (1988)
10. E.D.Arthur, Nucl.Sci.Eng. 76,137(1980); LA-UR-94-3104 (1994)
11. M.B.Chadwick and P.G.Young, Nucl.Sci.Eng. 123, 17 (1996)
12. F.D.Becchetti, Jr. and G.W.Greenlees, Phys. Rev. 182,1190 (1969)
13. J.C.Ferrer,J.D.Carlson, and J.Rapaport, Nucl.Phys. A275,325 (1977)
14. R.W.Finlay et al., Phys. Rev. C 30, 796 (1984)
15. A.Prince, Int. Conf. on Nucl. Data, Antwerp ,1982
16. P.A.Moldauer, Nucl. Phys. 47,65(1963)
17. J.Petler,M.S.Islam, and R.W.Finlay, Phys. Rev. C 32 ,673 (1985)
18. A.B.Smith,P.T.Guenther,J.F.Whalen, Nucl. Phys. A415,1 (1984)
19. S.Igarasi, Japan At.Ener.Res. Insti. 1228 , 41 (1973)
20. Japan At.Ener.Res. Insti., JNDC FP Nucl. Data WG
21. J.P.Delaroche, Proc.Int.Conf.on Neut.Phys. for Reactors, Harwell (1978)
22. D.Wilmore and P.E.Hodgson, Nucl. Phys. 55,673 (1964)
23. O.Bersillon, CEA Report CEA-N-2284 (1982) p.130; see also NEANDC-222U
24. J.P.Delaroche et al., Int. Conf. on Nucl. Data, Knoxville,TN,1979
26. G.Vladuca, A.Tudora, and M.Sin, Rom. J. Phys.,tome 41, no. 7-8 (1996) 515-526
27. C.A.Engelbrecht and H.Fiedeldey, Ann. Phys. 42,262-295 (1967)
28. D.G.Madland, OECD/NEA Specialists Meeting on Opt.Mod.to 200 MeV, Paris,1997
29. P.G.Young,E.D.Arthur,M.Bozian,T.R.England,G.M.Hale,R.J.LaBauve, R.C.Little,et al., LANL Report LA-11753-MS (1990); see also LA-8630-PR, p2 (1980)
30. E.D.Arthur and C.Philis, Report LA-8630-PR,p2 (1980)
31. R.Macklin and P.G.Young, Nucl.Sci.Eng. 95, 189 (1987)

32. R.Macklin and P.G.Young, Nucl.Sci.Eng. 97, 239 (1987)
33. P.G.Young, LANL Progress Report LA-11972-PR (1990) p.9
34. R.L.Varner,W.J.Thompson,T.L.McAbee,E.J.Ludwig,T.B.Clegg, Phys.Rep. 201,57 (1991)
35. R.L.Walter and P.P.Guss, Rad. Effects 92, 1079 (1985) [1985 Santa Fe Conf. Proc.]
36. A.J.Koning, J.J.van Wijk, J.P.Delaroche, OECD/NEA Specialists Meeting on Opt.Mod.to 200 MeV,Paris,1997
37. E.D.Arthur and P.G.Young, LA-8626-MS(ENDF-304) (1980);BNL-51245, p751 (1980); LA-UR-94-3104 (1994)
38. E.D.Arthur,P.G.Young,W.Matthes, BNL-51245,751 (1980); LA-UR-94-3104 (1994)
39. E.D.Arthur, Nucl.Sci.Eng. 76,137 1980)
40. P.G.Young and E.D.Arthur, LA-UR-84-2767 (1984); LA-UR-94-3104 (1994)
41. M.B.Chadwick and P.G.Young, Proc.Int. Particle Therapy Meeting and PTCOG XXIV, 24-26 Apr. 1996,Detroit,Mich.
42. F.G.Perey, Phys. Rev. 131,745 (1963)
43. F.D.Becchetti Jr. and G.W.Greenlees, Phys. Rev. 182,1190 (1969)
44. J.J.H.Menet,E.E.Gross,J.J.Malanify, and A.Zucker, Phys. Rev. C4, 1114 (1971)
45. G.S.Mani, Nucl. Phys. A165,225 (1972)
46. K.Kwiatkowski and N.S.Wall, Nucl. Phys. A301,349 (1978)
47. D.M.Patterson et al. Nucl. Phys. A263,261 (1976)
48. C.H.Johnson et al. Phys. Rev. Lett.39,1604(1977); Phys. Rev. C20, 2052(1979)
49. D.S.Flynn et al. Phys. Rev. C. 31, 87 (1985)
50. H.Sagaguchi et al. Phys. Rev. C 26, 944 (1982)
51. E.Cereda et. al., Phys. Rev. C 26, 1941 (1982)
52. A.Feigel et. al., Phys. Rev. C 21, 2666 (1980)
53. S.Kailas et al, Phys. Rev. C 20, 1272(1979); Pramana.J.Phys.27, 139(1986)
54. Y.P.Viyogi, Ph.D Thesis (Calcutta University 1983)
55. R.L.Walter and P.P.Guss, Rad. Effects 92, 1079 (1985) [1985 Santa Fe Conf. Proc.]
56. C.M.Perey and F.G.Perey, Phys. Rev. 132,755 (1963)
57. J.M.Lohr and W.Haeberli, Nucl. Phys. A232,381(1974)
58. O.P.Bilanyuk et al, Sov. J. Nucl. Phys. 35,317 (1982)
59. J.Bojowald et al, Phys. Rev. C 38,1153(1988)
60. R.Hardekopf et al, Phys. Rev. C 21,830 (1980)
61. F.D.Becchetti Jr. and G.W.Greenlees, Ann. Rept. J.H.Williams Lab., Univ. Minnesota (1969)
62. P.P.Urone et al, Nucl. Phys. A163,225 (1971)
63. P.Schwandt et al, Phys. Rev. C 26,369 (1982)
64. H.H.Chang et al, Nucl. Phys. A297,105 (1978)
65. C.B.Fulmer and J.C.Hafele, Phys. Rev. C 8,172 (1973)
66. P.P.Urone et al, Nucl. Phys. A163,225(1971)
67. M.Hyakutake et al, Nucl. Phys. A311,161 (1978)
68. A.Djaloeis et al, Nucl. Phys. A306,221 (1978)
69. N.Willis et al, Nucl. Phys. A204,454(1973)
70. H.J.Trost et al, Nucl. Phys. A337,377(1980)
71. P.P.Singh et al, Pramana. J. Phys. 27,747 (1986)
72. E.D.Arthur and P.G.Young, Report LA-8636-MS(ENDF-304) (1980)
73. E.D.Arthur,P.G.Young,W.Matthes, Report BNL-51245,751(1980)
74. L.McFadden and G.R.Satchler, Nucl. Phys. 84, 177 (1966)
75. J.R.Huizenga and G.Igo, Nucl. Phys. 29,462 (1962)
76. B.Strohmaier et al, Paper at the IAEA Advisory Group Meeting ,1981
77. O.F.Lemos, Orsay, Series A ,No.136 (1972)
78. V.Avrigeanu,P.E.Hodgson, and M.Avrigeanu, Report OUNP-94-02(1994); Phys. Rev. C49,2136 (1994)

5 Level Densities

Coordinator: A.V. Ignatyuk

Level densities represent one of key ingredients of nuclear reaction cross section calculations. Present Chapter, dealing with practical formalisms of nuclear level densities and their parameterization, is subdivided into three parts. First, the statistical model, notoriously used to calculate low energy nuclear reactions, needs detailed knowledge of total level densities and these are described in Section 5.1. Second, fission represents very specific reaction channel within the statistical model, and the corresponding fission level densities together with fission barriers are described separately in Section 5.2. Finally, extremely useful preequilibrium models of nuclear reactions require partial (particle-hole) level densities and these are described in Section 5.3.

5.1 Total Level Densities

Coordinator: A.V. Ignatyuk

Summary

For any applications of the statistical theory of nuclear reactions it is very important to obtain the parameters of the level density description from the reliable experimental data. The cumulative numbers of low-lying levels and the average spacings between neutron resonances are usually used as such data. The level density parameters fitted to such data are compiled in the RIPL Starter File for the tree models most frequently used in practical calculations:

i) For the Gilbert-Cameron model the parameters of the Beijing group, based on a rather recent compilations of the neutron resonance and low-lying level densities and included into the **beijing_gc.dat** file, are chosen as recommended. As alternative versions the parameters provided by other groups are given into the files: *jaeri_gc.dat*, *bombay_gc.dat*, *obninsk_gc.dat*. Additionally the *iljinov_gc.dat* and *mengoni_gc.dat* files include sets of the level density parameters that take into account the damping of shell effects at high energies.

ii) For the backed-shifted Fermi gas model the **beijing_bs.dat** file is selected as the recommended one. Alternative parameters of the Obninsk group are given in the *obninsk_bs.dat* file and those of Bombay in *bombay_bs.dat*.

iii) For the generalized superfluid model the Obninsk group parameters included into the **obninsk_bcs.dat** file are chosen as recommended ones and the *beijing_bcs.dat* file is included as an alternative set of parameters.

iv) For the microscopic approach to the level densities the files are: *obninsk_micro.for* — FORTRAN 77 source for the microscopical statistical level density code developed in Obninsk by Ignatyuk and coworkers, *moller_levels.gz* — Möller single-particle level and ground state deformation data base, *moller_levels.for* — retrieval code for Möller single-particle level scheme.

5.1.1 Introduction

The statistical properties of excited nuclear levels have been a matter of concern and study for over fifty years. One of the basic statistical properties of levels is their density. For the description of the level densities the Fermi-gas and constant temperature models are used frequently with parameters obtained from fitting some experimental data. But the physical assumptions upon which both these models are based are not sophisticated enough to allow them to account properly for variations of level densities over wide energy interval from the ground state to energies much higher than the neutron separation energy. This is not surprising, as the models discussed were initiated more than fifty years ago, when nuclear physics was in its infancy.

Some of the most important concepts, upon which current understanding of the structure of low-lying nuclear levels is based, include shell effects, pairing correlations and collective phenomena. All these concepts have been incorporated into the Generalized Superfluid Model (GSM) developed by many authors over the last 20 years. The phenomenological versions of the model convenient for an analysis of experimental data were developed intensively during the last years.

For practical applications of the statistical models it is very important to obtain parameters of the level density description from reliable experimental data. The cumulative numbers of low-lying levels and the average distances between neutron resonances are usually used as such data. The main problems of the corresponding parameter systematics are discussed briefly in this report. The systematics of the level density parameters developed during given RIPL project are considered below.

5.1.2 Composite Gilbert-Cameron Formula

Simple analytical expression expressions for the state density $\rho(U)$ of a nucleus with a given excitation energy U and the level density $\rho(U,J)$ of a nucleus with a given angular momentum J have been obtained by Bethe on the basis of the Fermi gas model [5.1]:

$$\begin{aligned} \rho(U) &= \frac{\sqrt{\pi}}{12a^{1/4}U^{5/4}}\exp(2\sqrt{aU}), \\ \rho(U,J) &= \frac{2J+1}{2\sqrt{2\pi}\sigma^3}\rho(U)\exp\left[-\frac{(J+1/2)^2}{2\sigma^2}\right]. \end{aligned} \tag{5.1}$$

Here $a = \pi^2 g/6$ is the level density parameter, which is proportional to the single-particle state density g near the Fermi energy, and σ^2 is the spin cutoff parameter.

For the Fermi gas model the state equations determining the dependence of the excitation energy U, the entropy S and other thermodynamic functions of a nucleus on its temperature t have a simple form:

$$U = at^2, \qquad S = 2at, \qquad \sigma^2 = < m^2 > gt, \tag{5.2}$$

where $< m^2 >$ is the mean square value of the angular momentum projections for the single-particle states around the Fermi energy, which may also be associated with the moment of inertia of a heated nucleus $\mathcal{I} = g < m^2 >$. The connection of thermodynamic functions (5.2) with the state and level densities (5.1) is obvious.

The main parameters of the Fermi-gas model may be estimated rather simply using the semi-classical approximation:

$$a = 2\left(\frac{\pi}{3}\right)^{4/3}\frac{m_0 r_0^2}{\hbar^2}A(1+\beta_s A^{-1/3}), \tag{5.3}$$

$$\mathcal{I}_0 = \frac{2}{5}\frac{m_0 r_0^2}{\hbar^2} A^{5/3}, \tag{5.4}$$

where m_0 is the nucleon mass, r_0 is the nuclear radius parameter, A is the mass number and β_s defines the surface component of the single-particle level density. Differences between various semi-classical determinations of the parameters (5.3) and (5.4) are mainly connected with large uncertainties of evaluation of β_s [5.2–5.5].

The most direct information on the level density of highly-excited nuclei is obtained from the average parameters of neutron resonances which were analyzed by many authors [5.6–5.15]. For the majority of nuclei the observed resonances correspond to s-neutrons, therefore the value of the average spacings D_0 is related to the level density of the compound nucleus by the relations:

$$D_0 = \begin{cases} \frac{1}{2}\left[\rho(B_n + \Delta E/2, I_0 + 1/2) + \rho(B_n + \Delta E/2, I_0 - 1/2)\right] & \text{for } I_0 \neq 0, \\ \frac{1}{2}\rho(B_n + \Delta E/2, 1/2) & \text{for } I_0 = 0, \end{cases} \tag{5.5}$$

were B_n is the neutron binding energy, ΔE is the energy interval for which the resonances are being examined, I_0 is the target nucleus spin, and the coefficient $1/2$ before the sum takes into account the fact that s-neutrons form resonances only of a particular parity. If necessary, resonances for p-neutrons can be taken into consideration analogously.

The experimental values of D_0 are normally used as source data, from which the magnitude of the level density parameter can be derived by means of Eqs. (5.1) and (5.5). Many authors have carried out such an analysis [5.8, 5.10, 5.11]. The regular differences of the level densities for even-even, odd and odd-odd nuclei analogous to the even-odd differences of the nuclear masses have been already noted on the first systematics of experimental data. To take this effect into account it is usual to introduce the so-called effective excitation energy, defined as:

$$U^* = U - \begin{cases} \delta_Z + \delta_N & \text{for even} - \text{even} \\ \delta_Z & \text{for even } Z \\ \delta_N & \text{for even } N \\ 0 & \text{for odd} - \text{odd}, \end{cases} \tag{5.6}$$

where δ_I is the corresponding phenomenological correction for even-odd differences of the nuclear binding energies.

Data on the cumulative numbers of low-lying nuclear levels are also very important for the level density analysis. Many years ago it has been noted [5.8, 5.16] that the observed energy dependence of the cumulative number of levels is described rather well by the function

$$N(U) = \exp[(U - U_0)/T], \tag{5.7}$$

where U_0 and T are free parameters determined by the fitting to corresponding data. The quantity $N(U)$ is related to the level density by the relation

$$\rho_{lev}(U) = \frac{\mathrm{d}N}{\mathrm{d}U} = \frac{1}{T}\exp\left[(U - U_0)/T\right], \tag{5.8}$$

and it is obvious that the parameter T corresponds simply to a nuclear temperature. Since the value of this parameter is assumed to be constant over the energy range considered, Eq. (5.8) is called the constant temperature model.

In order to obtain a description of the level density for the whole range of excitation energies the low-energy dependence Eq. (5.8) should be combined with the high-energy dependence predicted by the Fermi-gas model. The link between both models' parameters can be found from the condition of continuity for the level density and its first derivative at some matching energy

$$U_x = U_0 + T \ln \rho_{fg}(U_x). \tag{5.9}$$

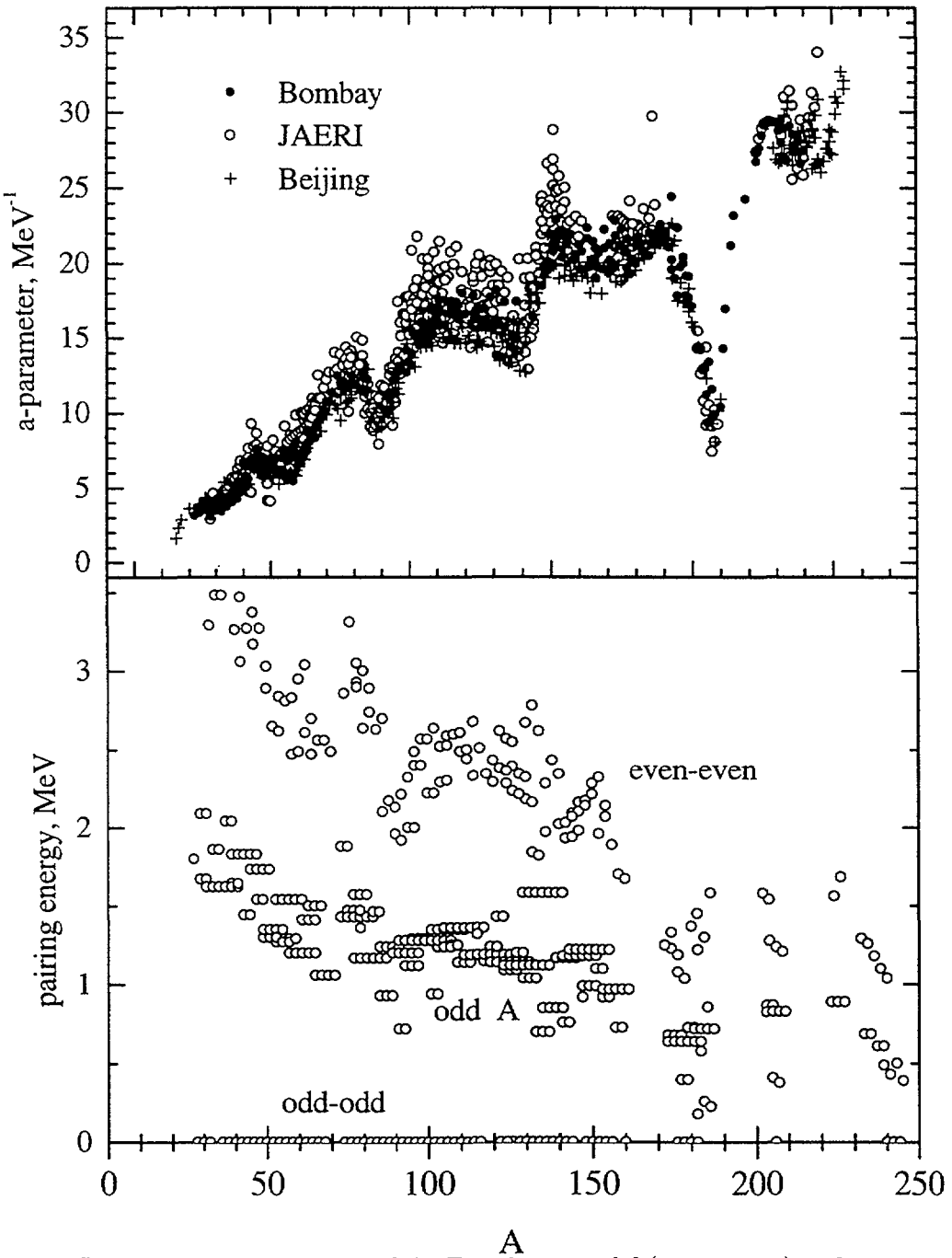

Figure 5.1: Level density parameters of the Fermi gas model (upper part) and pairing corrections to the nuclear binding energies (lower part).

The analysis of experimental data within the framework of this phenomenological approach has been carried out initially by Gilbert and Cameron [5.8], and the obtained parameters are shown in Figs. 5.1 and 5.2. The values of U_x determine the energies below which the level density description in terms of the Fermi-gas model becomes unsatisfactory, and one can see that for the majority of nuclei this energy is rather high.

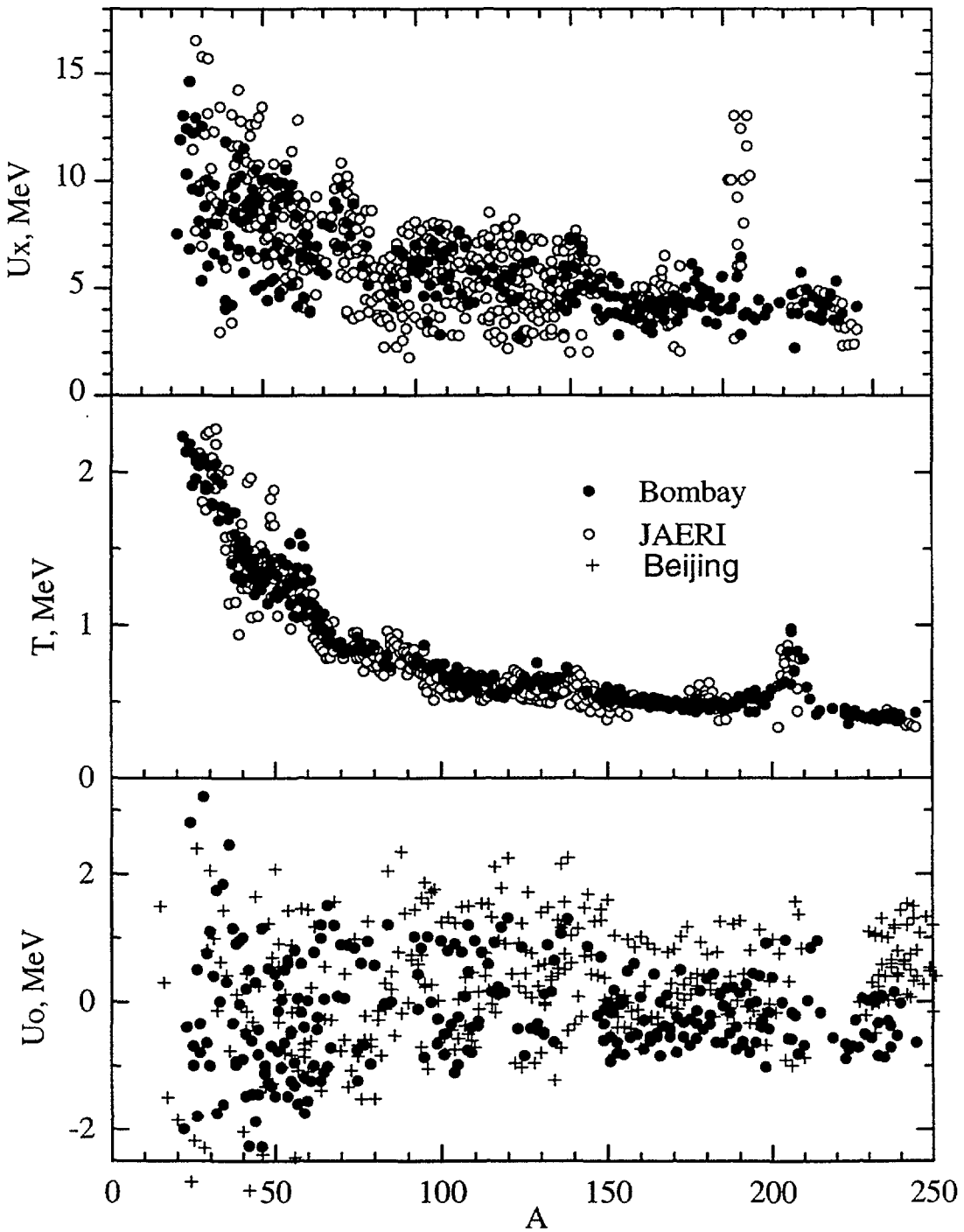

Figure 5.2: Level density parameters for the constant temperature model.

Gilbert and Cameron [5.8] developed the systematics of the even-odd corrections to excitation energies and suggested to approximate the shell changes of the level density parameters by the relation

$$\frac{a}{A} = 0.00917\,(S(Z) + S(N)) + Q(Z,N), \tag{5.10}$$

where $S(I)$ are the shell corrections for protons and neutrons, respectively, and $Q(Z,N) = 0.142$ for $54 < Z < 78$, $86 < N < 122$, and $Q(Z,N) = 0.120$ for $86 < Z < 122$, $130 < N < 182$. Such

a definition of the level density parameters was combined with the analysis of experimental data on the cumulative numbers of low-lying levels, performed by the Bombay and JAERI groups, and the parameters obtained are shown in Figs. 5.1 and 5.2. Tables of parameters are included in the corresponding contribution files of the present CRP.

It should be pointed out that the values of the a- parameters obtained depend to some extent on the determination of the spin cutoff parameter. The primary systematics [5.8, 5.10] used the value of $< m^2 >= 0.146A^{2/3}$, which corresponds to mean-square averaging of the proton and neutron angular momentum projections over all single-particle levels occupied in the ground state of a nucleus. More correct values of $< m^2 >= 0.24A^{2/3}$ or directly the rigid body values of the moment of inertia were mostly used in following analyses. The differences in the choice of the spin cutoff parameters as well as some variations in the even-odd corrections of excitation energies should be borne in mind while comparing the a- parameters obtained by different authors.

Some adjusted versions of the tables for the shell and pairing corrections were proposed in Refs. [5.17, 5.18]. The systematics of the a-parameters differ from Eq. (5.10) only by the values of the numerical coefficients and a slightly different definition of the functions $Q(Z,N)$. The parameters of the Beijing group [5.18] are based on a rather recent compilations of the neutron resonance densities and numbers of low-lying levels, and after some corrections of contradictive data they are recommended as the most reliable for the including into the Starter File of the level density parameters.

One of the serious defects of all systematics considered so far is energy independence of the a-parameters. The results of all consistent microscopic calculations of the nuclear level densities display the damping of the shell effect at high excitation energies [5.19–5.21]. To include the shell effect damping into consideration the level density parameters should be energy dependent. This dependence may be approximated by the formula

$$a(U,Z,A) = \tilde{a}(A)\left\{1 + \frac{\delta E_0}{U}\left[1 - \exp(-\gamma U)\right]\right\}, \tag{5.11}$$

where $\tilde{a}$ is the asymptotic level density parameter to which $a(U)$ tends for high excitation energies, $\delta E_0 = S(N) + S(Z)$ is the shell correction energy[3] and γ is the damping parameter [5.22]. The shell corrections are determined

$$\delta E_0 = M_{exp}(Z,A) - M_{ld}(Z,A,\beta), \tag{5.12}$$

where M_{exp} is the experimental value of the mass defect and M_{ld} is the liquid drop component of the mass formula calculated for the equilibrium nuclear deformations β [5.23]. The analysis of the neutron resonance densities on the basis of Eqs. (5.11) and (5.12) was performed recently by Iljinov *et al.* [5.15] and Mengoni and Nakajima [5.24]. The parameters obtained are shown in the upper part of Fig. 5.3 in the form of the ratio a/A. The shell corrections used are displayed in the lower part of Fig. 5.3. These level density parameters are included into the Starter File as other versions of parameters of the Gilbert-Cameron formula and are recommended at excitation energies higher than 10 MeV.

Other systematics of the shell corrections must be studied to obtain more consistent description of the level density parameters at broad energy region.

[3] Microscopic energies defined in Chapter 1 represent the difference compared to the spherical macroscopic energy, and not the macroscopic energy at equilibrium nuclear deformation, their use for the shell corrections needed in the level density formulations is not fully appropriate

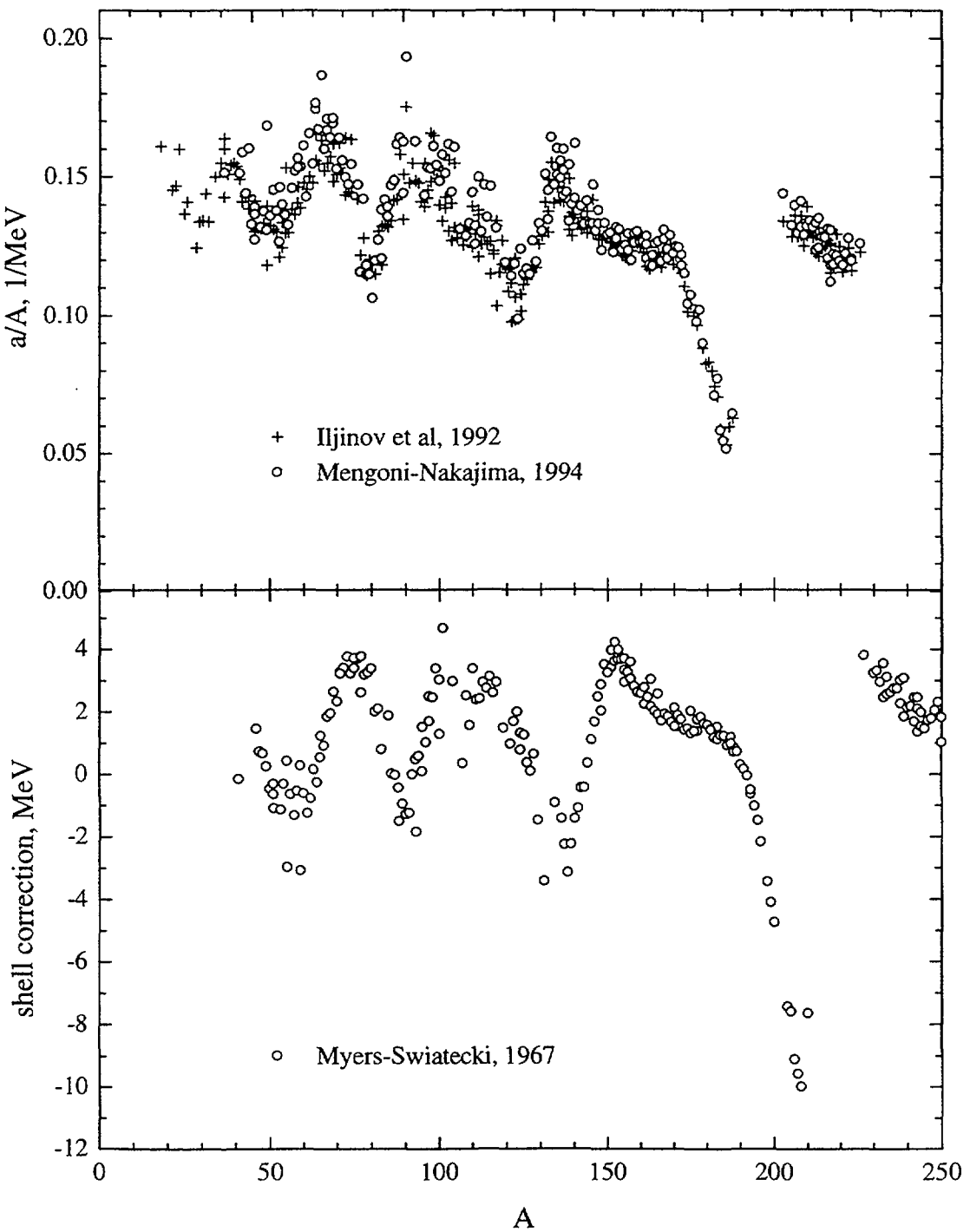

Figure 5.3: Ratio of the level density parameter a to the mass number A (upper part) and the shell corrections to the nuclear binding energies (lower part).

5.1.3 Back Shifted Fermi Gas Model

Another approach to the problem of simultaneous description of neutron resonance densities and low-lying levels was proposed in Ref. [5.12]. It has been assumed that both sets of experimental

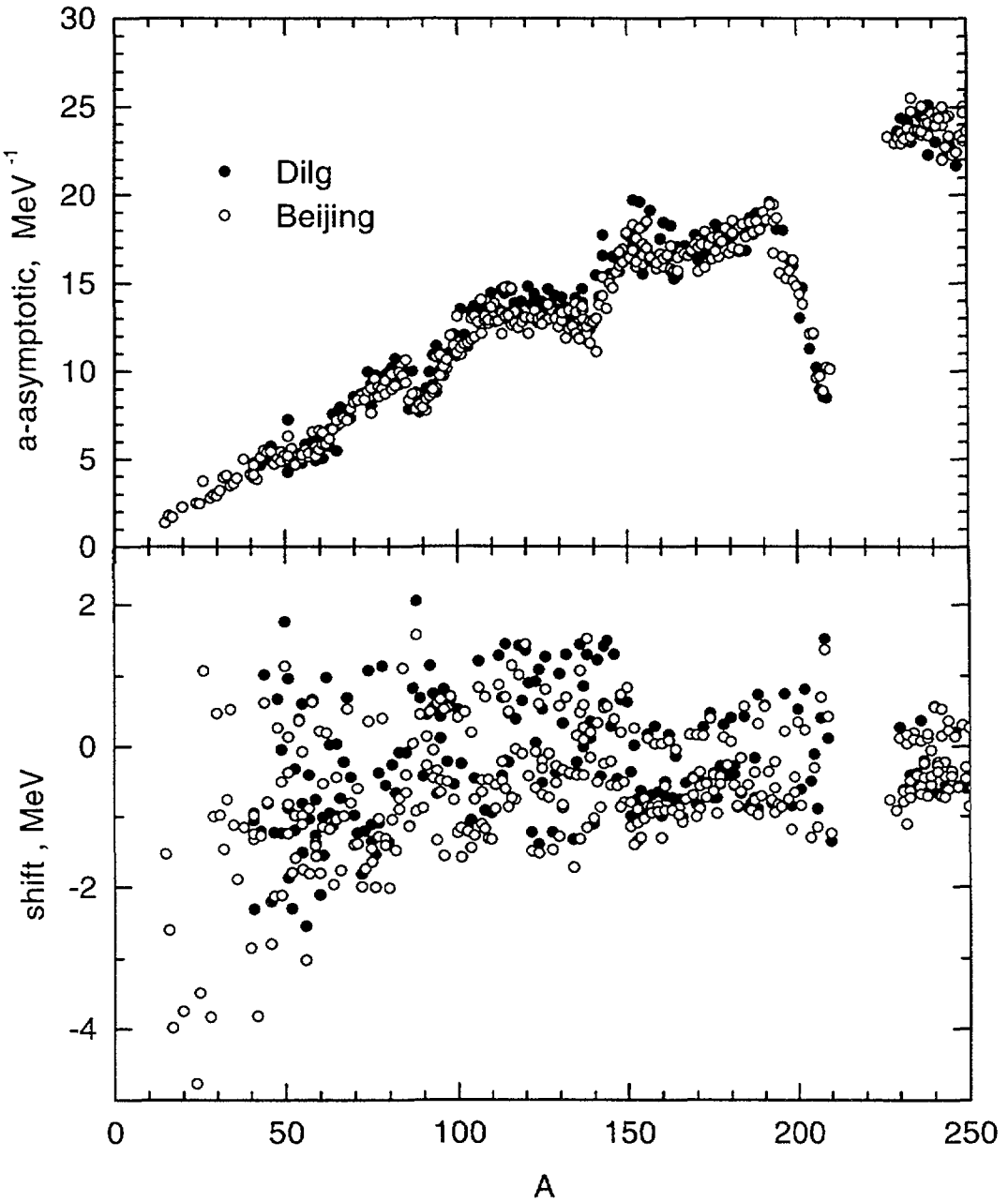

Figure 5.4: Level density parameters of the back-shifted Fermi gas model.

data can be described on the basis of the Fermi-gas relations if the level density parameter a and the excitation energy shift δ_{eff} are considered as free parameters for each nucleus. Since for odd-odd nuclei the displacement thus found is negative, the above approach has been called as the back-shifted Fermi-gas model. As the Fermi gas formulas are applied in this approach to a rather low excitation energies a more accurate estimation of a temperature is used

$$U - \delta_{eff} = at^2 - t. \tag{5.13}$$

U in denominator in the first line of Eq. (5.1) is to be replaced by $(U + t)$ [5.12].

Results of the corresponding analysis of the neutron resonance densities and low-lying nuclear levels are shown in Fig. 5.4. Due to another determination of effective excitation energies the values obtained for the a-parameter are naturally somewhat lower then those shown in Fig. 5.1. However, the shell effects in the mass dependence of a-parameters remain essentially invariable. The results of the recent analysis of more complete set of data performed by the Beijing group [5.25] are shown in Fig. 5.4 too. Difference between parameters obtained reflects improvements of experimental data achieved over recent years.

The spin cutoff parameters are determined in the model on the basis of the evaluation of the moment of inertia as the rigid body value or a half of this value. For many nuclei the available experimental data on the spins of low- lying levels can be used to analyze the statistical distribution of angular momentum. The distributions obtained agree rather with a half the rigid body values, but uncertainties of the spin-cutoff parameter estimations are still large for the final selection of the spin cutoff parameters.

Hence, both values for the moment of inertia are used in evaluation of the level density parameters. The parameters of Ref. [5.25] may be recommended as the Starter File for the back-shifted Fermi gas model. Again, as for the Gilbert-Cameron approach, it should be recommended to use Eq. (5.11) matched to these parameters to describe energy changes of the a-parameters above the neutron binding energies.

Up to now there is no a consistent systematics of parameters of the back-shifted Fermi gas model that could be used for parameter determination of nuclei for which there are no experimental data on the density of excited levels. Eq. (5.11) combined with the recent results of the low-lying nuclear level analysis [5.26] allow us to construct such a systematics, and this task can be recommended as the future stage of the RIPL development.

5.1.4 Generalized Superfluid Model

On the whole, all the results considered above let us to conclude that the Fermi-gas and constant temperature models provide us with comparatively simple and convenient formulas for parameterizing experimental data on nuclear level densities. However, these models do not give any explanation for the shifts of excitation energies and shell changes of the level density parameters. An interpretation of these effects must be obtained on the basis of more rigorous models that take into consideration shell inhomogenities of single-particle level spectra, on the one hand, and the superfluid and collective effects produced by the residual interaction of nucleons, on the other. A detailed discussion of such models can be found in the monograph [5.27]. However, rigorous microscopic methods of level density calculations are extremely laborious and this severely limits their application to experimental data analysis. For this reason there is a need for level density description, which takes into account the basic ideas of microscopic approaches concerning the structure of highly excited nuclear levels, while being sufficiently simple and convenient for broad application.

The influence of pairing correlations of super-conductive type on nuclear properties can be characterized by the value of the correlation functions $\Delta_{0\tau}$, which directly determine the even-odd differences in the nuclear binding energies and the energy gap $2\Delta_{0\tau}$ in the spectrum of quasi-particle excitations of even-even nuclei. The critical temperature t_c of the phase transition from a super-conductive (superfluid) state to normal one is also related to the correlation function:

$$t_c = 0.567\Delta_0. \tag{5.14}$$

The excitation energy corresponding to the critical temperature may be written as:

$$U_c = \frac{\pi^2}{6} g t_c^2 + \frac{1}{4} g \Delta_0^2 - n\Delta_0, \tag{5.15}$$

where $n = 0$, 1 and 2 for even-even, odd and odd-odd nuclei, respectively.

Above the critical energy the level density and other nuclear thermodynamic functions can be described by the Fermi gas relations in which the effective excitation energy is defined as

$$U^* = U - E_{cond}. \tag{5.16}$$

Here E_{cond} is the condensation energy that determines a reduction of the nuclear ground state energy due to the pairing correlations:

$$E_{cond} = \frac{1}{4} g \Delta_0^2 - n\Delta_0. \tag{5.17}$$

Below the phase transition point (5.14) the expressions for thermodynamic functions of a nucleus are rather complex, and they will not be considered here. Complete expressions can be found in Refs. [5.27–5.29].

If coherent collective effects are included into consideration of excited level structure, the nuclear level density may be expressed as

$$\rho(U) = \rho_{qp}(U) K_{vibr}(U) K_{rot}(U), \tag{5.18}$$

where ρ_{qp} is the level density due to quasi-particle excitations only, and K_{vibr} and K_{rot} are the corresponding enhancement coefficients due to vibration-al and rotational excitations, respectively.

In adiabatic approximation the rotational enhancement of the level density depends on the nuclear shape symmetry and can be written as [5.30]:

$$K_{rot} = \begin{cases} 1 & \text{for spherical nuclei,} \\ \mathcal{I}_\perp t & \text{for deformed nuclei,} \end{cases} \tag{5.19}$$

where $\mathcal{I}_\perp$ is the moment of inertia relatively to the perpendicular axis. This formula is obtained if the mirror and axial symmetry of deformed nuclei is assumed. The most stable nuclei of the rare- earth elements ($150 \leq A \leq 190$) and the actinide $A \geq 230$ have this shape. For non-axial forms the rotational enhancement of the level density becomes greater [5.30].

The vibrational enhancement coefficient is determined in the microscopic approach by the relation

$$K_{vibr} = \prod_i \left[\frac{1 - \exp(-\omega_i^0/t)}{1 - \exp(-\omega_i/t)} \right]^{g_i}, \tag{5.20}$$

where ω_i is the energy of vibrational excitations, ω_i^0 is the energy of corresponding quasi-particle excitation and g_i is the degeneracy of such excitations. The presence of quasi-particle energies in Eq. (5.20) reflects some account of non-adiabatic effects in excited nuclei. Due to symmetry conditions imposed on the nuclear Hamiltonian the rotational and vibrational excitations become connected in consistent microscopic approach [5.27]. As a result the calculated collective enhancement coefficients turn out always reduced in comparison to the adiabatic estimation.

It can readily be seen that adiabatic estimation of K_{rot} increases the nuclear level densities by a factor of 50–100 compared with the calculations based on quasi-particle excitations alone. The increase of the level density due to vibrational excitations will be appreciable only for low-energy excitations with $\omega_i < 1$–2 MeV.

During the last twenty years some microscopic models have been developed in order to consider collective effects in highly excited nuclei. The results of all these models demonstrate

damping of level density enhancement factors with the increase of excitation energy. On the basis of the level density calculations within the SU-3 model (the oscillator mean field with the quadrupole-quadrupole interaction of particles) Hansen and Jensen [5.31] obtained the empirical function

$$K_{rot}(U) = \frac{K_{rot}^{adiab}(U)}{1 + \exp[(U - U_r)/d_r]}, \tag{5.21}$$

that describes damping of the rotational enhancement factors. The parameters of this formula were estimated as

$$U_r = 120A^{1/3}\beta^2\text{MeV}, \qquad d_r = 1400A^{-2/3}\beta^2\text{MeV}, \tag{5.22}$$

where β is the quadrupole deformation parameter. Some other phenomenological descriptions for the enhancement factor damping were discussed in Refs. [5.32–5.34]. All such descriptions include at least one or two parameters that can fluctuate from one nucleus to another. Up to now rather big uncertainty exists in estimation of the collective enhancement damping and unfortunately we have no reliable experimental data that could be used for a crucial test of available model predictions.

The vibrational enhancement of the level density was approximated by the relation

$$K_{vibr} = \exp[\delta S - (\delta U/t)], \tag{5.23}$$

where δS and δU are changes in the entropy and excitation energy, respectively, resulting from the vibrational modes. These changes are described by the relations of the Bose gas:

$$\begin{aligned} \delta S &= \sum_i (2\lambda_i + 1)[(1 + n_i)\ln(1 + n_i) - n_i \ln n_i] \\ \delta U &= \sum_i (2\lambda_i + 1)\omega_i n_i, \end{aligned} \tag{5.24}$$

where ω_i are the energies, λ_i the multi-polarities and n_i the occupation numbers for vibrational excitations at a given temperature. To account for the disappearance of collective enhancement of the level density at high temperatures, the occupation numbers were approximated by the relation

$$n_i = \frac{\exp(-\gamma_i/2\omega_i)}{\exp(\omega_i/t) - 1}, \tag{5.25}$$

where γ_i are the spreading widths of the vibrational excitations. The spreading of collective excitations in nuclei should be similar to the zero-sound damping in a Fermi liquid and the corresponding width can be written as

$$\gamma_i = C(\omega_i^2 + 4\pi^2 t^2). \tag{5.26}$$

The value of $C = 0.0075A^{1/3}$ MeV^{-1} was obtained from the systematics of the neutron resonance densities of medium-weight nuclei [5.35]. In that analysis, the experimental values were employed for the energies of the first 2^+ excitation and $\omega = 50A^{-2/3}$ MeV for the octupole excitations, whose influence, however, is much weaker than of the quadrupole ones.

The shell inhomogenities of the single-particle level spectra result in a particular energy dependence of the level density parameter $a(U)$. The shell effects on the level density become weaker with an increase of excitation energy, and at sufficiently high energies the dependence of parameter a on the mass number tends to the semi-classical value (5.3). These important features of the behavior of the level density parameters can be explained in the framework of the shell correction method [5.27]. The strong correlation of shell corrections (5.12) with the observed values of the ratios a/A (Fig. 5.3) can be used to construct a phenomenological

systematics of the level density parameters [5.28]. The basis of the systematics is the relation, similar to (5.11),

$$a(U,Z,A) = \begin{cases} \tilde{a}(A)\left[1 + \delta E_0 \frac{f(U^*)}{U^*}\right] & \text{for } U \geq U_c \\ a_c(U_c,Z,A) & \text{for } U < U_c, \end{cases} \tag{5.27}$$

where the function $f(U) = 1 - \exp(-\gamma U)$ determines the energy changes of the level density parameter at lower energies. The shell damping parameter $\gamma = 0.40A^{-1/3}$ MeV^{-1} was estimated on the basis of both the theoretical calculations and the analysis of experimental data [5.13, 5.28].

Applying Eqs. (5.14) to (5.17) to the description of pairing correlation effects the values of level density enhancement coefficients were estimated from the experimental data on the densities of neutron resonances. In such analysis the asymptotic values of the level density parameters were defined as $\tilde{a} = 0.073A + 0.115A^{2/3}$ MeV, the shell corrections were taken from Ref. [5.36] and the correlation functions were approximated by $\Delta_0 = 12/A^{1/2}$ MeV. The coefficients obtained are shown in the upper part of Fig. 5.5. In the lower part the values of similar coefficients calculated in the adiabatic approximation are given. A correlation of both coefficients is very strong but as a rule the adiabatic evaluations give higher values of coefficients than the ones extracted from the observed density of neutron resonances. The difference of these two definitions of the level density enhancement factors demonstrates that the damping of the enhancement coefficients for highly excited nuclei should be taken into account. For the global description of the nuclear level densities this damping may be taken into account by means of the empirical functions similar to (5.21) and (5.25).

To take into account possible shortcomings of the global systematics of the pairing correlation functions and collective enhancement damping an additional shift of the excitation energies

$$U_{eff} = U^* + \delta_{shift} \tag{5.28}$$

was introduced into Eq. (5.27) [5.35, 5.34]. Within the framework of such approach the set of parameters $\tilde{a}$ and δ_{shift} was obtained from the simultaneous fitting of the cumulative numbers of low-lying levels and observed neutron resonance densities recommended by this CRP [5.37]. The similar analysis was performed by the Beijing group at their compilation of the low-lying levels and neutron resonance densities [5.38]. The parameters obtained are shown in Fig. 5.6. The Obninsk group parameters are obtained on the basis of more recent compilation of the neutron resonance densities, and therefore these parameters are included as recommended in the RIPL Starter File.

For any practical application the individual parameters are preferable of course. Uncertainties of parameters are not very important for a prediction of the level densities in an intermediate energy region if experimental data for the neutron resonances and low-lying levels were chosen correctly. For the study of the nuclear level densities the analysis of evaporation spectra of different particles is of great interest. The energy dependencies of the level densities obtained from the spectrum analysis of various threshold reactions are in good agreement with the calculations based on the individual parameters of GSM [5.35].

On the other hand, for many tasks we need level density parameters for nuclei for which no experimental data is available. For such goals the global parameters may be used effectively. Also some local systematics of parameters may be proposed based on extrapolations of the isotopic or isotonic changes of the individual parameters. In many cases experimental data on the cumulative number of low-lying levels might be very useful because such data permit to fit one of the individual parameters keeping the global systematics for others.

At first glance it might seem that the systematics of the level density parameters in terms of the Fermi gas and the generalized superfluid model are equally justified, since they give

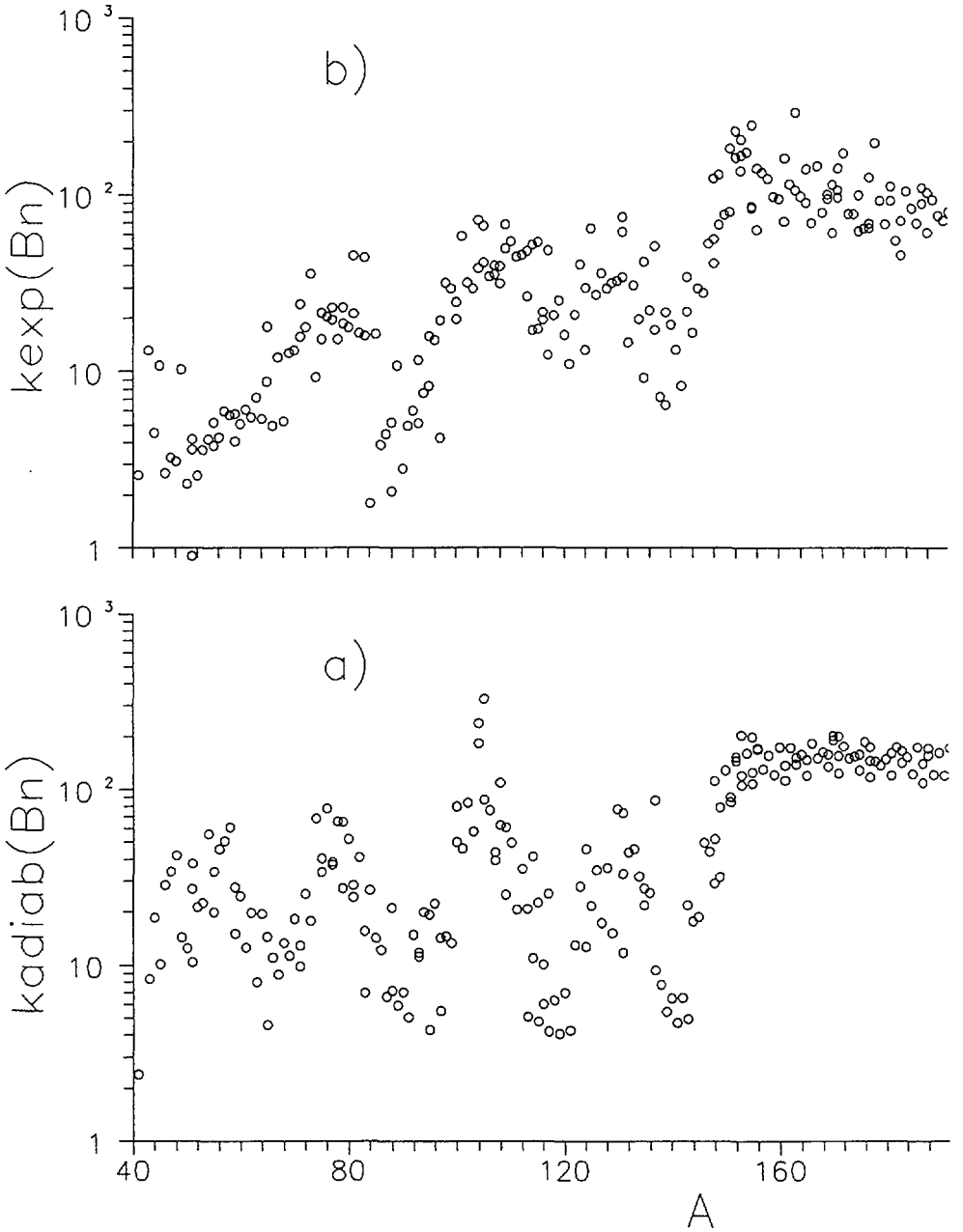

Figure 5.5: Collective enhancement factors calculated in the adiabatic approximation (a), and obtained as a ratio the observed density of neutron resonances to the calculated density of quasi-particle excitations (b).

approximately identical description of the level densities at excitation energies close to the neutron binding energy. However, these descriptions correspond to different absolute values of the level density parameters, because the inclusion of collective effects decreases the a-parameters obtained. These reduced values agree well enough with both the experimental data derived from the spectra of inelastically scattered neutrons with energies of up to 7 MeV and the theoretical calculations of the a-parameters for the single-particle level schemes of a Woods-Saxon potential [5.28]. This agreement of the data is very important, because the evaporation spectra are sensitive precisely to the value of the level density parameter. It is impossible to

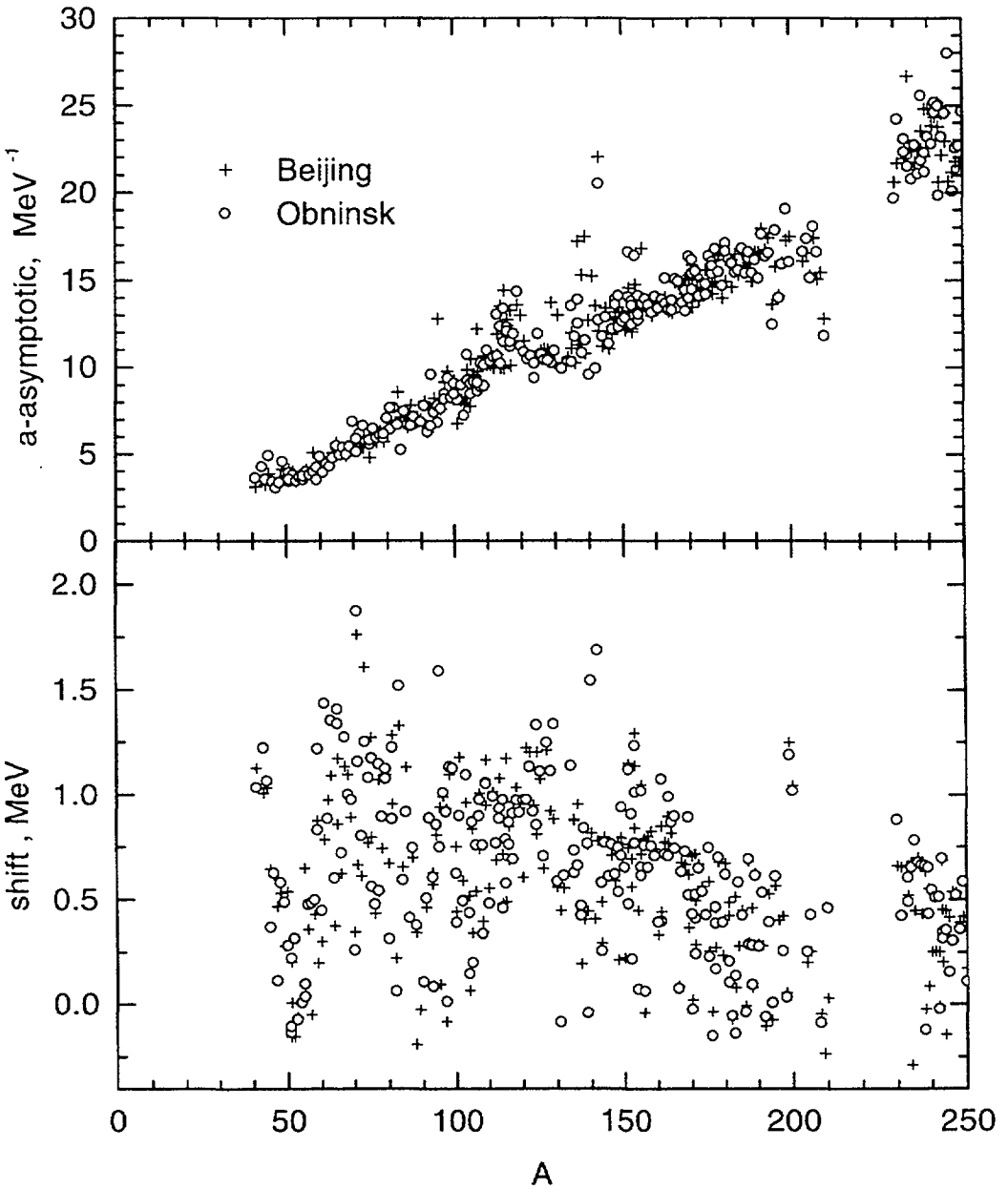

Figure 5.6: Level density parameters of the generalized superfluid model.

explain the differences between the values of a-parameter obtained from resonance data and from evaporation spectra in terms of the Fermi gas model without account of collective effects. Proper consideration of the level density collective enhancement is also very important for a consistent description of the observed fissilities of highly-excited nuclei [5.39].

Nowadays it seems almost obvious that in description of the level densities of excited nuclei we should use models which are more consistent than the Fermi-gas, but inevitably more complex. The success of the generalized superfluid model is attributed to the inclusion of the main well-known component of nuclear theory: the pairing correlations, shell effects and collective excitations. Some complexity of the model seems to be justified by the mutual consistency of the parameters obtained from the various experimental data and also by the close relation of the theoretical concepts used to describe the structure of low-lying nuclear levels and the statistical properties of highly excited nuclei.

5.1.5 Microscopic Generalized Superfluid Model

A more rigorous description of the level densities and other statistical characteristics of excited nuclei can be obtained in the framework of calculations performed with the realistic schemes of single-particle levels. The methods of such calculations are considered in details in the monograph [5.27]. The state equations for the thermodynamic functions of a excited nucleus, similar to Eq. (5.2) of the Fermi gas model, may be written in the form of

$$\begin{aligned} S &= \sum_i g_i[\beta E_i \overline{n}_i + \ln(1+\exp(-\beta E_i)], \\ U &= \frac{1}{2}\sum_i g_i[\sqrt{(\epsilon_i-\lambda)^2+\Delta_0^2} - E_i(1-2\overline{n}_i)] + \frac{\Delta_0^2-\Delta^2}{G}, \end{aligned} \tag{5.29}$$

Here $\beta = 1/t$ is the inverse temperature, E_i is the energy of quasiparticle nuclear excitations, $\overline{n}_i = [1+\exp(-\beta E_i)]^{-1}$ is the occupation numbers for the corresponding single-particle levels, g_i is the degeneracy of these levels and the sums over i include all single-particle levels for both protons and neutrons. The quasiparticle energies $E_i = [(\epsilon_i - \lambda_\tau)^2 + \Delta_\tau^2]^{1/2}$ are connected with the single-particle energies and the correlation function Δ_τ by the equations:

$$\begin{aligned} G_\tau^{-1} &= \frac{1}{4}\sum_i g_i \frac{1-2\overline{n}_i}{E_i}, \\ N_\tau &= \frac{1}{2}\sum_i g_i[1 - \frac{\epsilon_i-\lambda_\tau}{E_i}(1-2\overline{n}_i)], \end{aligned} \tag{5.30}$$

where N_τ is the number of protons or neutrons in a nucleus, λ_τ is the corresponding chemical potential and G_τ is the pairing force constant. For $t = 0$ Eqs. (5.30) determine the proton and neutron correlation functions for the ground state of a nucleus.

For given schemes of single-particle levels Eqs. (5.29) and (5.30) allow us to calculate the thermodynamic functions and the nuclear level densities without any additional parameter. To trace the difference between the behavior of the thermodynamic functions (5.29) and the Fermi gas ones (5.2), it is useful to determine the following functions:

$$\begin{aligned} a' &= S^2/4U, \qquad \overline{a} = \frac{\pi^2}{6}\beta\sum_i g_i\overline{n}_i(1-\overline{n}_i), \\ \overline{m^2} &= \frac{pi^2}{6\overline{a}}\beta\sum_i m_i^2 g_i\overline{n}_i(1-\overline{n}_i), \qquad \mathcal{I}_{\|} = \beta\sigma^2, \end{aligned} \tag{5.31}$$

which are equivalent to the Fermi gas model parameters. For low excitation energies the calculated values of the level density parameters (5.31) reproduce rather well the shell changes of the Fermi gas model parameters observed in experimental data (Figs. 5.1 and 5.4) [5.27]. At high excitation energies (> 50 MeV) the mass number dependence of calculated parameters is very close to the semiclassical (5.3).

The codes for microscopic calculations of the nuclear level densities are also given in the RIPL Starter File. The collective effects are included into the codes on the basis of the same approximations as for the phenomenological generalized superfluid model. As recommended ones for such calculations the single-particle level schemes of Möller *et al.* [5.40] are chosen. These schemes were used for calculations of the recommended nuclear binding energies, shell corrections and deformations (see Chapter 1). So their application to the level density calculations provides the consistency of the ground state and excited nucleus descriptions.

The single-particle level schemes and ground state deformations obtained in Ref. [5.40] are tabulated in the database *moller_levels.gz*. This set of single-particle level schemes was included in the RIPL in order to provide reliable and consistent single-particle level data set for microscopic nuclear level density calculations. The retrieval code *moller_levels.for* for the Möller data base is also provided. This is a modified version of the original code written by Nix [5.41]. It allows to extract interactively single particle level schemes for an given list of nuclides. The format of the output files is compatible with the microscopic nuclear level density codes *capote_micro.for* (Chapter 5.3) and *obninsk_micro.for* included in the RIPL Starter File.

5.1.6 Conclusions and Recommendations

Three level density models, the Gilbert-Cameron approach, the back-shifted Fermi gas model and the generalized superfluid model, are widely used in practical calculations of nuclear level densities. Therefore, recommended parameters for each level density model are presented in the RIPL Starter File.

The files of the level density parameters provided by the Beijing, Bologna, Bombay, JAERI and Obninsk groups were included into the Starter File as complete compilations of the level density parameters in computer readable format. Differencies among parameters obtained by different groups reflect different choices of input data on the neutron resonance spacings and on cumulative numbers of low-lying levels.

The following sets of parameters are included into the Starter File as recommended for each model:
i) For the Gilbert-Cameron model the parameters of the Beijing group [5.38], based on a recent compilation of the neutron resonance densities and numbers of low-lying levels, seem to be the best ones. The energy changes of these parameters at high excitation energies should be taken into account on the basis of formulae similar to Eq. (5.11). Such changes are particularly important for near magic nuclei. As an alternative version that includes more consistent description of shell effects at high energies, the parameters by Iljinov *et al.* [5.34] and Mengoni-Nakajima [5.24] could be used.
ii) For the back-shifted Fermi gas model, the parameters of Ref. [5.25] are included with two versions used for the moment of inertia. Again, as in the case of the Gilbert-Cameron approach, it is recommended to use Eq. (5.11) to describe energy changes of the a-parameter above neutron binding energy.
iii) For the generalized superfluid model, the Obninsk group parameters, obtained on the basis of more recent compilation of neutron resonance densities, are recommended.

A new analysis of available data on cumulative numbers of low-lying levels was performed within the frame of this CRP [5.26]. The nuclear temperatures and even-odd energy shifts are estimated now for a much larger number of nuclei than considered in previous analyses. Some more accurate evaluations of the neutron resonance densities are also obtained, and only a part of them taken into account by current systematics of the level density parameters. Re-evaluation of the level density parameters on the basis the new data obtained for the low-lying levels and neutron resonances is recommended for the next stage of the Starter File development. Other systematics of the shell corrections should be studied to obtain more consistent description of the level density parameters in broad energy region.

The use of microscopic methods is an alternative to semiempirical formulae for nuclear level density calculations. Combining microscopic and semimicroscopic methods, and using consistent set of single-particle levels, a deeper understanding of nuclear level densities can be achieved.

5.2 Fission Level Densities

Coordinator: V.M. Maslov

Summary

Fission level densities (or fissioning nucleus level densities at fission saddle deformations) are required for statistical model calculations of actinide fission cross sections. Back-shifted Fermi-Gas Model, Constant Temperature Model and Generalized Superfluid Model (GSM) are widely used for the description of level densities at stable deformations. These models provide approximately identical level density description at excitations close to the neutron binding energy. It is at low excitation energies that they are discrepant, while this energy region is crucial for fission cross section calculations. A drawback of back-shifted Fermi gas model and traditional constant temperature model approaches is that it is difficult to include in a consistent way pair correlations, collective effects and shell effects. Pair, shell and collective properties of nucleus do not reduce just to the renormalization of level density parameter a, but influence the energy dependence of level densities. These effects turn out to be important because they seem to depend upon deformation of either equilibrium or saddle-point. These effects are easily introduced within GSM approach [5.28]. Fission barriers are another key ingredients involved in the fission cross section calculations. Fission level density and barrier parameters are strongly interdependent. This is the reason for including fission barrier parameters along with the fission level densities in the Starter File.

The recommended file is **maslov.dat** — fission barrier parameters. Recent version of actinide fission barrier data obtained in Obninsk (*obninsk.dat*) should only be considered as a guide for selection of initial parameters. These data are included in the Starter File, together with the fission barrier parameters recommended by CNDC (*beijing.dat*), for completeness.

5.2.1 Introduction

Fission level densities and fission barrier parameters are key ingredients of actinide fission calculations. The important point is that fission level density and barrier parameters are strongly interdependent. The level density of deformed nucleus depends on the collective properties, pair correlations, and shell structure of a nucleus. These effects are easily introduced within the framework of the Generalized Superfluid Model [5.28]. Data on neutron-induced fission cross sections provide a sound basis for extraction of fission barrier parameters and for modeling level density approach. We proceed within the full-scale Hauser-Feshbach theory, coupled channel optical model and double-humped fission barrier model [5.42]. This approach is supported by many experimental signatures which demonstrate the importance of the collective, pairing, and shell effects both at equilibrium and saddle deformation.

Total nuclear level density is represented as a product of quasi-particle and collective contributions. The collective contribution to the level density at a saddle point is defined by the order of symmetry of a saddle point, which can be adopted according to the calculations within the shell correction method, such as the ones by Howard and Möller [5.43]. These saddle asymmetries depend on Z and N of the fissioning nucleus.

The effect of the pair correlations on the level density was demonstrated in the measurements of statistical γ–decay spectra on even rare-earth nuclei [5.44, 5.45]. In case of even-even

fissioning nuclei step-like structure of the K_o^2 parameter, defining the angular anisotropy of fission fragments, is interpreted as being due to few-quasi-particle excitations. These excitations are essential for state density calculation at low intrinsic excitation energies. Contrary to the fission cross section, the structure observed in the behavior of the K_o^2 parameter, is virtually insensitive to the detailed shape of the fission level density. It was demonstrated that the observed irregularities in neutron-induced fission cross sections can be attributed to the interplay of few-quasi-particle excitations in the level density of fissioning and residual nuclei [5.46, 5.47].

The shell structure effects are introduced through the dependence of the level density $a-$parameter on the excitation energy. Damping of the shell effects influences the shape of first-chance fission cross section at excitation energies above fission threshold. The impact of pairing correlations and of collective and shell effects, on the calculated fission cross sections depends on the excitation energy [5.48, 5.49].

It was demonstrated that the sophisticated level density approach, involving pair, shell and collective effects, is unavoidable.

5.2.2 Fission Level Densities

In the adiabatic approximation the total nuclear level density $\rho(U, J, \pi)$ is represented as a product of quasi-particle and collective contributions,

$$\rho(U, J, \pi) = K_{rot}(U, J) K_{vib}(U) \rho_{qp}(U, J, \pi), \tag{5.32}$$

where $\rho_{qp}(U, J, \pi)$ is the quasi-particle level density, and $K_{rot}(U, J)$ and $K_{vib}(U)$ are rotational and vibrational enhancement factors. The collective contribution to the level density of a deformed nucleus is defined by the symmetry order of nuclear deformation. The actinide nuclei equilibrium deformation is axially symmetric. The symmetry order of nuclear shape at inner and outer saddle point is adopted according to the calculations performed using shell correction method [5.43].

Level densities at equilibrium deformations should reproduce both: (i) the average neutron resonance spacings and (ii) the observed cumulative number of discrete levels $N^{exp}(U)$ (see previous Chapter). In the latter case, GSM model fails to describe the cumulative number of low-lying levels without introduction of the additional shift in the excitation energy δ_{shift}. Therefore, level densities at low excitation energies (i.e. just above the last discrete level where $N^{exp}(U) \sim N^{theor}(U)$) a modified constant temperature model is applied. The constant temperature approximation

$$\rho(U) = dN(U)/dU = T^{-1} \exp((U - U_o)/T), \tag{5.33}$$

is extrapolated up to the matching point U_c above which the GSM model [5.28] is adopted. The following condition is imposed:

$$U_c = U_o - T \ln(T\rho(U_c)). \tag{5.34}$$

Here, the odd-even energy shift $U_o = -n\Delta$, where $\Delta = 12/\sqrt{A}$ is the pairing correlation function, A is a mass number, and $n = 0$ for even-even, 1 for odd and 2 for odd-odd nuclei. The value of nuclear temperature T is defined by the matching conditions at excitation energy U_c. The constant temperature model parameters for some actinides are given in Table 5.1.

The respective parameters for axially symmetric fissioning nucleus (nuclear temperature T_f and excitation energy shift U_{of}) are defined at the matching energy U_{cf}, which is assumed to be the same as for the equilibrium deformation (U_c). This is a fair approximation because for ground state deformations the U_c value is not very much sensitive to the value of the $a-$parameter. The

Table 5.1: Constant temperature model parameters.

Parameter	^{246}Cm	^{245}Cm	^{241}Am	^{242}Am
U_c, MeV	3.6	2.4	3.6	2.4
U_o, MeV	-0.0068	-0.65311	-0.96455	-1.6452
T, MeV	0.37326	0.36246	0.40723	0.39241

effects of non-axiality and mass asymmetry are included afterwards. At excitation energies above U_{cf} the GSM model [5.28] is applied.

The parameters of the level density model for the inner (outer) saddle points and equilibrium deformations are:

- main level density parameters a_f and a,
- shell corrections $\delta W_{fA(B)}$ and δW,
- pairing correlation functions Δ_f and Δ , at equilibrium deformations $\Delta_o = 12/\sqrt{A}$,
- quadrupole deformation ε,
- moment of inertia at zero temperature $\mathcal{I}_0/\hbar^2$

Values of these parameters for actinides are given in Table 5.2. Shell corrections for ground state deformations are calculated as $\delta W = M^{exp} - M^{MS}$, where M^{MS} denotes liquid drop mass (LDM), calculated with Myers-Swiatecki parameters [5.23], and M^{exp} is the experimental nuclear mass. Shell correction values at inner and outer saddle deformations $\delta W_{fA(B)}$ are taken from the comprehensive review by Bjornholm and Lynn [5.50]. Correlation function $\Delta_f = \Delta_o + \delta$ at saddle-point depends on a_f/a ratio, which is a function of $(\delta W_f - \delta W)$.

Table 5.2: Level density parameters for fission and neutron emission channels in actinide nuclei.

Parameter	inner saddle (A)	outer saddle (B)	neutron channel
δW, MeV	2.5**	0.6	LDM
Δ, MeV	$\Delta_o + \delta$ *	$\Delta_o + \delta$ *	Δ_o
ε	0.6	0.8	0.24
$\mathcal{I}_0/\hbar^2$, MeV^{-1}	100	200	73

**) for axially asymmetric deformations, 1.5 MeV for axially symmetric deformations;
*) $\delta = \Delta_f - \Delta$ value is defined by fitting fission cross section in the plateau region.

Values of the $\tilde{a}-$parameter are determined by fitting neutron resonance spacings $\langle D_{obs} \rangle$. These, along with the $s-$wave neutron strength function $\langle S_o \rangle$, are obtained taking into account the correction for resonances missing due to their weakness and/or to poor experimental resolution [5.51]. Essentially, these values are consistent with those recommended for the RIPL Starter File (see file *obninsk.dat*). The shell correction dependence of $a-$parameter is defined using the following equation [5.28]:

$$a(U) = \begin{cases} \tilde{a}(1+ \delta W f(U - E_{cond})/(U - E_{cond})), & U > U_{cr} = 0.47 a_{cr} \Delta^2 - n\Delta \\ a(U_{cr}) = a_{cr} & U \leq U_{cr} = 0.47 a_{cr} \Delta^2 - n\Delta, \end{cases} \quad (5.35)$$

where $n = 0$, 1, 2 for even-even, odd-A and odd-odd nuclei, respectively; $f(x) = 1 - \exp(-\gamma x)$ is the dimensionless function describing damping of the shell effects; condensation energy $E_{cond} =$

$0.152a_{cr}\Delta^2$, where Δ is the correlation function; $\tilde{a}$ is the asymptotic a-parameter value at high excitation energies. It is assumed that $\tilde{a}$-values for equilibrium and saddle deformations are identical.

This means that the complete expression for the constant temperature approach to the total level density reads

$$\rho(U) = K_{rot}(U)K_{vib}(U)\frac{\omega_{qp}(U)}{\sqrt{2\pi}\sigma} = T^{-1}\exp((U-U_o)/T). \tag{5.36}$$

The quasi-particle state densities $\omega_{qp}(U)$ are renormalized at excitation energies $U < U_c$. Here, $\sigma^2 = \mathcal{I}_{||}\ t$ is the spin distribution parameter, t is thermodynamic temperature, the parallel moment of inertia $\mathcal{I}_{||} = 6/\pi^2 < m^2 > (1 - 2/3\varepsilon)$, where $< m^2 >$ is the average value of the squared projection of the angular momentum of the single-particle states, and ε is quadrupole deformation parameter.

For deformed axially symmetric nucleus it is assumed

$$K_{rot}(U) = \sigma_\perp^2 = \mathcal{I}_\perp t = 0.4mr_o^2\hbar^{-2}(1 + 1/3\varepsilon), \tag{5.37}$$

where $\sigma_\perp^2$ is the spin cutoff parameter, $\mathcal{I}_\perp$ is the nuclear moment of inertia (perpendicular to the symmetry axis). $\mathcal{I}_\perp$ is taken equal to the rigid-body value at high excitation energies (at which pairing correlations are destroyed), while experimental value is adopted at zero temperature. In the intermediate range, values interpolated using the GSM equations [5.28] are used.

For $\gamma-$asymmetric nuclides the rotational enhancement factor is

$$K_{rot}(U) = 2\sqrt{2\pi}\sigma_\perp^2\sigma. \tag{5.38}$$

The closed-form expressions for the thermodynamic temperature and other relevant equations needed to calculate $\rho(U, J, \pi)$ are provided by the GSM model [5.28]. Mass asymmetry increases level densities by a factor of 2.

The quasi-particle level density $\rho_{qp}(U, J, \pi)$ is defined as

$$\rho_{qp}(U, J, \pi) = \frac{(2J+1)\omega_{qp}(U)}{4\sqrt{2\pi}\sigma_\perp^2\sigma}\exp\left(-\frac{J(J+1)}{2\sigma_\perp^2}\right). \tag{5.39}$$

Few-quasi-particle effects, due to pairing correlations, are essential for state density calculation at low intrinsic excitation energies of recently. The section was shown to two-quasi-particle configurations ^{238}Pu [5.52]. The same effect is observed in the ^{238} U(n,γ) data due to (n,γ n') reaction competition [5.53]. It was demonstrated that effects are important for reproducing fission cross sections below ~2 MeV incident neutron energy [5.46, 5.54]. Observed irregularities in neutron-induced fission cross be attributed to the interplay of few-quasiparticle the level density of fissioning and residual nuclei. $n-$quasiparticle state densities, which sum-up to the intrinsic state density of quasiparticle excitations can be estimated using Bose-gas model predictions [5.52, 5.55]

$$\omega_{qp}(U) = \sum_n \omega_{nqp}(U) = \sum_n \frac{g^n(U-U_n)^{n-1}}{((n/2)!)^2(n-1)!}, \tag{5.40}$$

where $g = 6a_{cr}/\pi^2$ is a single-particle state density at the Fermi surface, and n is the number of quasi-particles. This equation provides energies. Partial state densities $\omega_{nqp}(U)$ depend critically on the excitation of the n-quasi-particle odd-A nuclei, n = 2, 4, ... for even-even and odd-odd

nuclei). The discrete character of few-quasi-particle excitations is unimportant only in the case of odd-odd nuclei. The values of U_n are given by [5.55]

$$U_n = \begin{cases} E_{cond}(3.23n/n_{cr} - 1.57n^2/n_{cr}^2), & \text{if } n < 0.446\ n_{cr} \\ E_{cond}(1 + 0.627n^2/n_{cr}^2), & \text{if } n \geq 0.446\ n_{cr}. \end{cases} \tag{5.41}$$

Here, $n_{cr} = 12/\pi^2(\ln 2)gt_{cr}$, $t_{cr} = 0.571\Delta$ is a critical temperature, and $E_{cond} = 0.152a_{cr}\Delta^2 - m\Delta$ is a condensation energy (with m=0, 1, 2 for even-even, odd-A and odd-odd nuclides, respectively). Eq.5.41 takes into account the energy dependence of the correlation function $\Delta(U)$ and a modified Pauli correction to the excitation energy. The angular momentum distribution parameter σ^2 can be written as

$$\sigma^2 = \sum_n n\langle m^2\rangle\omega_{nqp}(U) / \sum_n \omega_{nqp}(U), \tag{5.42}$$

where $\langle m^2\rangle = 0.24A^{2/3}$ is the average value of the squared projection of the angular momentum of the single-particle states on the symmetry axis.

The pairing is weakened by excitation of few-quasi-particle states. Actually, only the lowest-number quasi-particle states (n =2 for even nuclei and n =1 for odd nuclei) lead to the pronounced structure in the total level density for actinide nuclei [5.52]. In the case of even-even nuclei, at excitations below four-quasi-particle excitation threshold, the intrinsic state density $\omega_2(U)$ can be represented by Eq. (5.40) modified with a Woods-Saxon type factor:

$$\omega_2(U) = g^2(U_4 - U_2 - \alpha)\left[1 + \exp((U_2 - U + \beta)/\gamma)\right]^{-1}. \tag{5.43}$$

This estimate of $\omega_2(U)$ was obtained by modeling the structure of ^{238}Pu intrinsic state density in order to interpret observed step-like structure in the ^{239}Pu(n,2n) reaction near the threshold [5.52].

To avoid the use Bose-gas equations (Eq. (5.40)) for the intrinsic state densities, the step-like behavior can be simulated within the constant temperature model. At excitation energies above the pairing gap (i.e. $U > U_2$) but below the four-quasi-particle excitation threshold, the level density $\rho(U)$ of an axially symmetric fissioning nucleus is calculated as

$$\rho(U) = \rho(U_4 - \delta_4)/(1 + \exp(U_2 - U + \delta_a)/\delta_s). \tag{5.44}$$

This estimate almost coincides with the predictions of the Bose-gas model. The numerical values: δ_4 =0.5 MeV, $\delta_a = 0.1 \div 0.2$ MeV, $\delta_s = 0.1 \div 0.2$ MeV were extracted by fitting fission cross section data. Fission level density for even-even nuclide ^{234}U at outer saddle, as calculated within the current approach (Eq. (5.44)), are compared with the constant temperature model approximation on Fig. 5.7. Collective levels are used below the threshold for the 2-quasi-particle excitations (U_2). In case of axial symmetry at the inner saddle the band-heads spectra are similar to that at equilibrium deformation. In case of axial asymmetry at the inner saddle the 2^+ band-heads are sufficiently lowered. The position of negative parity band $K^\pi = 0^-$ at outer saddle is lowered due to mass asymmetry (see Table 5.3)

In the case of odd-even and even-odd nuclei the partial contributions $\omega_{nqp}(U)$ of $n-$quasiparticle states to the total intrinsic state density $\omega_{qp}(U)$ produce a distinct "jump" only below the 3-quasi-particle excitation threshold (U_3). The level density of the fissioning nucleus at excitations $U > U_3$ may be calculated introducing odd-even excitation energy shift: $\hat{U} = U + \Delta_f$, where Δ_f is the correlation function for the saddle point deformation. Nuclear level density $\rho(U)$ up to the 3-quasi-particle excitation threshold U_3 is actually independent on the excitation energy, since the intrinsic state density ($\omega_1 \sim g$) is constant. Therefore, level densities in this energy region can be written as

$$\rho(U) = T_f^{-1}\exp((U_3 + \Delta_f - U_o - \delta_3)/T_f) \sim \exp((\Delta_f - U_o)/T_f). \tag{5.45}$$

Table 5.3: Transition spectra band-heads of even-even nuclei.

inner saddle			outer saddle	
K^π	$E^{ax}_{K^\pi}$, MeV	$E^{nonax}_{K^\pi}$, MeV	K^π	E_{K^π}, MeV
0^+	0.0	0.0	0^+	0.0
2^+	0.5	0.1	2^+	0.5
0^-	0.4	0.4	0^-	0.2
1^-	0.4	0.4	1^-	0.5
2^+	0.5	0.5	2^+	
2^-	0.4	0.4	2^-	
0^+	0.8	0.8	0^+	
0^+	0.8	0.8	0^+	

Table 5.4: Transition spectra band-heads of Z-odd, N-even nuclei.

inner saddle		outer saddle	
K^π	E_{K^π}, MeV	K^π	E_{K^π}, MeV
$3/2^-$	0.0	$5/2^+$	0.0
$5/2^+$	0.140	$5/2^-$	0.0
$7/2^-$	0.180	$3/2^+$	0.08
$5/2^-$	0.180	$3/2^-$	0.08
		$1/2^+$	0.04
		$1/2^-$	0.04
		$1/2^+$	0.05
		$1/2^-$	0.05

Above the 3-quasi-particle states excitation threshold the constant temperature model is used. However, for the excitation energies between 3-quasi-particle and 5-quasi-particle excitation thresholds, the level density can be slightly increased, as compared with the constant temperature approximation:

$$\rho(U) = T_f^{-1} \exp((U - U_o + \delta_5)/T_f). \tag{5.46}$$

The discrete transition state spectra, for excitation energies up to 200 keV, can be constructed using one-quasi-particle states by Bolsterli *et al.* [5.56]. Each one-quasi-particle state in odd fissioning nucleus is assumed to have a rotational band built on it with a rotational constant, depending on the respective saddle-point deformation (see Tables 5.4i and 5.5). Due to the axial asymmetry at the inner saddle we additionally assume $(2J + 1)$ rotational levels for each J value. The positive parity bands $K^\pi = 1/2^+,\ 3/2^+,\ 5/2^+, \ldots$ at outer saddle are assumed to be doubly degenerated due to mass asymmetry [5.43]. The intrinsic 2-quasi-particle spectrum

Table 5.5: Transition spectra band-heads Z-even, N-odd nuclei.

inner saddle		outer saddle	
K^π	E_{K^π}, MeV	K^π	E_{K^π}, MeV
$1/2^+$	0.0	$1/2^+$	0.0
$5/2^+$	0.08	$1/2^-$	0.0
$1/2^-$	0.05	$3/2^+$	0.08
$3/2^-$	0.0	$3/2^-$	0.08
		$5/2^+$	0.0
		$5/2^-$	0.0

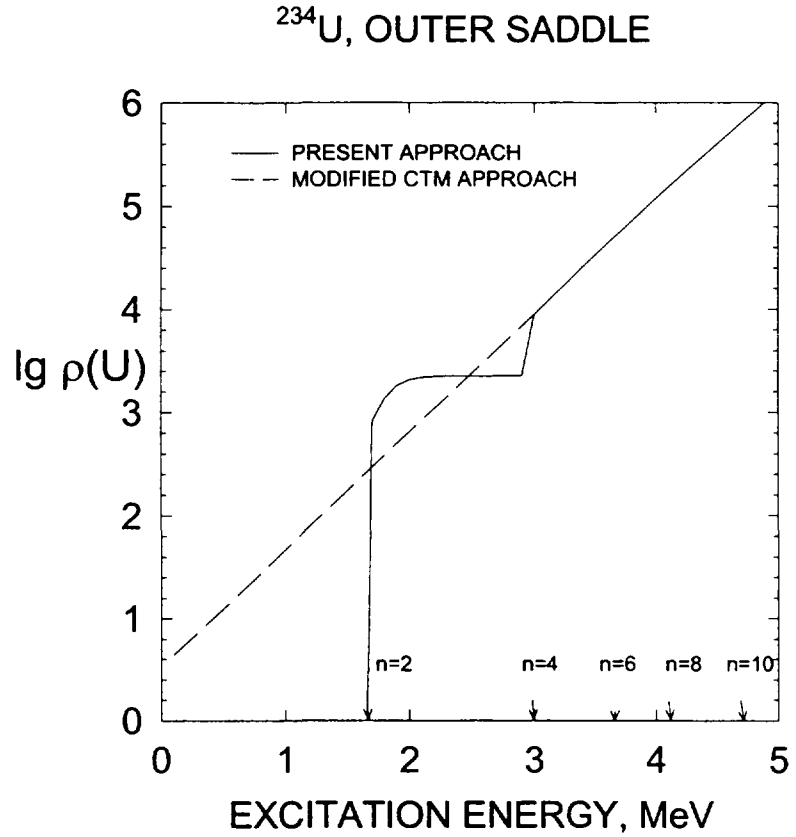

Figure 5.7: Level densities at outer saddle-point in ^{234}U. The arrows on the horizontal axis indicate excitation thresholds of even $n-$quasi-particle configurations.

of odd-odd nuclide ^{242}Am at equilibrium deformation can be obtained following Sood and Singh [5.57]. The expected location of still unobserved two-quasi-particle states was predicted (see Table 5.6). Using these intrinsic states as the band-head energies the rotational bands can be built in the same way as for Z-odd, N-even nuclei.

Table 5.6: Transition spectra band-heads of $Z-$odd, $N-$odd nuclei.

inner saddle		outer saddle	
K^π	E_{K^π}, MeV	K^π	E_{K^π}, MeV
1^-	0.0	1^-	0.0
0^-	0.044	0^-	0.044
5^-	0.049	5^-	0.049
6^-	0.170	6^-	0.170
1^-	0.220	1^-	0.220
3^-	0.242	$3-$	0.242
2^-	0.288	2^-	0.288

The values of δ_3 and δ_5 parameters can be defined by fitting fission cross section data. The level densities calculated with Eqs. (5.45) and (5.46) at the inner saddle-point of ^{239}Pu are shown on Fig. 5.8.

Adopting fission and total level densities modeling described above fission barrier parameters were extracted from the experimental neutron-induced fission cross sections on $^{232-238}$U, $^{238-244}$Pu, $^{241-243}$Am, and $^{242-248}$Cm targets [5.58-5.63]. Fission barrier parameters for Th, Pa,

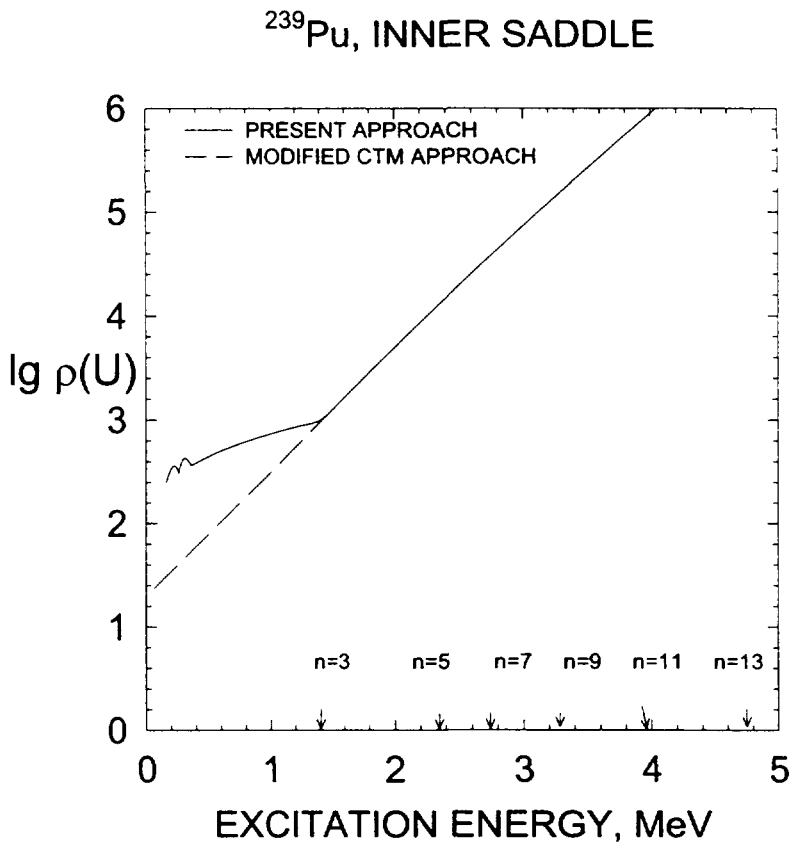

Figure 5.8: Level densities at inner saddle-point in ^{239}Pu. The arrows on the horizontal axis indicate excitation thresholds of odd $n-$quasi-particle configurations.

and Np nuclei were obtained essentially within the same approach [5.64–5.66]. In the latter case, however, the parameters should be treated as rather crude estimates, due to the more complex structure of fission barriers in Th and Pa as compared to the transuranium nuclei.

Fission barrier parameters: inner(A) and outer(B) barrier heights ($E_{fA(B)}$) and curvatures ($\hbar\omega_{A(B)}$) are given in Table 5.7. The symbol SYM denotes the symmetry of saddle point deformation. Comparison of the obtained results with the fission barriers determined by Smirenkin [5.67] shows the following: (i) for isotopes of uranium the agreement is rather good for outer fission barriers, while the isotopic dependencies for the inner barriers are similar, (ii) for Pu and Am the agreement is also good, except the americium outer barrier for neutron-deficient isotopes. It should be noted that the recommended barriers for neutron-deficient Am nuclei were determined from the analysis of the data for the ^{241}Am(n,f) reaction [5.59]. The largest discrepancies are observed in the case of outer barriers in Cm.

5.2.3 Conclusions and Recommendations

Recommended sophistication of the level density model, as compared to the conventional approaches, is needed in order to reproduce experimental data with the consistent level density and barrier parameters. It should be stressed, that the use of the recommended fission barriers also implies the use of the described approach to the level densities above the inner and outer saddle-points. The recommended fission barrier parameters are contained in **maslov.dat** file.

Table 5.7: Fission barrier parameters.

Nuclide	E_{fA},MeV	Sym.(A)	E_{fB},MeV	Sym.(B)	$\hbar\omega_A$,MeV	$\hbar\omega_B$,MeV	Δ_f,MeV
^{230}Th	6.1	S	6.8	MA	0.9	0.6	0.832
^{231}Th	6.0	S	6.7	MA	0.7	0.5	0.830
^{232}Th	5.8	S	6.7	MA	0.9	0.6	0.828
^{233}Th	5.1	S	6.65	MA	0.7	0.5	0.806
^{230}Pa	5.6	S	5.8	MA	0.6	0.4	0.802
^{231}Pa	5.5	S	5.5	MA	1.0	0.5	0.800
^{232}Pa	5.0	S	6.4	MA	0.6	0.4	0.828
^{233}Pa	5.7	S	5.8	MA	1.0	0.5	0.808
^{234}Pa	6.3	S	6.15	MA	0.6	0.4	0.806
^{231}U	4.4	S	5.5	MA	0.7	0.5	0.869
^{232}U	4.9	S	5.4	MA	0.9	0.6	0.848
^{233}U	4.35	S	5.55	MA	0.8	0.5	0.946
^{234}U	4.8	S	5.5	MA	0.9	0.6	0.889
^{235}U	5.25	S	6.0	MA	0.7	0.5	0.803
^{236}U	5.0	S	5.67	MA	0.9	0.6	0.833
^{237}U	6.4	GA	6.15	MA	0.7	0.5	0.809
^{238}U	6.3	GA	5.5	MA	1.0	0.6	0.818
^{239}U	6.45	GA	6.0	MA	0.7	0.5	0.816
^{236}Np	5.9	GA	5.4	MA	0.6	0.4	0.821
^{237}Np	6.0	GA	5.4	MA	1.0	0.5	0.819
^{238}Np	6.5	GA	5.75	MA	0.6	0.4	0.820
^{237}Pu	5.10	S	5.15	MA	0.7	0.5	0.799
^{238}Pu	5.6	S	5.1	MA	0.9	0.6	0.818
^{239}Pu	6.2	GA	5.7	MA	0.7	0.5	0.816
^{240}Pu	6.05	GA	5.15	MA	0.9	0.6	0.875
^{241}Pu	6.15	GA	5.50	MA	0.7	0.5	0.855
^{242}Pu	5.85	GA	5.05	MA	0.9	0.6	0.846
^{243}Pu	6.05	GA	5.45	MA	0.7	0.5	0.910
^{244}Pu	5.7	GA	4.85	MA	0.9	0.6	0.848
^{245}Pu	5.85	GA	5.25	MA	0.7	0.5	0.855
^{239}Am	6.00	GA	5.40	MA	0.8	0.5	0.776
^{240}Am	6.10	GA	6.00	MA	0.6	0.4	0.775
^{241}Am	6.00	GA	5.35	MA	0.8	0.5	0.773
^{242}Am	6.32	GA	5.78	MA	0.6	0.4	0.884
^{243}Am	6.40	GA	5.05	MA	1.0	0.5	0.770
^{244}Am	6.25	GA	5.9	MA	0.7	0.53	0.808
^{241}Cm	7.15	GA	5.5	MA	0.7	0.5	0.793
^{242}Cm	6.65	GA	5.0	MA	0.9	0.6	0.811
^{243}Cm	6.33	GA	5.4	MA	0.7	0.5	0.810
^{244}Cm	6.18	GA	5.10	MA	0.9	0.6	0.868
^{245}Cm	6.35	GA	5.45	MA	0.7	0.5	0.867
^{246}Cm	6.00	GA	4.80	MA	0.9	0.6	0.865
^{247}Cm	6.12	GA	5.10	MA	0.7	0.5	0.883
^{248}Cm	5.80	GA	4.80	MA	0.9	0.6	0.842
^{249}Cm	5.63	GA	4.95	MA	0.7	0.5	0.900

S - symmetric saddle point, GA - axially asymmetric saddle point, MA - mass asymmetric saddle point.

5.3 Partial Level Densities

Coordinator: M.B. Chadwick

Summary

Methods for calculating partial level densities for use in pre-equilibrium model calculations are described.

The RIPL Starter File includes a Fortran code **avrigeanu.for** by M. Avrigeanu for using various equidistant and Fermi-gas single-particle models, including models that incorporate pairing and shell effects within closed-form treatments and a Fortran code *capote_micro.for* by R. Capote, which uses a microscopic theory based on a convolution of shell-model single-particle states with BCS pairing.

5.3.1 Introduction

The partial level density (or "state density") is used in pre-equilibrium reaction calculations to describe the statistical properties of particle-hole excitations. Numerous theoretical methods have been developed to determine these partial level densities, and a variety of approaches have been used by researchers in pre-equilibrium calculations. Some of these approaches address theoretical methods for incorporating physical phenomena such as shell effects and pairing.

Despite the extensive amount of research that has been undertaken into the computation of partial level densities, even the most sophisticated theoretical predictions can significantly deviate from reality. There is a difficulty in testing the validity of calculated partial densities through comparisons between calculated and measured pre-equilibrium spectra because of uncertainties in our understanding of pre-equilibrium reaction mechanisms. A useful collection of articles on state-of-the-art methods for the calculation of partial level densities is the proceedings of the *Nuclear Level Densities* conference in Bologna [5.68].

One of the most widely used approaches is to determine partial level densities within an equidistant single-particle model, as proposed by Williams [5.69]. An important modification to limit the holes to excitation energies less than the nuclear well depth was made by Běták and Dobeš [5.70]. This is summarized below. A useful work which utilizes a computation of partial level densities from single-particle shell-model states within an applications-oriented Williams-type expression, is the work of M. Herman, G. Reffo *et al.* [5.71]. However, electronic files containing the numerical values determined in this work are unavailable.

5.3.2 Equidistant Formula with Well-Depth Restrictions

Since partial level densities based on equidistant levels are widely used in pre-equilibrium calculations because of their simplicity, we provide expressions for their determination below.

The density of p-particle h-hole states with residual nucleus energy U can be partitioned into the energy-dependent density multiplied by a spin distribution, $\rho(p,h,U,l) = \omega(p,h,U)\ R_n(l)$. The equidistant model expression for the energy dependent density with finite hole-depth re-

strictions is [5.70]

$$\omega(p,h,U) = \frac{g^n}{p!h!(n-1)!}\sum_{j=0}^{h}(-1)^j\binom{h}{j}(U-\Delta-A_{ph}-j\epsilon_F)^{n-1}$$

$$\times\ \Theta(U-\Delta-\alpha_{ph}-j\epsilon_F), \tag{5.47}$$

where $n = p+h$, g is the single particle density, ϵ_F is the Fermi energy, Δ is the pairing energy, and $A_{ph} = (p^2+h^2+p-3h)/4g$ accounts for Pauli blocking, and $\alpha_{ph} = (p^2+h^2)/2g$. The Θ-function is unity if its argument is positive, and zero otherwise. The single-particle density is often taken as $g = A/13$, which approximates the average single-particle density near the Fermi energy. Numerous possibilities for the pairing energy Δ have been suggested; a particularly useful approach is the "advanced pairing model" of Fu, which is mentioned below.

A Gaussian spin distribution is usually adopted,

$$R_n(l) = \frac{2l+1}{2\sqrt{2\pi}\sigma_n^3}\exp\left[-\frac{(l+1/2)^2}{2\sigma_n^2}\right], \tag{5.48}$$

where l is the spin and σ_n is the spin cut-off parameter, often taken as $\sigma_n^2 = 0.24nA^{2/3}$ [5.72].

The above expression is applicable in many pre-equilibrium model calculations. However, a useful extension of this formula to cases where the particle-excitations are also restricted, has been made by Obložinský [5.73]. This form is particularly useful in quantum mechanical multistep compound calculations where the particle excitations remain bound.

5.3.3 Analytical Formula

The RIPL Starter File includes a code, **avrigeanu.for**, written by Avrigeanu *et al.* [5.74], to calculate partial level densities from a variety of models. The partial level density models computed by this code are described in detail in Avrigeanu *et al.*'s extensive report [5.74], and are summarized below:

1. The one-component Williams formula, which uses equidistant single-particle levels [5.69];
2. The two component (i.e. distinguishing neutron and proton excitations) Williams formula, which uses equidistant single-particle levels;
3. The one and two component formula versions of the Williams formula with finite well-depth restrictions, due to Běták and Dobeš [5.70];
4. The one and two component formula versions of the Williams formula with finite well-depth and binding-energy restrictions, due to Obložinský [5.73];
5. The advanced pairing correction formulae of Fu [5.55], using the one-component Fu model;
6. The Kalbach formula for one-component partial level densities with pairing considerations [5.75];
7. The Kalbach formula based on single-particle and hole levels with a Fermi-gas energy dependence [5.76]. The nuclear potential finite-depth correction factor for a one-component Fermi-gas is also determined [5.76];
8. The Mao formula, including Pauli-exclusion effects [5.77].

5.3.4 Microscopic Theory

Most semi-empirical approaches to calculating partial level densities are based on various simplifying approximations. In particular, such approaches often inadequately account for shell effects, pairing effects and parity distributions. To address these deficiencies, more involved microscopical methods have been developed to calculate more realistic particle-hole level densities using the single-particle level scheme of the shell model. Additionally, the BCS formalism has been included in order to account more properly for pairing effects. In the combinatorial method the level density is calculated numerically by performing an exhaustive counting of the nuclear excited configurations.

The other file *capote_micro.for* is a Fortran code, included in the RIPL Starter File by R. Capote and R. Pedrosa [5.78]. It allows for microscopic calculations of particle-hole partial level densities (up to $3p-3h$ for even-even nuclei), which represent the dominant contribution to the pre-equilibrium component of emission spectra. Shell-model single-particle levels are taken from the Möller-Nix compilation [5.40].

The *capote_micro.for* code is a more recent (and rewritten) version of Herman and Reffo's ICAR code described in Ref. [5.79].

5.3.5 Conclusions and Recommendations

For detailed studies of the role of partial level densities in pre-equilibrium calculations, microscopic calculations using the *capote_micro.for* code may be performed. Such calculations include shell, and pairing effects. However, the results of such calculations should always be treated with caution, as the predictive capability of all partial level density theories is limited. For many pre-equilibrium calculations, particularly for applications, the more phenomenological models included in Avrigeanu's **avrigeanu.for** code are useful. Again, though, the limitations of such partial level density predictions should be kept in mind.

REFERENCES

[5.1] H. Bethe, Rev. Mod. Phys. **9**, 69 (1937).

[5.2] A.V. Ignatyuk, M.G. Itkis, V.N. Okolovich, G.N. Smirenkin and A.S. Tishin, J. Sov. Nucl. Phys. **21**, 612 (1975).

[5.3] S.K. Kataria and V.S. Ramamurthy, Nucl. Phys. **A349**, 10 (1980).

[5.4] W. Reisdorf, Z. Phys. **A300**, 227 (1981).

[5.5] J. Toke and W.J. Swiatecki, Nucl. Phys. **A372**, 141, (1981).

[5.6] J.M. Lang and K.J. Le Couteur, Proc. Phys. Soc. **A67**, 586 (1954).

[5.7] E. Erba, U. Facchini and E. Saetta-Menichella, Nuovo Cim. **22**, 1237 (1961).

[5.8] A. Gilbert and A.G.W. Cameron, Can. J. Phys. **43**, 1446 (1965).

[5.9] J.E. Lynn, *Theory of Neutron Resonance Reactions* (Clarendon Press, Oxford 1968).

[5.10] A.V. Malyshev, *Level Density and Structure of Atomic Nuclei* (in Russian). (Atomizdat, Moscow 1969).

[5.11] H. Baba, Nucl. Phys. **A159**, 625 (1970).

[5.12] W. Dilg, W. Schantl, H. Vonach and M. Uhl, Nucl. Phys. **A217**, 269 (1973).

[5.13] S.K. Kataria, V.S. Ramamurthy and S.S. Kapoor, Phys. Rev. **C18**, 549 (1978).

[5.14] G. Reffo, *in* Nuclear Theory for Applications. IAEA-SMR-43, Trieste, 1980, p. 205.

[5.15] A.S. Iljinov, M.V. Mebel *et al.*, Nucl. Phys. **A543**, 517 (1992).

[5.16] T. Ericson, Adv. Phys. **9**, 425 (1960).

[5.17] J.L. Cook, H. Ferguson and L. Musgrov, Aust. J. Phys. **20**, 477 (1967).

[5.18] Su Zongdi, Zhuang Youxiang, Wang Cuilan, Zhou Chunmei, Report INDC(CPR)-2 (IAEA Vienna 1985).

[5.19] A.V. Ignatyuk, V.S. Stavisski and Yu.N. Shubin, *in* Nuclear Data for Reactors. IAEA Vienna, 1970.

[5.20] V.S. Ramamurthy, S.S. Kapoor and S.K. Kataria, Phys. Rev. Lett. **25**, 386 (1970).

[5.21] S. Goriely, Nucl. Phys. **A605**, 28 (1996).

[5.22] A.V. Ignatyuk, G.N. Smirenkin and A.S. Tishin, J. Sov. Nucl. Phys. **21**, 255 (1975).

[5.23] W.D. Myers and W.J. Swiatecki, Ark. Fysik **36**, 593 (1967).

[5.24] A. Mengoni and Y. Nakajima, J. Nucl. Sci. Tech. **31**, 151 (1994).

[5.25] Huang Zhongfu, He Ping, Su Zongdi and Zhou Chunmei, Chin. J. Nucl. Phys., **13**, 147 (1991).

[5.26] T. Belgya, G. Molnár, B. Fazekas and J. Östör, Report INDC(NDS)-367 (IAEA Vienna 1997).

[5.27] A.V. Ignatyuk, *Statistical Properties of Excited Atomic Nuclei* (in Russian). (Energoatomizdat, Moscow 1983); Translated by IAEA, Report INDC-233(L) (IAEA Vienna 1985).

[5.28] A.V. Ignatyuk, K.K. Istekov and G.N. Smirenkin, Sov. J. Nucl. Phys. **29**, 450 (1979).

[5.29] A.V. Ignatyuk, J.L. Weil, S. Raman and S. Kahane, Phys. Rev. **C47**, 1504 (1993).

[5.30] A. Bohr, B. Mottelson, *Nuclear Structure, vol 2* (Benjamin Inc., New York and Amsterdam, 1974).

[5.31] G. Hansen and A. Jensen, Nucl. Phys. **A406**, 236 (1983).

[5.32] G. Maino, A. Mengoni and A. Ventura, Phys. Rev. **C42**, 988 (1990).

[5.33] E.M. Rastopchin, M.N. Svirin and G.N. Smirenkin, Sov. J. Nucl. Phys. **52**, 1258 (1990).

[5.34] A.V. Ignatyuk, *in* Nuclear Data Evaluation Methodology, Ed. Ch. Dunford (World Scientific, Singapore 1992), p. 411.

[5.35] O.T. Grudzevich, A.V. Ignatyuk, V.I. Plyaskin and A.V. Zelenetsky, *in* Nuclear Data for Science and Technology (Mito, 1988), JAERI, p. 187.

[5.36] W.D. Myers, Droplet Model of Atomic Nuclei. Plenum Press, 1977.

[5.37] A.V. Ignatyuk, Contribution to the 3rd CRP Meeting on RIPL, Trieste, 1997.

[5.38] Lu Guoxiong, Dong Liaoyuan, Huang Zhongfu, Qiu Guochun, Su Zongdi, Contribution to the 3-rd CRP Meeting on RIPL, Trieste, 1997.

[5.39] A.V. Ignatyuk, K.K. Istekov, V.N. Okolovich and G.N. Smirenkin G.N, *in* Physics and Chemistry of Fission, IAEA, Vienna, 1980, v. 1, p. 21.

[5.40] P. Möller, J.R. Nix, W.D. Myers and W.J. Swiatecki, Atomic Data Nucl. Data Tbl. **59**, 185 (1995).

[5.41] J.R. Nix, Private communication to M. Herman, 1988.

[5.42] V.M. Strutinsky, Nucl. Phys. **A95**, 420 (1967).

[5.43] W.M. Howard and P. Möller, Atomic Data Nucl. Data Tbl. **25**, 219 (1980).

[5.44] T. Dossing, T.I. Khoo, T. Lauritsen *et al.*, Phys. Rev. Lett. **75**, 1276 (1995).

[5.45] S.T. Boneva, V.A. Khitrov, Yu.V. Popov and A.M. Sukhovoj, *in* Proc. IV International Seminar on Interaction of Neutrons with Nuclei, Dubna, Russia, April 27-30, 1996, Report E3-96336 (JINR Dubna 1996), p. 183.

[5.46] V.M. Maslov, *in* Proc. IV International Seminar on Interaction of Neutrons with Nuclei, Dubna, Russia, April 27-30, 1996, Report E3-96336 (JINR Dubna 1996), p. 326.

[5.47] A.V. Ignatyuk and V.M. Maslov, Sov. J. Nucl. Phys. **54**, 392 (1991).

[5.48] A.V. Ignatyuk and V.M. Maslov, *in* Proc. Int. Symp. Nuclear Data Evaluation Methodology, Brookhaven,USA, October 12-16, 1992 (World Scientific, Singapore 1993), p. 440.

[5.49] V.M. Maslov and Y. Kikuchi, JAERI-Research 96-030, 1996.

[5.50] S. Bjornholm and J.E. Lynn, Rev. Mod. Phys. **52**, 725 (1980).

[5.51] Yu.V. Porodzinskij, E.Sh. Sukhovitskij and V.M. Maslov *in* Int. Conf. Nucl. Data Sci. and Technology, Trieste, Italy, May 19-23, 1997.

[5.52] V.M. Maslov, Z. Phys. **A347**, 211 (1994).

[5.53] V.M. Maslov, *in* Proc. 9th Int. Symp. Capture Gamma-Ray Spectroscopy and Related Topics, Budapest, Hungary, October 8-12, 1996, to be published.

[5.54] V.M. Maslov, *in* Int. Conf. Nucl. Data for Sci. and Technology, Trieste, Italy, May 19-23, 1997.

[5.55] C.Y. Fu, Nucl. Sci. Eng. **86**, 344 (1984); C.Y. Fu, Nucl. Sci. Eng. **92**, 440 (1986).

[5.56] M. Bolsterli, E.O. Fiset, J.R. Nix and J.L. Norton, Phys. Rev. **C5**, 1050 (1972).

[5.57] P.C. Sood and R.N. Singh, Nucl. Phys. **A373**, 519 (1982).

[5.58] V.M. Maslov *et al.*, Report INDC(BLR)-4 (IAEA Vienna 1996).

[5.59] V.M. Maslov *et al.*, Report INDC(BLR)-5 (IAEA Vienna 1996).

[5.60] V.M. Maslov and Y. Kikuchi, Nucl. Sci. Eng. **124**, 492 (1996).

[5.61] V.M. Maslov *et al.*, Report INDC(BLR)-7 (IAEA Vienna 1997).

[5.62] V.M. Maslov *et al.*, Report INDC(BLR)-9 (IAEA Vienna 1997).

[5.63] V.M. Maslov, submitted for publication to Sov. J. Nucl. Phys., 1997.

[5.64] V.M. Maslov, Ann. Nucl. Energy **19**, 181 (1992).

[5.65] V.M. Maslov, Yadernye Konstanty **1**, 80 (1992).

[5.66] V.M. Maslov, Yadernye Konstanty **4**, 19 (1987).

[5.67] G.N. Smirenkin, Report INDC(CCP)-359 (IAEA Vienna 1993).

[5.68] Proceedings of the Nov 15-17, 1989 conference in Bologna, *Nuclear Level Densities*, Ed. G. Reffo, M. Herman, and G. Maino (World Scientific, Singapore 1992).

[5.69] F.C. Williams, Nucl. Phys. **A166**, 231 (1971).

[5.70] E. Běták and J. Dobeš, Z. Phys. **A279**, 319 (1976).

[5.71] M. Herman, G. Reffo, *et al.*, Phys. Rev. **C40**, 2870 (1989).

[5.72] H. Gruppelaar, *in IAEA Advisory Group Meeting on Basic and Applied Problems on Nuclear Level Densities.* Ed. M.R. Bhat (Brookhaven National Laboratory 1983), p. 143.

[5.73] P. Obložinský, Nucl. Phys. **A453**, 127 (1986).

[5.74] M. Avrigeanu, A. Harangozo and V. Avrigeanu, "Development of Data Files with Partial Level Densities for Nuclear Data Calculations", IAEA Report (to be published); M. Avrigeanu, IAEA Research Contract No. 8886/RO/RBF.

[5.75] C. Kalbach, Nucl. Sci. Eng. **95**, 70 (1987); C. Kalbach, Z. Phys. **A332**, 157 (1989).

[5.76] C. Kalbach, Phys. Rev. **C32**, 1157 (1985).

[5.77] Mao Ming De and Guo Hua, J. Phys. **G19**, 421 (1993).

[5.78] R. Capote and R. Pedrosa, DENSIDAD code (1996), unpublished; Private communication to P. Obložinský of the IAEA (1997).

[5.79] M. Herman and G. Reffo, Phys. Rev. **C36**, 1546 (1987); M. Herman, G. Reffo and R.A. Rego, Phys. Rev. **C37**, 797 (1988).

6 Gamma-Ray Strength Functions

Coordinator: J. Kopecky

Summary

Gamma-ray strength functions are important for description of the gamma emission channel in nuclear reactions. This is an almost universal reaction channel since gamma rays, in general, may accompany emission of any other emitted particle.

The collected data bring information on experimental data and parameterizations of giant resonaces (mainly $E1$, but also $E2$ and $M1$) and the global systematics derived from experimental strength function data.

Recommended giant resonance parameters (not only those for giant dipole resonances) are summarized in **kopecky.readme**, and a tabular form of GDR parameters for specific nuclei is given in recommended file **beijing_gdr.dat**. Other file *varlamov.dat* brings additional useful information on GDR parameters.

Information on strength functions is also in **kopecky.readme** and an extensive systematics of global strength function data is in recommended file **kopecky.dat**.

6.1 Introduction

The impact of different models for gamma-ray strength functions f_{XL} on the calculation of neutron capture related experimental quantities, such as total radiative width, cross sections and gamma-ray spectra, has been studied in Refs. [6.1–6.11] and the results and recommendations are discussed in Chapter 6.2. Traditional models, used to describe radiative $E1$, $M1$ and $E2$ strength, namely the standard Lorentzian for $E1$ and the single-particle model for $M1$ and $E2$, result in a strong overestimation of all pertinent experimental quantities.

For $M1$ and $E2$ radiation we recommend strength functions derived from a standard Lorentzian with a global set of parameters. This formulation is superior to the traditionally applied single-particle models. For the dominant $E1$ strength, however, a generalized Lorentzian, with an energy dependent width and a finite limit as the energy tends to zero, is the best representation. It reproduces data reasonably well in the mass region A=50–200 with the exception of strongly deformed targets between A=150 and 170, underestimating the experimental values. In order to obtain $E1$ strength function model for the whole mass region an "enhanced generalized Lorentzian" is proposed, with two parameters depending smoothly on the mass number.

Important quantities for calculation of the gamma-ray strength functions are Lorentzian parameters of particular giant resonances. For $E1$ and $E2$ giant resonances they are traditionally derived from the analysis of the photoabsorption cross sections. However, this experimental data base is rather scarce and no experimental data are available for many target nuclei. Therefore several global systematic parameterizations of Lorentzian parameters have been derived for all multipolarities and they are quoted and discussed in Chapter 6.3.

The calculated gamma-ray strength functions can be directly compared to experimentally determined, usually averaged, strength functions. Earlier compilations of photon-strength functions, based on experimental data from resonance- or thermal-neutron capture and photonuclear

reactions, have been recently reviewed and updated with new data [6.12, 6.13, 6.14] together with their uncertainties. The individual experimental values have been used to test directly different strength function models, in particular for $E1$ radiation (see e.g. Ref. [6.15]). Further they resulted in derived global systematics of f_{E1} and f_{M1} values as a function of atomic mass A, which can be used for normalizations in statistical-model calculations. Brief description of the results is discussed in Chapter 6.4.

6.2 Models for γ-Ray Strength Functions

The gamma-ray strength function for multipole type XL is defined as the average reduced partial radiation $E_\gamma^{-(2L+1)}\langle\Gamma_{XL}(E_\gamma)\rangle$ per unit energy interval

$$f_{XL}(E_\gamma) = E_\gamma^{-(2L+1)}\langle\Gamma_{XL}(E_\gamma)\rangle/D \tag{6.1}$$

of resonances with average spacing D; E_γ is the transition energy. The corresponding gamma-ray transmission coefficient $T_{XL}(E_\gamma)$ is given by the relation

$$T_{XL}(E_\gamma) = 2\pi E_\gamma^{(2L+1)} f_{XL}(E_\gamma). \tag{6.2}$$

Therefore gamma-ray strength functions enter as important ingredients into compound nucleus model calculations of capture cross sections, gamma-ray production spectra, isomeric state populations and into the assessment of the competition between gamma-ray and particle emission. The relevant multipolarities in this context are $E1$, $M1$ and $E2$.

On Refs. [6.1–6.11] strength function models have been tested by comparison to various experimental data related to neutron capture. Cross sections and spectra depend on the gamma-ray strength at all transition energies but do not differentiate between multipolarities; so they are mainly sensitive to the dominant El strength. Analysis of resonance transitions allows to determine the multipolarity but the resulting strength functions compose only a narrow energy region.

The simplest model for gamma-ray strength functions is the single-particle model prescribing an energy independent strength [6.16]. We used this model for $M2$-, $E3$- and $M3$ radiation with a strength of one Weisskopf unit per MeV.

Gamma-ray strength functions may be related to the photoabsorption cross section. If the latter is dominated by a giant resonance (GR) of Lorentzian shape Brink's hypothesis [6.17] leads to a strength function derived from a **standard Lorentzian**

$$f_{XL}^{SLO}(E_\gamma) = \frac{26\times10^{-8}}{2L+1}\sigma_0\Gamma E_\gamma^{(3-2L)}\frac{\Gamma_0}{(E_\gamma^2-E_0^2)^2+E_\gamma^2\Gamma_0^2}\ \ [\mathrm{mb^{-1}MeV^{-2}}], \tag{6.3}$$

where the Lorentzian parameters (σ_0, E_0, Γ_0) respectively stand for peak cross section, energy and width of the GR. We used this model for $E1$, $M1$ (spin-flip giant resonance [6.18]) and $E2$ (isoscalar giant resonance [6.19]) radiation. For $E1$ the Lorentzian parameters were taken from the analysis of the photoabsorption cross section [6.18] of the compound or a neighbouring nucleus. Global parameters were employed for $M1$ and $E2$ radiation (see Chapter 6.2). For nuclei with a split GDR we used in Eqs. (6.3), (6.5) and (6.7) the incoherent sum of two analogue terms; the same parameters (k_0, ϵ_0) for each term were used in Eqs. (6.6) and (6.7). For targets with A=175–205 and for ^{93}Nb we included a standard Lorentzian pygmy resonance [6.1] with parameters determined by fitting the high-energy end of the gamma-ray production spectrum.

For the dominant $E1$ radiation the standard Lorentzian model severely overestimates the experimental data and improvements based on microscopic approaches are needed. The theory of Fermi liquids [6.20] predicts an energy and temperature dependent width of the giant dipole resonance (GDR) $\Gamma(E_\gamma, T) = \alpha(E_\gamma^2 + 4\pi^2 T^2)$, where α is a normalization constant. The first term reflects the spreading of particle hole states into more complex configurations while the second one accounts for collision of quasiparticles. The temperature T refers to the absorbing state and can be calculated within a level density model. Kadmenskij *et al.* [6.21] suggested to choose α so as to guarantee compatibility with photoabsorption data

$$\Gamma_K(E_\gamma, T) = \frac{\Gamma_0}{E_0^2}(E_\gamma^2 + 4\pi^2 T^2). \tag{6.4}$$

Generalized Lorentzian, as proposed by Kopecky and Chrien [6.15], consists of two terms: a Lorentzian with the energy dependent width according to Eq. (6.4) and the (non-zero) $E_\gamma \to 0$ limit of the model of Kadmenskij *et al.* [6.21]

$$f_{E1}^{GLO}(E_\gamma) = 8.68\times10^{-8}\sigma_0\Gamma_0\left[E_\gamma\frac{\Gamma_K(E_\gamma,T)}{(E_\gamma^2-E_0^2)^2+E_\gamma^2\Gamma_K^2(E_\gamma,T)} + 0.7\frac{\Gamma_K(E_\gamma=0,T)}{E_0^3}\right] \quad [\mathrm{mb}^{-1}\mathrm{MeV}^{-2}]. \tag{6.5}$$

Up to an energy around the neutron binding energy the $E1$ strength resulting from Eq. (6.5) and that from the model of Kadmenskij et al. [6.21] are very similar.[4] In Ref. [6.1] we showed for some selected spherical nuclei that the generalized Lorentzian model provides a reasonable simultaneous description of average resonance capture (ARC) data, capture cross sections and gamma-ray production spectra. To reproduce also data for strongly deformed nuclei we proposed in Refs. [6.3–6.5, 6.8] to use in Eq. (6.5) instead of $\Gamma_k(E_\gamma, T)$ the following *empirical* generalization of the energy dependent width

$$\Gamma_{En}(E_\gamma, T) = \left[k_0 + (1-k_0)\frac{(E_\gamma - \epsilon_0)}{E_0 - \epsilon_0}\right]\Gamma_K(E_\gamma, T), \tag{6.6}$$

which is determined by two parameters (k_0, ϵ_0). For $k_0 > 1$ the width is enhanced compared to the result of Eq. 6.2. In that case the resulting El strength, obtained by replacing in Eq. 6.3 $\Gamma_K(E_\gamma, T)$ with $\Gamma_{En}(E_\gamma, T)$, is denoted as derived from an **enhanced generalized Lorentzian**

$$f_{E1}^{EGLO}(E_\gamma) = 8.68\times10^{-8}\sigma_0\Gamma_0\left[E_\gamma\frac{\Gamma_{E_n}(E_\gamma,T)}{(E_\gamma^2-E_0^2)^2+E_\gamma^2\Gamma_{E_n}^2(E_\gamma,T)} + 0.7\frac{\Gamma_{E_n}(E_\gamma=0,T)}{E_0^3}\right] \quad [\mathrm{mb}^{-1}\mathrm{MeV}^{-2}]\,. \tag{6.7}$$

The enhancement k_0 can be used to reproduce the experimental $E1$ strength around the reference energy ϵ_0. Note, that
i) for $k_0 = 1$ the generalized Lorentzian model is obtained and
ii) $\Gamma_{En}(E_\gamma \to E_0, T \to 0) \to \Gamma_0$, i. e. compatibility with photoabsorption is maintained.

In order to study the behaviour of the k_0 enhancement factor, a large number of calculations have been performed [6.10, 6.11] in the mass region A=90–200. For these calculations of neutron capture cross sections and the resulting gamma-ray spectra the Hauser-Feshbach theory in the formulation of Moldauer [6.23] has been employed and an appropriate treatment of gamma-ray cascades. The calculations were performed with the code MAURINA [6.24].

[4] Very recently Plujko has presented a new model [6.22] for f_{E1} radiative strength function, based on microcanonical ensemble of initial states. The resulting formula has the same features as the Kadmenskij *et al.* approach [6.21], namely the energy and temperature dependence of the GDR width and the non-zero limit for $E_\gamma \to 0$. This work forms an independent theoretical support for the generalized Lorentzian formalism.

In the mass and energy region considered ($A > 100$, $E_n < 3$ MeV) charged particle emission can be neglected. Neutron optical potentials were taken from the literature and eventually slightly modified in order to improve the reproduction of total cross sections and (neutron) strength functions. For strongly deformed nuclei the neutron transmission coefficients were generated by coupled channels calculations.

For the level density, characterizing the excited states beyond the known levels, we used semi-empirical models with parameters relying on recent results for the average spacing of s-wave resonances D_0 and the number of low excited levels N_{lev}. For all nuclei calculations were performed employing the *backshifted Fermi gas model* [6.25] and the model by *Kataria, Ramamurthy and Kapoor* (KRK) [6.26] which accounts for shell effects in terms of the ground-state shell correction to the nuclear binding energy. The genuine KRK model is supplemented according to the Gilbert-Cameron prescription [6.27]: a conventional pairing shift and a constant temperature portion at lower excitation energy where the spin distribution parameter σ^2 is linearly interpolated between the value σ^2_{lev}, deduced from the levels and $\sigma^2(E_x)$, the value prescribed by the KRK model at the matching energy E_x. For comparisons we used in some cases also a more sophisticated level density model — the *generalized superfluid model* in its phenomenological version — which was developed by Ignatyuk and collaborators [6.28–6.30]. For each model the respective parameters are chosen so as to reproduce the same values D_0 and N_{lev}; in case of the generalized superfluid model this was achieved by an additional shift of the excitation energy as proposed in Ref. [6.29].

When employing a particular level density model we used the pertinent temperature T also in the expressions for the gamma-ray strength functions according to the models generalized Lorentzian and enhanced generalized Lorentzian (see Eqs. (6.4–6.7)). Under these conditions the $E1$ strength depends on the level density model employed. In case of the KRK model we use the genuine temperature prescription also in the constant temperature region.

As shown in Refs. [6.1–6.11] the generalized Lorentzian model reproduces the experimental data reasonably well in the mass region A=50–200 with the exception of targets between A=150–170. For this region a better fit of the experimental data has been obtained with the standard standard Lorentzian model. Consequently, neither the standard Lorentzian nor the generalized Lorentzian model can be used for model calculations in the whole mass region. The flexible enhanced generalized Lorentzian model could do the job if its parameters (k_0, ϵ_0) show a sufficiently smooth behaviour, so that it can be applied for cross section predictions. For a fixed reasonable value of the reference energy, namely $\epsilon_0 = 4.5$ MeV, we therefore determined for all nuclei considered in our studies the enhancement k_0, by simultaneously reproducing at least two pieces of experimental data. This was done by graphical comparisons [6.10, 6.11] between experimental data and the results obtained with different k_0. In this context we allowed for k_0, also values moderately smaller than 1. Because of the strong dependence of the results on the level density model we had to do this separately for the KRK and the backshifted Fermi gas model. The derived k_0 values only weakly depend on the reference energy ϵ_0 some test calculations indicated that a change of 1 MeV in ϵ_0 affects k_0 only by a few percent. The enhancements found in this way are displayed in Fig. 6.1 as function of the mass number of the compound nucleus. The error bars reflect uncertainties of the experimental data and the spacing D_0 as well as inconsistencies between the enhancements required for different types of data; they were found by rather rough assessments and not by detailed sensitivity studies. The trend of the enhancements can be described as a function of the mass number A by simple purely empirical expressions as e.g.

$$\begin{aligned} k_0(x) &= 1.5 && \text{for } A < 145 \\ &= 1.5 + 0.131(A-145)^2 \exp[-0.154(A-145)] && \text{for } A \geq 145 \end{aligned} \qquad (6.8)$$

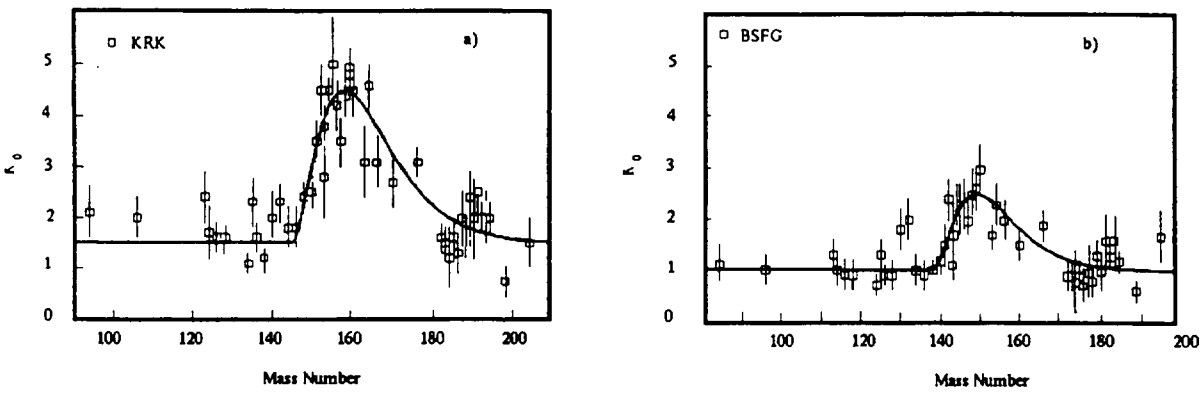

Figure 6.1: The enhancements k_0 plotted against the mass number of the compound nucleus. They are extracted from calculations employing the Kataria, Ramamurthy and Kapoor (a) and the backshifted Fermi gas model (b) for the level densities.

for the KRK model and

$$\begin{aligned} k_0(x) &= 1.0 && \text{for } A < 148 \\ &= 1.0 + 0.09(A-148)^2 \exp[-0.180(A-148)] && \text{for } A \geq 148 \end{aligned} \tag{6.9}$$

for the backshifted Fermi gas model, respectively. The expressions are actually the same as in Ref. [6.9]; the constants may change when we consider more nuclei with $A < 100$. Fig. 6.2 displays calculated average s-wave radiation width and the experimental value for the nuclei considered for the determination of k_0 and some more. For the calculations we employed the enhanced generalized Lorentzian model with the enhancement k_0 according to Eq. (6.8) or (6.9).

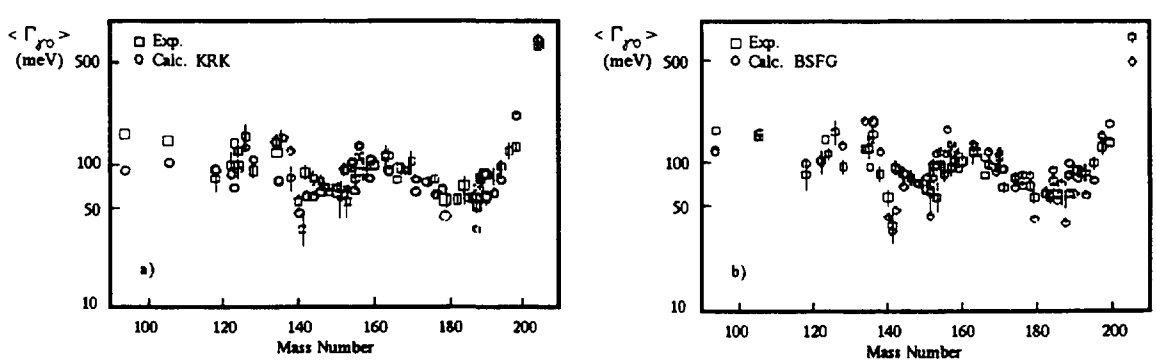

Figure 6.2: The calculated average s-wave radiation width and the corresponding experimental value. The calculations employ the enhanced generalized Lorentzian model for the *El* strength with k_0 values according to Eqs. (6.8) and (6.9), depending on the level density models employed, i.e. the Kataria, Ramamurthy and Kapoor model (a) and the backshifted Fermi gas model (b).

6.3 Giant Resonance Parameters

6.3.1 *E*1: Giant Dipole Resonance

Generally, giant resonance parameters can be obtained:
i) from the analysis of experimental photoabsorption cross sections of the compound nucleus,

ii) interpolated from experimental values of neighbouring nuclei assuming small dependence of these parameters on A,
iii) if no experimental information is available, global systematics of all parameters can be applied. It should, however, be noted, that no systematic is reliable for nuclei with $A < 50$. The shape of their excitation functions reveals quite complicated structure for every nucleus due to excitations in unbound individual $E1$ states. For more information on this subject see Ref. [6.32].

Recommended compilations of giant resonance parameters derived from experimental data are Refs. [6.31, 6.33, 6.34] and they are also quoted in **kopecky.readme** as the global trend of these parameters, and in a tabular form in the recommended file **beijing_gdr.dat**.

There is also another file, *varlamov.dat*, which contains additional useful information on giant dipole resonance parameters. The file contains 366 entries selected from the table published in [6.34]. The file provides GDR parameters deduced from photoabsorption cross sections, and also from total neutron production cross sections (total neutron production is often a good approximation to photoabsorption). In a few cases where this information is not available, GDR parameters are provided as deduced from either neutron yield, single neutron production, double neutron production or fission. It should be noted that GDR parameters given in the well known atlas by Dietrich and Berman [6.31] and included also into varlamov.dat, are based purely on total (photo)neutron production cross sections.

Global Parameterization

Spherical targets ($A > 50$)
(applied symbols have the usual meaning)

$E_0 = 31.2\ A^{-0.333} + 20.6\ A^{-0.167}$	MeV	[6.19]	
$\Gamma_0 = 0.026\ E_r^{1.91}$	MeV	[6.35]	
$\sigma_0 = 0.166\ A^{1.54}$	mb	[6.36]	(fit to experimental data)
$\sigma_0 = 1.2 \times 120\ NZ\ /\ (A\pi\Gamma_0)$	mb	[6.35]	(adjusted classical sum rule)

Deformed targets ($A > 50$)
(β = quadrupole deformation parameter)

$E_{01} = E_0\ /\ (1 + 0.666\beta)$	MeV	[6.37]
$E_{02} = E_0\ /\ (1 - 0.333\beta)$	MeV	[6.37]
$\Gamma_{01} = 0.026\ E_{01}^{1.91}$	MeV	[6.35]
$\Gamma_{02} = 0.026\ E_{02}^{1.91}$	MeV	[6.35]
$\sigma_{01} = 1.2 \times 120\ NZ\ /\ (A\pi\Gamma_0)$	mb	[6.35]
$\sigma_{02} = 1.2 \times 120\ NZ\ /\ (A\pi\Gamma_0)$	mb	[6.35]

Recently a comprehensive study (D'Arigo *et al.* [6.38]) has been completed, in which the following global expressions for all nuclei (based on the analysis of the experimental data from Dietrich and Berman [6.31]) have been derived:

Single GR hump targets ($A > 50$)

$E_0 = (49.336 + 7.34\ \beta)\ A^{0.2409}$	MeV
$\Gamma_0 = 0.3\ E_0$	MeV
$\sigma_0 = 10.6\ A\ /\ \Gamma_0$	mb

Double GR hump targets ($A > 50$)

$E_{02} = 50\ A^{-0.232}$	MeV
$\ln(E_{02}/E_{01}) = 0.946\ \beta$	
$\Gamma_{01} = (0.283 - 0.263\ \beta)\ E_{01}$	MeV
$\Gamma_{02} = (0.35 - 0.14\ \beta)\ E_{02}$	MeV
$\sigma_{01} = 3.48\ A\ /\ \Gamma_{01}$	mb
$\sigma_{02} = 1.464\ A\ /\ \Gamma_{02}$	mb

Other information on systematic giant resonance parameters treatment can be found in Refs. [6.39–6.41].

6.3.2 $M1$: Spin-Flip Giant Resonance

Spin-flip giant resonance mode, as proposed by Bohr and Mottelson [6.18], is recommended (see e.g. Refs. [6.1–6.11, 6.15]).

Global parameterization

$E_0 = 41\ A^{-1/3}$	MeV	[6.18]
$\Gamma_0 = 4$	MeV	[6.15]
σ_0 = adjusted to:		
1. experimental f_{M1} value		
2. $f_{M1} = 1.58\ A^{0.47}$	at ±7 MeV	[6.13]
3. $f_{E1}\ /\ f_{M1} = 0.0588\ A^{0.878}$	at ±7 MeV	[6.36]

6.3.3 $E2$: Isoscalar Giant Resonance

The description of $E2$ excitations in neutron capture as the isoscalar giant resonance mode are discussed in Refs. [6.10, 6.15, 6.42].

Global parameterization

$E_0 = 63\ A^{-1/3}$	MeV	[6.19]
$\Gamma_0 = 6.11 - 0.021\ A$	MeV	[6.42]
$\sigma_0 = 0.00014\ Z^2\ E_0\ /\ (A^{1/3}\ \Gamma_0)$	mb	[6.42]

6.4 Systematics of γ-Ray Strength Functions

6.4.1 Introduction

The compound nucleus mechanism is dominant for the neutron capture process up to incident neutron energy of several MeV. Therefore, the statistical model is generally used to describe and calculate the (n,γ) cross sections and spectra for these energies. An exception to this can occur in thermal and resonance regions (thus at low neutron energies) in mass regions, where non-statistical processes (potential and valence capture) may become important

The γ-ray transmission coefficient T_{XL}, usually used in the model calculations, is related to the γ-ray strength function f_{XL} as

$$T_{XL}(E_\gamma) = 2\pi E_\gamma^{2L+1} f_{XL}(E_\gamma), \tag{6.10}$$

where E_γ is the γ-ray energy and L indicates the multipolarity of the radiation. Therefore, both theoretical and experimental knowledge of γ-ray strength functions is a very important ingredient for description and calculation of photon-production data in all reaction channels, not only for the (n,γ) reaction.

In this survey we concentrate on experimental γ-ray strength functions, collected over a period of about forty years and based on measurements of partial radiative widths $\Gamma_{\gamma i}$. Such data originate from three different experiments. Most of the data are derived from discrete resonance-capture experiments using the method of slow neutron time-of-flight spectrometry. In some cases, the thermal neutron-capture data can be used, however, with some restrictions. The last source of data is set of the photonuclear data. Common in the analysis of all these experiments is a need to average over Porter-Thomas fluctuations, which govern the distribution of partial radiative widths.

The first compilation of McCullagh *et al.* [6.43] included about 50 nuclides with absolute partial widths originating from (n_{res},γ) and (γ,n) reactions, selected from data published before 1980 and averaged over the observed resonances. These data were analyzed in the frame of model dependent (single-particle model and Brink-Axel approximation) strength functions for $E1$ and $M1$ radiation. The mean energy for this data set was about 7 MeV. From fits to these data Kopecky [6.44] derived global formulae for the additional dependence of f_{E1} and f_{M1} on the mass A compared to the above models. We prefer the model independent definition of strength functions for dipole radiation, written as

$$f_{XL}(E_{\gamma i}) = \langle \Gamma_{\gamma i} / E_{\gamma i}^3 \rangle / D_0. \tag{6.11}$$

A first update of this data set was made by Kopecky and Uhl [6.12] in 1990. In their study a few new data have been added and the general reliability of the data was addressed.

6.4.2 Selected Data

The original set of data [6.43] has been extended with data published between 1981 and 1995 with, however, no claim on completeness. The preliminary results has been published in Ref. [6.13] and the present compilation is a slightly extended and updated version. The extensions include resolved-resonance measurements [6.45–6.53], thermal-capture measurements [6.54–6.56] and photonuclear data [6.57–6.59].

Two comments should be made concerning the interpretation of thermal capture data in terms of strength functions. Firstly, Bollinger [6.60] has demonstrated that the distribution of γ-ray intensities following the thermal capture follows only approximately the Porter-Thomas distribution, and in cases that both spin components contribute in thermal region, the distribution should be intermediate between χ^2 distributions with one and two degrees of freedom. Secondly, the conversion of thermal γ-ray intensities into partial radiative widths is based on the average value of the total radiative width, as derived from all measured resonances. This quantity, especially if resonances in a wide energy region are considered, may not be a good representation of the radiative width for the thermal region. Three of such measurements have been included in our data set; we have selected only those where the authors derived the $f_{E1,M1}$ values by themselves [6.54, 6.55, 6.56]. However, it should be mentioned that a huge wealth of

thermal capture data is available and it would certainly be worthwhile to consider making effort to convert well selected data into the γ-ray strength functions.

The final data sets (65 entries) of f_{E1} and f_{M1} values are listed in the electronic version of RIPL in the file **kopecky.dat**. In the original data base [6.43], only a small number of minor corrections have been carried out, most of the data have been adopted without changes. Values for two different resonance spins, treated separately in Ref. [6.43], have been combined. Given errors include statistical, normalization (assumed 20%) and Porter-Thomas uncertainties. Data posterior to Ref. [6.43] have been adopted without changes and their origin is quoted in the first column of Table 1 (see electronic version) by their reference. Further, the number of resonances and γ-rays used in evaluation of $f_{E1,M1}$ values is quoted, just to indicate the quality of averaging.

Another assessment concerned the mean energy E_γ at which $f_{E1,M1}$ values have been derived. Following Eq. (6.11) only the partial E_γ^3 reduction factor has been applied and no additional energy dependence was assumed. This is reasonably true if the energy region is narrow and the additional energy dependence which comes from the $E1$ ($M1$) giant-resonance model is negligible. The quoted $f_{E1,M1}$ value is then the mean value over all partial $f_{E1,M1}(E_{\gamma i})$ entries considered, assumed to correspond approximately to the mean value $< E_\gamma >$. This energy is quoted in Table 1 in a comment line. An inspection of these values shows, that the majority of data do not significantly deviate from earlier quoted $< E_\gamma > \approx$ 6 - 7 MeV. A fraction of the $f_{E1,M1}$ scatter may, however, stem from internal differences in distributions of partial data within the $< E_\gamma >$ range. The only data outside 6 - 7 MeV to be considered are the actinide data with $< E_\gamma > \approx$ 4.2 MeV. The energy correction due to additional energy dependence (e.g. assumed E_γ^2 for $E1$ radiation) increases f_{E1} values by factor of 2.5. The global trend of $f_{E1,M1}$ data is, however, not significantly influenced due to a relatively small number of such data points, as was shown in Ref. [6.44].

6.4.3 $E1$ Radiation

All surveyed data with their original values, denoted according to their experimental origin, are displayed in Fig. 6.3 together with a least-squares fit of a power dependence on mass number A (solid curve). Data follow reasonably well the expected smooth global trend with two exceptions, where some deviations above the general scatter of data may be considered. These large deviations belong to data in mass regions with $A < 40$ and $170 < A < 210$. There is no difference detected in data trend among the three experimental methods applied. For indication how the extension and revisions of the data set have influenced the general trend in f_{E1} data, the fitted curve from 1981 [6.44] is plotted for a comparison.

Reasons for a large scatter of the low-mass data ($A < 40$) can be surely attributed to an insufficient averaging together with pronounced single-particle character of many transitions. However, it seems that their mean value reasonably represents the general trend, as expected from the other data. The situation in the mass region with $170 < A < 210$ is more complex. Several strongly enhanced data points can be explained by the presence of a non-statistical mechanism, in particular those around the double-closed shell region. However, this enhancement is not a general feature of all data, some values seem to follow the general trend, as determined by data from the mass region with $100 < A < 170$. It is noticed, that the general data scatter around the trend curve in Fig. 6.3 can be characterized by a uncertainty factor of $k = 2$, which leaves about 10% of data points outside the uncertainty band (see Fig. 6.3). This data scatter probably masks the expected enhancement of f_{E1} values in other mass regions (e.g. A=150–170).

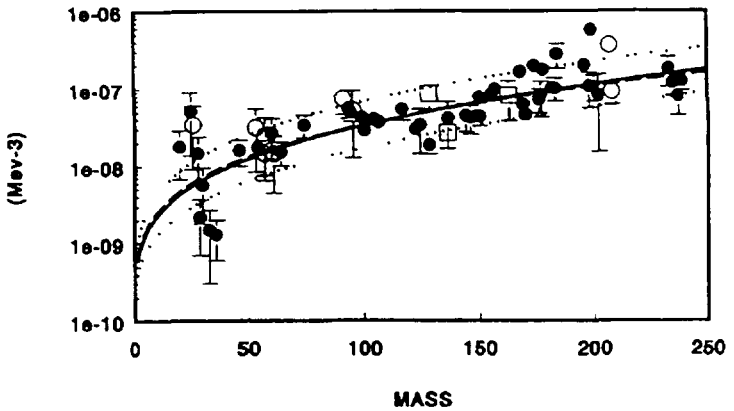

Figure 6.3: Plot of f_{E1} values [full circles (n_{res},γ), open circles (γ,n) and squares (n_{th},γ)] against the mass number. The full curve represent a LSQ fit to recent data, the fit from 1981 [6.32] is denoted by the dashed curve. Dotted curves display an uncertainty band with $k = 2$ (see Eq. (6.13)).

6.4.4 $M1$ Radiation

For $M1$ radiation, the situation is more complicated for several reasons. The systematic behaviour of the $M1$ strength function (see Fig. 6.4) shows a similar mass dependence as $E1$ radiation. These data, however, are scarce and statistically less accurate, often based on inadequate averaging. The uncertainty representing data scatter, determined in a similar way as for $E1$ radiation with about 10% data points outside, amounts to a factor of three (see Fig. 6.4). The curve fitted to data available in 1981 (Ref. [6.44]) differs very little from the present fit.

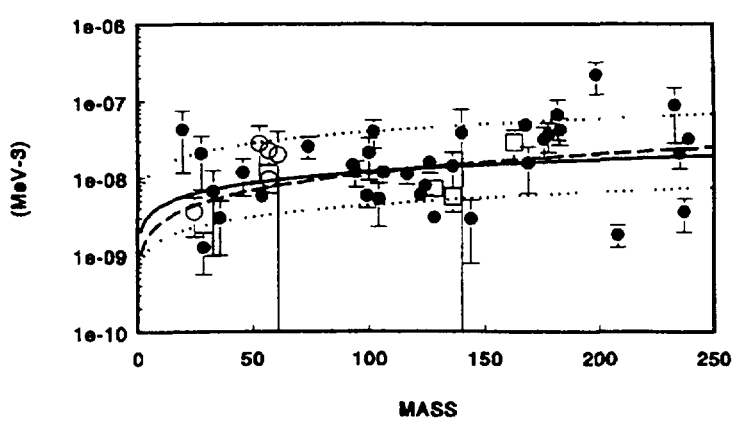

Figure 6.4: Plot of f_{M1} values, the uncertainty band has a value of $k = 3$ (used symbols are the same as in Fig. 6.1).

There is no well established general theoretical expression for f_{M1}. The frequently used single-particle estimate is at variance with a finite energy-weighted sum rule and is also ruled out by the observed mass dependence. The proposed giant resonance model [6.15], based on the Brink hypothesis [6.17] and the spin-flip $M1$ resonance, lacks a global description of the sum rule. The data display also some effects, which may be attributed to a non-statistical origin. Some of the enhanced data seem to cluster in a gross structure but a clear identification is difficult However, their influence on the general trend is marginal, as can be seen in Fig. 6.4.

Only in two original references the nonstatistical origin of data was identified.

6.4.5 Systematics

It was shown that there has been no significant influence on the global trend of the fitted strength functions as a function of mass by updating the basis data set since 1981. It was shown further that this global trend is also not influenced by data enhanced by non-statistical effects. The general reason for this is that the associated individual errors, dominated by Porter-Thomas uncertainties, are sometimes comparable to these effects and that the number of non-statistical entries is relatively small. Therefore, we have decided to apply only corrections to the those D_0 values in the original entries, which were obviously wrong. These changes are documented in Table 1 of the file **kopecky.dat**. The least-square fit to these data resulted in a recommended experimental (trend) systematics, which reads as

$$\begin{aligned} f_{E1}(exp) &= 9.23 \times 10^{-11} A^{1.34\pm0.14}, \\ f_{M1}(exp) &= 1.58 \times 10^{-9} A^{0.47\pm0.21}. \end{aligned} \tag{6.12}$$

These expressions are recommended for estimates of f_{E1} and f_{M1} values for normalization of calculations if the neutron binding energy is not too much different from a value of 6 to 7 MeV. The associated uncertainty factor k, defined as the minimal value which satisfies the condition

$$f_{XL}^{calc}/k < f_{XL}^{exp} < k f_{XL}^{calc}, \tag{6.13}$$

found to be $k = 2$ for $E1$ and $k = 3$ for $M1$ radiations. These, to some extent arbitrarily chosen uncertainty factors, agree reasonably with associated errors of the A power, as derived from the least-squared fit, resulting in k values 2.1 and 2.9.

6.5 Conclusions and Recommendations

A significant portion of information has been joined to **kopecky.readme** file. Summarising, we may state that the flexible enhanced generalized Lorentzian model for the $E1$ strength function is useful for the calculation of capture cross sections and related quantities as its parameters exhibit a reasonable smooth behaviour. The required enhancement depends on the level density model employed. The strong dependence of the calculated quantities (total radiative width, cross sections and gamma-ray spectra) and consequently of the extracted $E1$ enhancement parameter k_0 is not very satisfying. It probably represents the price for using too simple formulas which may fail to describe the energy dependence of the level density. Therefore a realistic level density model should always be used. It seems at present, that the backshifted Fermi gas model is the best solution for practical applications. This results also in the applicability of the enhanced generalized Lorentzian for nuclei outside the A=150–170 range, because k_0=1 in Eq. (6.9) and enhanced generalized Lorentzian = generalized Lorentzian. In view of our empirical formulation of the enhancement of the width of the generalized Lorentzian a better understanding of the effect and a subsequent theoretical description would be very helpful.

Recent experiments with Two-Step Cascade method [5.61–5.68] reveal additional information on the strength function predictions. This method is sensitive, not only to primary transitions, but also to secondary transitions via intermediate states. However, the interpretation of two-step cascade method results is complicated by its dependence on the final state parameters.

The global parametrization of the giant resonances (not only GDR) is contained in **kopecky.readme**. The recommended data file **beijing_gdr.dat** contains the giant dipole resonance

parameters for the gamma-ray strength functions. These parameters of Lorentz curves are based on compilation by Dietrich and Berman [6.31] extended by the Beijing group in later years especially for light nuclei (C, N, O, Al and Si). The recent compilation of Varlamov *et al.* [6.34] has been included into RIPL as other file *varlamov.dat*. It is of similar structure, covering period 1976–95 and containing more entries than the Beijing compilation.

The main systematics of various paremeters important for the γ emission is contained in **kopecky.dat**.

1. The original experimental data set for $E1$ and $M1$ gamma-ray strength functions [6.43] has been reviewed, and extended by recent data covering the period up to 1996 and listed in **kopecky.dat**. The resulting f_{E1} and f_{M1} values show a smooth increasing dependence on mass A, different to that expected from the single-particle model. Together with an additional energy dependence above the E^3 phase-shift factor (as detected in many averaged-resonance capture experiments), it may be concluded that the use of single-particle model should be disregarded for both $E1$ and $M1$ radiation. Extended information of this survey and update can be found in Ref. [6.14].
2. The data fluctuations around the fitted systematics are dominated by a combined effect of experimental uncertainties (including the averaging properties) and uncertainties in D_0 values, their possible corrections are discussed and in several cases applied. In order to cover the uncertainty in D_0 determinations, all previous and recent D_0 evaluations are listed in **kopecky.dat**. The size of these fluctuations complicates the interpretation of individual data in terms of statistical and non-statistical components, however, a global trend of data is detected.
3. The resulting set of f_{E1} values generally underestimates the predictions by the standard Lorentzian, as expected from previous studies. This behaviour forms a global argument for the use of the generalized Lorentzian with the energy-dependent width. The enhancements of $E1$ radiation above this model in mass regions $50 < A < 60$ and $150 < A < 170$, which influences all quantities such as f_{E1}, $< \Gamma_\gamma >$, σ_γ $\mathrm{d}\sigma_\gamma/\mathrm{d}E$ may be attributed to global non-statistical effects. However, it is not excluded that some of the Γ_γ enhancements are due to experimental effects.
4. For practical applications in statistical model calculations, the experimental ratio of Γ_γ/D_0 is probably the best normalization check. The derived systematics of f_{E1} and f_{M1}, if necessary combined with the trend in $E1/M1$ ratios, can be used as a reasonable approximation of the strength functions in model calculations, if experimental values are not available.

REFERENCES

[6.1] J. Kopecky and M. Uhl, Phys. Rev. **C41**, 1941 (1990).

[6.2] M. Uhl and J. Kopecky, Report INDC(NDS)-238 (IAEA Vienna 1990), p. 113.

[6.3] J. Kopecky, *in* Proc. VII. Int. Symposium on Capture Gamma-ray Spectroscopy and Related Topics. (AIP Conf. Proc. No. 238, New York 1991), p. 607.

[6.4] M. Uhl and J. Kopecky, *in* Proc. Int. Conf. Nuclear Data for Science and Technology, Jülich, 1991 (Spring Verlag, Berlin/Heidelberg, 1992), p. 977.

[6.5] J. Kopecky, M. Uhl and R.E. Chrien, Report ECN-RX–92-011 (ECN Petten 1992).

[6.6] J. Kopecky and M. Uhl, *in* Proc. Int. Symposium on Nuclear Data Evaluation Methodology, Brookhaven, 1992 (World Scientific, Singapore 1993), p.381.

[6.7] M. Uhl and J. Kopecky, Proc. Int. Symp. on Nuclear Astrophysics, Karlsruhe, 1992 (IOP Publishing 1993), p. 259.

[6.8] J. Kopecky, M. Uhl and R.E. Chrien, Phys. Rev. **C47**, 312 (1993).

[6.9] M. Uhl and J. Kopecky, Proc.Int.Conf. Nuclear Data for Science and Technology, Gatlinburg, 1994. (American Nuclear Soc., La Grange Park, 1994), p. 438.

[6.10] M. Uhl and J. Kopecky, Report INDC(NDS)-335 (IAEA Vienna 1995), p. 157.

[6.11] J. Kopecky, to be published in 1998.

[6.12] J. Kopecky and M. Uhl, *in* Proc. IAEA Specialists' Meeting on the Measurement, Calculation and Evaluation of Photon Production Cross Sections, Feb. 5-7, 1990, Smolenice, CSFR, Report INDC(NDS)- 238 (IAEA Vienna 1990), p. 103.

[6.13] J. Kopecky and M. Uhl, Report ENEA/NSC/Doc (95) 1, 119.

[6.14] J. Kopecky, *in* the final CRP document on "Measurement, Calculation and Evaluation of Photon Production data", INDC(NDS), to be published in 1998.

[6.15] J. Kopecky and R.E. Chrien, Nucl. Phys. **A468**, 285 (1987).

[6.16] M. Blatt and V.F. Weisskopf, *Theoretical Nuclear Physics*, (J. Wiley, New York 1952), p. 647.

[6.17] D.M. Brink, Ph.D. Thesis, Oxford University, (1955).

[6.18] A.G. Bohr and B.R. Mottelson, *Nuclear Structure, Vol. II* (Benjamin London 1975), p. 636.

[6.19] J. Speth and A. van de Woude, Rep. Prog. Phys. **44**, 719 (1981).

[6.20] D. Pines and D. Nozier, em The theory of Quantum Liquids (Benjamin, New York 1966).

[6.21] S.G. Kadmenskij, V.P. Markushev and V.L. Furman, Sov. J. Nucl. Phys. **37**, 165 (1983).

[6.22] V.A. Plujko, Contribution to Int.Conf. Nuclear Data for Science and Technology, Trieste, May 1997, to be published.

[6.23] P. A. Moldauer, Nucl. Phys. **A344**, 185 (1980).

[6.24] M. Uhl (unpublished).

[6.25] W. Dilg, W. Schantl, H. Vonach and M. Uhl, Nucl. Phys. **A217**, 269 (1973).

[6.26] S.K. Kataria, V.S. Ramamurthy, and S.S. Kapoor, Phys. Rev. **C18**, 549 (1978).

[6.27] A. Gilbert and A.G.W. Cameron, Can. J. Phys. **43**, 1446 (1965).

[6.28] A.V. Ignatyuk, K.K. Istekov, and G.N. Smirenkin, Sov. J. Nucl. Phys. **29**, 450 (1979),

[6.29] O.T. Grudzevich, A.V. Ignatyuk, V.L. Plyaskin and A.V. Zelenetsky, *in* Proc. Int. Conf. Nuclear Data for Science and Technology, May 30 - June 3, 1988 Mito, Japan. Ed. S. Igarasi, Saikon, Japan (1988), p. 187.

[6.30] A.V. Ignatyuk, em in Proc. Int. Symposium on Nuclear Data Evaluation Methodology, 12-16 Oct, 1992, Brookhaven National Laboratory, Upton, New York. (World Scientific, Singapore 1993), p. 411.

[6.31] S.S. Dietrich and B.L. Berman, Atomic Nucl. Data Tbl. **38**, 199 (1988).

[6.32] Liu Jianfeng, Su Zongdi and Zuo Yixin, contribution to the 2nd CR Meeting on Development of Reference Input Parameter Library for Nuclear Model Calculations of Nuclear Data, INDC(NDS)-350, March 1996.

[6.33] Sub-library of Giant Dipole Resonance Parameters (BEIJING_GDP_1_1.DAT;1), described in Zuo Yixin, Liu Jianfeng, Zhang Xizhi, Ge Zhigang and Su Zongdi, Comm. of Nuclear Data Progress **11**, 95 (1996).

[6.34] V.V. Varlamov, V.V. Sapunenko, M.E. Stepanov, *Photonuclear Data 1976–1995. Index* (in Russian). (Moscow University Press, 1996).

[6.35] N. Kishida, *in* Symposium on Nuclear Data Evaluation Methodology, (World Sci., Singapore 1993) p.598.

[6.36] J. Kopecky, unpublished data base.

[6.37] A. Ignatyuk, private communication.

[6.38] A.D'Arigo, G. Giardina, A. Lamberto, G.F. Rappazzo, R. Sturiale, A. Taccone, M. Herman and G. Reffo, private communication and to be published in Journal of Physics.

[6.39] D.G. Gardner in "Neutron Radiative Capture". Ed. R.E. Chrien (Pergamon Press 1985), p. 62.

[6.40] D.G. Gardner, M.A. Gardner and R.W. Hoff, Report UCRL-100547 Supplement (1989).

[6.41] G. Reffo, ENEA Report RT/FI (78) 11; and G. Reffo, M. Blann, T. Komoto and R.J. Howerton, Nucl. Instr. Methods **A267**, 408 (1988).

[6.42] W.V. Prestwich *et al.*, Z. Phys. **A315**, 103 (1984).

[6.43] C.M. McCullagh, M. Stelts and R.E. Chrien, Phys. Rev. **C23**, 1394 (1981).

[6.44] J. Kopecky, *in* Neutron-Capture Gamma Ray Spectroscopy and Related Topics 1981, (The Institute of Physics, Bristol and London, 1982), p. 423.

[6.45] F. Bečvář *et al.*, Journal of Nuclear Physics (in Russian), **44**, 3 (1986).

[6.46] O. Shahal, S. Raman, G.G. Slaughter, C. Coceva and M. Stefanon, Phys. Rev. **C25**, 1283 (1982).

[6.47] S. Kahane, S. Raman, G.G. Slaughter, C. Coceva and M. Stefanon, Phys. Rev. **C30**, 807 (1984).

[6.48] C. Coceva, M1 transitions from p-wave neutron resonances of ^{53}Cr, Contr. to the 8th International Symposium on Capture Gamma-ray Spectroscopy and Related Topics, Fribourg (Switzerland), September 20-24, 1994.

[6.49] C. Coceva, Radiative transitions from neutron capture in ^{53}Cr resonances, to be published in Il Nuovo Cimento A, 1994.

[6.50] F. Bečvář *et al.*, Journal of Nuclear Physics (in Russian), **46**, 3 (1987).

[6.51] F. Bečvář, *in* Capture Gamma Ray Spectroscopy 1987. (Institute of Physics Conference Series 88, Institute of Physics, Bristol, 1988) p. 649; and private communication.

[6.52] F. Bečvář *et al.*, *in* Int. Conference on Neutron Physics, Kiev (USSR), 2-6 October, 1983, p. 8.

[6.53] S. Pospíšil *et al.*, Annual Report 1995, Frank Laboratory of Neutron Physics JINR Dubna, p. 84.

[6.54] M.A. Islam, T.J. Kennett and W.V. Prestwich, Z. Physik, **A 335**, 173 (1990).

[6.55] M.A. Islam, T.J. Kennett and W.V. Prestwich, Phys. Rev., **C42**, 207 (1990).

[6.56] H.H. Schmidt *et al.*, Nucl. Phys. **A504**, 1 (1989); and F. Bečvář, private communication.

[6.57] C. Coceva, Y.K. Ho, M. Magnani, A. Mauri and P. Bartolomei, *in* Capture Gamma Ray Spectroscopy 1987, (Institute of Physics Conference Series 88, Institute of Physics, Bristol, 1988) p. 676.

[6.58] C. Coceva, Y.K. Ho, M. Magnani, A. Mauri and P. Bartolomei, see Ref. [6.57], p. 679.

[6.59] C. Coceva, private communication.

[6.60] L.M. Bollinger, Phys. Rev. **C3**, 2071 (1971).

[6.61] F. Bečvář, P. Cejnar, R.E. Chrien and J. Kopecky, *in* Proc. 7th International Symposium on Capture Gamma-Ray Spectroscopy and Related Topics, ed. R.W. Hoff, AIP Conf. Proc. No.238 (AIP New York 1991), p. 287.

[6.62] F. Bečvář, P. Cejnar, R.E. Chrien and J. Kopecky, Phys.Rev. **C46**, 1276 (1992).

[6.63] J. Honzátko, K. Konečný, I. Tomandl, F. Bečvář, P. Cejnar and R.E.Chrien, *in* Proc. 8th International Symposium on Capture Gamma-Ray Spectroscopy and Related Topics, Ed. J. Kern (World Scientific, Singapore 1994) p. 572.

[6.64] J. Honzátko, K. Konečný, I. Tomandl, F. Bečvář and P. Cejnar, *in* Proc. 8th International Symposium on Capture Gamma-Ray Spectroscopy and Related Topics, Ed. J. Kern (World Scientific, Singapore 1994), p. 590.

[6.65] J. Honzátko, K. Konečný, I. Tomandl, F. Bečvář and P. Cejnar, *in* Proc. 2nd International Seminar on Interaction of Neutrons with Nuclei, Report E3-94-419 (JINR Dubna 1994), p. 154.

[6.66] J. Honzátko, I. Tomandl, F. Bečvář and P. Cejnar, *in* Proc. of the 3rd International Seminar on Interaction of Neutrons with Nuclei, Report E3-95-307 (JINR Dubna 1995), p. 109.

[6.67] J. Honzátko, K. Konečný, I. Tomandl, F. Bečvář and P. Cejnar, Physica Scripta **T56**, 253 (1995).

[6.68] F. Bečvář, P. Cejnar, J. Honzátko, K. Konečný, I. Tomandl and R.E.Chrien, Phys. Rev. **C52**, 1278 (1995).

7 Continuum Angular Distributions

Coordinator: M.B. Chadwick

Summary

This chapter discusses methods for determining continuum angular distributions for use in nuclear reaction calculations and evaluated data files. We recommend the Kalbach systematics for most applications due to their wide-ranging applicability, and due to the fact that emission spectra can then be represented in a convenient compact form in evaluated data libraries. A computer code **kalbach_systematics.for** is included in the RIPL library to compute the Kalbach systematics angular distributions. We also recommend the use of a physics-based formula by Chadwick and Obložinský for analyses in which a fundamental physical derivation is preferred. A code **losalamos_analytical.for** is provided to calculate distributions with this theory. We also briefly discuss photonuclear angular distributions, and discuss how these can also be calculated using the **kalbach_systematics.for** code.

7.1 Introduction

Evaluated nuclear data files usually require a description of the angular distributions of emitted particles. The Kalbach systematics [7.1] provide a very successful characterization of these distributions, and have been widely used in evaluations. A drawback of these systematics is that they were not originally developed to include photon-induced reactions. However, Chadwick *et al.* have adapted the Kalbach systematics for use in photonuclear reactions in the quasideuteron regime (above about 40 MeV) [7.2].

A computer code obtained from Kalbach has been modified so that angular distributions in photon-induced, as well as nucleon-induced, reactions can be computed. This code, **kalbach_systematics.for**, is provided as part of RIPL.

In recent years a physics-based theory for calculating preequilibrium angular distributions has been developed by Chadwick and Obložinský [7.3]. This theory has been successfully applied in exciton model calculations [7.3], and in a Monte Carlo version of the hybrid model [7.4], and is described in some detail in the next subsection.

7.2 Theory for Preequilibrium Angular Distributions

The angular distribution of emitted particles is a subject which has attracted a great deal of interest from a physics perspective, since the angular effects give information about the underlying reaction mechanisms involved in the evolution of a quantum system towards equilibrium. Here we review some recent developments in the modeling of angular distributions which are of use in nuclear data evaluation work.

Particles ejected during the early stages of a nuclear reaction are typically of high energy and have forward-peaked angular distributions, since they are emitted prior to nuclear equilibration and partially preserve the incident projectile's direction of motion [7.5–7.11] These preequilibrium particles account for the continuum region of double differential emission spectra. Theoretical attempts to understand such spectra span from semiclassical approaches, notably exciton

and hybrid models, up to recent quantum mechanical multistep theories [7.12]. The quantum mechanical approaches have been used with a certain amount of success for analyzing nucleon reactions up to 200 MeV. However, they still face open questions regarding the formulation of multistep processes [7.13], multiple particle emission, and the emission of complex particles. Semiclassical models have provided a clear insight into the physics of preequilibrium processes and have successfully explained many angle-integrated spectra, though they were initially not formulated to account for angular effects. Therefore a widely-adopted approach [7.5–7.8] is to use these angle-integrated spectra, and obtain angular distributions from the Kikuchi-Kawai [7.14] nucleon-nucleon scattering kernel in a Fermi-gas. While this has been able to explain certain features of the forward-peaking, it has not been able to account for many of the systematic properties of continuum angular distributions [7.1]. Furthermore, most works assume a fast leading-particle that carries all the directional information during the cascade. This is in contradiction to the equiprobability assumption used in the exciton model which puts all the excited particles and holes on an equal footing, and does not follow the individual particle's motion [7.6].

In the absence of a sufficient theoretical understanding of the general properties of continuum angular distributions, Kalbach developed phenomenological systematics to describe them [7.1]. She analyzed a large body of experimental measurements (over 900 data sets) in nucleon and alpha-induced reactions at energies up to several hundreds of MeV, and found simple angular variations and a surprising similarity between angular distributions in reactions involving varying types of projectile and ejectile. While these systematics are very useful for describing and predicting differential cross sections, their physical basis has remained obscure. The fact that observed continuum preequilibrium cross sections tend to vary smoothly with angle and energy, and lend themselves to simple parameterization [7.1], suggests that they should be describable using a relatively simple model of the reaction process. Here we show how momentum considerations are fundamental to the description of continuum angular distributions, and using a semiclassical preequilibrium model we derive Kalbach's parameterization of the forward-peaking shape.

An important step in reconciling the role of linear momentum in the preequilibrium cascade with the statistical assumptions of the exciton model was made by Mädler and Reif in 1980 [7.9]. They abandoned the leading particle assumption and treated the cascade in a fully statistical manner. As in the usual exciton model, it was assumed that exciton states compatible with energy conservation can be excited in a transition (so one implicitly assumes that there is mixing between particle-hole states within a given exciton class). But in addition, accessible states were restricted to those that satisfy momentum conservation. To do this the concept of the linear-momentum dependence of state densities was introduced. Recent work on exciton model angular distributions also uses this picture of the preequilibrium cascade [7.10, 7.11, 7.3]. However, the partition function technique used by Mädler and Reif to derive the state densities is impractical for numerical computations. In contrast, the approach of Refs. [7.3, 7.4] uses new and computationally tractable methods for determining the state densities with linear momentum.

7.2.1 General Features of Preequilibrium Angular Distributions

Kalbach's work [7.1] on the systematical properties of angular distributions highlighted a number of features of the measured angular distribution data that must be modeled correctly in applications:

1. The shape of a preequilibrium angular distribution has the general form of $\exp(a \cos\theta)$, where a is a parameter that governs the magnitude of the forward-peaking. Thus, when

data is plotted on a logarithmic scale against angle, it exhibits a cosine shape. This functional form for the angular distributions applies (approximately) to all types of reactions, independent of the projectile/ejectile type.

2. The a parameter is independent of target mass.

3. The a parameter is approximately independent of projectile/ejectile mass.

4. The a parameter, to a good approximation for energies up to 130 MeV, is a function of emission energy, but not incident energy.

7.2.2 State Densities with Linear Momentum

The state density with linear momentum can be expressed [7.11] as the product of a state density in energy space, $\rho(p,h,E)$, and a linear momentum distribution function $M(p,h,E,\mathbf{K})$,

$$\rho(p,h,E,\mathbf{K}) = \rho(p,h,E)\ M(p,h,E,\mathbf{K}), \tag{7.1}$$

in analogy to the usual partitioning of the angular-momentum state density. It has units of $\mathrm{MeV}^{-1}(\mathrm{MeV/c})^{-3}$, is independent of the direction of $\mathbf{K}$, and yields the energy-dependent state density when integrated over all momenta, $\int \rho(p,h,E,\mathbf{K}) 4\pi K^2 dK = \rho(p,h,E)$. The individual momenta of the particles and holes are oriented in random directions, and the state density with linear momentum counts all configurations which sum to the required total energy and total momentum. The Central Limit Theorem implies that the ensemble of the various particle and hole momenta sum to yield a distribution of total momenta which follows a Gaussian,

$$M(p,h,E,\mathbf{K}) = \frac{1}{(2\pi)^{3/2}\sigma^3} \exp(-K^2/2\sigma^2), \tag{7.2}$$

where σ is the momentum cut-off (representing the width of the distribution). The momentum cut-off can be obtained by considering the average-squared value of the exciton momentum projections on the direction of $\mathbf{K}$ in a Fermi-gas nucleus, giving

$$\sigma^2 = n \left(\frac{2m\epsilon_{\mathrm{av}}}{3}\right), \tag{7.3}$$

where m is the nucleon mass, $n = p + h$, and ϵ_{av} is the average exciton energy relative to the bottom of the nuclear well. Thus, as n increases with more excited particles and holes, the width of the total momentum distribution increases. If the excitation energy is less than the Fermi energy (ϵ_F) and $p \approx h$, then $\epsilon_{\mathrm{av}} \approx \epsilon_F$, but in general in an equidistant single-particle model it is given by

$$\epsilon_{\mathrm{av}} = \frac{2p(p+1)}{ng} \frac{\rho(p+1,h,\tilde{E})}{\rho(p,h,\tilde{E})} - \frac{\tilde{E}}{n} + \epsilon_F, \tag{7.4}$$

with the notation that $\tilde{E}$ denotes the excitation energy relative to the Fermi-level, $\tilde{E} = E - (p-h)\epsilon_F$, and the state densities in Eq. (7.4) are taken from the equidistant model with finite well-depth restrictions [7.15].

Recently, analogous values for the average exciton energy in a Fermi-gas (with single-particle energies increasing as the square root of energy) have been presented [7.4].

7.2.3 Preequilibrium Angular Distribution Formula

In the exciton model the emission rate from the r^{th} preequilibrium stage containing p particles and h holes, leaving p_r particles and h_r holes in the residual nucleus, is obtained by applying detailed balance. By explicitly conserving linear momentum we obtain an angle-dependent rate for emission with energy ϵ and direction Ω given by

$$\frac{d^2\lambda_n(\epsilon,\Omega)}{d\epsilon d\Omega} = \frac{2\mu\epsilon\sigma_{\text{inv}}}{\pi^2\hbar^3}\frac{\rho(p_r,h_r,E-\epsilon_\Omega,\mathbf{K}-\mathbf{k}_\Omega)}{4\pi\ \rho(p,h,E,\mathbf{K})}, \tag{7.5}$$

where for clarity we have omitted model-dependent factors which may be applied to account for the type of ejectile particle [7.12]. Here, μ is the ejectile reduced mass, and the reaction cross section for the inverse process is σ_{inv}. The composite system total energy and momentum before particle emission are E and $\mathbf{K}$, respectively, and the residual nucleus energy and momentum after emission are $E-\epsilon_\Omega$ and $\mathbf{K}-\mathbf{k}_\Omega$, respectively, all these quantities being measured relative to the bottom of the nuclear well. The energy and momentum of the emitted particle relative to the bottom of the nuclear well are $\epsilon_\Omega = \epsilon + B_{\text{em}} + \epsilon_F$ and $\mathbf{k}_\Omega$, where $|\mathbf{k}_\Omega| = \sqrt{2\mu\epsilon_\Omega}$, B_{em} being the emission particle separation energy. Momentum, like energy, is not transferred to the whole residual nucleus; rather, it is carried solely by the excited particles and holes. The forward-peaked angular variation for a given emission energy follows directly from the variation of $\rho(p_r,h_r,E-\epsilon_\Omega,\mathbf{K}-\mathbf{k}_\Omega)$ with angle Ω in Eq. (7.5). This in turn follows from the inclusion of Fermi-motion and Pauli-blocking in the state-densities, and ignores deviations from center-of-mass isotropy in nucleon-nucleon scattering. During the preequilibrium cascade the model assumes that particle-hole states can be populated providing that both energy and momentum are conserved, and the memory of the initial projectile direction is not maintained solely by a fast leading-particle, but rather it is carried by both the excited particles and the holes.

Following the preequilibrium emission of a particle with momentum $\mathbf{k}_\Omega$, the squared absolute value of the residual nucleus momentum is

$$|\mathbf{K}-\mathbf{k}_\Omega|^2 = K^2 + k_\Omega^2 - 2Kk_\Omega\cos\theta,$$

where θ is the angle of emission in relation to the projectile direction. This residual-nucleus momentum appears in the state density in the numerator of Eq. (7.5) and accounts for the angular-dependence of the emission rate. Since the cross section for emission is proportional to the emission rate, we obtain:

$$\frac{d^2\sigma_n(\epsilon,\Omega)}{d\epsilon d\Omega} = \frac{d\sigma_n(\epsilon)}{d\epsilon}\ \frac{1}{4\pi}\frac{2a_n}{e^{a_n}-e^{-a_n}}\exp(a_n\cos\theta), \tag{7.6}$$

where $d\sigma_n(\epsilon)/d\epsilon$ is the n^{th}-stage angle-integrated exciton model cross section, the pre-exponential factor arises from the normalization conditions, and

$$a_n = \frac{3Kk_\Omega}{2n_r m\epsilon_{\text{av}}}, \tag{7.7}$$

where $n_r = p_r + h_r$. The total preequilibrium emission is a sum of the above contributions for all preequilibrium stages. Conservation of linear momentum, and hence angle-energy correlation, is maintained for all orders of scattering. As would be expected, the forward-peaking increases with incident and emission energy, and decrease with increasing n as the incident momentum is shared among more particles and holes. Eq. (7.6) has exactly the same functional form that Kalbach used to describe the preequilibrium angular distributions. While the Kalbach-systematics formula is of the same functional form as the theoretical result, her expression applies to the full preequilibrium spectrum whereas the theory applies to each preequilibrium stage

component. The variable "a" that she parameterized by comparisons with many measurements can be understood as an averaged value of a_n over all preequilibrium stages.

The model also provides a framework for understanding previously-unexplained features of the systematic behavior of angular distributions:

1. The angular variation as an exponential in $\cos\theta$ results from the Gaussian accessible phase space, and the vector addition of momenta using the cosine formula. The model therefore explains the general shape of measured continuum angular distributions [7.1] and its applicability to various projectile and ejectile types.
2. The independence of the angular distribution on target mass mass, since the momentum cut-off (unlike the spin cut-off) is independent of A.
3. The independence of a on projectile and ejectile mass is harder to show exactly, though possible explanations can be easily seen. In the case of composite projectiles, the increased number of excitons in the initial state due to cluster fragmentation approximately cancels the extra incident momentum. As for ejected clusters, models such as the pickup cluster model of Iwamoto and Harada include extra nucleons participating in the pick-up mechanism which again increases n.
4. The (approximate) independence of Kalbach's a parameter on incident energy below 130 MeV arises because of the approximate canceling of the incident energy dependence in the expression for a_n with the increasing number of preequilibrium stages (each with successively flatter angular distributions) that contribute.

There are similarities between this model and exciton models which use the Kikuchi-Kawai angular kernel (see Fig. 7.1). If instead of using the Gaussian (statistical) solution, the state densities with linear momentum are determined in a Fermi-gas by convoluting single-particle densities while conserving energy and momentum, the Kikuchi-Kawai result follows for 1-step scattering [7.11]. But the result for multistep scattering differs from a convolution of Kikuchi-Kawai kernels since we do not make a leading-particle assumption. We showed in Ref. [7.11] that the Gaussian solution approximates the exact Fermi-gas result very well even when the number of excitons is small. We are further encouraged to use the Gaussian solution since Reffo and Herman [7.16] found that a Gaussian angular momentum distribution described shell-model with BCS pairing calculations well, even when there are just two excitons.

7.2.4 Comparison with Measurements

Comparisons between angular distributions predicted by the linear-momentum conserving exciton model and experimental measurements have been presented in Refs. [7.3, 7.4]. Even though the model includes the quantum phenomena of Fermi-motion and Pauli-blocking, it does not account for other quantum effects such as refraction and diffraction from the nuclear potential, and finite-size effects. At low incident energies these have been shown to be important for obtaining sufficient backward-angle emission [7.6–7.8, 7.17], and result in a flatter angular distribution. A simple applications-oriented way to account for these effects is to modify a_n in Eq. (7.7) so that it is decreased by an energy-dependent parameter ζ. Writing a_n in terms of channel energies we then obtain for nucleon reactions:

$$a_n = \frac{3\sqrt{(\epsilon_{\rm in} + B_{\rm in} + \epsilon_F)(\epsilon + B_{\rm em} + \epsilon_F)}}{\zeta\,(n-1)\epsilon_{\rm av}}, \tag{7.8}$$

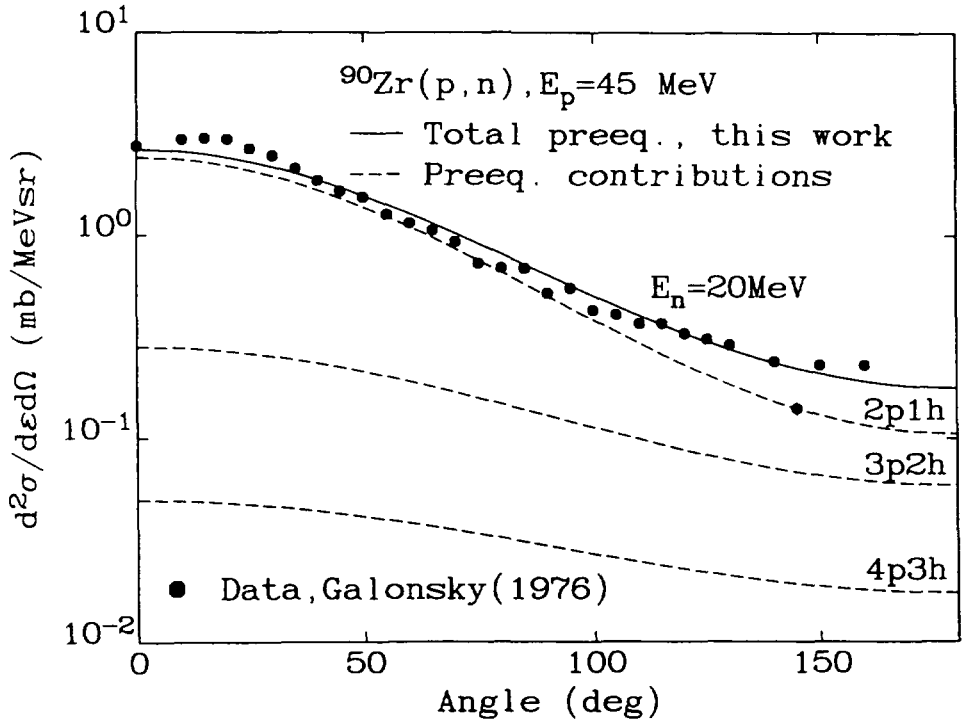

Figure 7.1: Comparison of measured (p,xn) continuum angular distributions with the theory of Ref. [7.3] applied within an exciton-model context. Data from Galonsky *et al.* [7.19]. Taken from Ref. [7.3].

and we take the Fermi-energy as 35 MeV. By analyzing a few experimental data sets we have found that the simple parameterization $\zeta = \max(1, 9.3/\sqrt{\epsilon})$, with ϵ in MeV, works fairly well up to 80 MeV. This factor tends to 1 for the higher emission energies where the quantum effects become small, and increases to 2 at 20 MeV.

Figures 7.1 and 7.2 show comparisons between prediction of the Chadwick-Obložinský theory with measured angular-distribution theory, taken from Refs. [7.3, 7.4]. The results shown in Figure 7.1 are also those used in the sample input file for the **losalamos_analytical.for** code included in the RIPL library.

7.2.5 Photonuclear Reactions

The photonuclear reaction model in Refs. [7.22, 7.23] describes the photonuclear absorption as a giant resonance excitation at low energies, and a quasideuteron mechanism at higher energies. In the case of the quasideuteron regime, the initial interaction produces particle-hole excitations and initiates a preequilibrium cascade. We follow Blann's prescription of treating the initial configuration as a $2p$-$1h$ state, to account for correlations in the two hole's degrees of freedom.

Kalbach did not include photonuclear processes in her systematics work. The model described above for angular distributions can be easily applied in this case, using the above formulae. In comparison to nucleon-induced reactions, photonuclear preequilibrium emission would be expected to be less forward-peaked due to the small momentum that a photon carries. Refs. [7.22, 7.23] shows comparisons between this model and experimental data.

Alternatively, it has been shown [7.2] that the above physical principles can be used to adapt Kalbach's nucleon-induced systematics for photon projectiles, by modifying the forward-

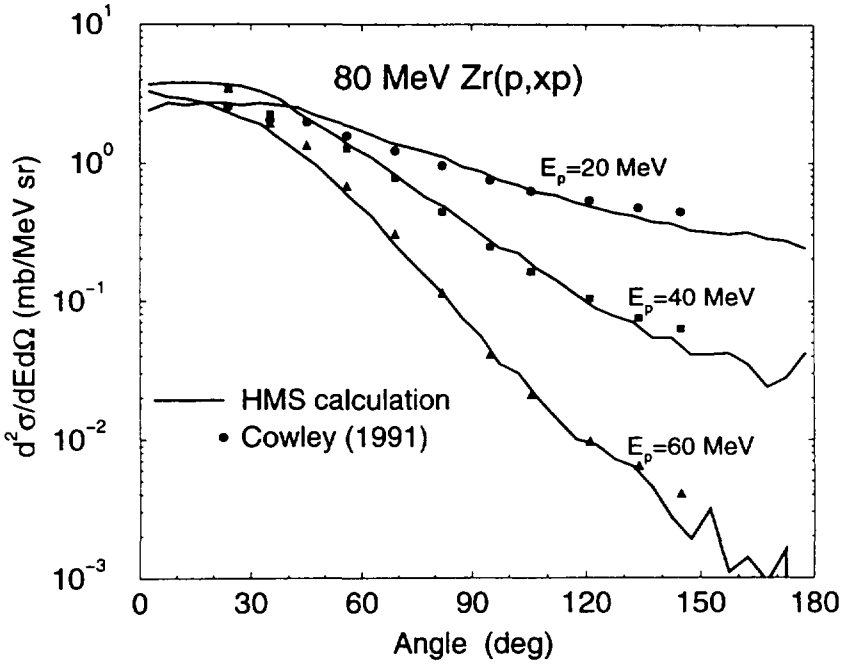

Figure 7.2: Comparison of measured (p,xp) continuum angular distributions with the theory of Ref. [7.3] applied within a Monte Carlo hybrid model context. Data from Cowley *et al.* [7.20]. Taken from Ref. [7.4].

peaking a-parameter. This approach, described in detail in Ref. [7.2], is incorporated into the RIPL **kalbach_systematics.for** code.

Finally, we stress that this approach cannot be applied in the Giant Dipole Resonance region, where a dipole-shaped angular distribution is often observed experimentally.

7.3 Formats

KALBACH_SYSTEMATICS.FOR:

1st Line:	Ac, Zc, Za, Na, Zb, Nb
2nd Line:	Einc
3rd Line:	Nem
Next Nem Lines:	Eem, dxs, fmsd

Where:

Ac, Zc	are the A and Z values for the compound nucleus (before any particle emission occurs).
Za, Na	are the projectile Z and N values.
Zb, Nb	are the ejectile Z and N values.
Einc	is the projectile lab incident energy in MeV.

Nem	is the number of emission energies considered.
Eem, dxs, fmsd	are the emission energy in MeV, the angle-integrated (energy-differential) cross section at this emission energy in mb/MeV, and the preequilibrium fraction (use fmsd=1 as a rough guidance for all but the very low energies) at this emission energy, respectively.

Note that photonuclear reactions in the quasideuteron regime are assumed when Za=Na=0.

LOSALAMOS_ANALYTICAL.FOR:

1st Line:	ein, eout, bindin, bindout, efermi, dsde, amass
2nd Line:	nstages
Next nstages Lines:	rat(i)

Where:

ein, eout	are the incident and emission energies in MeV.
bindin and bindout	are the separation energies for projectile and ejectile from the composite nucleus, in MeV.
efermi	is the Fermi energy (35 MeV).
dsde	is the angle-integrated preequilibrium cross section at emission energy eout.
amass	is the target A value.
nstages	is the number of preequilibrium stages to be included.
rat(i)	is the relative contribution of the preequilibrium stage i to the total preequilibrium spectrum, for emission energy eout.

7.4 Conclusions and Recommendations

The Kalbach systematics provide an invaluable tool for predicting angular distributions in evaluation work since they have a high degree of predictability, they are computationally straightforward to apply, and they are fairly comprehensive in describing most projectile/ejectile types of interest in applications. On the other hand, the Chadwick-Obložinský theory is useful for nuclear model calculations and evaluations since: (a) it is grounded in theory and explains many features of the phenomenological systematics; (b) it can be applied to reactions not considered by Kalbach, for instance photonuclear reactions in the quasideuteron regime; and (c) the model provides a different angular distribution for each preequilibrium step of the reaction and includes the physically-expected behavior of a decrease in forward-peaking as the system moves towards equilibrium.

Our recommendations are:
For nuclear data evaluations, for nucleon reactions up to approximately 200 MeV and for photonuclear reactions in the 40-140 MeV range, continuum angular distributions can be determined with the Kalbach systematics as incorporated in the **kalbach_systematics.for** code.
If an analysis based on a fundamental physical derivation is required, we recommend use of the Chadwick-Obložinský theory [7.3, 7.4] for preequilibrium angular distributions, as implemented in the **losalamos_analytical.for** code.

REFERENCES

[7.1] C. Kalbach, Phys. Rev. **C37**, 2350 (1988).

[7.2] M.B. Chadwick, P.G. Young and S. Chiba, J. Nucl. Sci. Tech. **32**, 1154 (1995).

[7.3] M.B. Chadwick and P. Obložinský, Phys. Rev. **C50**, 2490 (1994).

[7.4] M. Blann and M.B. Chadwick, "New precompound decay model: Angular distributions", to be published in Physical Review C (1998).

[7.5] Sun Ziyang, Wang Shunuan, Zhang Jingshang, Zhou Yizhong, Z. Phys. **A305**, 61 (1982).

[7.6] C. Costa, H. Gruppelaar and J.M. Akkermans, Phys. Rev. **C28**, 587 (1983).

[7.7] A. Iwamoto and K. Harada, Nucl. Phys. **A419**, 472 (1984).

[7.8] M. Blann, W. Scobel and E. Plechaty, Phys. Rev. **C30**, 1493 (1984).

[7.9] P. Mädler and R. Reif, Nucl. Phys. **A337**, 445 (1980).

[7.10] M.B. Chadwick and P. Obložinský, Phys. Rev. **C44**, R1740 (1991)

[7.11] M.B. Chadwick and P. Obložinský, Phys. Rev. **C46**, 2028 (1992)

[7.12] E. Gadioli and P.E. Hodgson, *Pre-equilibrium Nuclear Reactions* (Clarendon Press, Oxford 1992).

[7.13] H. Feshbach, Phys. Rev. **C48**, R2553 (1993).

[7.14] K. Kikuchi and M. Kawai, *Nuclear Matter and Nuclear Reactions* (North-Holland, Amsterdam 1968), p. 44; M.L. Goldberger, Phys. Rev. **74**, 1269 (1948).

[7.15] F.C. Williams, Nucl. Phys. **A166**, 231 (1971); E. Běták and J. Dobeš, Z. Phys. **A279**, 319 (1976).

[7.16] G. Reffo and M. Herman, Nuovo Cimento Lett. **34**, 261 (1982).

[7.17] K. Sato, Phys. Rev. **C32**, 647 (1985).

[7.18] P.G. Young, E.D. Arthur and M.B. Chadwick, Report LA-12343-MS (Los Alamos National Laboratory 1992).

[7.19] A. Galonsky, R.R. Doering, D.M. Patterson and H.W. Bertini, Phys. Rev. **C14**, 748 (1976).

[7.20] A.A. Cowley, A. van Kent, J.J. Lawrie, S.V. Fortsch, D.M. Whittal, J.V. Pilcher, F.D. Smit, W.A. Richter, R. Lindsay, I.J. van Heerden, R. Bonetti and P.E. Hodgson, Phys. Rev. **C43**, 678 (1991).

[7.21] A. Marcinkowski, R.W. Finlay, G. Randers-Pehrson, C.E. Brient, R. Kurup, S. Mellema, A. Meigooni and R. Taylor, Nucl. Sci. Eng. **83**, 13 (1983).

[7.22] M.B. Chadwick and P.G. Young, "Photonuclear reactions in the GNASH code: Benchmarking model calculations for reactions on lead up to 140 MeV", Lawrence Livermore National Laboratory Document UCRL-ID-118721 (1994).

[7.23] M.B. Chadwick and P.G. Young, Acta Phys. Slov. **45**, 633 (1995).

Appendix I

SUMMARY OF RIPL FILES

I.1 On-line Access

Numerical files of the Reference Input Parameter Library (RIPL Starter File) are stored at the DEC Alpha server of the Nuclear Data Section, IAEA Vienna. Access, restricted to read only, can be achieved via the Web interface or by using FTP (File Transfer Protocol).

1. Web access
   - http://www-nds.iaea.or.at/ripl/
2. FTP access
   - ftp iaeand.iaea.or.at
   - username: ripl

   with no password required.

I.2 Directory Tree

The structure of directories of the RIPL Starter File is shown below in a form of a tree. The main directory is ripl, there are altogether 8 basic directories, including readme and 7 segments with actual numerical data. Each segment (for densities each of 3 subsegments) has 2 subdirectories, for recommended files and for other files.

Main Directory	Basic Directory	Subdirectory	Subdirectory
	README		
	.....	.....	.....
	MASSES		RECOMMENDED
			OTHER_FILES
	.....	.....	.....
	LEVELS		RECOMMENDED
			OTHER_FILES
	.....	.....	.....
	RESONANCES		RECOMMENDED
			OTHER_FILES
	.....	.....	.....
	OPTICAL		RECOMMENDED
			OTHER_FILES
	.....	.....	.....
RIPL		TOTAL	RECOMMENDED
			OTHER_FILES
		.....	.....
	DENSITIES	FISSION	RECOMMENDED
			OTHER_FILES
		.....	.....
		PARTIAL	RECOMMENDED
			OTHER_FILES
	.....	.....	.....

```
                GAMMA                          RECOMMENDED
                                               OTHER_FILES
                ...............  ............  ............
                ANGULAR                        RECOMMENDED
                                               OTHER_FILES
--------------  ---------------  ------------  ------------
```

The above tree shows the sequence of directories in a way the RIPL Handbook is arranged, rather than in the alphabetical sequence generated automatically by the DEC Alpha computer.

I.3 Directory Names

The RIPL Starter File is located at the disk No 4, therefore the full name of the main directory, as generated by the Open VMS operating system, is UD4:[RIPL]. In the following, we will skip this full notation and indicate plain names only. These names will be sufficient for users, particularly for those accessing the library via the Web interface.

The names of basic directories and subdirectories are as follows:

Basic directory	Comment
README	RIPL readme and RIPL Handbook
MASSES	1st Segment, Masses and Deformations
LEVELS	2nd Segment, Discrete Level Schemes
RESONANCES	3rd Segment, Average Neutron Resonance Parameters
OPTICAL	4th Segment, Optical Model Parameters
DENSITIES	5th Segment, Level Densities (Total, Fission, Partial)
GAMMA	6th Segment, Gamma-Ray Strength Functions
ANGULAR	7th Segment, Continuum Angular Distributions

Each basic directory makes between recommended files and other files by providing two subdirectories

Subdirectory	Comment
*.RECOMMENDED	For recommended files
*.OTHER_FILES	For other files

I.4 Structure of File Names

As a rule, file names are created by coupling together 3 words, yielding full names with the structure

`originator_explanation.type`

As *originator* we use the name of a laboratory if the file came from a participant of the RIPL Coordinated Research Project (CRP). In (a few) cases where files came from individuals outside

the CRP, names of these individuals are used. The *ripl* is used for files generated by the whole RIPL team. Thus, the main *originators* are *beijing, bologna, bombay, budapest, jaeri, livermore, losalamos, obninsk* and *ripl.* In addition, the individual originators are *avrigeanu, capote, iljinov, kalbach, kopecky, maslov, mengoni* and *moller.*

Explanation indicates the contents of the file. Since the name of the basic directory serves this purpose, explanation is generally omitted. However, it is always given when more than one file in one subdirectory has the same originator

Type reflects the type of data in the file·

Type	Comment
dat	Data file
for	FORTRAN source code
gz	Compressed file using gzip (GNU distribution)
readme	Text file
tex	LaTeX file
ps	PostScript file

I.5 File Names

Listed below are files with their full names as contained in each basic directory. Each file name has its readme file, however only one readme file is provided for a group of files of the same originator in one subdirectory.

In several instances a subdirectory has its readme file as a short explanation of the contents of the subdirectory, applied to the cases where this is not self-explanatory

README

File name	Comment
ripl.readme	Brief description of RIPL
ripl_handbook.ps	Handbook, PostScript files (complete and 9 partial files)
ripl_handbook.tex	Handbook, LaTeX files (driver and 9 input files)

1. MASSES: Atomic Masses and Deformations

File name	Comment
all.readme	Recommended file, readme for all files
audi_95.dat	Recommended file, Audi-Wapstra 1995 recommended masses
audi_95.readme	Recommended file
moller.dat	Recommended file, extensive table of Moller et al

moller.readme	Recommended file
all.readme	Other file, readme for all files listed below
beijing.dat	Other file, masses only
beijing.readme	Other file
jaeri_deform.dat	Other file, deformations only
jaeri.readme	Other file

2. LEVELS: Discrete Level Schemes

File name	Comment
budapest.readme	Recommended file
budapest_levels.dat	Recommended file, discrete level schemes
budapest_cumulative.dat	Recommended file, cumulative number of levels
all.readme	Other file, readme for all files listed below
beijing.dat	Other file, discrete level schemes and branchings
beijing.readme	Other file
bologna.dat	Other file, Bologna nuclear level file
bologna.readme	Other file
jaeri.dat	Other file, level schemes, restricted data set
jaeri.readme	Other file
livermore.dat	Other file, Livermore biological file (A<18)
livermore.readme	Other file
obninsk.readme	Other file
obninsk_branchings.dat	Other file, experimental branchings
obninsk_levels.dat	Other file, experimental levels schemes

3. RESONANCES: Average Neutron Resonance Parameters

File name	Comment
obninsk.dat	Recommended file, s-resonance parameters
obninsk.readme	Recommended file
all.readme	Other file, readme for all files listed below
beijing.dat	Other file, resonances and other parameters
beijing.readme	Other file
minsk.dat	Other file, resonance parameter for actinides
minsk.readme	Other file

4. OPTICAL: Optical Model Parameters

File name	Comment
losalamos.readme	Recommended file
losalamos_omlib.dat	Recommended file, optical model potentials
all.readme	Other file, readme for all files listed below
beijing.dat	Other file, potentials collected in Beijing
beijing.readme	Other file
jaeri.dat	Other file, potentials used in JENDL evaluations
jaeri.readme	Other file
losalamos.readme	Other file
losalamos_omcode.for	Other file, utility code for losalamos_omlib.dat

5. DENSITIES: Level Densities

5.1. TOTAL: Total Level Densities

File name	Comment
all.readme	Recommended file, readme for all files
beijing.readme	Recommended file
beijing_bs.dat	Recommended file, back-shifted model
beijing_gc.dat	Recommended file, Gilbert-Cameron model
obninsk.readme	Recommended file
obninsk_bcs.dat	Recommended file, superfluid (BCS) model
all.readme	Other file, readme for all files listed below
beijing.for	Other file, retrieval code for Beijing files
beijing.readme	Other file
beijing_bcs.dat	Other file, superfluid (BCS) model
bombay.readme	Other file
bombay_bs.dat	Other file, back-shifted model
bombay_gc.dat	Other file, Gilbert-Cameron model
iljinov.readme	Other file
iljinov_gc.dat	Other File, Gilbert-Cameron model, by Iljinov et al
jaeri.readme	Other file
jaeri_gc.dat	Other file, parameters used in JENDL evaluations
mengoni.readme	Other file
mengoni_gc.dat	Other File, Gilbert-Cameron model, by Mengoni et al
obninsk_bcs.for	Other file, code to calculate BCS densities
obninsk_bcs.readme	Other file
obninsk_bs.dat	Other file, back-shifted model
obninsk_gc.dat	Other file, Gilbert-Cameron model
obninsk_gc_bs.readme	Other file

moller.readme	Other file
moller_levels.gz	Other file, single-particle levels, compressed
moller_levels.for	Other file, retrieval code for moller_levels.gz
obninsk_micro.for	Other file, code, microscopic total level densities
obninsk_micro.readme	Other file

5.2 FISSION Fission Level Densities

File name	Comment
maslov.dat	Recommended file, fission barriers
maslov.readme	Recommended file
all.readme	Other file, readme for all files listed below
beijing.dat	Other file, 3 compilations of fission barriers
beijing.readme	Other file
obninsk.dat	Other file, fission barriers from Obninsk
obninsk.readme	Other file

5.3 PARTIAL Partial Level Densities

File name	Comment
avrigeanu.for	Recommended file, code with analytical formulas
avrigeanu.readme	Recommended file
all.readme	Other file, readme for all files listed below
capote_micro.for	Other file, code for microscopic densities
capote_micro.readme	Other file
moller.readme	Other file, microscopic densities, see also 5.1

6. GAMMA: Gamma-Ray Strength Functions

File name	Comment
all.readme	Recommended file, readme for all files below
beijing readme	Recommended file
beijing_gdr dat	Recommended file, experimental GDR parameters
kopecky.readme	Recommended file
kopecky.dat	Recommended file, exper systematics of strength functions
varlamov.readme	Other file
varlamov dat	Other file, experimental GDR parameters by Varlamov

7. ANGULAR: Continuum Angular Distributions

File name	Comment
all.readme	Recommended file, readme for all files below
kalbach.readme	Recommended file
kalbach_systematics.for	Recommended file, code for Kalbach systematics
losalamos.readme	Recommended file
losalamos_analytical.for	Recommended file, code with analytical expressions based on linear momentum approach

Appendix II

EXPERIENCE AT LOS ALAMOS WITH USE OF THE OPTICAL MODEL FOR APPLIED NUCLEAR DATA CALCULATIONS

(Report LA-UR-94-3104)

P.G. Young
Los Alamos National Laboratory

Summary

While many nuclear models are important in calculations of nuclear data, the optical model usually provides the basic underpinning of analyses directed at data for applications. An overview is given here of experience in the Nuclear Theory and Applications Group at Los Alamos National Laboratory in the use of the optical model for calculations of nuclear cross section data for applied purposes. We consider the direct utilization of total, elastic, and reaction cross sections for neutrons, protons, deuterons, tritons, ^{3}He and alpha particles in files of evaluated nuclear data covering the energy range of 0 to 200 MeV, as well as transmission coefficients for reaction theory calculations and neutron and proton wave functions in direct-reaction and Feshbach-Kerman-Koonin analyses. Optical model codes such as SCAT and ECIS and the reaction theory codes COMNUC, GNASH, FKK-GNASH, and DWUCK have primarily been used in our analyses. A summary of optical model parameterizations from past analyses at Los Alamos will be given, including detailed tabulations of the parameters for a selection of nuclei.

I. INTRODUCTION

The optical model frequently provides the basis for theoretical analyses and/or data evaluations that are used in providing nuclear data for applied purposes. In addition to offering a convenient means for calculation of reaction, shape elastic, and (neutron) total cross sections, optical model potentials are widely used in quantum-mechanical preequilibrium and direct-reaction theory calculations and, most importantly, in supplying particle transmission coefficients for Hauser-Feshbach statistical-theory analyses used in nuclear data evaluations. This paper collects and reviews optical model potentials developed over the last several years for applied nuclear data analyses in the Nuclear Theory and Applications Group at Los Alamos National Laboratory.

Section II outlines the methodology used for determining many of the potentials described here. Section III includes tabulations of a selection of spherical optical model potentials that have been utilized at Los Alamos in nuclear data calculations, and Section IV gives a similar summary for coupled-channels optical model potentials. Finally, conclusions and recommendations are given in Section V.

II. METHODOLOGY

In the sections that follow a standard form is used for the optical model potential and the various components of the potential.[1] In particular, the potential is represented by a combination of Woods-Saxon volume and surface derivative terms with (V_R, r_R, a_R), (W_V, r_V,

a_V), (W_D, r_D, a_D), and (V_{SO}, r_{SO}, a_{SO}) indicating the real central, volume imaginary, surface derivative imaginary, and real spin-orbit components. In the parameterizations given below, the abbreviations

$$\eta = \frac{N-Z}{A} = 1 - \frac{2Z}{A} \tag{1}$$

and

$$\Delta V_c = 0.4 \frac{zZ}{A^{1/3}} \tag{2}$$

are employed in the isospin and coulomb correction terms, respectively. In Eqs. (1) and (2) the quantities N, Z, and A are the neutron, proton, and atomic mass numbers of the target nucleus, respectively, and z is the charge number of the projectile. Note that when plus or minus signs are used with the isospin terms in general expressions for proton or neutron potentials, the minus sign is used for neutrons and the positive sign for protons.

For our calculations we typically use the spherical optical model codes SCAT2 by Bersillon[2] or SNOOPY8 by Schwandt.[3] In the case of SCAT2, we have extended the option to call built-in parameterizations to include many additional global and regional parameterizations. For coupled-channels calculations we use either the ECIS code by Raynal[4] or the JUPITOR code, as modified by Rebel et al.[5] In cases where detailed neutron optical model analyses are required, we typically combine the SPRT method[6] (fitting experimental values of s- and p-wave neutron strengths, potential scattering radii, and low energy neutron total cross sections) with fits to differential elastic scattering data at higher energies. We often combine analyses of neutron and proton data using a simple Lane model. In cases where accuracy requirements are not too demanding, we use existing global or regional parameterizations in calculations.

III. SPHERICAL OPTICAL MODEL POTENTIALS

A. Global Potentials at Incident Energies Below 50 MeV

A number of global optical model potentials have been developed for nuclear physics calculations at incident energies below ~ 50 MeV, especially for neutrons. A review of neutron global parameters is given in Ref. 1, and the older review by Perey and Perey[7] is still useful for charged-particle potentials. A global neutron potential developed since the 1985 review that has proven useful for calculations of nuclear data for fusion reactions is a modification by Yamamuro[8] of the surface imaginary term in the Walter and Guss[9] potential below an incident neutron energy of 20 MeV, as follows:

$$\begin{aligned} W_D\,(\text{MeV}) &= 5.0 - 14.94\,\eta + 0.271\,E_n \qquad 0 \le E_n \le 10\ \text{MeV} \\ &= 7.71 - 14.94\,\eta \qquad\qquad\quad 10 \le E_n \le 20\ \text{MeV} \end{aligned} \tag{3}$$

All other parameters are taken from the Walter and Guss potential, and that potential is used intact at neutron energies above 20 MeV. We have found the Yamamuro/Walter potential to be quite useful in cases where detailed optical model analyses are not available.

B. Global Potentials at Incident Energies Above 50 MeV

Possibilities for global optical model parameterizations above 50 MeV are considerably more restricted. Starting from a global proton potential by Schwandt et al.,[10] Madland[11] developed a potential that covers a wider energy range and that is generalized for neutrons and protons through the Lane model. The Madland potential was developed by analyzing data for 3 nuclides in the mass range $27 \leq A \leq 208$ and the energy range $50\ MeV \leq E_{n,p} \leq 400\ MeV$. We have incorporated a form of the Madland potential[12] modified for nonrelativistic calculations over the range $50\ MeV \leq E_{n,p} \leq 140\ MeV$ into the SCAT2 code; this potential is listed in Table 1.

Table 1. Global spherical optical model potentials for incident neutrons and protons over the incident energy range $50\ MeV \leq E_{n,p} \leq 140\ MeV$ and for the mass range $24 \leq A \leq 208$

NEUTRONS

Well Depth (MeV)	Geometry (fm)
$V_R = 105.5 - 16.5\eta - 0.4*Z/A^{1/3} - 17.14375 \ln(E_n)$	$r_R = 1.125 + 0.001\ E_n$ $a_R = 0.675 + 0.00031\ E_n$
$W_D = 0.0$	
$W_V = 2.4346 + 0.1016\ E_n - (9.288E\text{-}4)\ E_n^2 + (3.87E\text{-}6)\ E_n^3$	$r_V = 1.650 - 0.0024\ E_n$ $a_V = 0.328 + 0.00244\ E_n$
$V_{SO} = 19.0 + 3.75\eta - 3.154 \ln(E_n)$	$r_{SO} = 0.920 + 0.0305\ A^{1/3}$ $= 0.98\ (A \leq 40)$ $a_{SO} = 0.768 - 0.0012\ E_n$

PROTONS ($r_C = 1.20$ fm)

Well Depth (MeV)	Geometry (fm)
$V_R = 105.5 + 16.5\eta - 17.14375 \ln(E_p)$	$r_R = 1.125 + 0.001\ E_p$ $a_R = 0.675 + 0.00031\ E_p$
$W_D = 0.0$	
$W_V = 2.4346 + 0.1016\ E_p - (9.288E\text{-}4)\ E_p^2 + (3.87E\text{-}6)\ E_p^3$	$r_V = 1.650 - 0.0024\ E_p$ $a_V = 0.328 + 0.00244\ E_p$
$V_{SO} = 19.0 - 3.75\eta - 3.154 \ln(E_p)$	$r_{SO} = 0.920 + 0.0305\ A^{1/3}$ $= 0.98\ (A \leq 40)$ $a_{SO} = 0.768 - 0.0012\ E_p$

For deuterons, tritons, ^{3}He and alpha particles, we have modified the SCAT2 code to include a simplified Watanabe model[13] to derive potentials at medium energies. Details of the Watanabe transformation are also described by Madland.[11]

Other techniques for simplifying and facilitating development of optical model potentials are summarized in Ref. 1. These include the method of approximating an odd-A rotational nucleus in coupled-channels calculations by using appropriately chosen fictitious levels in an adjacent even-A (K=0) nucleus.[14] This procedure can reduce the computer time required to perform coupled-channels calculations for odd-A rotational nuclei, although some penalty in accuracy and setup time must be paid. Another technique that has good potential but that has had little use is the method outlined by Madland and Young[15] that permits the adaptation of spherical optical model potentials for coupled-channels calculations by simply scaling the imaginary surface potential by the relation

$$\frac{W_D a_D}{W_D' a_D'} = \alpha \quad , \tag{4}$$

where the primed and unprimed quantities refer to the spherical and deformed potentials, respectively, and α is a constant that can be optimally adjusted but which is typically ≈ 0.7.[1]

C. Regional and Local Potentials

1. Neutron, Proton, and Alpha Potentials for Analysis of n + ^{27}Al Reactions

A reaction theory analysis of neutron cross sections on ^{27}Al has been carried out with the FKK-GNASH code in some detail to 40 MeV for a planned update of the ENDF/B-VI data file, and in less detail to 100 MeV for comparison with high-resolution γ-ray measurements.[16] In this study the neutron potential of Petler et al.[17] was found to reproduce the available experimental data up to 60 MeV or so, and at higher energies the Madland potential[11] appeared to reliably track the total and reaction cross sections to above 100 MeV. For proton channels a form of the Perey proton potential[18] was used for proton energies below 30 MeV, with the following modification to the imaginary surface potential:

$$W_D(\text{MeV}) = 13.5 - 0.15\, E_p \, . \tag{5}$$

In the energy range 30 MeV $\le E_p \le$ 100 MeV, the Madland global potential[11] was employed for protons. The alpha-particle potential was taken from an analysis of n + ^{54,56}Fe reactions[19] (see next section) and was used up to 100 MeV.

These potentials produce good agreement with elastic scattering, (n,p), (n,n'), (n,α), and nonelastic cross sections over the range of available data, and give reasonable agreement with neutron, proton, and alpha-particle emission spectrum measurements at 14 MeV. Additionally, reasonable agreement is observed in calculations of discrete gamma-ray production cross sections for (n,n'γ) and (n,2nγ) reactions to 60 MeV.[16] The optical model potentials for neutrons and alpha particles are given in Table 2.

Table 2. Spherical optical model potentials for $^{27}Al + n$ calculations over the incident neutron energy range 1 keV $\leq E_n \leq$ 100 MeV. For $E_n > 60$ MeV, the global potential of Madland[11] was used for neutrons (Table 1).

NEUTRONS

Well Depth (MeV)	Range (MeV)	Geometry (fm)	
$V_R = 51.55 - 0.308\ E_n$	$0 < E_n < 60$	$r_R = 1.18$	$a_R = 0.64$
$W_D = 6.07$	$0 < E_n < 15$	$r_D = 1.26$	$a_D = 0.58$
$= 6.07 - 0.10\ (E_n - 15)$	$15 \leq E_n \leq 60$		
$W_V = 0.00$	$0 < E_n < 15$	$r_V = 1.26$	$a_V = 0.58$
$= -2.625 + 0.175\ E_n$	$15 \leq E_n \leq 60$		
$V_{SO} = 6.0$	$0 < E_n < 60$	$r_{SO} = 1.01$	$a_{SO} = 0.50$

ALPHA PARTICLES ($r_c = 1.4$ fm)

Well Depth (MeV)	Range (MeV)	Geometry (fm)	
$V_R = 193.0 - 0.15\ E_\alpha$	$0 < E_\alpha < 100$	$r_R = 1.37$	$a_R = 0.56$
$W_D = 0.00$	$0 < E_\alpha < 100$		
$W_V = 21.0 + 0.25\ E_\alpha$	$0 < E_\alpha < 100$	$r_V = 1.37$	$a_V = 0.56$

2. Neutron, Proton, and Alpha Potentials for Analysis of n + ^{54,56}Fe Reactions

Starting from an analysis of reactions on ^{54,56}Fe and nearby nuclei,[19] an optical model parameterization was developed for use in calculating neutron and proton reactions to 100 MeV.[20] These parameters have been used recently to calculate n + ^{56}Fe cross sections to 40 MeV for a planned update of ENDF/B-VI and to compare with experimental measurements of alpha particle spectra from the Weapons Neutron Research (WNR) facility.[21] Calculated cross sections agree reasonably with the available experimental data, including ^{56}Fe(p,n) and (p,2n) measurements as well as (n,xγ) data and neutron elastic angular distributions. The neutron, proton, and alpha particle optical model parameters are included in Table 3.

3. Neutron, Proton, and Alpha Potentials for Analysis of n + ^{59}Co Reactions

Similar to the above calculations on Fe, reaction theory analyses that were made earlier for n + ^{59}Co reactions[22] have been modified slightly for a planned extension of the ENDF/B-VI library to 40 MeV and for calculations of alpha particle spectra to compare with recent measurements from WNR.[23] Again, these parameters result in good agreement with the available total, elastic, nonelastic, inelastic, and (n,2n) cross section measurements and reasonable agreement with (n,p) and (n,α) data. The parameters are listed in Table 4. It should be noted that reaction theory calculations using these parameters have only been performed to ~ 50 MeV but reasonable total and reaction cross sections are calculated out to 100 MeV. Also note that the earlier set of alpha parameters given in Ref. 22 also give good results, especially at lower neutron energies.

Table 3. Spherical optical model potentials for $^{54,56}Fe$ + n calculations over the incident neutron energy range 1 keV $\leq E_n \leq$ 100 MeV. Above 62 MeV for neutrons and 28 MeV for protons, the Madland global potential[11] is used (Table 1).

NEUTRONS TO 62 MeV

	Well Depth (MeV)	Range (MeV)	Geometry (fm)	
V_R	= 49.747 - 0 297 E_n - 0.0003 E_n^2	$0 < E_n < 62$	$r_R = 1.287$	$a_R = 0.56$
W_D	= 6.00 + 0.42 E_n	$0 < E_n < 6$	$r_D = 1.345$	$a_D = 0.47$
	= 8 52 - 0.224 (E_n - 6)	$6 \leq E_n \leq 62$		
W_V	= 0.00	$0 < E_n < 8.9$	$r_V = 1.287$	$a_V = 0.56$
	= -1.60 + 0.18 E_n	$8.9 \leq E_n \leq 62$		
V_{SO}	= 6.20	$0 < E_n < 62$	$r_{SO} = 1.12$	$a_{SO} = 0.47$

PROTONS TO 28 MeV (r_c = 1.25 fm)

	Well Depth (MeV)	Range (MeV)	Geometry (fm)	
V_R	= 58.384 - 0.55 E_p	$0 < E_p < 28$	$r_R = 1.25$	$a_R = 0.65$
W_D	= 13.5 - 0.15 E_p	$0 < E_p < 28$	$r_D = 1.25$	$a_D = 0.47$
W_V	= 0	$0 < E_p < 28$		
V_{SO}	= 7.5	$0 < E_p < 28$	$r_{SO} = 1.25$	$a_{SO} = 0.47$

ALPHA PARTICLES (r_c = 1.4 fm)

	Well Depth (MeV)	Range (MeV)	Geometry (fm)	
V_R	= 193 - 0.15 E_α	$0 < E_\alpha < 100$	$r_R = 1.37$	$a_R = 0.56$
W_D	= 0.00	$0 < E_\alpha < 100$		
W_V	= 21.0 + 0.25 E_α	$0 < E_\alpha < 100$	$r_V = 1.37$	$a_V = 0.56$

4. Neutron, Proton, and Alpha Potentials for Analysis of n + $^{64,66,68}Zn$ Reactions

A set of optical model parameters for Zn isotopes was developed in support of 14.8-MeV activation measurements of the $^{64}Zn(n,p)^{64}Cu$ and $^{64}Zn(n,2n)^{63}Zn$ cross sections, covering the incident neutron energy range up to 20 MeV.[24] The parameters were obtained by fitting elastic angular distribution and total cross section measurements, and were validated in calculations of activation cross sections for neutron reactions on $^{64,66,68}Zn$ and for (p,n) reactions on ^{63}Cu and ^{65}Cu. The optical model parameters that resulted are given in Table 5.

5. Neutron and Proton Potentials for Analysis of Neutron Reactions on Sr, Y, and Zr Isotopes

Results of a detailed analysis of neutron and proton reactions on Sr, Y, and Zr isotopes at incident energies from 50 keV to 20 MeV were reported in 1980.[25] The optical model parameters obtained in that study were thoroughly tested against experimental data over that energy range

Table 4. Spherical optical model potentials for $^{59}Co + n$ calculations over the incident neutron energy range 1 keV $\leq E_n \leq$ 100 MeV. Above 62 MeV for neutrons and 23 MeV for protons, the Madland global potential[11] is used.

NEUTRONS

Well Depth (MeV)	Range (MeV)	Geometry (fm)
$V_R = 47.604 - 0.3636\ E_n - 0.0003\ E_n^2$	$0 < E_n < 62$	$r_R = 1.2865$ $a_R = 0.561$
$W_D = 8.047 + 0.0805\ E_n$	$0 < E_n < 6$	$r_D = 1.3448$ $a_D = 0.473$
$= 8.530 - 0.2509\ (E_n - 6)$	$6 \leq E_n \leq 62$	
$W_V = 0.00$	$0 < E_n < 0.5$	$r_V = 1.3448$ $a_V = 0.473$
$= -0.0721 + 0.1475\ E_n$	$0.5 \leq E_n \leq 62$	
$V_{SO} = 6.20$	$0 < E_n < 62$	$r_{SO} = 1.12$ $a_{SO} = 0.47$

PROTONS TO 23 MeV ($r_c = 1.25$ fm)

Well Depth (MeV)	Range (MeV)	Geometry (fm)
$V_R = 57.175 - 0.55\ E_p$	$0 < E_p < 23$	$r_R = 1.25$ $a_R = 0.65$
$W_D = 13.5 - 0.15\ E_p$	$0 < E_p < 23$	$r_D = 1.25$ $a_D = 0.47$
$W_V = 0$	$0 < E_p < 23$	
$V_{SO} = 7.5$	$0 < E_p < 23$	$r_{SO} = 1.25$ $a_{SO} = 0.47$

ALPHA PARTICLES ($r_c = 1.4$ fm)

Well Depth (MeV)	Range (MeV)	Geometry (fm)
$V_R = 217.0 - 0.15\ E_\alpha$	$0 < E_\alpha < 100$	$r_R = 1.416$ $a_R = 0.493$
$W_D = 0.00$	$0 < E_\alpha < 100$	
$W_V = 24.0$	$0 < E_\alpha < 100$	$r_V = 1.416$ $a_V = 0.493$

Table 5. Optical Model Parameters for Neutron Reactions with Zn Isotopes.

Well Depth (MeV)	Range (MeV)	Geometry (fm)
$V_R = 49.11 - 16\ \eta - 0.376E_n$	$0 \leq E_n \leq 20$	$r_R = 1.295$ $a_R = 0.58$
$W_D = 8.545 - 8\eta$	$0 \leq E_n \leq 20$	$r_D = 1.295$ $a_D = 0.48$
$W_V = -0.094 + 0.197E_n$	$0 \leq E_n \leq 20$	$r_V = 1.295$ $a_V = 0.58$
$V_{SO} = 6.2$	$0 \leq E_n \leq 20$	$r_{SO} = 1.12$ $a_{SO} = 0.48$

Since that time, the optical model analyses and reaction theory calculations have been extended to higher energies. Calculations of neutron-induced reactions on ^{89}Y have been compared with higher energy (n,xγ) measurements from WNR.[26] Similarly, in the case of ^{90}Zr proton-induced reactions were calculated to 160 MeV for the recent NEA-sponsored intermediate energy data calculations.[27] The optical model potentials for protons and neutrons used in these studies are given in Table 6.

Table 6. Spherical optical model potentials for proton and neutron reactions on Sr, Y, and Zr isotopes in the vicinity of A = 90. At energies above the maxima indicated, the global potential of Madland[11] was used for protons and neutrons.

n + ^{89}Y

Well Depth (MeV)	Range (MeV)	Geometry (fm)	
$V_R = 49.5 - 0.28\ E_n$	$0 < E_n < 21$	$r_R = 1.24$	$a_R = 0.62$
$W_D = 4.63 + 0.3\ E_n$	$0 < E_n < 10$	$r_D = 1.26$	$a_D = 0.58$
$= 7.63 - 0.13\ E_n$	$10 \le E_n < 21$		
$W_V = 0$	$0 < E_n \le 10.9$	$r_V = 1.24$	$a_V = 0.62$
$= -1.42 + 0.13\ E_n$	$10.9 < E_n < 21$		
$V_{SO} = 6.2$	$0 < E_n < 21$	$r_{SO} = 1.12$	$a_{SO} = 0.47$

n + ^{90}Zr

Well Depth (MeV)	Range (MeV)	Geometry (fm)	
$V_R = 49.0 - 0.28\ E_n$	$0 < E_n < 20$	$r_R = 1.24$	$a_R = 0.62$
$W_D = 3.4 + 0.3\ E_n$	$0 < E_n < 10$	$r_D = 1.26$	$a_D = 0.58$
$= 6.4 - 0.13\ E_n$	$10 \le E_n < 20$		
$W_V = 0$	$0 < E_n \le 10.9$	$r_V = 1.24$	$a_V = 0.62$
$= -1.42 + 0.13\ E_n$	$10.9 < E_n < 21$		
$V_{SO} = 6.2$	$0 < E_n < 20$	$r_{SO} = 1.12$	$a_{SO} = 0.47$

p + Sr ($r_c = 1.25$ fm)

Well Depth (MeV)	Range (MeV)	Geometry (fm)	
$V_R = 56.4 + 24\eta + \Delta V_c - 0.32\ E_p$	$0 < E_p < 21$	$r_R = 1.20$	$a_R = 0.68$
$W_D = 3.0 + 0.60\ E_p$	$0 < E_p < 17.5$	$r_D = 1.225$	$a_D = 0.40$
$= 13.5 - 0.15\ E_p$	$17.5 \le E_p < 21$		
$W_V = 0$	$0 < E_p < 21$		
$V_{SO} = 6.4$	$0 < E_p < 21$	$r_{SO} = 1.03$	$a_{SO} = 0.63$

p + Y ($r_c = 1.25$ fm)

Well Depth (MeV)	Range (MeV)	Geometry (fm)	
$V_R = 56.4 + 24\eta + \Delta V_c - 0.32\ E_p$	$0 < E_p < 21$	$r_R = 1.20$	$a_R = 0.73$
$W_D = 4.0 + 0.5\ E_p$	$0 < E_p < 17.5$	$r_D = 1.30$	$a_D = 0.40$
$= 12.75 - 0.15\ E_p$	$17.5 \le E_p < 21$		
$W_V = 0$	$0 < E_p < 21$		
$V_{SO} = 6.4$	$0 < E_p < 21$	$r_{SO} = 1.03$	$a_{SO} = 0.63$

IV. REGIONAL AND LOCAL COUPLED-CHANNELS OPTICAL MODEL POTENTIALS

A. Incident Neutron and Proton Potentials for Nuclides in the Region $63 \leq Z \leq 82$

A number of coupled-channels optical model analyses have been performed at Los Alamos for use in reaction theory calculations, including several rare earth and transition elements. In all cases modified SPRT[6] approaches were used to determine the neutron parameters, requiring reasonable agreement with low-energy resonance data and neutron total cross sections, as well as with elastic and inelastic scattering measurements if available. Inclusion of proton data in most cases was accomplished using a simple Lane model.

An analysis was performed of neutron-induced reactions with ^{165}Ho and ^{169}Tm to establish reasonable optical parameters for reaction theory calculations on Tm isotopes.[28] The parameters are based mainly on fits to ^{169}Tm low-energy resonance and total cross section data, and to a neutron elastic scattering angular distribution measurement for ^{165}Ho at 11 MeV. The parameters are listed in Table 7.

In preparation for a major update of the ENDF/B-V cross sections, a coupled-channels optical model analysis was performed on the W isotopes.[29] That analysis included high-resolution neutron elastic and inelastic scattering data below 4 MeV, neutron total cross sections, 16-MeV (p,p') differential cross sections, and low-energy resonance data. A set of neutron parameters specific to each major isotope was obtained in the analysis, and the potentials produce good agreement with the available data to 20 MeV. Since that time, a general form of the potential was extended to higher energies[28] and was used to calculate data libraries to 100 MeV for incident neutrons and protons.[20] The generalized potential is included in Table 8.

Table 7. Coupled-Channels Optical Model and Deformation Parameters for Proton and Neutron Reactions with ^{165}Ho and ^{169}Tm (r_c = 1.25 fm).

Well Depth (MeV)	Range(MeV)	Geometry (fm)	
$V_R = 49.8 \pm 16\eta + \Delta V_c - 0.25E$	$0 \leq E \leq 100$	$r_R = 1.26$	$a_R = 0.63$
$W_D = 5.020 \pm 8\eta + 0.51E$	$0 \leq E \leq 6.5$	$r_D = 1.26$	$a_D = 0.48$
$= 8.335 \pm 8\eta - 0.092(E-6.5)$	$6.5 \leq E \leq 100$		
$W_V = 0$	$0 \leq E \leq 8.3$	$r_V = 1.26$	$a_V = 0.63$
$= -1.0 + 0.12E$	$8.3 \leq E \leq 100$		
$V_{SO} = 6.0$	$0 \leq E \leq 100$	$r_{SO} = 1.26$	$a_{SO} = 0.63$
β_2 (^{165}Ho) = 0.30	β_4 (^{165}Ho) = -0.02	(3 States Coupled)	
β_2 (^{169}Tm) = 0.29	β_4 (^{169}Tm) = -0.01	(5 States Coupled)	

Table 8. Deformed optical potential for proton and neutron reactions on W isotopes over the energy range 10 keV to 100 MeV.

Well Depth (MeV)	Range(MeV)	Geometry (fm)	
$V_R = 49.73 \pm 16\eta + \Delta V_c - 0.25E$	$0 \le E \le 100$	$r_R = 1.26$	$a_R = 0.61$
$W_D = 4.95 \pm 8\eta + 0.76E$	$0 \le E \le 4.5$	$r_D = 1.24$	$a_D = 0.45$
$= 8.37 \pm 8\eta - 0.10(E - 4.5)$	$4.5 \le E \le 100$		
$W_V = 0$	$0 \le E \le 5.8$	$r_V = 1.26$	$a_V = 0.61$
$= -0.70 + 0.12\ E$	$5.8 \le E \le 100$		
$V_{SO} = 7.5$	$0 \le E \le 100$	$r_{SO} = 1.26$	$a_{SO} = 0.61$
(3 States Coupled)		$r_c = 1.20$	

$\beta_2(^{182}W) = 0.223$	$\beta_4(^{182}W) = -0.054$
$\beta_2(^{183}W) = 0.220$	$\beta_4(^{183}W) = -0.055$
$\beta_2(^{184}W) = 0.209$	$\beta_4(^{184}W) = -0.056$
$\beta_2(^{186}W) = 0.195$	$\beta_4(^{186}W) = -0.057$

Because of a need to provide radiative capture cross section calculations for Eu and Re isotopes, very similar coupled-channels potentials were developed for the two systems covering the neutron energy range up to 20 MeV. The results were utilized in (n,γ) cross section calculations for $^{151,153}Eu$[30] and $^{185,187}Re$.[31] The parameterizations are included in Tables 9 and 10. Similarly, a requirement to perform (n,xγ) calculations on ^{197}Au led to an investigation of coupled-channels potentials for that system. In that case the potential of Delaroche[32] was found to be highly suitable and was used to perform extensive calculations to 20 MeV.[33] The potential, which was later used to calculate data for the ENDF/B-VI evaluation, is given in Table 11.

An optical model potential coupling in vibrational states was developed for n + ^{208}Pb reactions, primarily for use in analyzing high-resolution (n,xγ) measurements[34] and in performing calculations for the NEA intermediate energy data calculations.[27] Beginning with the coupled-channels neutron potential by Shamu and Young[35] (obtained for experimental neutron data in the range 8.5 to 10 MeV), the potential was modified and extended to both lower and higher neutron energies by matching the available experimental neutron total, elastic scattering, and nonelastic scattering data. The collective model assumed for ^{208}Pb was a first-order vibrational model with complex coupling. Excited states included in these calculations were all the ^{208}Pb states below 10 MeV excitation energy known from various alpha-particle, proton and/or electron inelastic scattering experiments to be highly collective, as follows: discrete states at 2.615(3^-), 4.085(2^+), 4.323(4^+), 4.424(6^+), and 4.610(8^+) MeV; and a low-energy octupole resonance (LEOR) state, centered at 5.38 MeV (3^-). The β_L used for the discrete states were adopted proton values,[36] except at $E_x = 2.615$ MeV where $\beta_3 = 0.115$, and $E_x = 5.38$ where $\beta_3 = 0.10$ was used. The potential that resulted, which is presented in Table 12, gives a reasonable representation of the available neutron total, elastic, and nonelastic scattering data to approximately 200 MeV.

Table 9. Coupled-Channels Optical Model and Deformation Parameters for ^{151,153}Eu Isotopes

Well Depth (MeV)	Range(MeV)	Geometry (fm)	
$V_R = 49.8 \pm 16\,\eta + \Delta V_c - 0.325E_n$	$0 \le E_n \le 20$	$r_R = 1.28$	$a_R = 0.63$
$W_D = 4.02 \pm 8\eta + 0.51E_n$	$0 \le E_n \le 10$	$r_D = 1.28$	$a_D = 0.48$
$= 9.12 \pm 8\eta - 0.09(E_n - 10)$	$10 \le E_n \le 20$		
$W_V = 0$	$0 \le E_n \le 8$	$r_V = 1.28$	$a_V = 0.63$
$= -2.0 + 0.25E_n$	$8 \le E_n \le 20$		
$V_{SO} = 6.0$		$r_{SO} = 1.28$	$a_{SO} = 0.63$

β_2 (^{151}Eu) = 0.16 β_2 (^{153}Eu) = 0.30 β_4 (^{151,153}Eu) = 0 (3 States Coupled)

Table 10. Coupled-Channels Optical Model and Deformation Parameters for Neutron Reactions with ^{185,187}Re

Well Depth (MeV)	Range(MeV)	Geometry (fm)	
$V_R = 49.8 \pm 16\eta + \Delta V_c - 0.30E_n$	$0 \le E_n \le 20$	$r_R = 1.26$	$a_R = 0.61$
$W_D = 4.02 \pm 8\eta + 0.75E_n$	$0 \le E_n \le 9$	$r_D = 1.26$	$a_D = 0.47$
$=10.77 \pm 8\eta - 0.05(E_n - 9)$	$9 \le E_n \le 20$		
$W_V = 0$	$0 \le E_n \le 9$	$r_V = 1.26$	$a_V = 0.61$
$= -1.8 + 0.2E_n$	$9 \le E_n \le 20$		
$V_{SO} = 7.5$	$0 \le E_n \le 20$	$r_{SO} = 1.26$	$a_{SO} = 0.61$

β_2 (^{185}Re) = 0.22 β_4 (^{185}Re) = -0.085 (3 States Coupled)
β_2 (^{187}Re) = 0.21 β_4 (^{187}Re) = -0.085 (3 States Coupled)

Table 11. Deformed optical potential for proton and neutron reactions on ^{197}Au over the energy range 10 keV to 57 MeV.

Well Depth (MeV)	Range(MeV)	Geometry (fm)	
$V_R = 49.9 \pm 18\eta + \Delta V_c - 0.25E$	$0 \le E \le 57$	$r_R = 1.26$	$a_R = 0.64$
$W_D = 4.20 \pm 9\eta + 0.50E$	$0 \le E \le 10$	$r_D = 1.26$	$a_D = 0.47$
$= 9.20 \pm 9\eta - 0.18(E - 10)$	$10 \le E \le 57$		
$W_V = 0$	$0 \le E \le 10$	$r_V = 1.26$	$a_V = 0.63$
$= -8.54 + 2.7\sqrt{E}$	$10 \le E \le 57$		
$V_{SO} = 6.2$	$0 \le E \le 57$	$r_{SO} = 1.12$	$a_{SO} = 0.47$
		$r_C = 1.10$	

$\beta_2 = 0.30$ $\beta_4 = -0.02$ (3 States Coupled)

Table 12. Coupled-channels optical model potential for ^{208}Pb + n calculations over the neutron energy range 1 keV $\leq E_n \leq$ 200 MeV

Well Depth (MeV)	Range(MeV)	Geometry (fm)	
$V_R = 53.425 - 16\eta - 0.279 E_n$	$0 < E_n < 60$	$r_R = 1.183$	$a_R = 0.6966$
$= 114.477 - 16\eta - 19 \ln E_n$	$60 \leq E_n \leq 200$		
$W_D = 2.692 - 8\eta + 0.2502 E_n$	$0 < E_n < 14$	$r_D = 1.273$	$a_D = 0.699$
$= 7.414 - 8\eta - 0.08705 E_n$	$14 \leq E_n \leq 65.7$		
$= 0$	$65.7 \leq E_n \leq 200$		
$W_V = 0$	$0 < E_n < 14.4$	$r_V = 1.273$	$a_V = 0.699$
$= -2.60 + 0.18 E_n$	$14.4 \leq E_n \leq 40$		
$= 2.20 + 0.06 E_n$	$40 \leq E_n \leq 100$		
$= 8.20$	$100 \leq E_n \leq 200$		
$V_{SO} = 6.18$	$0 < E_n < 200$	$r_{SO} = 1.16$	$a_{SO} = 0.677$

B. Actinide Potentials for Incident Neutrons and Protons

Coupled-channels optical potentials have been developed for several actinides in order to provide theoretical analyses[37-39] for ENDF/B evaluations. The analyses use as a starting point the potentials determined by Lagrange,[40] with modifications to enhance agreement with data, especially above 10 MeV. As described above, low-energy resonance data, neutron total and differential elastic and inelastic data were used to optimize the potentials. In this manner potentials have been determined for neutron reactions on $^{235,237,238}U$, ^{237}Np, $^{239,242}Pu$, and ^{241}Am, and the parameters are listed in Table 13.

In conjunction with our work in extending data libraries to higher energies, a generalized neutron/proton potential was developed for ^{238}U that was used in reaction theory calculations to 100 MeV [20] This parameterization is included in Table 14.

V. CONCLUSIONS

In this paper a variety of optical model potentials used in reaction theory analyses at Los Alamos National Laboratory have been assembled and presented. While many other potentials have been used that are not included here, the present list is a reasonable sampling of our efforts and includes the systems for which more concentrated efforts have been made. In all cases presented, however, we expect that refinements and improvements can be made Our hope is that the present parameterizations will be adequate with minimal revision for some applications and will provide an initial basis for future detailed analyses.

The parameterizations included here become progressively less certain as the incident energy increases In our view substantial additional work is needed at higher energies and into the medium energy region in order to put optical model characterizations on a sound basis In addition to the Madland potential described here,[11] Kozack and Madland have combined Dirac

phenomenology with a relativistic generalization of the Lane model to fit both neutron total cross sections and proton elastic scattering data for ^{208}Pb between 95 and 300 MeV.[41] It is our view that a systematic study utilizing both a Schrödinger and Dirac approach is needed to develop a reliable global nucleon-nucleus optical model potential that extends into the medium energy region.

Table 13. Optical Model and Deformation Parameters Used in the Coupled-Channel Calculations for Actinides

n + ^{235}U Parameters (E_n = 0 - 30 MeV)

Well Depth (MeV)	Range(MeV)	Geometry (fm)	
$V_R = 46.4 - 0.3E_n$	$0 \le E_n \le 30$	$r_R = 1.26$	$a_R = 0.63$
$W_D = 3.3 + 0.4E_n$	$0 \le E_n \le 8$	$r_D = 1.24$	$a_D = 0.50$
$= 6.5 - 0.046(E_n - 8)$	$8 \le E_n \le 30$		
$W_V = 0$	$0 \le E_n \le 7$	$r_V = 1.26$	$a_V = 0.63$
$= -0.7 + 0.1E_n$	$7 \le E_n \le 30$		
$V_{SO} = 6.2$	$0 \le E_n \le 30$	$r_{SO} = 1.12$	$a_{SO} = 0.47$

$\beta_2 = 0.215$ $\beta_4 = 0.075$ (3 States Coupled)

n + ^{237}U Parameters (E_n = 0 - 30 MeV)

Well Depth (MeV)	Range(MeV)	Geometry (fm)	
$V_R = 46.25 - 0.275E_n$	$0 \le E_n \le 30$	$r_R = 1.26$	$a_R = 0.63$
$W_D = 3.206 + 0.4E_n$	$0 \le E_n \le 8$	$r_D = 1.26$	$a_D = 0.52$
$= 6.406 - 0.046(E_n - 8)$	$8 \le E_n \le 30$		
$W_V = 0$	$0 \le E_n \le 8$	$r_V = 1.26$	$a_V = 0.63$
$= -1.4 + 0.175\ E_n$	$8 \le E_n \le 30$		
$V_{SO} = 6.2$	$0 \le E_n \le 30$	$r_{SO} = 1.12$	$a_{SO} = 0.47$

$\beta_2 = 0.195$ $\beta_4 = 0.060$ (6 States Coupled)

n + ^{238}U Parameters (E_n = 0 - 30 MeV)

Well Depth (MeV)	Range(MeV)	Geometry (fm)	
$V_R = 46.2 - 0.275E_n$	$0 \le E_n \le 30$	$r_R = 1.26$	$a_R = 0.63$
$W_D = 3.18 + 0.4E_n$	$0 \le E_n \le 8$	$r_D = 1.26$	$a_D = 0.52$
$= 6.38 - 0.046(E_n - 8)$	$8 \le E_n \le 30$		
$W_V = 0$	$0 \le E_n \le 8$	$r_V = 1.26$	$a_V = 0.63$
$= -1.4 + 0.175\ E_n$	$8 \le E_n \le 30$		
$V_{SO} = 6.2$	$0 \le E_n \le 30$	$r_{SO} = 1.12$	$a_{SO} = 0.47$

$\beta_2 = 0.198$ $\beta_4 = 0.057$ (3 States Coupled)

n + ^{237}Np Parameters (E_n = 0 - 30 MeV)

Well Depth (MeV)	Range(MeV)	Geometry (fm)	
V_R = 46.2 - 0.3E_n	0 ≤ E_n ≤ 30	r_R = 1.26	a_R = 0.63
W_D = 3.6 + 0.4E_n	0 ≤ E_n ≤ 8	r_D = 1.24	a_D = 0.52
= 6.8 - 0.046(E_n - 8)	8 ≤ E_n ≤ 30		
W_V = 0	0 ≤ E_n ≤ 7	r_V = 1.26	a_V = 0.63
= -0.7 + 0.1E_n	7 ≤ E_n ≤ 30		
V_{SO} = 6.2	0 ≤ E_n ≤ 30	r_{SO} = 1.12	a_{SO} = 0.47

β_2 = 0.214 β_4 = 0.074 (3 States Coupled)

n + ^{239}Pu Parameters (E_n = 0 - 30 MeV)

Well Depth (MeV)	Range(MeV)	Geometry (fm)	
V_R = 46.2 - 0.3E_n	0 ≤ E_n ≤ 30	r_R = 1.26	a_R = 0.63
W_D = 3.3 + 0.45E_n	0 ≤ E_n ≤ 8	r_D = 1.24	a_D = 0.50
= 6.9 - 0.046(E_n - 8)	8 ≤ E_n ≤ 30		
W_V = 0	0 ≤ E_n ≤ 7	r_V = 1.26	a_V = 0.63
= -0.7 + 0.1E_n	7 ≤ E_n ≤ 30		
V_{SO} = 6.2	0 ≤ E_n ≤ 30	r_{SO} = 1.12	a_{SO} = 0.47

β_2 = 0.205 β_4 = 0.075 (7 States Coupled)

n + ^{242}Pu Parameters (E_n = 0 - 20 MeV)

Well Depth (MeV)	Range(MeV)	Geometry (fm)	
V_R = 53.016 - 0.344E_n - 24.5η	0 ≤ E_n ≤ 20	r_R = 1.203	a_R = 0.30 + 1.492η
W_D = 8.905 - 0.255E_n - 13.6η	0 ≤ E_n ≤ 20	r_D = 1.306	
		a_D = 0.25 + (0.733E-2)E_n + 1.42η	
W_V = 0	0 ≤ E_n ≤ 2.7	r_V = 1.306	
= -0.566 + 0.21E_n	2.7 ≤ E_n ≤ 20	a_V = 0.25 + (0.733E-2)E_n + 1.42η	
V_{SO} = 6.2	0 ≤ E_n ≤ 20	r_{SO} = 1.01	a_{SO} = 0.75

β_2 = 0.260 β_4 = 0.036 (5 States Coupled)

n + ^{241}Am Parameters (E_n = 0 - 30 MeV)

Well Depth (MeV)	Range(MeV)	Geometry (fm)	
V_R = 46.23 - 0.3E_n	0 ≤ E_n ≤ 30	r_R = 1.25	a_R = 0.60
W_D = 3.314 + 0.45E_n	0 ≤ E_n ≤ 8	r_D = 1.24	a_D = 0.55
= 6.914 - 0.046(E_n -8)	8 ≤ E_n ≤ 30		
W_V = 0	0 ≤ E_n ≤ 8	r_V = 1.24	a_V = 055
= -1.6 + 0.2E_n	8 ≤ E_n ≤ 30		
V_{SO} = 6.2	0 ≤ E_n ≤ 30	r_{SO} = 1.01	a_{SO} = 0.75

β_2 = 0.210 β_4 = 0.0756 (5 States Coupled)

Table 14. Coupled-Channels Optical Model and Deformation Parameters for Neutron and Proton Reactions with ^{238}U to 100 MeV

n + ^{238}U Parameters ($E_{n,p}$ = 0 - 100 MeV)

Well Depth (MeV)	Range(MeV)	Geometry (fm)
$V_R = 49.8 \pm 16\eta + \Delta V_c - 0.29E + 0.0005E^2$	$0 \le E \le 100$	$r_R = 1.26$ $a_R = 0.63$
$W_D = 4.995 \pm 8\eta + 0.4E$	$0 \le E \le 8$	$r_D = 1.26$ $a_D = 0.52$
$= 8.195 - 0.046(E - 8)$	$8 \le E \le 100$	
$W_V = 0$	$0 \le E \le 7$	$r_V = 1.26$ $a_V = 0.63$
$= -0.7 + 0.10\ E$	$7 \le E \le 100$	
$V_{SO} = 6.2$	$0 \le E \le 100$	$r_{SO} = 1.12$ $a_{SO} = 0.47$
$\beta_2 = 0.198$ $\beta_4 = 0.057$	(3 States Coupled)	

REFERENCES

1. P. G. Young, "Global and Local Optical Model Parameterizations," Proc. *Specialists' Meeting on Use of the Optical Model for the Calculation of Neutron Cross Sections below 20 MeV*, sponsored by the NEANDC, Nov. 13-15, 1985, Chateau de la Muette, Paris, France, OECD/NEA report NEANDC-222'U' (1986) p. 127.

2. O. Bersillon, "SCAT2 - Un Programme de Modele Optique Spherique," Commissariat a l'Energie Atomique report CEA-N-2227 (1978), and Proc. ICTP Workshop on *Computation and Analysis of Nuclear Data Relevant to Nuclear Energy and Safety*, 10 February - 13 March, 1992, Trieste, Italy.

3. P. Schwandt, Indiana University, private communication to D. Madland, May 1984.

4. J. Raynal, "Optical Model and Coupled-Channel Calculations in Nuclear Physics," International Atomic Energy Agency report IAEA SMR-9/8 (1970) p. 281.

5. H. Rebel et al., Karlsruhe report KFK-1333 (1971).

6. J. P. Delaroche et al., "The Optical Model with Particular Considerations of the Coupled-Channel Optical Model," IAEA-190 (1976) p. 251.

7. C. M. Perey and F. G. Perey, *Atomic Data and Nuclear Data Tables* **17**, 1 (1976).

8. N. Yamamuro, "Nuclear Cross Section Calculations with a Simplified-Input Version of ELIESE-GNASH Joint Program," Proc. *Int. Conf. on Nucl. Data for Sci. and Tech.*, May 30-June 3, 1988, Mito, Japan (LA-UR 88-1618) (Ed. S. Igarasi, Saikon Publ. Co., Ltd., 1988) p. 489.

9. R. L. Walter and P. P. Guss, "A Global Optical Model for Neutron Scattering for A>53 and 10 MeV<E<80 MeV," Proc. Int. Conf. Nuclear Data for Basic and Applied Science, Santa Fe, N.M., May 13-17, 1985 [Gordon and Breach Science Pub., Inc. (1986)] p. 1079.

10. P. Schwandt et al., *Phys. Rev. C.* **26**, 55 (1982).

11. D. G. Madland, "Recent Results in the Development of a Global Medium-Energy Nucleon-Nucleus Optical-Model Potential," Proc. Specialists' Mtg. Preequilibrium Nuclear Reactions, Semmering, Austria, 10-12 February 1988 [Ed: B. Strohmaier, NEANDC-245 'U' (1988)] p. 103.

12. D. G. Madland, personal communication, December, 1986.

13. S. Watanabe, *Nucl. Phys.* **8**, 484 (1958).

14. Ch. Lagrange, O. Bersillon, and D. G. Madland, *Nucl. Sci. Eng.* **83**, 396 (1983).

15. D. G. Madland and P. G. Young, "Neutron-Nucleus Optical Potential for the Actinide Region," Proc. *Int. Conf. on Neutron Physics and Nuclear Data for Reactors and Other Applied Purposes*, Harwell, England, Sept. 25-29, 1978 [published by the OECD (1978)], p. 349.

16. H. Hitzenberger, A. Pavlik, H. Vonach, R. C. Haight, R. O. Nelson, and P. G. Young, "Study of ^{27}Al (n,xγ) Reaction up to E_n = 400 MeV," Proc. Int. Conf. on *Nuclear Data for Sci. and Tech.*, 9-13 May 1994, Gatlinburg, Tenn. (LA-UR 93-3808).

17. J. S. Petler, M. S. Islam, R. W. Finlay, and F. S. Dietrich, *Phys. Rev. C* **32**, 673 (1985).

18. F. G. Perey, *Phys. Rev.* **131**, 745 (1963).

19. E. D. Arthur and P. G. Young, "Evaluated Neutron-Induced Cross Sections for ^{54,56}Fe to 40 MeV," Los Alamos National Laboratory report LA-8636-MS (ENDF-304) (1980).

20. P. G. Young, E. D. Arthur, M. Bozoian, T. R. England, G. M. Hale, R. J. LaBauve, R. C. Little, R. E. MacFarlane, D. G. Madland, R. T. Perry, and W. B. Wilson, "Transport Data Libraries for Incident Proton and Neutron Energies to 100-MeV," Los Alamos National Laboratory report LA-11753-MS (July 1990).

21. S. M. Sterbenz, F. B. Bateman, T. M. Lee, R. C. Haight, Rc C. Goeckner, C. E. Brient, S. M. Grimes, H. Vonach, P. Maier-Komor, P. G. Young, and M. B. Chadwick, "The ^{56}Fe(n,xα) Reaction from Threshold to 30 MeV," Proc. Int. Conf. on *Nuclear Data for Sci. and Tech.*, 9-13 May 1994, Gatlinburg, Tenn. (LA-UR-93-3626).

22. E. D. Arthur, P. G. Young, and W. K. Matthes, "Calculation of ^{59}Co Neutron Cross Sections Between 3 and 50 MeV, "Proc. *Symp. on Neutron Cross Sections from 10 to 50 MeV*, BNL (May 1980), p. 751.

23. T. M. Lee, F. B. Bateman, P. G. Young, *et al.*, "The ^{59}Co(n,α) Reaction from Threshold to 30 MeV," Proc. Int. Conf. on *Nuclear Data for Sci. and Tech.*, 9-13 May 1994, Gatlinburg, Tenn. (LA-UR-93-3627).

24. P. G. Young and D. A. Rutherford, "Calculation of Neutron Cross Sections of $^{64, 66, 68}$Zn for Fusion Applications," Proc. *IAEA Advisory Group Mtg. on Nuclear Theory for Fast Neutron Data Evaluation*, 12-16 Oct., 1987, Beijing China (LA-UR 87-3189), International Atomic Energy Agency report IAEA-TECDOC-483 (1988) p. 167.

25. E. D. Arthur, *Nucl. Sci. Eng.* **76**, 137 (1980).

26. H. A. O'Brien, R. O. Nelson, C. M. Laymon, S. A. Wender, and P. G. Young, "Studies of Higher-Order (n,xγ) Reactions in ^{89}Y Targets," Proc. *7th International Symposium on Capture Gamma-Ray Spectroscopy and Related Topics*, Asilomar, California, 14-19 October 1990, LA-UR-90-3498 (October, 1990).

27. P. G. Young and M. B. Chadwick, "Calculation of Proton and Neutron Emission Spectra from Proton Reactions with ^{90}Zr and ^{208}Pb to 160 MeV with the GNASH Code", Proc. OECD Nuclear Energy Agency Specialists Meeting on *Intermediate Energy Nuclear Data,* May 30 - June 1, 1994, Issy-les-Moulineaux, France, to be published (LA-UR-94-1830).

28. E. D. Arthur, "Extension of Theoretical Calculations of Nucleon-Induced Reactions on Tungsten Isotopes to 50 MeV," in *Applied Nuclear Data Research and Development, June 1 - Nov. 30 1985,* Los Alamos Scientific Laboratory report LA-10689-PR (1986) p. 27.

29. E. D. Arthur and C. A. Philis, "New Calculations of Neutron-Induced Cross Sections on Tungsten Isotopes," in *Applied Nuclear Data Research and Development, July 1 - Sept. 30, 1980,* Los Alamos Scientific Laboratory report LA-8630-PR (1980) p. 2.

30. R. L. Macklin and P. G. Young, *Nucl. Sci. Eng.* **95**, 189 (1987).

31. R. L. Macklin and P. G. Young, *Nucl. Sci. Eng.* **97**, 239 (1987).

32. J. P. Delaroche, "Potentiel Optique Nucleon-^{197}Au Entre 10 keV et 57 MeV," Proc. *Int. Conf. on Neutron Physics and Nuclear Data for Reactors and Other Applied Purposes,* Harwell, England, Sept. 25-29, 1978 [published by the OECD (1978)], p. 366.

33. P. G. Young and E. D. Arthur, "Analysis of n + ^{197}Au Cross Sections for E_n = 0.01-209 MeV," Proc. *5th Int. Symp. on Capture Gamma Ray Spectroscopy and Related Topics,* Oak Ridge Nat. Lab., Knoxville, Tenn., Sept. 9-14, 1984, AIP Proceedings No. 125, p. 530 (LA-UR-84-2767).

34. H. Vonach, A. Pavlik, M. B. Chadwick, R. C. Haight, R. O. Nelson, S. A. Wender, and P. G. Young, "^{207,208}Pb(n,xnγ) Reactions for Neutron Energies up to 200 MeV," accepted for publication in *Phys. Rev. C* (1994).

35. R. E. Shamu and P. G. Young, *J. Phys. G: Nucl. Part. Phys.* **19**, L169 (1993).

36. M. J. Martin, *Nucl. Data Sheets* **47**, 797 (1986).

37. D. G. Madland and P. G. Young, "Evaluation of n + ^{242}Pu Reactions from 10 keV to 20 MeV," Los Alamos National Laboratory report LA-7533-MS (1978).

38. P. G. Young and E. D. Arthur, "Calculation of ^{235}U(n,n') Cross Sections for ENDF/B-VI, Proc. *Int. Conf. on Nucl. Data for Sci. and Tech.*, May 30-June 3, 1988, Mito, Japan (LA-UR-99-1740) (Ed. S. Igarasi, Saikon Publ. Co., Ltd., 1988), p. 603.

39. P. G. Young and E. D. Arthur, "Theoretical Analyses of (n,xn) Reactions on ^{235}U, ^{238}U, ^{237}Np, and ^{239}Pu for ENDF/B-VI," Proc. Int. Conf. on Nuclear Data for Science and Technology, Jülich, Germany, 13-17 May 1991 (LA-UR-91-1424), [Ed. S. M. Qaim, Springer-Verlag, Germany (1992)], p. 894.

40. G. Haouat, J. Lachkar, Ch. Lagrange et al., *Nucl. Sci. Eng.* **81**, 491 (1982).

41. R. Kozack and D. G. Madland, *Phys. Rev. C.* **39**, 1461 (1990).

Appendix III

STATUS OF OPTICAL MODEL ACTIVITIES AT LOS ALAMOS NATIONAL LABORATORY

(Report LA-UR-95-3654)

P.G. Young
Los Alamos National Laboratory

Summary

An update will be given of activities at Los Alamos National Laboratory aimed at developing optical model potentials for applied calculations. Recent work on a coupled-channels potential for neutron reactions on ^{241,243}Am and spherical neutron potential updates for ^{56}Fe and ^{59}Co will be presented, together with examples of their application in nuclear reaction calculations with the GNASH code system. New potentials utilized in evaluations at Livermore for ^{12}C, ^{14}N, and ^{16}O are described and additional potentials from earlier analyses at Los Alamos of Ti, V, and Ni data are made available for possible inclusion in the Reference Input Parameter Library (RIPL) for nuclear model calculations of nuclear data. Specific activities directed at development of the optical potential segment of the RIPL will be summarized.

I. INTRODUCTION

At the First Research Coordination Meeting on Development of Reference Input Parameter Library for Nuclear Model Calculations of Nuclear Data in 1994, a number of spherical and coupled-channels optical model potentials developed at Los Alamos National Laboratory for applied calculations were presented.[1] In this paper we update the parameterizations for two materials that were included in the previous paper and provide additional ones that have been employed both at Los Alamos and Livermore in nuclear data calculations. We present selected comparisons with experimental data to demonstrate the validity of the potentials.

II. SPHERICAL OPTICAL MODEL POTENTIALS

A. Neutron and Proton Potentials for ^{12}C, ^{14}N, and ^{16}O Target Nuclei

Recently new evaluations have been completed at Lawrence Livermore National Library for neutron- and proton-induced reactions on ^{12}C, ^{14}N, and ^{16}O for neutron and proton radiotherapy applications. The neutron evaluations[2,3] cover the energy range up to 100 MeV, and the proton evaluations[4] cover the range to 250 MeV. We include here the neutron and proton potentials used for major parts of those evaluations.

The neutron potentials used for ^{12}C are taken from the analysis of Arthur[5] for neutron energies below 10 MeV and from Dimbylow[6] for neutrons in the 10 - 65 MeV range. Above 65 MeV the global potential of Madland[7] is used. The proton potentials were obtained by applying the Lane isospin model to the neutron potentials. The parameters for these potentials are included in Table 1.

Table 1. Spherical optical model potentials for neutron and proton reactions with ^{12}C over the incident energy range 1 keV $\leq E_{n,p} \leq$ 100 MeV. Above an energy of 65 MeV, the Madland global potential[7] is used. Note that the symbol $W_{D'}$ indicates a gaussian form factor for the surface derivative potential.

NEUTRONS BELOW 10 MeV

Well Depth (MeV)	Range (MeV)	Geometry (fm)	
$V_R = 49.0 - 0.20\ E_n + 0.00008\ E_n^2$	$0 < E_n < 10$	$r_R = 1.35$	$a_R = 0.60$
$W_D = 2.50 + 0.125\ E_n$	$0 < E_n < 6$	$r_D = 1.26$	$a_D = 0.45$
$= 4.00 - 0.02\ (E_n - 6)$	$6 \leq E_n < 10$		
$W_V = 0.00$	$0 < E_n < 10$		
$V_{SO} = 7.0$	$0 < E_n < 10$	$r_{SO} = 1.30$	$a_{SO} = 0.66$

NEUTRONS FROM 10 TO 65 MeV

Well Depth (MeV)	Range (MeV)	Geometry (fm)	
$V_R = 47.75 - 0.345\ E_n$	$10 \leq E_n < 65$	$r_R = 1.23$	$a_R = 0.60$
$W_{D'} = 6.50 + 0.01\ E_n$	$10 \leq E_n < 65$	$r_D = 1.23$	$a_D = 1.20$
$W_V = 0.00$	$10 \leq E_n < 65$		
$V_{SO} = 7.0$	$10 \leq E_n < 65$	$r_{SO} = 1.23$	$a_{SO} = 0.60$

PROTONS BELOW 10 MeV

Well Depth (MeV)	Range (MeV)	Geometry (fm)	
$V_R = 50.50 - 0.20\ E_p + 0.00008\ E_p^2$	$0 < E_p < 10$	$r_R = 1.35$	$a_R = 0.60$
$W_{D'} = 2.50 + 0.25\ E_p$	$0 < E_p < 6$	$r_D = 1.26$	$a_D = 0.45$
$= 4.00 - 0.02\ (E_p - 6)$	$6 \leq E_p < 10$		
$W_V = 0.00$	$0 < E_p < 10$		
$V_{SO} = 7.0$	$0 < E_p < 10$	$r_{SO} = 1.30$	$a_{SO} = 0.66$
	$0 < E_p < 10$	$r_C = 1.25$	

PROTONS FROM 10 TO 65 MeV

Well Depth (MeV)	Range (MeV)	Geometry (fm)	
$V_R = 48.80 - 0.345\ E_p$	$10 \leq E_p < 65$	$r_R = 1.23$	$a_R = 0.60$
$W_{D'} = 6.50 + 0.01\ E_p$	$10 \leq E_p < 65$	$r_D = 1.23$	$a_D = 1.20$
$W_V = 0.00$	$10 \leq E_p < 65$		
$V_{SO} = 7.0$	$10 \leq E_p < 65$	$r_{SO} = 1.23$	$a_{SO} = 0.60$
	$10 \leq E_p < 65$	$r_C = 1.25$	

For ^{14}N and ^{16}O, the neutron potentials are taken from Arthur[5] below 20 MeV for ^{14}N and below 10 MeV for ^{16}O, and from Islam et al.[8] in the energy range 20 - 60 MeV for ^{14}N and 10 - 50 MeV for ^{16}O. At higher energies, the Madland Semmering potential[7] is again employed. The Lane isospin model is again used to determine the proton potentials. The parameterizations of these potentials are included in Table 2 for ^{14}N and Table 3 for ^{16}O.

B. Neutron Potential for Analysis of n + $^{54,56}Fe$ Reactions

The neutron potential included in our previous CRP paper[1] for $^{54,56}Fe$ targets was based on an analysis by Arthur and Young[9] but including modifications that were suggested by the ENDF/B-VI evaluation.[10] Over the past year we have discovered that our modifications lead to poorer agreement with elastic scattering angular distributions at energies above ~8 MeV than was previously obtained with the Arthur and Young potential. Consequently, we have revised the $^{54,56}Fe$ potential to rely on the original Arthur and Young potential to 26 MeV but have introduced new modifications in the volume imaginary potential that improve the reaction cross section at higher energies. We now utilize this revised potential to an incident neutron energy of 52 MeV and switch to the Madland Semmering potential[7] at higher energies.

The problem in the n + Fe elastic scattering angular distributions with our previous CRP potential is shown in Fig. 1, where calculated angular distributions using our previous and present potentials are compared with experimental data at 14.1 and 24.8 MeV. The revised potential clearly leads to improved agreement with the measurements. The calculated total and reaction cross sections for n + ^{56}Fe are compared to experimental data for natural Fe in Fig. 2. The revised neutron optical model parameters are included in Table 4.

C. Neutron Potential for Analysis of n + ^{59}Co Reactions

Similar to the above calculations on Fe, optical model parameters that were given in our earlier paper[1] for n + ^{59}Co reactions have been modified slightly on the basis of an analysis of recent measurements from Weapons Neutron Research facility at Los Alamos. In particular, it is not possible to achieve suitable agreement with new measurements of neutron-induced alpha particle emission spectra by Grimes et al.[11] at energies above 30 MeV with the previous set of parameters, as is shown in Fig. 3. It was found that, although the Madland Semmering potential[7] was derived for energies above 50 MeV, it results in much better agreement with the alpha emission measurements even at lower energies. Because the Madland potential produces elastic and reaction cross sections that are consistent with the lower energy ^{59}Co potential[12] near 26 MeV, the transition to the Madland Semmering potential is now made at that energy. Calculations of angle-integrated alpha emission cross sections with the revised potential are included in Fig. 3

The revised n + ^{59}Co parameters are listed in Table 5. Calculated neutron total and nonelastic cross sections are compared to experimental data in Fig. 4. It should be noted that although the reaction theory and optical model calculations using these parameters are only shown here to ~ 50 MeV, reasonable total and reaction cross sections result from the combination of this potential with the Madland Semmering potential for neutron energies to 100 MeV or higher.

Table 2. Spherical optical model potentials for neutron and proton reactions with ^{14}N over the incident energy range 1 keV $\leq E_{n,p} \leq$ 100 MeV. Above an energy of 60 MeV, the Madland global potential[7] is used.

NEUTRONS BELOW 20 MeV

Well Depth (MeV)	Range (MeV)	Geometry (fm)	
$V_R = 48.0 - 0.20\ E_n - 0.0008\ E_n^2$	$0 < E_n < 20$	$r_R = 1.35$	$a_R = 0.70$
$W_D = 2.50 + 0.625\ E_n$	$0 < E_n < 4.8$	$r_D = 1.261$	$a_D = 0.51$
$= 5.50$	$4.8 \leq E_n < 20$		
$W_V = 0.00$	$0 < E_n < 20$		
$V_{SO} = 7.0$	$0 < E_n < 20$	$r_{SO} = 1.312$	$a_{SO} = 0.66$

NEUTRONS FROM 10 TO 60 MeV

Well Depth (MeV)	Range (MeV)	Geometry (fm)	
$V_R = 52.40 - 0.29\ E_n$	$20 \leq E_n \leq 60$	$r_R = 1.197$	$a_R = 0.593$
$W_D = 8.64 - 0.145\ E_n$	$20 \leq E_n \leq 60$	$r_D = 1.388$	$a_D = 0.449$
$W_V = 0.0$	$20 \leq E_n < 22$	$r_V = 1.388$	$a_V = 0.449$
$= -5.86 + 0.267\ E_n$	$22 \leq E_n \leq 60$		
$V_{SO} = 6.0$	$20 \leq E_n \leq 60$	$r_{SO} = 1.010$	$a_{SO} = 0.500$

PROTONS BELOW 20 MeV

Well Depth (MeV)	Range (MeV)	Geometry (fm)	
$V_R = 59.673 - 0.55\ E_p$	$0 < E_p < 20$	$r_R = 1.25$	$a_R = 0.65$
$W_D = 13.5$	$0 < E_p < 20$	$r_D = 1.25$	$a_D = 0.47$
$W_V = 0.00$	$0 < E_p < 20$		
$V_{SO} = 7.5$	$0 < E_p < 20$	$r_{SO} = 1.25$	$a_{SO} = 0.65$
	$0 < E_p < 20$	$r_C = 1.25$	

PROTONS FROM 20 TO 70 MeV

Well Depth (MeV)	Range (MeV)	Geometry (fm)	
$V_R = 53.73 - 0.29\ E_p$	$20 \leq E_p \leq 70$	$r_R = 1.197$	$a_R = 0.593$
$W_D = 8.64 - 0.145\ E_p$	$20 \leq E_p \leq 70$	$r_D = 1.388$	$a_D = 0.449$
$W_V = 0.0$	$20 \leq E_p < 22$	$r_V = 1.388$	$a_V = 0.449$
$= -5.86 + 0.267\ E_p$	$22 \leq E_p \leq 70$		
$V_{SO} = 6.0$	$20 \leq E_p \leq 70$	$r_{SO} = 1.010$	$a_{SO} = 0.500$
	$20 \leq E_p \leq 70$	$r_C = 1.20$	

Table3. Spherical optical model potentials for neutron and proton reactions with ^{16}O over the incident energy range 1 keV $\leq E_{n,p} \leq$ 100 MeV. Above an energy of 50 MeV, the Madland global potential[7] is used.

NEUTRONS BELOW 20 MeV

Well Depth (MeV)	Range (MeV)	Geometry (fm)	
$V_R = 49.0 - 0.20\ E_n + 0.00008\ E_n^2$	$0 < E_n < 20$	$r_R = 1.35$	$a_R = 0.60$
$W_D = 2.50 + 0.25\ E_n$	$0 < E_n < 14$	$r_D = 1.26$	$a_D = 0.45$
$= 6.0 - 0.02(E_n - 14)$	$14 \leq E_n < 20$		
$W_V = 0.00$	$0 < E_n < 20$		
$V_{SO} = 7.0$	$0 < E_n < 20$	$r_{SO} = 1.30$	$a_{SO} = 0.66$

NEUTRONS FROM 20 TO 50 MeV

Well Depth (MeV)	Range (MeV)	Geometry (fm)	
$V_R = 53.50 - 0.297\ E_n$	$20 \leq E_n \leq 50$	$r_R = 1.153$	$a_R = 0.646$
$W_D = -0.01 + 0.31\ E_n$	$20 \leq E_n < 21$	$r_D = 1.376$	$a_D = 0.473$
$= 10.0 - 0.166\ E_n$	$21 \leq E_n \leq 50$		
$W_V = 0.$	$20 \leq E_n < 21$	$r_V = 1.376$	$a_V = 0.473$
$= -3.50 + 0.167\ E_n$	$21 \leq E_n \leq 50$		
$V_{SO} = 4.31$	$20 \leq E_n \leq 50$	$r_{SO} = 1.110$	$a_{SO} = 0.450$

PROTONS BELOW 10 MeV

Well Depth (MeV)	Range (MeV)	Geometry (fm)	
$V_R = 49.80 - 0.20\ E_p - 0.00008\ E_p$	$0 < E_p \leq 10$	$r_R = 1.35$	$a_R = 0.60$
$W_D = 2.50 + 0.25\ E_p$	$0 < E_p \leq 6$	$r_D = 1.26$	$a_D = 0.45$
$= 4.00 - 0.02(E_p - 6)$	$6 < E_p \leq 10$		
$W_V = 0.00$	$0 < E_p \leq 10$		
$V_{SO} = 7.0$	$0 < E_p \leq 10$	$r_{SO} = 1.30$	$a_{SO} = 0.66$
	$0 < E_p \leq 10$	$r_C = 1.25$	

PROTONS FROM 20 TO 70 MeV

Well Depth (MeV)	Range (MeV)	Geometry (fm)	
$V_R = 54.78 - 0.297\ E_p$	$10 < E_p \leq 50$	$r_R = 1.153$	$a_R = 0.646$
$W_D = -0.01 + 0.31\ E_p$	$10 < E_p < 21$	$r_D = 1.376$	$a_D = 0.473$
$= 10.0 - 0.166\ E_p$	$21 \leq E_p \leq 50$		
$W_V = 0.$	$10 < E_p < 21$	$r_V = 1.376$	$a_V = 0.473$
$= -3.50 + 0.167\ E_p$	$21 < E_p \leq 50$		
$V_{SO} = 4.31$	$10 < E_p \leq 50$	$r_{SO} = 1.110$	$a_{SO} = 0.450$
	$10 < E_p \leq 50$	$r_C = 1.21$	

Table 4. Spherical optical model potentials for $^{54,56}Fe$ + n calculations over the incident neutron energy range 1 keV ≤ E_n ≤ 100 MeV. Above a neutron energy of 52 MeV, the Madland global potential[7] is used.

NEUTRONS TO 52 MeV

	Well Depth (MeV)	Range (MeV)	Geometry (fm)	
V_R	= 49.747 - 0.429 E_n - 0.0003 E_n^2	0 < E_n ≤52	r_R = 1.287	a_R = 0.56
W_D	= 6.053 + 0.074 E_n	0 < E_n < 6	r_D = 1.345	a_D = 0.47
	= 6.497- 0.325 (E_n - 6)	6 ≤ E_n < 25.99		
	= 0	25.99 ≤ E_n ≤ 52		
W_V	= 0.00	0 < E_n < 0.82	r_V = 1.345	a_V = 0.47
	= -0.207 + 0.253 E_n	0.82 ≤ E_n < 25.67		
	= 4.717 + 0.0612 E_n	25.67 ≤ E_n ≤ 52		
V_{SO}	= 6.20	0 < E_n ≤ 52	r_{SO} = 1.12	a_{SO} = 0.47

Table 5. Spherical optical model potentials for ^{59}Co + n calculations over the incident neutron energy range 1 keV ≤ E_n ≤ 100 MeV. Above a neutron energy of 27.6 MeV, the Madland global potential[7] is used.

NEUTRONS

	Well Depth (MeV)	Range (MeV)	Geometry (fm)	
V_R	= 47.604 - 0.3636 E_n - 0.0003 E_n^2	0 < E_n ≤ 27.6	r_R = 1.2865	a_R = 0.561
W_D	= 8.047 + 0.0805 E_n	0 < E_n < 6	r_D = 1.3448	a_D = 0.473
	= 8.530 - 0.2509 (E_n - 6)	6 ≤ E_n ≤ 27.6		
W_V	= 0.00	0 < E_n < 0.5	r_V = 1.3448	a_V = 0.473
	= -0.0721 + 0.1475 E_n	0.5 ≤ E_n ≤ 27.6		
V_{SO}	= 6.20	0 < E_n ≤ 27.6	r_{SO} = 1.12	a_{SO} = 0.47

D. Neutron Potentials for Analysis of n + Ti and n + V Reactions

A study of neutron-induced activation cross sections of $^{45,46}Ti$ and $^{50,51}V$ was reported in 1984 by Muir and Arthur.[13] In order to carry out the calculations, optical model parameters were obtained for both elements by fitting resonance data (s- and p-wave strengths and scattering radii) and neutron total and scattering cross sections. Good agreement was obtained between measurements of various reaction cross sections and calculations with the GNASH code.[14] Muir and Arthur's analysis only extended to 20 MeV. Presumably it would not be difficult to extend the results to a slightly higher energy where a match with the Madland Semmering potential should be possible. Muir and Arthur's neutron potential for Ti isotopes is given in Table 6 and the potential for V isotopes is given in Table 7.

Table6. Spherical optical model potentials for neutron reactions on Ti isotopes over the incident neutron energy range 1 keV $\leq E_n \leq$ 20 MeV.

NEUTRONS TO 20 MeV

	Well Depth (MeV)	Range (MeV)	Geometry (fm)	
V_R	= 49.46 - 0.192 E_n	$0 < E_n \leq 20$	r_R = 1.261	a_R = 0.60
W_D	= 3.975 + 0.074 E_n	$0 < E_n < 6$	r_D = 1.364	a_D = 0.42
	= 4.419 - 0.10 (E_n - 6)	$6 \leq E_n \leq 20$		
W_V	= 0.00	$0 < E_n < 1.4$	r_V = 1.261	a_V = 0.60
	= -0.544 + 0.39 E_n	$1.4 \leq E_n \leq 20$		
V_{SO}	= 6.20	$0 < E_n \leq 20$	r_{SO} = 1.12	a_{SO} = 0.47

Table 7. Spherical optical model potentials for neutron reactions on V isotopes over the incident neutron energy range 1 keV $\leq E_n \leq$ 20 MeV.

NEUTRONS TO 20 MeV

	Well Depth (MeV)	Range (MeV)	Geometry (fm)	
V_R	= 48.86 - 0.43 E_n + 0.0003 E_n^2	$0 < E_n \leq 20$	r_R = 1.292	a_R = 0.6076
W_D	= 4.910 + 0.074 E_n	$0 < E_n < 6$	r_D = 1.3685	a_D = 0.429
	= 5.354 - 0.17 (E_n - 6)	$6 \leq E_n \leq 20$		
W_V	= 0.00	$0 < E_n < 0.8$	r_V = 1.292	a_V = 0.6076
	= -0.207 + 0.253 E_n	$0.8 \leq E_n \leq 20$		
V_{SO}	= 6.20	$0 < E_n \leq 20$	r_{SO} = 1.12	a_{SO} = 0.47

E. Neutron Potentials for Analysis of n + ^{58,60}Ni Reactions

Measurements of activation cross sections for 14.2-MeV neutrons on targets of ^{27}Al, ^{58}Ni, ^{93}Nb, and ^{197}Au are compared to calculations with the GNASH code in a 1982 publication by Harper and Alford.[15] The analysis that led to the optical model parameterizations for Ni isotopes was performed at Los Alamos under the tutelage of E. D. Arthur. The optical model analysis was carried out in the same manner as described in Section D for Ti and V isotopes. The potential was validated by calculating a number of reaction cross sections for which experimental data exist. Good agreement with experimental was obtained in most cases, for example, the ^{58}Ni(n,2n), ^{58,60}Ni(n,p), ^{58}Ni(p,pn), ^{54}Fe(α,n), and ^{59}Co(p,xn) cross sections. The optical model parameterizations that resulted for neutron, proton, and alpha reactions to 20 MeV are given in Table 8. Again, these parameterizations could probably be extended to higher energies by making use of the Madland Semmering potential.[7]

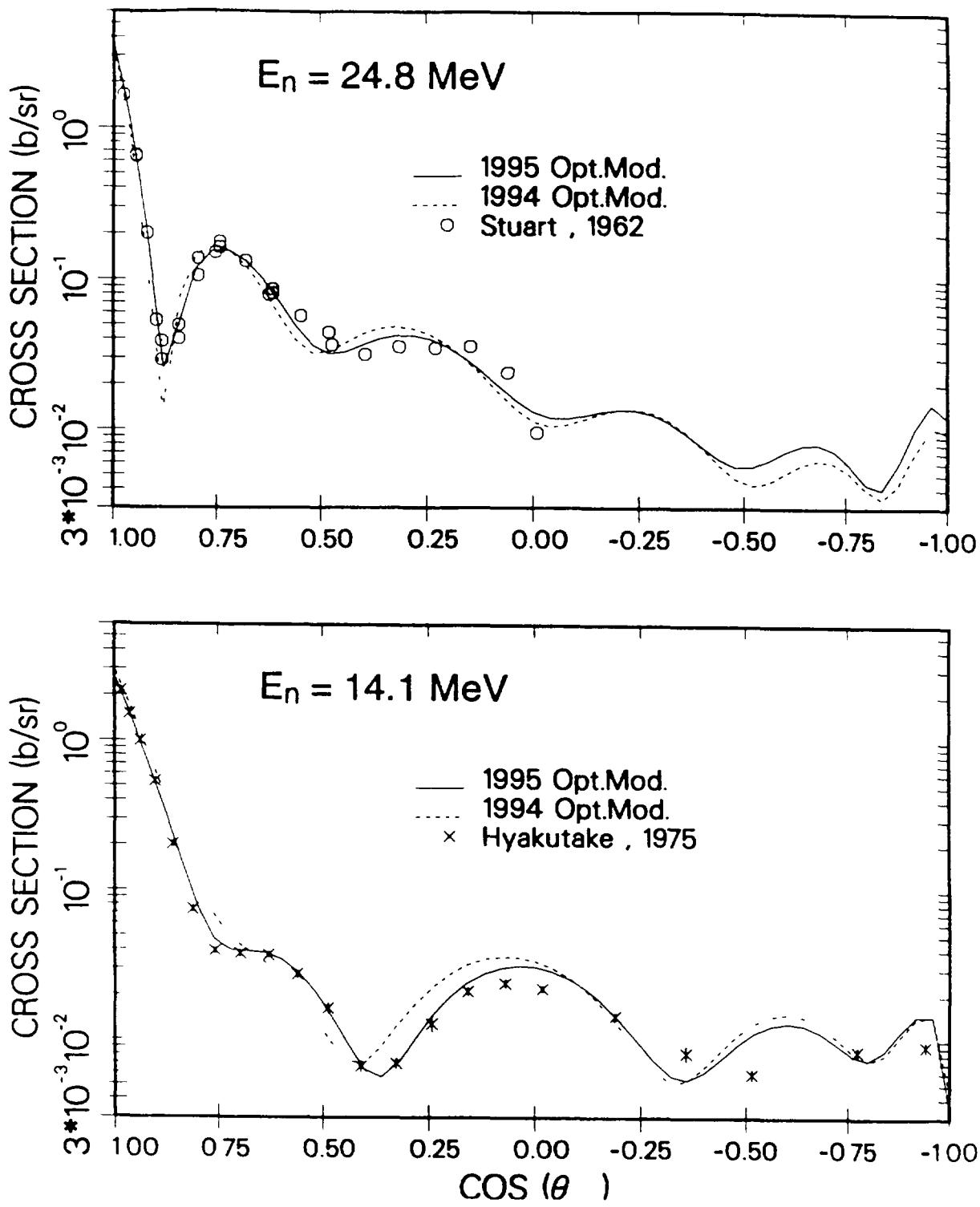

Fig. 1. Angular distributions of 14.1- and 24.8-MeV neutrons elastically scattered from Fe

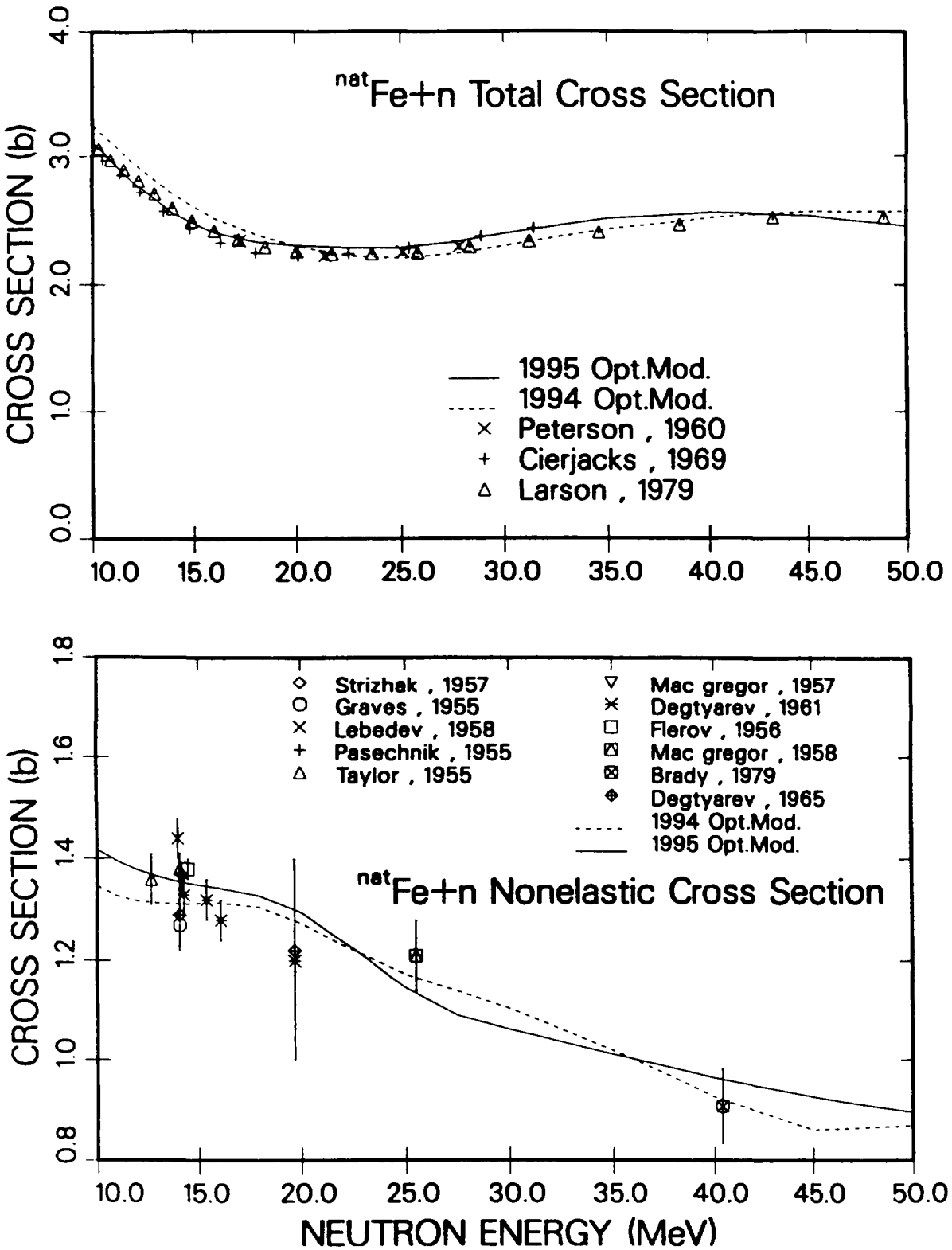

Fig. 2. Calculated and measured neutron total and reaction cross sections from n + Fe reactions.

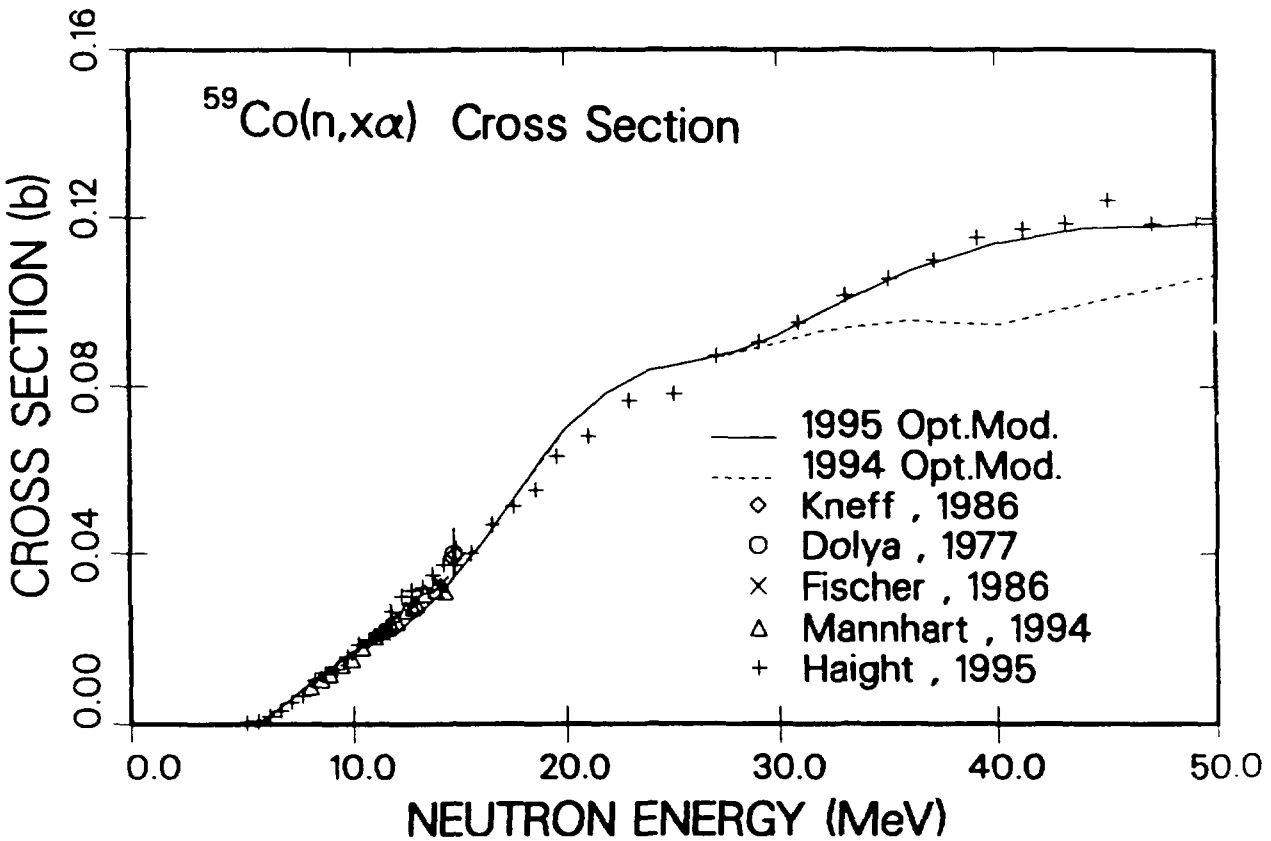

Fig. 3. Comparison of measured and calculated alpha-production cross sections from the $^{59}Co(n,x\alpha)$ reaction.

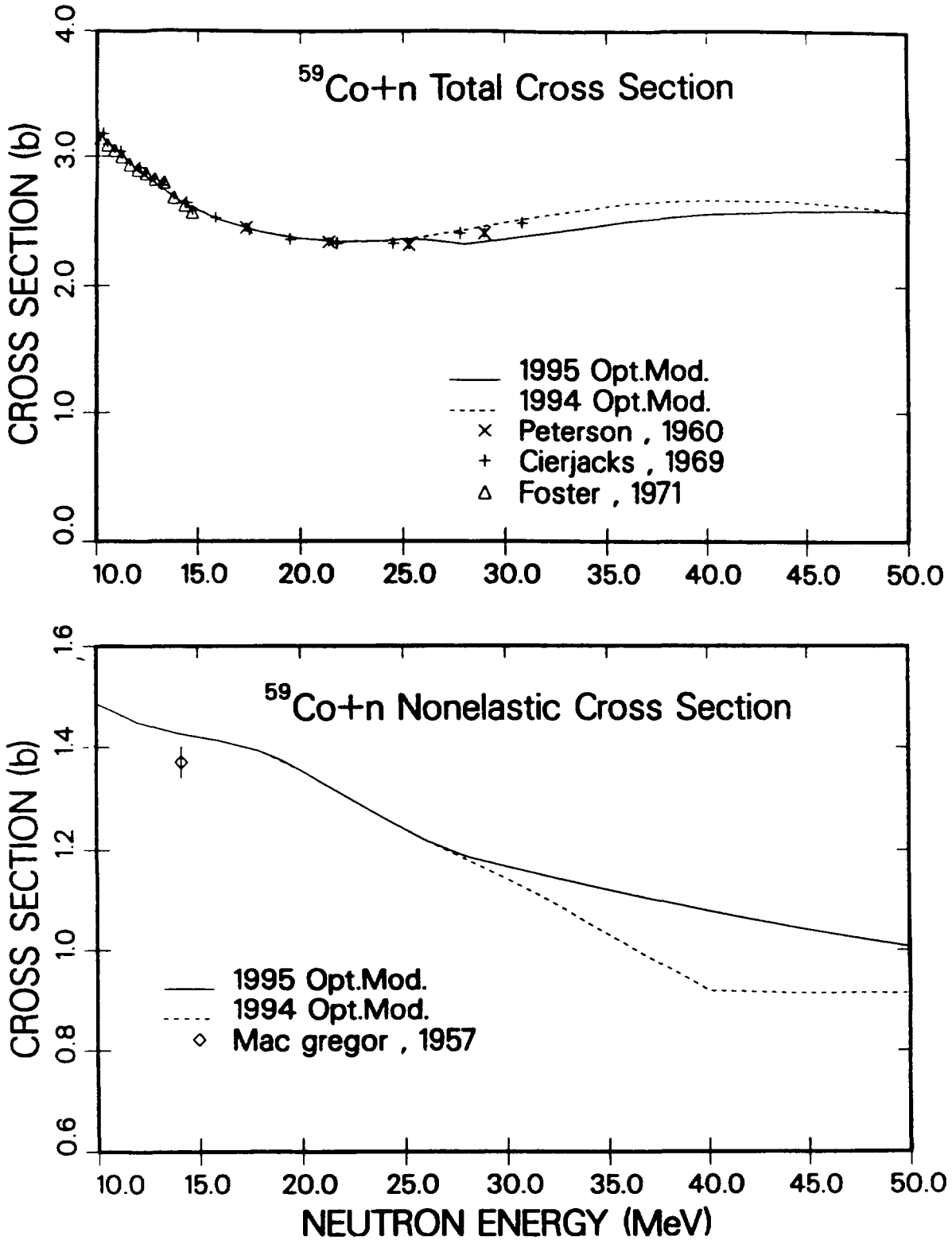

Fig. 4. Calculated and measured neutron total and reaction cross sections from n + ^{59}Co reactions.

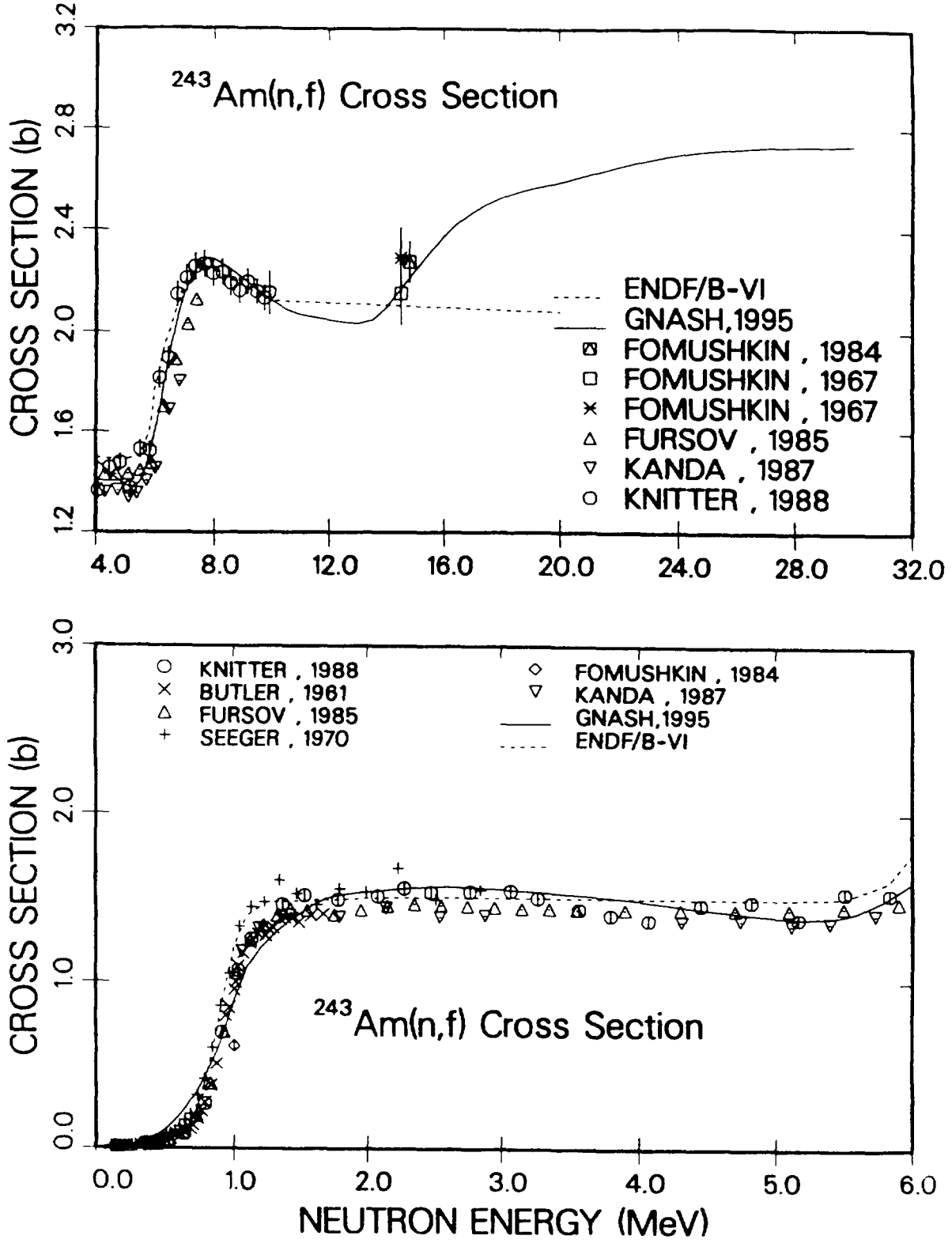

Fig. 5. Comparison of experimental ^{243}Am(n,f) cross section data with the ENDF/B-VI evaluation (dashed curve) and the results of the GNASH calculations (solid curve).

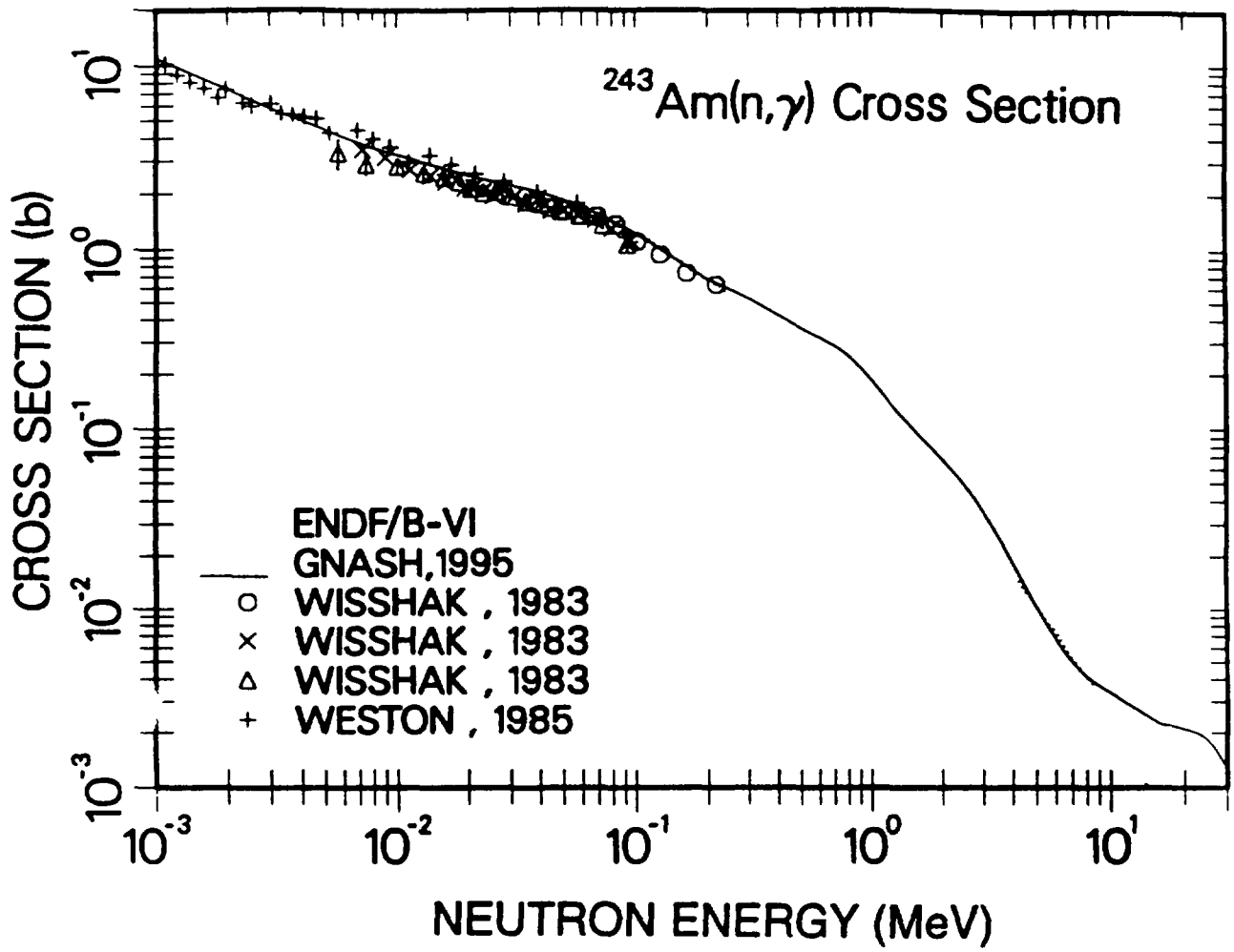

Fig. 6. Comparison of the GNASH calculation of the ^{243}Am(n,γ) cross section with the experimental data base and with the ENDF/B-VI evaluation (dotted curve).

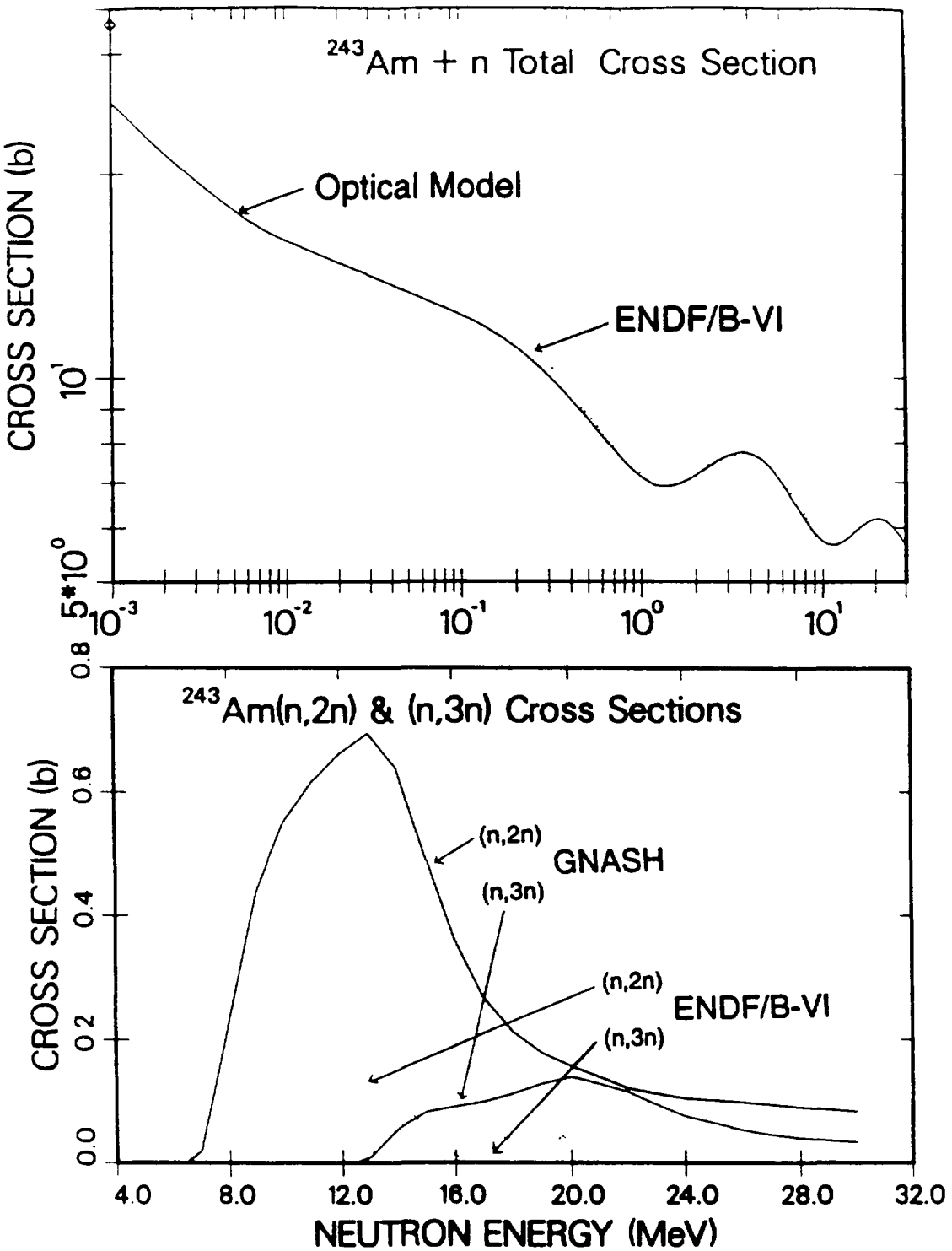

Fig. 7. Comparison of the optical model calculation of the n + ^{243}Am total cross section (upper half) and the GNASH calculations of the (n,xn) and (n,3n) cross sections (lower half) with the existing ENDF/B-VI data evaluation of these quantities.

Table 8 Spherical optical model potentials for neutron reactions on Ni isotopes over the incident neutron energy range 1 keV ≤ E_n ≤ 20 MeV, and proton and alpha energy ranges from effective threshold to 20 MeV.

NEUTRONS TO 20 MeV

Well Depth (MeV)	Range (MeV)	Geometry (fm)	
V_R = 50.06 - 0.3721 E_n	$0 < E_n \leq 20$	r_R = 1.287	a_R = 0.56
W_D = 4.876 + 0.27 E_n	$0 < E_n < 6$	r_D = 1.345	a_D = 0.47
= 6.496 - 0.2251 (E_n - 6)	$6 \leq E_n \leq 20$		
W_V = 0.00	$0 < E_n < 0.5$	r_V = 1.287	a_V = 0.56
= -0.0941 + 0.1973 E_n	$0.5 \leq E_n \leq 20$		
V_{SO} = 6.20	$0 < E_n \leq 20$	r_{SO} = 1.12	a_{SO} = 0.47

PROTONS TO 20 MeV (r_c = 1.25 fm)

Well Depth (MeV)	Range (MeV)	Geometry (fm)	
V_R = 57.95 - 0.55 E_p	$0 < E_p \leq 20$	r_R = 1.25	a_R = 0.65
W_D = 13.5 - 0.10 E_p	$0 < E_p \leq 20$	r_D = 1.25	a_D = 0.47
W_V = 0	$0 < E_p \leq 20$		
V_{SO} = 7.5	$0 < E_p \leq 20$	r_{SO} = 1.25	a_{SO} = 0.47
	$0 < E_p \leq 20$	r_c =	

ALPHA PARTICLES (r_c = 1.4 fm)

Well Depth (MeV)	Range (MeV)	Geometry (fm)	
V_R = 193.0 - 0.15 E_α	$0 < E_\alpha \leq 20$	r_R = 1.37	a_R = 0.56
W_D = 0.00	$0 < E_\alpha \leq 20$		
W_V = 21.0 + 0.25 E_α	$0 < E_\alpha \leq 20$	r_V = 1.37	a_V = 0.56
	$0 < E_\alpha \leq 20$	r_c =	

III. COUPLED-CHANNELS OPTICAL MODEL POTENTIAL FOR Am ISOTOPES

In our previous paper[1] we presented a coupled-channels potential for neutron reactions on ^{241}Am. Since that time we have performed an analysis of neutron cross sections on ^{243}Am. For the new work, we formulated the ^{241}Am potential in an isospin-dependent form and used it for ^{243}Am. The generalized Am coupled-channels neutron potential is given in Table 9. The results of the fission cross section analysis utilizing transmission coefficients from this potential are compared in Fig. 5 with experimental data and the ENDF/B-VI evaluation. Similarly, the calculated ^{243}Am(n,γ) cross section is compared to measurements and the ENDF/B-VI evaluation in Fig. 6. Finally, the calculated ^{243}Am + n total and (n,2n) cross sections are compared to the ENDF/B-VI evaluation in Fig. 7.

Table 9 Coupled-channels optical model and deformation parameters for neutron reactions with Am isotopes to 30 MeV. The lowest five members of the ground-state rotational band are coupled in the calculation for each isotope The quantity η is given for each isotope by $\eta = (N - Z) / A$.

n + ^{241,243}Am Parameters (E_n = 0 - 30 MeV)

Well Depth (MeV)	Range(MeV)	Geometry (fm)
$V_R = 52.102 - 27.75\eta - 0.30E$	$0 \le E \le 30$	$r_R = 1.25$ $a_R = 0.60$
$W_D = 5.3243 - 9\ 4995\eta + 0.45E$	$0 \le E < 8$	$r_D = 1.24$ $a_D = 0.55$
$= 8.9243 - 9.4995\eta - 0.046(E - 8)$	$8 \le E \le 30$	
$W_V = 0$	$0 \le E < 8$	$r_V = 1.24$ $a_V = 0.55$
$= -1.6 + 0.20\ E$	$8 \le E \le 30$	
$V_{SO} = 6.2$	$0 \le E \le 30$	$r_{SO} = 1.01$ $a_{SO} = 0.75$

Deformation Parameters

Isotope	β_2	β_4
^{241}Am	0.2100	0.0756
^{243}Am	0.2102	0.0629

IV STATUS OF THE REFERENCE INPUT PARAMETER LIBRARY

In the time period since the first research coordination meeting organized by the IAEA for development of the Reference Input Parameter Library (RIPL),[1] a preliminary format for the RIPL has been developed and a number of spherical and coupled-channels optical model parameterizations have been cast in the format and provided to the Nuclear Data Section. More details on this activity are given in the paper by S. B. Garg and A. Kumar[16] in this meeting.

IV. CONCLUSIONS

In our previous paper,[1] we presented a variety of optical model potentials used in reaction theory analyses at Los Alamos National Laboratory. In this paper we have refined the Fe and Co potentials and included additional potentials for Ti, V, Ni, and Am isotopes Additionally, we have included potentials from Lawrence Livermore National Laboratory that are highly successful in reproducing measured data for neutron and proton reactions on ^{12}C, ^{14}N, and ^{16}O As was pointed out in our previous paper, we expect that refinements and improvements can be made to all these potentials. Our hope again is that the present parameterizations will be adequate with minimal revision for some applications and will provide a starting point for future detailed analyses

As was also mentioned in our previous paper, it is our view that substantial additional work is needed at higher energies in order to put optical model characterizations on a sound basis. We feel that a systematic study utilizing both a Schrödinger and Dirac approach is needed to develop a global nucleon-nucleus optical model potential that is reliable into the medium energy region.

Significant progress has been made over the past year in specifying and initiating a library of reference input optical model parameters for nuclear model calculations. After approval of a format, we will complete a base library and begin considering default or recommended initial parameters for a variety of applied problems.

REFERENCES

1. P. G. Young, "Experience at Los Alamos With Use of the Optical Model for Applied Nuclear Data Calculations," International Atomic Energy Agency report INDC(NDS)-335 (1994) p. 109.

2. M. B. Chadwick, L. J. Cox, P. G. Young, and A. S. Meigooni, "Calculation and Evaluation of Cross Sections and Kerma Factors for Neutrons Up to 100 MeV on Carbon," to be published in Nucl. Sci. Eng. (1995).

3. M. B. Chadwick and P. G. Young, "Calculation and Evaluation of Cross Sections and Kerma Factors for Neutrons Up to 100 MeV on ^{16}O and ^{14}N," submitted to Nucl. Sci. Eng. (1995).

4. M. B. Chadwick, Lawrence Livermore National Laboratory, personal communication (1995).

5. E. D. Arthur, Los Alamos National Laboratory progress report LA-9841-PR (1983).

6. P. J. Dymbylow, Phys. Med. Biol. **25**, 637 (1980).

7. D. G. Madland, "Recent Results in the Development of a Global Medium-Energy Nucleon-Nucleus Optical-Model Potential," Proc. *Specialists' Mtg. Preequilibrium Nuclear Reactions*, Semmering, Austria, 10-12 February 1988 [Ed: B. Strohmaier, NEANDC-245 'U' (1988)] p. 103.

8. M. S. Islam, R. W. Finlay, J. S. Petler, J. Rapaport, R. Alarcon, and J. Wierzbicki, Phys. Med. Biol. **33**, 315 (1988).

9. E. D. Arthur and P. G. Young, "Evaluated Neutron-Induced Cross Sections for $^{54,56}Fe$ to 40 MeV," Los Alamos National Laboratory report LA-8636-MS (ENDF-304) (1980).

10. C. Y. Fu and D. M. Hetrick, "Update of ENDF/B-V Mod-3 Iron: Neutron-Producing Reaction Cross Sections and Energy-Angle Correlations," Oak Ridge National Laboratory report ORNL/TM-9964 (1986).

11. S. M. Grimes, C. E. Brient, F. C. Goeckner, F. B. Bateman, Mc B. Chadwick, R. C. Haight, T. M. Lee, S. M. Sterbenz, P. G. Young, O. A. Wasson, and H. Vonach, "The $^{59}Co(n,\alpha)$ Reaction from 5 to 50 MeV," Nucl. Sci. Engr., to be published (1995).

12. E. D. Arthur, P. G. Young, and W. K. Matthes, "Calculation of ^{59}Co Neutron Cross Sections Between 3 and 50 MeV, "Proc. *Symp. on Neutron Cross Sections from 10 to 50 MeV*, BNL (May 1980), p. 751.

13. D. W. Muir and E. D. Arthur, J. of Nucl. Materials **122 & 123**, 1058 (1984).

14. P. G. Young, E. D. Arthur, and M. B. Chadwick, "Comprehensive Nuclear Model Calculations: Introduction to the Theory and Use of the GNASH Code," Los Alamos National Laboratory report LA-12343-MS (1992).

15. R. C. Harper and W. L. Alford, J. Phys. G: Nucl. Phys. **8**, 153 (1982).

16. S. B. Garg and A. Kumar: "Starter File of Optical Model Potential Parameters and Nuclear Data Computations of Nd-Isotopes," *Second Research Co-ordination Meeting on Development of Reference Input Parameter Library for Nuclear Model Calculations of Nuclear Data*, 19-23 September 1994, Vienna, Austria (present meeting).

CONTRIBUTORS TO DRAFTING AND REVIEW

Bersillon, O.
Service de Physique et Techniques Nucléaires
Centre d'Etudes Nucléaires de Bruyères-le-Châtel
B.P. 12
F-91680 Bruyères-le-Châtel
France
E-mail: bersil@bruyeres.cea.fr

Běták, E.
Institute of Physics
Slovak Academy of Sciences
84228 Bratislava
Slovakia
E-mail: betak@savba.sk

Capote Noy, R.
Centro de Estudios Aplicados al Desarollo Nuclear
Calle 30 No. 502 e/5ta y 7ma
Miramar, Playa
11300 Ciudad de la Habana
Cuba
E-mail: rcapote@ceaden.edu.cu

Chadwick, M.B.
Group T-2, MS B243
Los Alamos National Laboratory
Los Alamos, NM 87545
USA
E-mail: chadwick@t2e.lanl.gov

Fukahori, T.
Nuclear Data Center
Japan Atomic Energy Research Institute
Tokai-mura, Naka-gun
Ibaraki-ken 319-1195
Japan
E-mail: fukahori@cracker.tokai.jaeri.go.jp

Ignatyuk, A.V.
(Chairman)
Institute of Physics and Power Engineering
Bondarenko Sq. 1
249020 Obninsk, Kaluga Region
Russian Federation
E-mail: ignatyuk@cjd.obninsk.su

Kailas, S.
Nuclear Physics Division
Bhabha Atomic Research Center
Trombay, Mumbai 400 085
India
E-mail: kailas@magnum.barc.ernet.in

Kopecky, J.	JUKO Research Kalmanstraat 4 NL-1817 HX Alkmaar Netherlands E-mail: juka@wxs.nl
Maslov, V.M.	Radiation Physics and Chemistry Problems Institute Belarus Academy of Science 220109 Minsk-Sosny Belarus E-mail: maslov@ndel.belpak.minsk.by
Molnár, G.	Institute of Isotopes Hungarian Academy of Sciences P.O. Box 77 H-1525 Budapest Hungary E-mail: molnar@alpha0.iki.kfki.hu
Obložinský, P. *(Scientific Secretary)*	International Atomic Energy Agency Wagramerstrasse 5, P.O. Box 100 A-1400 Vienna Austria E-mail: oblozinsky@iaeand.iaea.or.at
Reffo, R.	Nuclear Data Center E.N.E.A. Via Martiri di Monte Sole, 4 I-40129 Bologna Italy E-mail: reffo@nudace.arcoveggio.enea.it
Su, Z.	China Institute of Atomic Energy P.O. Box 275 (41) Beijing 102413 China E-mail: zdsu@mipsa.ciae.ac.cn
Uhl, M. (†)	Institut für Radiumforschung und Kernphysik Boltzmanngasse 3 A-1090 Vienna Austria
Young, P.G.	Group T-2, MS B243 Los Alamos National Laboratory Los Alamos, NM 87545 USA E-mail: pgy@lanl.gov

† Deceased